2018

Development And Utilization Of Ultrasound Imaging Techniques To Evaluate The Role Of Vascularity In Adult And Aged Rat Achilles Tendon Healing

Corinne Nicole Riggin
University of Pennsylvania, cnriggin@gmail.com

Development And Utilization Of Ultrasound Imaging Techniques To Evaluate The Role Of Vascularity In Adult And Aged Rat Achilles Tendon Healing

Abstract

Tendons are hypovascular tissues, undergoing angiogenesis only during development, wound healing, and pathogenesis. Injured tendons exhibit a healing response with vascular ingrowth during the proliferative phase and vascular regression during remodeling. Despite this normal healing response, tendons never fully regain their original structure or composition. Additionally, aging further increases tendon risk of rupture and impairs healing response. Since the optimal vascularization level and timing during tendon healing is currently unknown, modulating the vascular response during healing could elucidate the role of angiogenesis in tendon injury and ultimately improve the tendon healing outcome. Furthermore, new ultrasound technologies allow for the evaluation of vascular response after injury, which could provide a measure for evaluating tendon healing in vivo. Therefore, the objective of this study is to develop methods for, and evaluate the effect of, vascular modulation in adult and aged rat Achilles tendons during healing using both in vivo ultrasound imaging measures of vascularity and structure and ex vivo measures of tendon compositional and mechanical properties. In Specific Aim 1, we will validate the use of in vivo high-frequency ultrasound technologies to measure vascular changes in rat Achilles tendons. In Specific Aim 2, we will develop methodologies for vascular modulation in an Achilles tendon injury model using the delivery of pro- and anti-angiogenic factors. Finally, in Specific Aim 3, we will apply methods of vascular modulation and ultrasound imaging to determine the role of angiogenesis in adult and aged Achilles tendon healing models. To achieve these goals, we will perform bilateral partial-rupture injuries in the Achilles tendons of adult and aged rats, followed by injections to modulate their vascular response after injury. The animals will receive vascular endothelial growth factor (VEGF), anti-VEGF antibody (B20.4-1-1, Genentech), or saline injections following injury. They will be evaluated using B-mode, color Doppler, photoacoustic, and contrast-enhanced ultrasound imaging weekly post-injury. Additionally, they will undergo in vivo functional assays to assess gait and passive ankle motion. Animals will be sacrificed for histological and mechanical analyses. This study will validate new in vivo methods for evaluating vascularity in tendon injury models, develop potential angiogenic therapies for improved healing outcome, and elucidate the differences in vascular response with age after tendon injury and vascular modulation.

Degree Type
Dissertation

Degree Name
Doctor of Philosophy (PhD)

Graduate Group
Bioengineering

First Advisor
Louis J. Soslowsky

DEVELOPMENT AND UTILIZATION OF ULTRASOUND IMAGING
TECHNIQUES TO EVALUATE THE ROLE OF VASCULARITY IN ADULT AND
AGED RAT ACHILLES TENDON HEALING

Corinne Nicole Riggin

A DISSERTATION

in

Bioengineering

Presented to the Faculties of the University of Pennsylvania

in

Partial Fulfillment of the Requirements for the

Degree of Doctor of Philosophy

2018

Supervisor of Dissertation   Graduate Group Chair

_____   _____

Louis J. Soslowsky, Ph.D.   Ravi Radhakrishnan, Ph.D.
Fairhill Professor of   *Professor of Bioengineering and*
Orthopaedic Surgery   *Chemical and Biomolecular Engineering*

Dissertation Committee

Robert L. Mauck, Ph.D.
Mary Black Ralston Professor for Education and Research in Orthopaedic Surgery

Chandra M. Sehgal, Ph.D.
Research Professor of Radiology, University of Pennsylvania

Daniel C. Farber, M.D.
Assistant Professor of Clinical Orthopaedic Surgery, University of Pennsylvania

DEVELOPMENT AND UTILIZATION OF ULTRASOUND IMAGING

TECHNIQUES TO EVALUATE THE ROLE OF VASCULARITY IN ADULT AND

AGED RAT ACHILLES TENDON HEALING

DEDICATION

I dedicate my dissertation to my family, who have always believed in me and encouraged me to believe in myself. I would not be the person that I am today without their unconditional love and support.

ACKNOWLEDGMENTS

and I really appreciate everything they have done for me. I also want to thank Susan Schultz from the small animal imaging facility. She taught me how to do live animal ultrasound imaging and helped me with all of my imaging logistics. Finally, I want to thank all of the staff in the Soslowsky lab over the years, and in particular Courtney Nuss, Carrie Barnum, James Boorman-Padgett, Kerrie Tiedeman, and Molly Minnig.

Finally, I want to thank my family. My parents, Karen and Ron Riggin, love and support me in everything that I do. They always believe in me and encourage me to believe in myself. Completing a PhD is no easy task, and I think it would have been nearly impossible without their support. Also, my sister and brother-in-law, Alyse and Mike Talbott. Spending time together with them can always brighten my day, and I feel grateful to be so close to my siblings. I also want to thank my Grandmom (Marcia Davis) and Grampy and Grammy (Dr. Charles and Jean Warner), who have been an important part of my life and have helped shape me into the person I am today. Throughout my life, my Grandmom has always shared her love of art with me. While I am pursuing a career in science and engineering, art still remains important to me and is a relaxing and fulfilling hobby. My Grammy and Grampy have played a large role in developing my interest in science from a young age. I have so many fond memories of doing little science experiments, learning how to use a compass, or even learning about nutrition (and reading all the nutrition facts in the grocery store!) with them. Their love to learn, explore, and try new things has forever been ingrained in me, and I can't thank them enough for that. Finally, I want to thank my boyfriend Dr. Justin Thomas. Justin and I have shared all of the highs and lows of our graduate experiences together, and I am so thankful for his love and support.

ABSTRACT

DEVELOPMENT AND UTILIZATION OF ULTRASOUND IMAGING

TECHNIQUES TO EVALUATE THE ROLE OF VASCULARITY IN ADULT AND

AGED RAT ACHILLES TENDON HEALING

Corinne N. Riggin

Dr. Louis J. Soslowsky

Tendons are hypovascular tissues, undergoing angiogenesis only during development, wound healing, and pathogenesis. Injured tendons exhibit a healing response with vascular ingrowth during the proliferative phase and vascular regression during remodeling. Despite this normal healing response, tendons never fully regain their original structure or composition. Additionally, aging further increases tendon risk of rupture and impairs healing response. Since the optimal vascularization level and timing during tendon healing is currently unknown, modulating the vascular response during healing could elucidate the role of angiogenesis in tendon injury and ultimately improve the tendon healing outcome. Furthermore, new ultrasound technologies allow for the evaluation of vascular response after injury, which could provide a measure for evaluating tendon healing in vivo. Therefore, the objective of this study is to develop methods for, and evaluate the effect of, vascular modulation in adult and aged rat Achilles tendons during healing using both in vivo ultrasound imaging measures of vascularity and structure and ex vivo measures of tendon compositional and mechanical properties. In Specific Aim 1, we will validate the use of in vivo high-frequency ultrasound technologies to measure

vascular changes in rat Achilles tendons. In Specific Aim 2, we will develop methodologies for vascular modulation in an Achilles tendon injury model using the delivery of pro- and anti-angiogenic factors. Finally, in Specific Aim 3, we will apply methods of vascular modulation and ultrasound imaging to determine the role of angiogenesis in adult and aged Achilles tendon healing models. To achieve these goals, we will perform bilateral partial-rupture injuries in the Achilles tendons of adult and aged rats, followed by injections to modulate their vascular response after injury. The animals will receive vascular endothelial growth factor (VEGF), anti-VEGF antibody (B20.4-1-1, Genentech), or saline injections following injury. They will be evaluated using B-mode, color Doppler, photoacoustic, and contrast-enhanced ultrasound imaging weekly post-injury. Additionally, they will undergo in vivo functional assays to assess gait and passive ankle motion. Animals will be sacrificed for histological and mechanical analyses. This study will validate new in vivo methods for evaluating vascularity in tendon injury models, develop potential angiogenic therapies for improved healing outcome, and elucidate the differences in vascular response with age after tendon injury and vascular modulation.

TABLE OF CONTENTS

CHAPTER 1: INTRODUCTION

CHAPTER 2: ANALYSIS OF COLLAGEN ORGANIZATION IN MOUSE ACHILLES TENDON USING HIGH-FREQUENCY ULTRASOUND IMAGING

CHAPTER 3: METHODS FOR MODULATION OF VASCULAR RESPONSE AFTER INJURY

**CHAPTER 4: EFFECT OF VASCULAR MODULATION ON ACHILLES
TENDON HEALING IN AN ADULT RAT INJURY MODEL**

CHAPTER 5: EFFECT OF VASCULAR MODULATION ON ACHILLES TENDON HEALING WITH AGING

List of Tables

LIST OF FIGURES

CHAPTER 1: INTRODUCTION

A. INTRODUCTION

Musculoskeletal injuries are common and represent a significant burden to the health care system. A recent study reported over 61 million musculoskeletal injuries treated nationwide. Of these injuries, the greatest single group involves injuries to tendons or ligaments, namely sprains, strains, and ruptures, with 18.4 million injuries resulting in a visit to a health care professional.[25, 67, 117, 125] The frequency of musculoskeletal injury is expected to increase greatly in the coming decades with both increased life expectancy and a sustained higher level of activity with aging. This is estimated to have an exponential effect on injuries to tendons and ligaments.[58]

Tendon rupture is defined by the partial or full thickness tearing of tendon fibers. This condition can be either acute, in the case of an individual experiencing a rupture from a single high load impact, or chronic, in the case where the tendon is weakened due to degeneration and can rupture at a lower load.[117] The Achilles tendon is one of the most frequently injured tendons in the human body and commonly tears at the midsubstance.[28] Unfortunately, after rupture, tendons primarily form scar tissue during healing and never fully regain the same structure, composition, and organization of healthy tissue. This sustained decrease in the mechanical properties increases the potential for re-rupture.[80] Aging also has significant effects on tendon homeostatic maintenance, increasing the risk of rupture, as well as impairing healing capacity after injury.[1, 89, 103]

An important component of the tendon healing process is angiogenesis, the

formation of new blood vessels. Blood vessels have numerous roles within tissues to facilitate the healing process, including the delivery of oxygen and nutrients, the removal of waste, the transport of regulatory factors, and the control of the immune response.[49] However, while angiogenesis is a necessary component to tendon healing, prolonged hypervascularization following tendon injury is not always believed to be beneficial.[121] As seen in various vascular diseases, an imbalance of pro- and anti-angiogenic factors could promote abnormal angiogenesis creating vessels with structural and functional deficits, causing inflammation, inefficient nutrient exchange, and potentially hypoxia despite increased vessel density.[49] Conversely, it is possible that the angiogenic response following tendon injury is not sufficient, and that increasing vascular formation could promote a more robust healing response.[139] Therefore, there is uncertainty regarding the balance of angiogenic processes in the progression of tendon healing.[35]

Angiogenic treatments have been evaluated primarily in the context of vascular diseases such as ischemic injury or tumor growth. However, there has been some evidence supporting their use for musculoskeletal conditions. While studies have demonstrated the ability to increase[65, 69, 73, 137, 139] or decrease[24, 56, 57, 98] vascularity in tendon and ligament applications, many of these studies fail to correlate vascular changes to mechanical properties and therefore healing outcomes. Therefore, a comprehensive evaluation of both pro- and anti-angiogenic treatments after tendon injury is needed to fully understand the mechanism of vascularity in tendon healing.

In addition to studying mechanical outcomes in basic science research, there is the need for methodologies that can longitudinally evaluate the tendon healing process and

therefore ultimately be translated to clinical use. Ultrasound imaging is a method currently used for diagnosing tendon injury or disease but infrequently used to track the progression of tendon healing. Additionally, there are multiple new ultrasound technologies that allow for the quantitative evaluation of vascular and structural properties within tissues that are currently not used in the tendon field.

Therefore, the objective of this work is to develop methods for, and evaluate the effect of, vascular modulation in adult and aged rat Achilles tendons during healing using both *in vivo* ultrasound imaging measures of structure and vascularity and *ex vivo* measures of tendon compositional and mechanical properties. Specifically, this work will develop a model for the study of vascular growth within tendons. Additionally, it will provide insight into the role of the tendon vascular response to injury throughout aging by studying healing outcomes after the delivery of angiogenic therapies. Finally, this work will investigate the use of multiple ultrasound imaging modalities to quantify tendon properties *in vivo*, which has the capability to be translated to clinical practice.

A subset of the information in this chapter is provided from a previously published book chapter on tendinopathies.[110]

B. BACKGROUND

B-1. Achilles Tendon Overview

<u>Tendon Anatomy</u>: The Achilles tendon is the largest and strongest tendon in the human body and can endure loads over 3700 N during activity.[42] The origin of the tendon is in the mid-calf, where it fuses with the medial and lateral heads of the gastrocnemius

muscle and inserts on the posterior surface of the calcaneus (Figure 1.1). Deep to the gastrocnemius is the soleus muscle, which forms a second branch in the Achilles tendon. The plantaris originates on the femur, runs parallel to the Achilles on the medial side, and inserts on the medial side of the calcaneus.[28] The Achilles has an average length of 15 cm, with a width of 4-6cm near the myotendinous junction, 1-2cm at the midsubstance, and 2-4cm at the insertion.[4, 20] The gastrocnemius, soleus, and plantaris muscles all act as ankle flexors, while the gastrocnemius also acts as a knee flexor. The gastrocnemius plays an active role in motions such as walking, running, and jumping, and is therefore comprised of primarily fast-twitch (type II) muscle fibers.[114] The soleus muscle, by contrast, has a stabilizing role in the ankle, and is comprised of slow-twitch (type I) fibers.[114]

Figure 1.1: Achilles tendon and associated muscle anatomy [Reprinted from Danish Medical Journal, Open Access].[6]

Vascular Anatomy: Similar to other tendons in the body, the Achilles tendon is a relatively hypovascular tissue. Its blood supply comes from two main arteries: the posterior tibial artery, which perfuses the proximal and distal sections, and the peroneal artery, which perfuses the mid-section of the tendon (Figure 1.2).[28, 121] The tendon is primarily supplied by these arteries from the anterior side, with vessels that pass through

or around the tendon to perfuse the posterior surface.[20] Vascular supply mainly runs through the paratenon, which is the highly vascularized sheath surrounding the tendon.[20] The proximal third of the tendon also receives blood supply through the vessels in the muscle that continue into the endotendon at the musculotendinous junction. Similarly, the distal third receives vascularization from small vessels starting at the insertion and continuing up the endotenon.[28] The structure of the vessels in the tendon comprise of larger transverse vessels that run on the surface of the tendon perpendicular to the fibers, and then branching vessels that that run longitudinally between tendon fibers and fascicles, but do not penetrate the collagen bundles.[97] The mid-substance region of the tendon, supplied by the peroneal artery, is significantly less vascular than the proximal and distal regions. The poor vascularization of this region of the Achilles tendon has been hypothesized to contribute to the frequent incidence of inflammation, pathology, and rupture at this site.[20, 97]
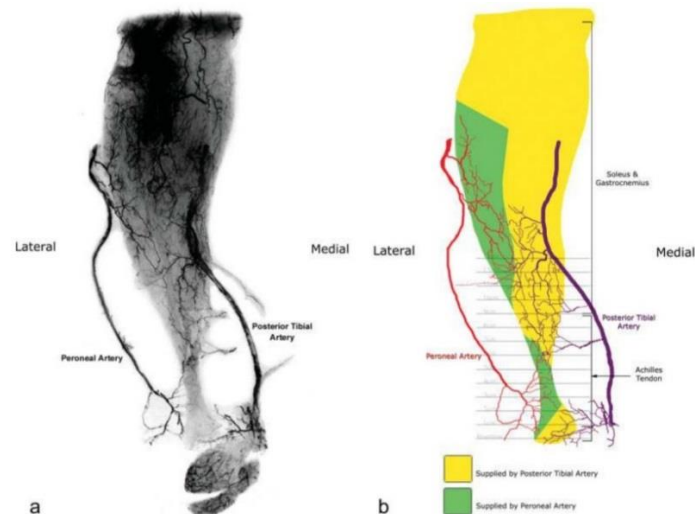
Figure 1.2: (A) Radiograph and (B) schematic of the vascular supply of the Achilles tendon and muscle unit. The posterior tibial artery supplies the proximal and distal sections, while the peroneal artery supplies the mid-section [Reprinted with permission from John Wiley and Sons].[20]

5

Tendon Biology: The main cell type within tendons are tenocytes (tendon fibroblasts), comprising 90-95% of the cells within the tissue. The remaining 5-10% of cells consist of chondrocytes, vascular, synovial, and smooth muscle cells.[28] These cells are embedded in an extracellular matrix (ECM), comprised of collagens (types I, II, V, IX, and X), proteoglycans (PG), elastin, and fibronectin.[38, 43] Collagen is the primary component of the ECM making up 70% of the dry weight of the tendon.[62] Collagen fibers are organized into a hierarchical network from macro-scale bundles of fascicles, down to nano-scale fibrils (Figure 1.3). Fascicles are surrounded by endotenon, encompassing nerve, blood, and lymphatic vessels. The groups of fascicles forming the full tendon are surrounded by the epitenon and then the paratenon.[68] In healthy tendon, 90% of the collagen content is type I.[82] However, tendon biology and composition can change with age, loading environment, disease, and injury, which can alter tissue function and lead to changes in mechanical properties. For example, in injured tendon, type III collagen is produced during tendon repair, which is less organized and less resistant to tensile forces.[84]
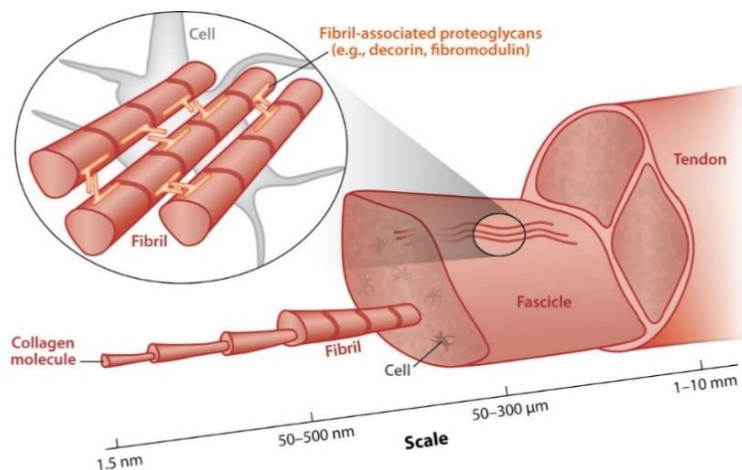
Figure 1.3: The hierarchical structure of the tendon [Reprinted with permission from Annual Reviews, Inc]. [127]

Tendon Mechanics: Tendons are uniquely designed to transmit forces created by the muscle to the bone to facilitate joint movement. The collagen fibers aligned along the axis of loading are the primary load bearing components of mature tissue. Tendons exhibit a non-linear, strain-dependent, viscoelastic behavior. This is due to both the structure and organization of the collagen fibers, as well as the glycosaminoglycan (GAG) and PG content, which attracts water due to their high negative charge.[2] At rest, the collagen fibrils within the tendon have a crimped structure. At low strains, the uncrimping of this structure and the associated increase in collagen alignment gives way to the non-linear toe region of the stress-strain curve.[37] After 2-4% strain, most of the uncrimping has occurred, and the collagen fibers begin to undergo a linear response to increasing strain until microfailure yielding and eventually rupture occurs (Figure 1.4).[90] Other structural elements, such as GAGs and elastin, connect adjacent fibrils and are believed to play a role in the loading response of tendon.[2, 51] However, the specific structure-function relationships of these ECM components is not fully understood. These specific tendon mechanical properties enable the tendon to respond and adapt to loading. The viscoelastic behavior of the tendon allows the storage and release of energy during loading. This protects the tissue from damage, while also providing the elastic spring-like properties to the Achilles tendon, enabling the high-energy propulsion forces during normal physiological activities.[101] Tendon mechanical properties change drastically with injury as the composition and structure is altered through the progression of healing.[84]
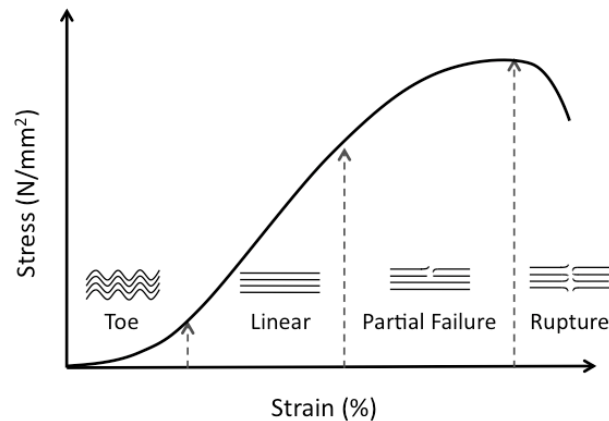
Figure 1.4: Schematic of a typical stress vs. strain curve of a tendon, demonstrating the toe, linear, and failure regions.[110]

B-2. Achilles Tendon Injury

Despite its strength, the Achilles tendon is commonly affected by spontaneous rupture. Achilles tendon pathology is estimated to make up as much as 50% of all sports-related injuries.[61] While some ruptures occur in sedentary patients, 75% of ruptures occur during recreational activities, primarily in men between 30-40 years old.[61] The etiology of Achilles tendon ruptures is unclear. One theory is that chronic degeneration can lead to a rupture without the need for excessive loads. It is hypothesized that low blood flow to the midsubstance of the tendon can result in hypoxia and altered metabolism, ultimately reducing cellular capacity for maintenance and repair of the tissue and leading to ECM degeneration.[31, 66] However, evidence also suggests that Achilles tendon ruptures can occur in healthy tendons, where an incident of excessive force can cause rupture without prior degeneration.[31] It was found that the motion with the greatest risk of rupture is when the tendon is loaded obliquely at a short initial length with maximum muscle contraction, such as in a push-off type activity.[7] Additionally, this risk can be amplified in individuals who are less able to control excessive and uncoordinated muscle contractions, a quality

often seen in the "weekend warrior" population.[31]

Once ruptured, the tendon undergoes a healing response that occurs in three main stages: (1) inflammation, (2) proliferation, and (3) remodeling (Figure 1.5).[15, 132] The inflammatory phase of healing begins immediately after injury and lasts for up to 7 days. Initially, hemostasis occurs, where the injury site is infiltrated with red blood cells and platelets from damaged vessels at the injury site. Platelets aggregate and form a fibrin clot to stabilize the injury while releasing pro-inflammatory markers to recruit immune cells, mainly neutrophils. Damaged cells at the injury site, as well as recruited neutrophils, also release chemotactic factors to attract macrophages. Macrophages phagocytose necrotic tissue, as well as release growth factors to initiate ECM formation, tenocyte proliferation, and angiogenesis.[59] Mechanical stretching is thought to be harmful to healing during this initial inflammatory phase.[112]
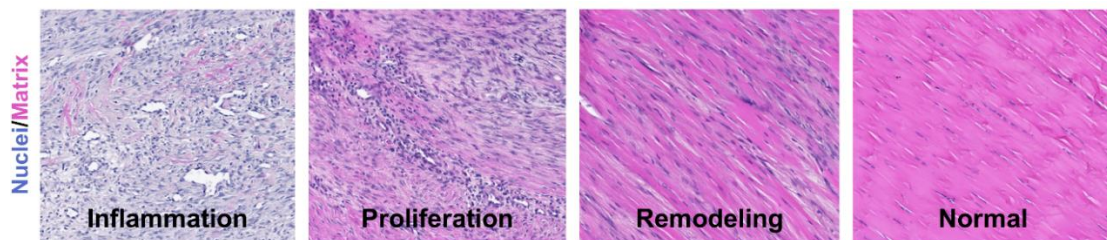
Figure 1.5: Histological sections of tendon tissue during the 3 stages of healing compared to normal tendon.

The proliferative phase of healing begins 3-7 days after injury and continues for weeks. During this phase, tenocytes and macrophages proliferate and initiate tissue synthesis. Production of type I collagen decreases, whereas the production of type III collagen increases significantly. The ECM becomes filled in with large amounts of disorganized collagen as well as non-collagenous proteins, including PGs and GAGs,

maintaining a high water content. Passive stretching during this phase of healing has been shown to promote synthesis of collagen by tenocytes, increasing tensile strength, tendon diameter, PGs, and collagen crosslinks.[71, 118, 129]

The remodeling phase of healing happens over the course of months to years after injury. During this phase, tenocytes begin to turn over type III collagen into type I collagen, and the granulation scar tissue becomes progressively more aligned and fibrous. Cell density and cell activity decrease. While this increased organization improves the tensile mechanical properties towards normal tendon, the repaired tissue is still fibrous scar, and will never completely regain the structural, compositional, or functional properties it had prior to injury. Unfortunately, this leads to a relatively high rate of re-rupture as well as tendon lengthening during healing, causing loss of calf muscle strength and ankle function.

B-3. Tendon Vascular Response to Injury

Blood vessels have numerous roles within tissues, including the delivery of oxygen and nutrients, the removal of waste products, the transport of growth factors, cytokines, and hormones, and the control of blood flow to regulate immune response.[49] Wound healing relies heavily on all of these functions, and so angiogenesis is induced in order to enhance these functions after injury. Angiogenesis is a complex process that involves the interplay between multiple pro- and anti-angiogenic factors. The stages of angiogenesis include: (1) increase in pro- to anti-angiogenic ratio, (2) vessel destabilization, (3) vessel sprouting, (4) endothelial proliferation and pericyte recruitment, and (5) vessel maturation (Figure 1.6).[49] During the initiation of angiogenesis, vascular endothelial growth factor

(VEGF) is the major pro-angiogenic factor produced by many different cell types as a response to hypoxia and inflammation. Regulated by VEGF, Angiopoietin-2 (Ang-2) is the primary factor responsible for vessel destabilization, and is localized to areas of vascular remodeling. In the absence of VEGF, Ang-2 vessel destabilization leads to vessel regression. However, in the presence of VEGF, Ang-2 vessel destabilization initiates angiogenesis and vessel growth. Ang-2 also induces MMP expression to breakdown the ECM and allow for vessel growth in the tissue. Angiopoietin-1 (Ang-1), which competes for the same receptor as Ang-2, is more broadly expressed. Along with platelet-derived growth factor (PDGF), Ang-1 initiates endothelium stabilization, which is necessary for proper vessel maturation and function.[14, 33, 49]
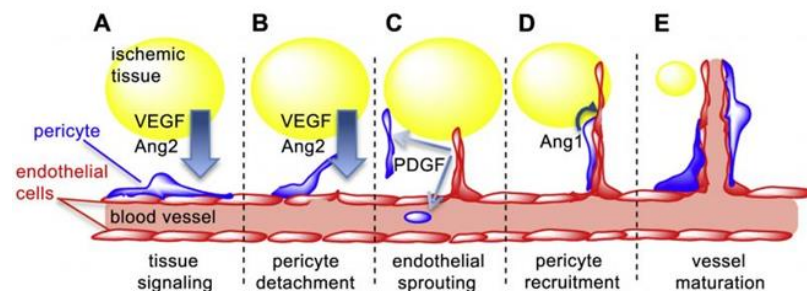
Figure 1.6: Schematic of the stages of angiogenesis and associated angiogenic factors and vascular cells [Reprinted with permission from Elsevier].[14]

Similar to other soft tissues, angiogenesis is an important process during tendon healing.[49] However, unlike other highly vascularized tissues, prolonged or excessive hypervascularization following tendon injury is not always believed to be beneficial, as healthy tendons are usually poorly vascularized and degenerated tendons are highly vascularized.[121] As with many vascular diseases, an imbalance of pro- and anti-angiogenic factors could promote abnormal angiogenesis, creating vessels with structural and

functional deficits, causing inflammation, inefficient nutrient exchange, and hypoxia despite increased vessel density.[49] Conversely, it is possible that the angiogenic response following tendon injury is not sufficient, and that increasing vascular formation could promote a more robust healing response.[139] Therefore, there is uncertainty regarding the role of vasculature in the progression of tendon healing and degeneration.[35]

Vascular ingrowth in tendons increases after rupture, reaching a maximum vessel density at 2 weeks[45], and then decreasing for weeks to months thereafter.[122] The degree of vascular response depends on the conditions of the tendon injury. Ruptures elicit a greater increase in vessel formation than degeneration alone. However, severe degeneration within a ruptured tendon causes a further increase in vessel formation than acute rupture only.[120] Additionally, smaller full thickness tears show a robust repair response, with increased cellularity, inflammation, and vascular density. However, these changes diminish as tear size increases, potentially reducing their overall healing capacity.[88]

The expression of angiogenic factors, particularly VEGF, has been evaluated in cases of tendon injury. While VEGF is expressed during tendon development, it is not expressed in healthy adult tendons except in cases of injury[106] or degeneration.[102] It is highly expressed locally at the site of injury, but less so in regions of the tendon distal to the injury.[11] The expression of VEGF precedes vascular ingrowth, with maximum expression seen at 7-10 days, and levels returning to normal 14 days after injury.[85] There are multiple factors throughout healing that influence the expression of VEGF. Tissue hypoxia due to vessel damage induces hypoxia-inducible factor 1 alpha (HIF-1α) expression, which upregulates VEGF expression and initiates angiogenesis.[85]

Inflammatory cytokines present in early stages of healing and mechanical stimulation after injury also upregulate VEGF expression.[32, 107] Finally, VEGF can stimulate MMP production and inhibit TIMP production, facilitating the ECM degradation required for invasion of new blood vessels.[10, 85, 107] Due to the increased MMP expression, it is possible that prolonged VEGF expression or vessel ingrowth could inhibit tissue remodeling and decrease tissue organization.

B-4. Vascular Modification

Angiogenesis is important for proper tissue repair. However, uncontrolled angiogenesis can promote hypervascular conditions such as what is observed in tumor growth, and inadequate angiogenesis can lead to ischemic conditions as seen in coronary artery disease. Pro- and anti-angiogenic therapies have been investigated as a means to correct these vascular conditions. Pro-angiogenic treatments involve cell based, genetic, or proteomic delivery of growth factors (mainly VEGF and basic fibroblast growth factor (bFGF)). Most anti-angiogenic drugs are direct VEGF antagonists (such as Bevacizumab), tyrosine kinase inhibitors (such as Sunitinib), or VEGF secretion blockades (such as Gefitinib).[83]

Pro-Angiogenic Treatments: Coronary artery disease, myocardial infarction, and ischemic injury diseases, are all caused by inadequate vasculature or angiogenic response to injury, creating ischemia and cell death in the tissue. These conditions can greatly benefit from pro-angiogenic therapies to help promote vessel growth to restore health and function.[100] There are three main methods for therapeutic angiogenesis: (1) protein

therapy, (2) gene therapy, and (3) cell therapy. Protein therapy is beneficial because it allows a finite temporal exposure with titratable dosing, easy administration, decreased risk of inflammatory response, and no exposure to exogenous genetic material. However, growth factors generally have a short half-life, so they need frequent administration at higher doses to be effective. On the contrary, gene and cell therapies allow for sustained production of factors for a prolonged exposure, but they introduce the risk of viral vectors, inflammation, and do not allow for precise modulation of expression.[3] In this work, we are most interested in protein delivery due to easy administration and precise dosage and timing of delivery.

The most commonly delivered proteins for induced angiogenesis are VEGF and bFGF. Multiple human trials delivering recombinant VEGF-165 protein to patients with coronary artery disease demonstrated improved myocardial perfusion and angina compared to no treatment.[50, 52, 53] Animal models of myocardial infarction and coronary artery disease demonstrated improved vascularization, cardiac function, and capillary density after the delivery of VEGF or bFGF.[9, 115, 128] Treatment of ischemic wound healing with VEGF-165 or bFGF injection improved granulation tissue formation and percent survival of ischemic tissue, and showed increased endothelial cells and higher vessel density.[23, 34, 75] These studies demonstrate the efficacy of delivering pro-angiogenic factors in cases of ischemic tissue disease.

<u>Anti-Angiogenic Treatments</u>: There are many diseases in which uncontrolled angiogenesis can lead to detrimental and debilitating conditions, such as cancer, diabetic nephropathy, arthritis, and retinopathy, among others.[100] Often in these conditions,

structural abnormalities in vessels lead to hypoxia or inflammation in the tissue, causing abnormally increased expression of angiogenic factors. This can further increase vessel density, causing ECM disruption and reduced function, increased pain, and in cases of cancer, tumor growth.[49] Multiple classes of drugs are used for anti-angiogenic therapies for cancer treatment. Direct VEGF inhibitors, such as bevacizumab, reduce tumor vascularity[86] and tumor size.[99] Tyrosine kinase inhibitors, such as sunitinib and sorafenib, decrease tumor vessel density, vessel size, and tumor growth.[26, 48, 87] Finally, other studies have evaluated Ang-1 and -2 specific inhibitors to alter vessel growth and normalization.[33]

Angiogenic Treatments in Musculoskeletal Tissues: While angiogenic treatments are more commonly evaluated in the vascular diseases discussed above, a few groups have begun to test these therapies in musculoskeletal conditions. Similar to ischemic disease treatments, pro-angiogenic factors VEGF and bFGF have been evaluated for tendon repair. VEGF injected at the site of a rat Achilles tendon repair improved mechanical properties during healing.[69, 139] While this implies that vascular changes during the course of healing were responsible for the improved healing outcome, these studies did not directly evaluate changes in vasculature, so the mechanism remains unknown. Conversely, some studies demonstrate improved vascular response that is not supported by improved mechanical outcome. For example, the administration of VEGF or bFGF in the knee after ACL repair increases vascularization of the graft.[65, 73, 137] However, these studies demonstrate either no change or inferior healing outcome, and one study did not evaluate mechanical properties. Additionally, the injection of bFGF in a patellar tendon defect increased cell proliferation and type III collagen deposition, but showed no change in mechanical parameters.[18] While

this work all demonstrates that translating pro-angiogenic therapies for tendon and ligament healing could be beneficial, they collectively fail to correlate vascular changes induced to healing outcomes, and therefore do not fully elucidate the role of vasculature in tendon healing.

Tendon degeneration is accompanied by a non-beneficial increase in vasculature that could contribute to the pathology of disease. Therefore, it is possible that reducing vascularity with anti-angiogenic therapy could be beneficial in some tendon injury conditions. In an acute injury caused by collagenase injection in rat patellar and Achilles tendons, treatment with intra-tendinous injection of bevacizumab was shown to reduce neovessels and improve collagen organization.[24] Tendinopathy in human patients treated by injection of a sclerosing agent that disrupts the vasculature showed decreased pain scores.[56, 57, 98] However, despite potentially positive outcomes, animal studies evaluating the mechanical response of anti-angiogenic treatments in tendon injury have yet to be evaluated. While it is generally hypothesized that increased vascularity during tendon healing is beneficial, it is unknown if prolonged hypervascularity is detrimental for healing outcome, similar to what is seen in cases of hypervascular tendon degeneration. Therefore, a comprehensive evaluation of both pro- and anti-angiogenic treatments after tendon injury is needed to fully understand the mechanism of vascularity in tendon healing.

B-5. Aging

Tendon Maintenance and Healing with Aging: Aging alters both the cell and the ECM, which subsequently impacts tissue mechanical properties. Tenocytes show

decreased cell growth, proliferation, differentiation potential, and self-renewal capabilities with aging.[72, 123] Additionally, they become less organized within the ECM[103] with increased cellular senescence.[62, 96, 123] Aging also causes increased lipid deposition, decreased expression of ECM proteins, and decreased vascularity.[74, 96] However, due to reduced collagen turnover capacity, there is increased type I collagen volume density.[62, 96] Further, MMP production increases, favoring tendon degradation over synthesis, and leading to overall decreased organization and strength of the tissue.[103, 111, 138] Changes in ECM properties in aged tendons cause significant decreases in failure load and modulus leaving older tendons weaker and more susceptible to rupture.[77, 103]

Vascularity and Aging: Aging not only has significant effects on tendon health and wound healing, but has also been shown to alter tissue vascularity. Human studies have mostly evaluated blood flow in tendons using ultrasound imaging. Intratendinous blood flow in the supraspinatus tendon and peritendinous blood flow around the Achilles tendon significantly decrease in elderly patients.[44, 79, 113] Additionally, cells harvested from ACL reconstruction in young patients have higher numbers of vascular endothelial cells (CD34+) with higher cell expansion and differentiation potential than cells from older age groups.[124] Finally, endostatin, an angiogenic inhibitor, is higher in adults than in younger patients.[105] This data suggests that aging tendons are subject to changes in vasculature that could alter their cellular responses and healing capacity. These alterations could contribute to the pathogenesis of conditions such as mucoid or lipoid degeneration as well as hypoxic or calcifying tendinopathy commonly seen in the aged population.[41, 66, 89, 96]

B-6. Ultrasound Imaging Methods

Ultrasound imaging is beneficial for the evaluation of both structural and functional characteristics of soft tissues. Importantly, it allows real time imaging, which can detect movement to evaluate properties such as blood flow within tissues. The following sections outline the main ultrasound imaging techniques relevant to this dissertation.

Brightness Mode Ultrasound: Ultrasound images are created by transmitting sound waves that propagate through a tissue and reflect off boundaries of impedance mismatches. These reflected sound waves are then detected by the same ultrasound transducer. Depending on the time it takes for the ultrasound wave to return, and how much of the wave was absorbed or scattered by the tissue, the ultrasound system can re-construct an image, called brightness mode (B-mode) imaging, depicting the location and absorption of the tissue boundaries.[22, 95] Ultrasound transducers operate at a range of frequencies, where the higher the frequency, the higher the resolution of the image, but the lower the depth penetration into the tissue. Clinical ultrasound is in the range of 2-15 MHz with a corresponding axial resolution 400-100μm, and high-frequency ultrasound, mostly used in animal research, is in the range of 15-55 MHz with an axial resolution of 75-30μm.[126]

In the clinic, B-mode ultrasound is primarily used for qualitatively evaluating tendon structure. A healthy Achilles tendon will look straight with hyperechoic striations created from aligned collagen fibers and fascicles (Figure 1.7A).[55] An injured Achilles will appear more hypoechoic, less striated, and is often thickened in the region of degeneration or injury (Figure 1.7B).[55] While these characteristics can clearly identify a tendon as being pathologic, a simple qualitative evaluation is not always helpful for

determining progression of degeneration or healing when evaluated longitudinally. A quantitative measure evaluating the collagen fiber organization, or striations in the image, could provide a useful tool for longitudinally evaluating tendon health. A number of studies have implemented methods for quantifying the structural changes identified in ultrasound images of pathological tendons. Specifically, mechanical property changes have been correlated to changes in ultrasound echogenicity,[17, 30] and tendinopathy has been identified through the analysis of the degree of speckle patterning using Fourier analyses.[8, 76] However, these methods do not quantify tendon collagen alignment specifically, which is known to directly relate to tendon mechanical properties.[29, 46, 78, 90, 91] Therefore, a method for the quantification of collagen alignment from B-mode ultrasound images could be used to monitor healing or progress during treatment and ultimately improve patient outcomes.
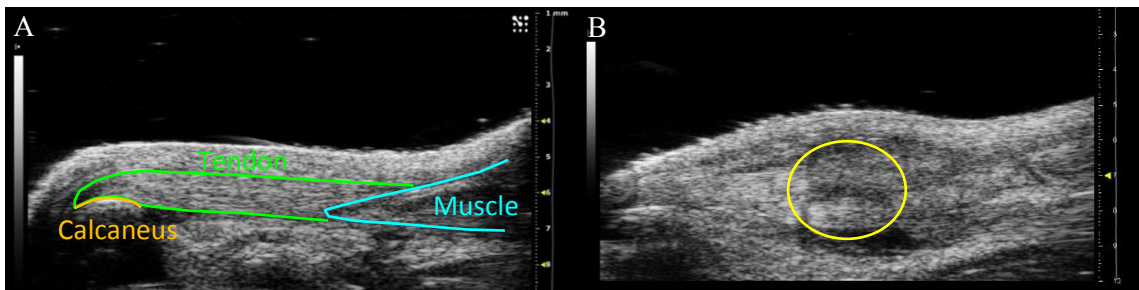
Figure 1.7: Sagittal rat Achilles tendon B-mode images depicting (A) normal and (B) injured tendon samples, with the hypoechoic, thickened injury region circled in yellow.

Color Doppler Ultrasound: Doppler ultrasound imaging utilizes a phenomenon called the "Doppler Effect" to detect movement within the tissue, specifically, blood cells moving within vessels. When a sound wave hits a stationary object, the reflected wave (f_R) is the same frequency as the initial wave frequency (f_0). However, when a sound wave hits

a moving object, the movement of the object either expands or compresses the wave (depending on the direction the object is moving), which changes the frequency of the reflected wave. The change in the frequency detected by the transducer can be used to determine the velocity (v) of the moving object (Figure 1.8A).[22, 95] The velocity measurements are displayed using a color scale and overlaid on the B-mode ultrasound image, where red and blue colors indicate blood flow towards and away from the probe, respectively (Figure 1.8B).

A

$$\Delta f = f_r - f_0 = \frac{2f_0 v}{c} \cos\theta$$
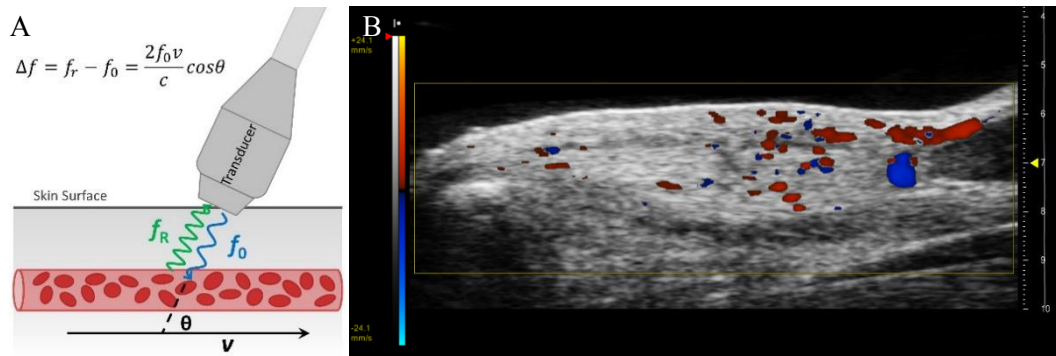
Figure 1.8: (A) Schematic of color Doppler ultrasound theory and associated equation to determine blood flow velocity. (B) Representative image of color Doppler ultrasound imaging of an injured rat Achilles tendon.

Doppler ultrasound is commonly used for the diagnosis of tendinopathy due to the increased vascular density observed in that condition. However, quantification of the Doppler signal is generally only used for basic science research.[116] Color Doppler ultrasound can be quantified to determine the mean color level (MCL - average velocity of colored pixels), the fractional area (FA - percent of colored pixels in region of interest), and the color weighted fractional area (CWFA - average flow per total unit area of the tissue) for a region of interest (ROI) in the ultrasound image.[116, 119] These metrics provide

information about both the velocity of the blood flow detected, as well as the amount of blood flow detected within the tissue. While this imaging modality is able to provide this specific quantifiable vascular data, it is only sensitive to larger vessels with faster blood flow velocities. It is not sensitive to capillary-sized vessels, which is why there is essentially no signal detected in uninjured tendons that only contain dispersed, small vessels. For that reason, color Doppler ultrasound can be paired with other imaging modalities, such as photoacoustic and contrast-enhanced ultrasound discussed in the next few sections, to provide additional information about the vascular properties of the tissue.

Photoacoustic Imaging: Photoacoustic imaging is a hybrid technology that uses both acoustic and optical imaging properties. Instead of the transducer sending out a sound wave like in traditional ultrasound, it sends an optical laser pulse into the tissue. Tissue components that exhibit absorption at the transmitted optical wavelength will undergo thermoelastic expansion and subsequent relaxation, inducing an acoustic wave that is then detected by the ultrasound transducer. The photoacoustic system can generate a range of optical wavelengths to provide physiological information, such as blood oxygen saturation, due to the different absorption spectrums of oxygenated (750nm) and deoxygenated (850nm) hemoglobin (Figure 1.9).[13, 70, 94]
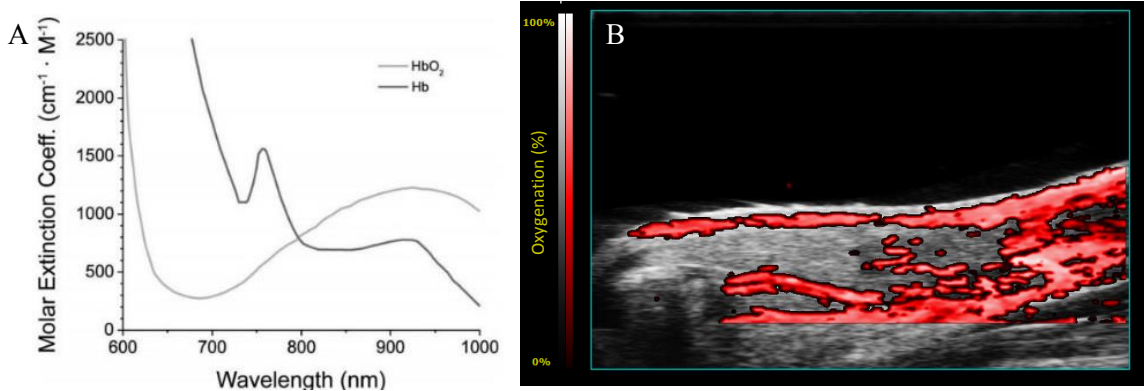
Figure 1.9: (A) Optical absorption spectra of oxygenated (HbO$_2$) and deoxygenated hemoglobin (Hb).[94] (B) Representative image of photoacoustic imaging of a rat Achilles tendon.

Photoacoustics has been implemented in research areas of microcirculation,[60] tumor characterization,[12, 136] brain perfusion,[47] and in the development of endogenous and exogenous photoacoustic contrast agents.[54, 64, 94, 140] Only a few studies have used photoacoustics in the context of musculoskeletal research. These studies aimed to identify arthritis in the ankle and knee joints of rats,[108, 109] and evaluate microvascular changes in mouse Achilles tendons after collagenase-induced tendinopathy.[130] However, these musculoskeletal studies use a laser wavelength specific to the absorption of red components (532nm), which would detect primarily blood, but does not detect differences in hemoglobin oxygenation specifically and therefore cannot obtain blood oxygenation levels. Therefore, no current studies have used photoacoustics for the quantification of tissue oxygenation in tendons or ligaments.

Non-Linear Contrast-Enhanced Ultrasound: Ultrasound is a mechanical wave and therefore requires a medium to travel through. Because of this, ultrasound travels very poorly through air, making microbubbles an ideal medium for a contrast agent due to the

high reflectance of sound against the air bubbles.[36] Microbubbles are small gas-filled and self-assembling microspheres that have distinct acoustic properties. Advancements in microsphere technology, such as the incorporation of a thin shell and heavy molecular-weight gas, have improved stability and survival under high pressures experienced in circulation throughout the body. Low acoustic pressures cause linear oscillations of microbubbles, where the frequency of the transmitted and reflected acoustic waves are equal. However, higher acoustic pressures induce a non-linear expansion and compression of the microbubbles, causing the emission of non-linear harmonic acoustic waves (Figure 1.10A). Specific pulse sequences can be developed to cancel out the linear signal response, and detect only non-linear frequencies. This will maximize detection efficiency for signals arising from the microbubble contrast agent, and suppress signal from the surrounding tissue.[27, 93]
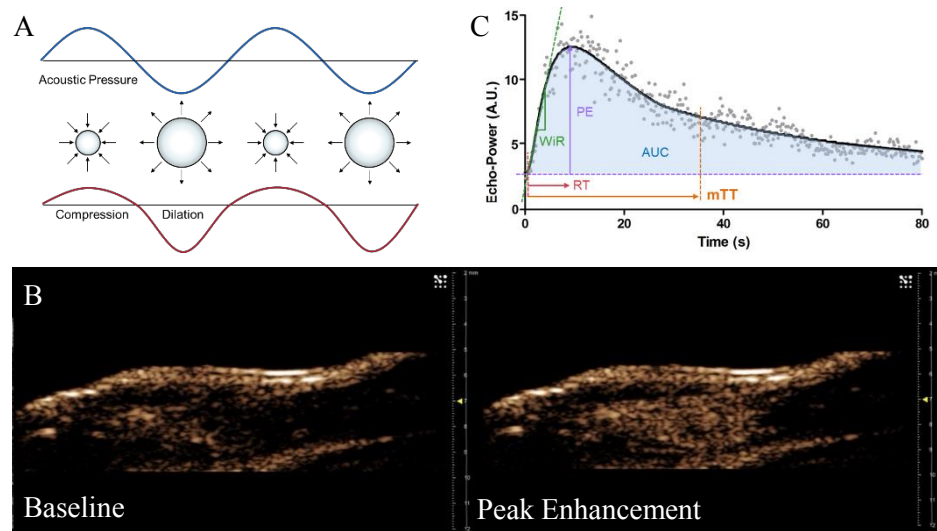
Figure 1.10: (A) Schematic of non-linear oscillations of microbubbles under acoustic pressure. (B) Representative images of baseline and peak contrast signal in a rat Achilles tendon. (C) Schematic of echo-power vs. time curve and associated parameters for the contrast analysis.

Contrast-enhanced ultrasound has been widely used in echocardiography[5, 92] and oncology,[40, 81, 133] among other fields. Most commonly, the single frame exhibiting peak enhancement is quantified as a measure of tissue perfusion. However, with the delivery of a bolus injection of contrast, an echo-intensity vs. time curve can be created, and both time and amplitude based parameters can be calculated to provide more comprehensive evaluation of the flow of contrast through the tissue (Figure 1.10B-C).[93]

C. SIGNIFICANCE OF STUDIES

C-1. Novel Ultrasound Imaging in a Rat Achilles Tendon

Ultrasound imaging has been used in medicine for over 70 years,[16] and advancements in ultrasound technologies continue to improve the resolution and utility of ultrasound for many different medical applications. In current clinical practice, both B-mode and Doppler ultrasound imaging are routinely used to evaluate soft tissue injuries, including tendon ruptures. However, these scanners are operating at low frequencies, between 2-15 MHz, which do not have the resolution to evaluate finer collagen structure or to evaluate smaller vessels with low flow velocities. While high frequency ultrasound imaging has been widely used in animal research, very little tendon-specific research has utilized this technology. In this dissertation, I investigated the use of these high frequency (40-55HMz) ultrasound imaging techniques in mouse and rat Achilles tendons for both B-mode and Doppler imaging analyses. Additionally, only a couple groups have used photoacoustic imaging for evaluating vascularity in musculoskeletal applications, none of which evaluate hemoglobin oxygenation. [108, 131] In this work, I have evaluated tissue and

blood oxygenation changes, which indicate the functionality and efficiency of the vessels. Furthermore, I used contrast-enhanced ultrasound to detect more subtle changes in vascular perfusion not captured with Doppler or photoacoustic imaging. Therefore, this work is the first to comprehensively evaluate multiple *in vivo* ultrasound imaging modalities along with *ex vivo* tissue properties, to correlate these imaging parameters to healing properties in tendon tissue.

C-2. Vascular Modulation Techniques Translated to Tendon Model

Modulation of vascularity has primarily been performed either to induce angiogenesis in ischemic disease, such as after a myocaridial infarction, or to inhibit angiogenesis, such as in tumor growth. There have only been a few studies that have evaluated vascular modulation using VEGF in tendons,[69, 139] and only one study that evaluated the delivery of anti-angiogenic factors in tendons.[24] However, none of these evaluated both the vascular response to the treatment as well as the mechanical outcome. Additionally, vascular modulation studies generally administer the factor immediately after injury, and do not evaluate the effect of delayed administration during different phases of healing and angiogenesis. In this dissertation, I have evaluated the administration of both pro- and anti-angiogenic factors at two different delivery schedules, as well as *in vivo* vascular changes, *in vivo* functional response, and *ex vivo* histological and mechanical tissue properties. Both increasing and decreasing vascularity, as well as comprehensively evaluating the tendon response to the vascular modulation, can provide the necessary insight into the role of vascularity in tendon healing.

C-3. Evaluation of Vascularity in an Aging Model

Distinct vascular changes occur in uninjured tendons due to aging.[44, 79, 89, 105, 124] There is also evidence of impaired cellular response and reduced healing outcome in aged tissues after injury.[74, 104, 138] However, there is little to no research evaluating how aging effects the vascular response to injury in tendon, and how that might affect healing outcomes. By modulating the vascular response during healing throughout aging, we evaluated how vascularity impacts the ability for the aged population to recover after injury, and if there is an angiogenic therapy that could be administered to improve healing outcome.

D. SPECIFIC AIMS

Tendons are hypovascular tissues, undergoing angiogenesis only during development, wound healing, and pathogenesis.[121] Injured tendons undergo a healing response with vascular ingrowth during the proliferative phase and vascular regression during remodeling. However, the remodeled tendon often does not regain its natural structural, compositional, or mechanical properties, leading to reduced function or increased incidence of re-rupture.[39, 110] Modulating the vascular response during healing could ultimately improve the tendon healing outcome.

Angiogenesis is a process highly regulated by a multitude of both pro- and anti-angiogenic factors. Many research fields have investigated the delivery of pro- and anti-angiogenic factors as a therapy for vascular diseases.[26, 33, 50, 53, 86, 115, 128] However, there has been little research evaluating the effect of modulating vascularity in the context of

tendon healing.[18, 69, 139] Increased vascularity could allow for more efficient exchange of nutrients, growth factors, and cytokines to improve tendon healing. However, prolonged durations of heightened vascularity could inhibit proper tissue structure remodeling or increase pain.[121] The optimal vascularization level and timing for tendon healing is currently unknown. Additionally, due to variations in both vascular function and healing potential with age, it is also unknown how the vascular response to injury changes over the course of aging. Finally, new ultrasound technologies provide higher sensitivity measures and more structural and functional information than traditional clinical ultrasounds currently used to evaluate tendon conditions.[13, 19, 70, 134] These technologies could provide useful tools for evaluating the progression and outcome of tendon healing, specifically by determining the *in vivo* vascular response during healing. **Therefore, the objective of this study is to develop methods for, and evaluate the effect of, vascular modulation in adult and aged rat Achilles tendons during healing using both *in vivo* ultrasound imaging measures of structure and vascularity and *ex vivo* measures of tendon compositional and mechanical properties.**

Specific Aim 1: Validate the use of *in vivo* high-frequency ultrasound technologies to measure structural and vascular changes in Achilles tendons.

> **Hypothesis 1a:** Quantification of collagen alignment from B-mode ultrasound images will detect changes across treatment groups and reflect differences seen in mechanical outcome.

> **Hypothesis 1b:** Color Doppler, photoacoustics, and contrast-enhanced ultrasound

will all detect changes between treatment groups due to alterations in vascular density and structure. While Doppler and photoacoustics will show the most changes at early time points, contrast-enhanced ultrasound will detect changes in perfusion with more sensitivity, and therefore detect changes at later time points as well.

Hypothesis 1c: Vascular ultrasound changes will support histological measures of vascularity, and will be able to predict stages in the angiogenic and healing processes.

Specific Aim 2: Develop methodologies for vascular modulation in an Achilles tendon injury model using the delivery of pro- and anti-angiogenic factors.

Hypothesis 2a: The delivery of pro-angiogenic factors will cause an increase in vasculature as measured by both histological and ultrasonic measures. Delivery after the initial inflammatory phase will produce the greatest increase in vasculature, resulting in improved failure properties and increased cross-sectional area of the healing tendon.

Hypothesis 2b: The delivery of anti-angiogenic factors will cause a decrease in vasculature as measured by both histological and ultrasonic measures. This will result in more organized collagen fibers, but reduced failure properties and cross-sectional area.

Specific Aim 3: Apply methods of vascular modulation and ultrasound imaging to determine the role of angiogenesis during healing in adult and aged Achilles tendon models.

Hypothesis 3a: Pro-angiogenic treatment will improve tendon mechanical healing outcomes in aged animals to a greater extent than in adult animals.

Hypothesis 3b: Anti-angiogenic treatment at early time points will cause a decrease in healing outcomes in all age groups with adult animals showing the largest change.

This study will validate new *in vivo* methods for evaluating vascularity in a tendon injury model, develop potential angiogenic therapies for improved healing outcome, and elucidate the differences in vascular response across age groups after tendon injury and vascular modulation.

E. STUDY DESIGN

E-1. Overview

In this dissertation, vascular response was evaluated in situations of induced or inhibited angiogenesis throughout healing in adult and aged rats. Following the development of appropriate dosage to induce the intended angiogenic changes, an Achilles incisional injury was created followed by the administration of a pro-angiogenic factor, an anti-angiogenic drug, or saline control. Treatment delivery occurred either immediately after injury or delayed 4 days following injury, each for 3 consecutive days. Multiple advanced ultrasound imaging techniques were validated to evaluate *in vivo* measures of tendon structure (collagen organization and echogenicity) as well as *in vivo* measures of vascular parameters (e.g. blood flow velocity, tissue perfusion, and blood oxygenation)

(Aim 1). These ultrasound imaging parameters of vascularity and structure were compared to *ex vivo* measures of vasculature using immunohistochemistry, as well as healing parameters including mechanical and compositional properties, to determine effect of modulated angiogenesis on healing (Aim 2). Finally, using the optimal timing of factor delivery determined in the first two aims, the effect of modulated vascularity on healing in aged animals was evaluated (Aim 3).

E-2. Animal Model Justification

In order to validate the use of ultrasound imaging for quantification of collagen alignment, a mouse Achilles tendon model was used. This model was selected because the small size of a mouse tendon enabled simultaneous imaging with our cross-polarizer system, which was our standard for comparing against our novel high-frequency ultrasound analysis algorithm. Additionally, the Achilles tendon's straight and superficial anatomical position made this system an ideal first step toward direct translation to future *in vivo* studies. An *ex vivo* environment was necessary for this study so that the cross-polarizer system could be used, and also so that the exact loading conditions, and therefore the collagen alignment, could be precisely controlled.

For the evaluation of tendon vascularity and healing, the rat Achilles tendon incisional injury model was used. This tendon model is ideal for the proposed study due to its clinical relevance, optimal size, and superficial anatomy. Clinically, vascular abnormalities are found within the Achilles tendon that are related to tendon pathology. For example, the midsubstance region of the Achilles tendon is hypovascular, which is

believed to be a contributing factor to spontaneous rupture.[63] In opposition, Achilles tendinopathy demonstrates hypervascularity accompanying hypertrophy and disorganization.[135] Additionally, there is a significant patient population with partial midsubstance Achilles tendon ruptures who heal without surgical repair, similar to our model injury.[21] While our acute, full-thickness partial-width rupture injury model does not fully replicate the clinical situation, it allows for a more stable and consistent injury without the complications of a full-thickness rupture, such as the need to immobilize the limb (which could alter blood flow) or use suture for the repair (creating artifact in ultrasound images). The rat Achilles tendon anatomy is ideally sized for using high frequency ultrasound to allow for sufficient penetration while maintaining high resolution images. The Achilles in particular is superficial and parallel to the skin surface, making imaging simpler and quantitative measures more consistent. Additionally, the Achilles is one of the largest tendons in the body, allowing for intratendinous injections without causing significant damage to the tendon tissue due to the needle puncture. Therefore, a partial rupture of the rat Achilles tendon is the ideal model to answer the questions posed in this study.

E-3. Animal Use and Study Design

To validate the quantification of collagen alignment using B-mode ultrasound imaging (Chapter 2), 18 Achilles tendons were harvested from C57BL/6 mice. Tendons were tested in two experimental situations known to cause changes in tendon collagen alignment: (1) incremental increase in load (n=11) and (2) induction of an excisional injury

(n=7) (Figure 1.11). All analysis of cross-polarizer and ultrasound measures were performed paired so that each tendon specimen could be compared against itself across changes in alignment and between imaging modalities.
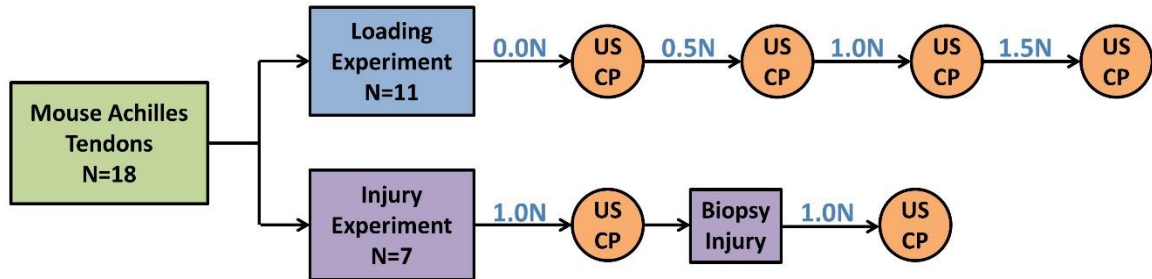
Figure 1.11: Study design for the validation of using B-mode ultrasound imaging for the quantification of changes in tendon collagen alignment. US and CP represent simultaneous ultrasound and cross-polarizer imaging after each loading or injury condition.

To develop methodologies for modulating vascular response after injury (Chapter 3), a total of 56 Sprague Dawley rats (4-6 months old) were used and divided into two pilot studies: (1) the evaluation of VEGF injection and (2) the evaluation of anti-VEGF antibody (B20.4-1-1, Genentech) injection after tendon injury. For the first study, 24 rats underwent unilateral Achilles tendon incisional injury, followed by bilateral injections intratendinously with 5µg VEGF at either 0-2 days (early) or 4-6 days (late) post-injury. Color Doppler ultrasound imaging was performed on both injured and uninjured tendons on days 7, 10, and 14 after injury, and animals were sacrificed at either day 7 or 14 for histological evaluation (n=4 tendons/group) (Figure 1.12). For the second study, 32 rats underwent bilateral Achilles tendon incisional injury followed by bilateral intratendinous injection with either 50, 250, or 500 µg anti-VEGF antibody (B20) on days 4-6 post-injury. Color Doppler and Photoacoustic imaging was performed on days 7 and 14 after injury, and animals were sacrificed at either day 7 or 14 for histological analysis (n=8

tendons/group) (Figure 1.13). These two studies validated the methods for vascular

modulation and *in vivo* evaluation that will be used in the primary studies discussed in

Chapters 4 and 5.

Day														
0	1	2	3	4	5	6	7	8	9	10	11	12	13	14

Figure 1.12: Study Design for the evaluation of VEGF delivery on vascular response after injury. "US" represents ultrasound imaging time points and "O" represents sacrifice for histological evaluation.

Day														
0	1	2	3	4	5	6	7	8	9	10	11	12	13	14

Figure 1.13: Study Design for the evaluation of ant-VEGF antibody (B20) delivery on vascular response after injury. "US" represents ultrasound imaging time points and "O" represents sacrifice for histological evaluation.

To evaluate the effect of vascular modulation on Achilles tendon healing in adult

animals (Chapter 4), a total of 180 Fisher (F-344) rats (4 months) were used, divided into

6 groups. These animals were first divided into (1) early and (2) late delivery of treatment,

and then further divided into three treatments: (1) VEGF, (2) B20, and (3) Saline injections.

All animals underwent bilateral Achilles tendon incisional injuries, and were sacrificed at

7, 14, or 28 days post-injury. One limb was used for mechanical analysis (n = 12, days 14 and 28) and one limb for histological (n = 6, days 7, 14, and 28) analysis. The remaining 6 limbs were harvested and stored for future biological analysis (n=6, days 7, 14, and 28). Ultrasound analysis (U) was performed on days 3 (early only), 7, 14, 21, and 28 on the animals sacrificed at 28 days. Functional measures (F) were performed on days 3 (early only), 7, 10, and 14 on the animals sacrificed at 14 days (Figure 1.14).

				Week				
Group				**0**	**1**	**2**	**3**	**4**
Adult	Early	Surgery	B20		O			
				F	F F F X			
				U	U U	U	U X	
			SAL		O			
				F	F F F X			
				U	U U	U	U X	
			VEGF		O			
				F	F F F X			
				U	U U	U	U X	
	Late	Surgery	B20		O			
				F	F F X			
				U	U	U	U X	
			SAL		O			
				F	F F X			
				U	U	U	U X	
			VEGF		O			
				F	F F X			
				U	U	U	U X	

Figure 1.14: Study Design for the effect of vascular modulation on tendon healing in adult animals. "F" represents functional joint and ambulation measures, "U" represents ultrasound imaging, "O" represents sacrifice for histological and biological assays only, and "X" represents sacrifice for mechanical, histological, and biological assays.

To assess the use of aged animals as a model for impaired vascular response (Chapter 5), 5 adult (4-5 months) and 5 aged (14-16 months) Sprague Dawley rats were used. All animals underwent a bilateral Achilles tendon incisional injury followed by

ultrasound imaging on day 7 post-injury and sacrifice at day 7 for histological evaluation

(8-9 tendons/group) (Figure 1.15).

Day	0	1	2	3	4	5	6	7
Adult	Surgery							U O
Aged	Surgery							U O

Figure 1.15: Study Design to evaluate the effect of age on vascular response after injury. "U" represents ultrasound imaging, and "O" represents sacrifice for histological evaluation.

To evaluate the effect of vascular modulation on Achilles tendon healing in aged

animals, a total of 36 Fisher (F-344) rats (19 months) were used, divided into 3 treatment

groups: (1) VEGF, (2) B20, and (3) Saline injections. Only the delivery schedule and time

point that provided the largest change in the adult rats was used in the evaluation of this

age group. All animals underwent bilateral Achilles tendon incisional injuries and were

sacrificed at 14 days post-injury. One limb was used for mechanical analysis (n = 12, day

14) and one limb for histological analysis (n = 6, day 14). The remaining 6 limbs were

harvested and stored for future biological analysis. Ultrasound analysis (U) was performed

on days 7 and 14 post-injury (Figure 1.16).

Week	0		1		2
Aged	Surgery	B20	U	U	X
		SAL	U	U	X
		VEGF	U	U	X

Figure 1.16: Study Design for the effect of vascular modulation on tendon healing in aged animals. "U" represents ultrasound imaging and "X" represents sacrifice for mechanical, histological, and biological assays.

F. CHAPTER OVERVIEW

Chapter 2 will describe the development and validation of the method for using B-mode ultrasound imaging to quantify tendon collagen organization. Chapter 3 will describe the validation of our angiogenic treatments through ultrasound and histological evaluation of timing and dosage. Chapter 4 will describe the effects of vascular modulation on tendon healing in an adult model, and Chapter 5 will describe the effects of vascular modulation on tendon healing in an aged model. Finally, Chapter 6 will summarize the conclusions of the previous chapters and provide future directions for this area of research.

G. REFERENCES

1.   Ackerman J.E., Bah I., Jonason J.H., Buckley M.R. and Loiselle A.E. Aging does not alter tendon mechanical properties during homeostasis, but does impair flexor tendon healing. *J Orthop Res* 2017.

2.   Ahmadzadeh H., Connizzo B.K., Freedman B.R., Soslowsky L.J. and Shenoy V.B. Determining the contribution of glycosaminoglycans to tendon mechanical properties with a modified shear-lag model. *J Biomech* 2013; 46(14): 2497-2503.

3.   Al Sabti H. Therapeutic angiogenesis in cardiovascular disease. *J Cardiothorac Surg* 2007; 2: 49.

4.   Apaydin N., Bozkurt M., Loukas M., Vefali H., Tubbs R.S. and Esmer A.F. Relationships of the sural nerve with the calcaneal tendon: An anatomical study with surgical and clinical implications. *Surg Radiol Anat* 2009; 31(10): 775-780.

5.   Appis A.W., Tracy M.J. and Feinstein S.B. Update on the safety and efficacy of commercial ultrasound contrast agents in cardiac applications. *Echo Res Pract* 2015; 2(2): R55-62.

6.   Barfod K.W. Achilles tendon rupture; assessment of nonoperative treatment. *Dan Med J* 2014; 61(4): B4837.

7.   Barfred T. Achilles tendon rupture. Aetiology and pathogenesis of subcutaneous rupture assessed on the basis of the literature and rupture experiments on rats. *Acta Orthop Scand Suppl* 1973: 3-126.

8. Bashford G.R., Tomsen N., Arya S., Burnfield J.M. and Kulig K. Tendinopathy discrimination by use of spatial frequency parameters in ultrasound b-mode images. *IEEE Trans Med Imaging* 2008; 27(5)**:** 608-615.

9. Battler A., Scheinowitz M., Bor A., Hasdai D., Vered Z., Di Segni E., Varda-Bloom N., Nass D., Engelberg S., Eldar M. and et al. Intracoronary injection of basic fibroblast growth factor enhances angiogenesis in infarcted swine myocardium. *J Am Coll Cardiol* 1993; 22(7)**:** 2001-2006.

10. Berglund M.E., Hart D.A., Reno C. and Wiig M. Growth factor and protease expression during different phases of healing after rabbit deep flexor tendon repair. *J Orthop Res* 2011; 29(6)**:** 886-892.

11. Bidder M., Towler D.A., Gelberman R.H. and Boyer M.I. Expression of mrna for vascular endothelial growth factor at the repair site of healing canine flexor tendon. *J Orthop Res* 2000; 18(2)**:** 247-252.

12. Bohndiek S.E., Sasportas L.S., Machtaler S., Jokerst J.V., Hori S. and Gambhir S.S. Photoacoustic tomography detects early vessel regression and normalization during ovarian tumor response to the antiangiogenic therapy trebananib. *J Nucl Med* 2015; 56(12)**:** 1942-1947.

13. Bouchard R., Sahin O. and Emelianov S. Ultrasound-guided photoacoustic imaging: Current state and future development. *IEEE Trans Ultrason Ferroelectr Freq Control* 2014; 61(3)**:** 450-466.

14. Brudno Y., Ennett-Shepard A.B., Chen R.R., Aizenberg M. and Mooney D.J. Enhancing microvascular formation and vessel maturation through temporal control over multiple pro-angiogenic and pro-maturation factors. *Biomaterials* 2013; 34(36)**:** 9201-9209.

15. Buckwalter J.A. and Hunziker E.B. Orthopaedics. Healing of bones, cartilages, tendons, and ligaments: A new era. *Lancet* 1996; 348 Suppl 2**:** sII18.

16. Campbell S. A short history of sonography in obstetrics and gynaecology. *Facts Views Vis Obgyn* 2013; 5(3)**:** 213-229.

17. Chamberlain C.S., Duenwald-Kuehl S.E., Okotie G., Brounts S.H., Baer G.S. and Vanderby R. Temporal healing in rat achilles tendon: Ultrasound correlations. *Ann Biomed Eng* 2013; 41(3)**:** 477-487.

18. Chan B.P., Fu S., Qin L., Lee K., Rolf C.G. and Chan K. Effects of basic fibroblast growth factor (bfgf) on early stages of tendon healing: A rat patellar tendon model. *Acta Orthop Scand* 2000; 71(5)**:** 513-518.

19. Chang K.V., Lew H.L., Wang T.G. and Chen W.S. Use of contrast-enhanced ultrasonography in musculoskeletal medicine. *Am J Phys Med Rehabil* 2012; 91(5)**:** 449-457.

20.	Chen T.M., Rozen W.M., Pan W.R., Ashton M.W., Richardson M.D. and Taylor G.I. The arterial anatomy of the achilles tendon: Anatomical study and clinical implications. *Clin Anat* 2009; 22(3)**:** 377-385.

21.	Chiodo C.P., Glazebrook M., Bluman E.M., Cohen B.E., Femino J.E., Giza E., Watters W.C., 3rd, Goldberg M.J., Keith M., Haralson R.H., 3rd, Turkelson C.M., Wies J.L., Raymond L., Anderson S., Boyer K. and Sluka P. Diagnosis and treatment of acute achilles tendon rupture. *J Am Acad Orthop Surg* 2010; 18(8)**:** 503-510.

22.	Coltrera M.D. Ultrasound physics in a nutshell. *Otolaryngol Clin North Am* 2010; 43(6)**:** 1149-1159, v.

23.	Corral C.J., Siddiqui A., Wu L., Farrell C.L., Lyons D. and Mustoe T.A. Vascular endothelial growth factor is more important than basic fibroblastic growth factor during ischemic wound healing. *Arch Surg* 1999; 134(2)**:** 200-205.

24.	Dallaudiere B., Lempicki M., Pesquer L., Louedec L., Preux P.M., Meyer P., Hess A., Durieux M.H., Hummel V., Larbi A., Deschamps L., Benayoun Y., Journe C., Perozziello A., Schouman-Claeys E., Michel J.B. and Serfaty J.M. Acceleration of tendon healing using us guided intratendinous injection of bevacizumab: First pre-clinical study on a murine model. *Eur J Radiol* 2013; 82(12)**:** e823-828.

25.	DeFranco M.J., Derwin K. and Iannotti J.P. New therapies in tendon reconstruction. *J Am Acad Orthop Surg* 2004; 12(5)**:** 298-304.

26.	Denorme M., Yon L., Roux C., Gonzalez B.J., Baudin E., Anouar Y. and Dubessy C. Both sunitinib and sorafenib are effective treatments for pheochromocytoma in a xenograft model. *Cancer Lett* 2014; 352(2)**:** 236-244.

27.	Dijkmans P.A., Juffermans L.J., Musters R.J., van Wamel A., ten Cate F.J., van Gilst W., Visser C.A., de Jong N. and Kamp O. Microbubbles and ultrasound: From diagnosis to therapy. *Eur J Echocardiogr* 2004; 5(4)**:** 245-256.

28.	Doral M.N., Alam M., Bozkurt M., Turhan E., Atay O.A., Donmez G. and Maffulli N. Functional anatomy of the achilles tendon. *Knee Surg Sports Traumatol Arthrosc* 2010; 18(5)**:** 638-643.

29.	Dourte L.M., Perry S.M., Getz C.L. and Soslowsky L.J. Tendon properties remain altered in a chronic rat rotator cuff model. *Clin Orthop Relat Res* 2010; 468(6)**:** 1485-1492.

30.	Duenwald-Kuehl S., Lakes R. and Vanderby R., Jr. Strain-induced damage reduces echo intensity changes in tendon during loading. *J Biomech* 2012; 45(9)**:** 1607-1611.

31.	Egger A.C. and Berkowitz M.J. Achilles tendon injuries. *Curr Rev Musculoskelet Med* 2017; 10(1)**:** 72-80.

32. Eliasson P., Andersson T. and Aspenberg P. Influence of a single loading episode on gene expression in healing rat achilles tendons. *J Appl Physiol (1985)* 2012; 112(2)**:** 279-288.

33. Falcon B.L., Hashizume H., Koumoutsakos P., Chou J., Bready J.V., Coxon A., Oliner J.D. and McDonald D.M. Contrasting actions of selective inhibitors of angiopoietin-1 and angiopoietin-2 on the normalization of tumor blood vessels. *Am J Pathol* 2009; 175(5)**:** 2159-2170.

34. Fayazzadeh E., Ahmadi S.H., Rabbani S., Boroumand M.A., Salavati A. and Anvari M.S. A comparative study of recombinant human basic fibroblast growth factor (bfgf) and erythropoietin (epo) in prevention of skin flap ischemic necrosis in rats. *Arch Iran Med* 2012; 15(9)**:** 553-556.

35. Fenwick S.A., Hazleman B.L. and Riley G.P. The vasculature and its role in the damaged and healing tendon. *Arthritis Res* 2002; 4(4)**:** 252-260.

36. Ferrara K., Pollard R. and Borden M. Ultrasound microbubble contrast agents: Fundamentals and application to gene and drug delivery. *Annu Rev Biomed Eng* 2007; 9**:** 415-447.

37. Franchi M., Fini M., Quaranta M., De Pasquale V., Raspanti M., Giavaresi G., Ottani V. and Ruggeri A. Crimp morphology in relaxed and stretched rat achilles tendon. *J Anat* 2007; 210(1)**:** 1-7.

38. Freedman B.R., Bade N.D., Riggin C.N., Zhang S., Haines P.G., Ong K.L. and Janmey P.A. The (dys)functional extracellular matrix. *Biochim Biophys Acta* 2015; 1853(11 Pt B)**:** 3153-3164.

39. Freedman B.R., Gordon J.A. and Soslowsky L.J. The achilles tendon: Fundamental properties and mechanisms governing healing. *Muscles Ligaments Tendons J* 2014; 4(2)**:** 245-255.

40. Frohlich E., Muller R., Cui X.W., Schreiber-Dietrich D. and Dietrich C.F. Dynamic contrast-enhanced ultrasound for quantification of tissue perfusion. *J Ultrasound Med* 2015; 34(2)**:** 179-196.

41. Fu S.C., Rolf C., Cheuk Y.C., Lui P.P. and Chan K.M. Deciphering the pathogenesis of tendinopathy: A three-stages process. *Sports Med Arthrosc Rehabil Ther Technol* 2010; 2**:** 30.

42. Fukashiro S., Komi P.V., Jarvinen M. and Miyashita M. In vivo achilles tendon loading during jumping in humans. *Eur J Appl Physiol Occup Physiol* 1995; 71(5)**:** 453-458.

43. Fukuta S., Oyama M., Kavalkovich K., Fu F.H. and Niyibizi C. Identification of types ii, ix and x collagens at the insertion site of the bovine achilles tendon. *Matrix Biol* 1998; 17(1)**:** 65-73.

44. Funakoshi T., Iwasaki N., Kamishima T., Nishida M., Ito Y., Kondo M. and Minami A. In vivo visualization of vascular patterns of rotator cuff tears using contrast-enhanced ultrasound. *Am J Sports Med* 2010; 38(12)**:** 2464-2471.

45. Gelberman R.H., Khabie V. and Cahill C.J. The revascularization of healing flexor tendons in the digital sheath. A vascular injection study in dogs. *J Bone Joint Surg Am* 1991; 73(6)**:** 868-881.

46. Gimbel J.A., Van Kleunen J.P., Mehta S., Perry S.M., Williams G.R. and Soslowsky L.J. Supraspinatus tendon organizational and mechanical properties in a chronic rotator cuff tear animal model. *J Biomech* 2004; 37(5)**:** 739-749.

47. Giustetto P., Filippi M., Castano M. and Terreno E. Non-invasive parenchymal, vascular and metabolic high-frequency ultrasound and photoacoustic rat deep brain imaging. *J Vis Exp* 2015; (97).

48. Grenier N., Douws C., Perot V., Ferriere J.M. and Ravaud A. Combined radiofrequency ablation and antiangiogenic drug for the treatment of recurrent renal tumor. *Urology* 2009; 73(4)**:** 928 e911-922.

49. Hall K. and Ran S. Regulation of tumor angiogenesis by the local environment. *Front Biosci (Landmark Ed)* 2010; 15**:** 195-212.

50. Hendel R.C., Henry T.D., Rocha-Singh K., Isner J.M., Kereiakes D.J., Giordano F.J., Simons M. and Bonow R.O. Effect of intracoronary recombinant human vascular endothelial growth factor on myocardial perfusion: Evidence for a dose-dependent effect. *Circulation* 2000; 101(2)**:** 118-121.

51. Henninger H.B., Underwood C.J., Romney S.J., Davis G.L. and Weiss J.A. Effect of elastin digestion on the quasi-static tensile response of medial collateral ligament. *J Orthop Res* 2013; 31(8)**:** 1226-1233.

52. Henry T.D., Annex B.H., McKendall G.R., Azrin M.A., Lopez J.J., Giordano F.J., Shah P.K., Willerson J.T., Benza R.L., Berman D.S., Gibson C.M., Bajamonde A., Rundle A.C., Fine J. and McCluskey E.R. The viva trial: Vascular endothelial growth factor in ischemia for vascular angiogenesis. *Circulation* 2003; 107(10)**:** 1359-1365.

53. Henry T.D., Rocha-Singh K., Isner J.M., Kereiakes D.J., Giordano F.J., Simons M., Losordo D.W., Hendel R.C., Bonow R.O., Eppler S.M., Zioncheck T.F., Holmgren E.B. and McCluskey E.R. Intracoronary administration of recombinant human vascular endothelial growth factor to patients with coronary artery disease. *Am Heart J* 2001; 142(5)**:** 872-880.

54. Ho C.J., Balasundaram G., Driessen W., McLaren R., Wong C.L., Dinish U.S., Attia A.B., Ntziachristos V. and Olivo M. Multifunctional photosensitizer-based contrast agents for photoacoustic imaging. *Sci Rep* 2014; 4**:** 5342.

55.   Hodgson R.J., O'Connor P.J. and Grainger A.J. Tendon and ligament imaging. *Br J Radiol* 2012; 85(1016)**:** 1157-1172.

56.   Hoksrud A., Ohberg L., Alfredson H. and Bahr R. Ultrasound-guided sclerosis of neovessels in painful chronic patellar tendinopathy: A randomized controlled trial. *Am J Sports Med* 2006; 34(11)**:** 1738-1746.

57.   Hoksrud A., Torgalsen T., Harstad H., Haugen S., Andersen T.E., Risberg M.A. and Bahr R. Ultrasound-guided sclerosis of neovessels in patellar tendinopathy: A prospective study of 101 patients. *Am J Sports Med* 2012; 40(3)**:** 542-547.

58.   Hootman J.M., Macera C.A., Ainsworth B.E., Martin M., Addy C.L. and Blair S.N. Association among physical activity level, cardiorespiratory fitness, and risk of musculoskeletal injury. *Am J Epidemiol* 2001; 154(3)**:** 251-258.

59.   Hope M. and Saxby T.S. Tendon healing. *Foot Ankle Clin* 2007; 12(4)**:** 553-567, v.

60.   Hu S., Maslov K. and Wang L.V. Noninvasive label-free imaging of microhemodynamics by optical-resolution photoacoustic microscopy. *Opt Express* 2009; 17(9)**:** 7688-7693.

61.   Inglis A.E. and Sculco T.P. Surgical repair of ruptures of the tendo achillis. *Clin Orthop Relat Res* 1981; (156)**:** 160-169.

62.   Ippolito E., Natali P.G., Postacchini F., Accinni L. and De Martino C. Morphological, immunochemical, and biochemical study of rabbit achilles tendon at various ages. *J Bone Joint Surg Am* 1980; 62(4)**:** 583-598.

63.   Jarvinen T.A., Kannus P., Maffulli N. and Khan K.M. Achilles tendon disorders: Etiology and epidemiology. *Foot Ankle Clin* 2005; 10(2)**:** 255-266.

64.   Jeon M., Song W., Huynh E., Kim J., Helfield B.L., Leung B.Y., Goertz D.E., Zheng G., Oh J., Lovell J.F. and Kim C. Methylene blue microbubbles as a model dual-modality contrast agent for ultrasound and activatable photoacoustic imaging. *J Biomed Opt* 2014; 19(1)**:** 16005.

65.   Ju Y.J., Tohyama H., Kondo E., Yoshikawa T., Muneta T., Shinomiya K. and Yasuda K. Effects of local administration of vascular endothelial growth factor on properties of the in situ frozen-thawed anterior cruciate ligament in rabbits. *Am J Sports Med* 2006; 34(1)**:** 84-91.

66.   Kannus P. and Jozsa L. Histopathological changes preceding spontaneous rupture of a tendon. A controlled study of 891 patients. *J Bone Joint Surg Am* 1991; 73(10)**:** 1507-1525.

67.   Kannus P. and Natri A. Etiology and pathophysiology of tendon ruptures in sports. *Scand J Med Sci Sports* 1997; 7(2)**:** 107-112.

68.   Kastelic J., Galeski A. and Baer E. The multicomposite structure of tendon. *Connect Tissue*

Res 1978; 6(1)**:** 11-23.

69. Kaux J.F., Janssen L., Drion P., Nusgens B., Libertiaux V., Pascon F., Heyeres A., Hoffmann A., Lambert C., Le Goff C., Denoel V., Defraigne J.O., Rickert M., Crielaard J.M. and Colige A. Vascular endothelial growth factor-111 (vegf-111) and tendon healing: Preliminary results in a rat model of tendon injury. *Muscles Ligaments Tendons J* 2014; 4(1)**:** 24-28.

70. Kim J., Lee D., Jung U. and Kim C. Photoacoustic imaging platforms for multimodal imaging. *Ultrasonography* 2015; 34(2)**:** 88-97.

71. Kjaer M. Role of extracellular matrix in adaptation of tendon and skeletal muscle to mechanical loading. *Physiol Rev* 2004; 84(2)**:** 649-698.

72. Klatte-Schulz F., Pauly S., Scheibel M., Greiner S., Gerhardt C., Schmidmaier G. and Wildemann B. Influence of age on the cell biological characteristics and the stimulation potential of male human tenocyte-like cells. *Eur Cell Mater* 2012; 24**:** 74-89.

73. Kobayashi D., Kurosaka M., Yoshiya S. and Mizuno K. Effect of basic fibroblast growth factor on the healing of defects in the canine anterior cruciate ligament. *Knee Surg Sports Traumatol Arthrosc* 1997; 5(3)**:** 189-194.

74. Kostrominova T.Y. and Brooks S.V. Age-related changes in structure and extracellular matrix protein expression levels in rat tendons. *Age (Dordr)* 2013; 35(6)**:** 2203-2214.

75. Kryger Z., Zhang F., Dogan T., Cheng C., Lineaweaver W.C. and Buncke H.J. The effects of vegf on survival of a random flap in the rat: Examination of various routes of administration. *Br J Plast Surg* 2000; 53(3)**:** 234-239.

76. Kulig K., Landel R., Chang Y.J., Hannanvash N., Reischl S.F., Song P. and Bashford G.R. Patellar tendon morphology in volleyball athletes with and without patellar tendinopathy. *Scand J Med Sci Sports* 2013; 23(2)**:** e81-88.

77. LaCroix A.S., Duenwald-Kuehl S.E., Brickson S., Akins T.L., Diffee G., Aiken J., Vanderby R., Jr. and Lakes R.S. Effect of age and exercise on the viscoelastic properties of rat tail tendon. *Ann Biomed Eng* 2013; 41(6)**:** 1120-1128.

78. Lake S.P., Miller K.S., Elliott D.M. and Soslowsky L.J. Effect of fiber distribution and realignment on the nonlinear and inhomogeneous mechanical properties of human supraspinatus tendon under longitudinal tensile loading. *J Orthop Res* 2009; 27(12)**:** 1596-1602.

79. Langberg H., Olesen J., Skovgaard D. and Kjaer M. Age related blood flow around the achilles tendon during exercise in humans. *Eur J Appl Physiol* 2001; 84(3)**:** 246-248.

80. Lin T.W., Cardenas L. and Soslowsky L.J. Biomechanics of tendon injury and repair. *J Biomech* 2004; 37(6)**:** 865-877.

81.   Liu H., Jiang Y., Dai Q., Zhu Q., Wang L. and Lu J. Peripheral enhancement of breast cancers on contrast-enhanced ultrasound: Correlation with microvessel density and vascular endothelial growth factor expression. *Ultrasound Med Biol* 2014; 40(2)**:** 293-299.

82.   Longo U.G., Ronga M. and Maffulli N. Achilles tendinopathy. *Sports Med Arthrosc* 2009; 17(2)**:** 112-126.

83.   Mac Gabhann F., Qutub A.A., Annex B.H. and Popel A.S. Systems biology of pro-angiogenic therapies targeting the vegf system. *Wiley Interdiscip Rev Syst Biol Med* 2010; 2(6)**:** 694-707.

84.   Maffulli N., Ewen S.W., Waterston S.W., Reaper J. and Barrass V. Tenocytes from ruptured and tendinopathic achilles tendons produce greater quantities of type iii collagen than tenocytes from normal achilles tendons. An in vitro model of human tendon healing. *Am J Sports Med* 2000; 28(4)**:** 499-505.

85.   Magnan B., Bondi M., Pierantoni S. and Samaila E. The pathogenesis of achilles tendinopathy: A systematic review. *Foot Ankle Surg* 2014; 20(3)**:** 154-159.

86.   Mancuso M.R., Davis R., Norberg S.M., O'Brien S., Sennino B., Nakahara T., Yao V.J., Inai T., Brooks P., Freimark B., Shalinsky D.R., Hu-Lowe D.D. and McDonald D.M. Rapid vascular regrowth in tumors after reversal of vegf inhibition. *J Clin Invest* 2006; 116(10)**:** 2610-2621.

87.   Matsumoto S., Saito K., Takakusagi Y., Matsuo M., Munasinghe J.P., Morris H.D., Lizak M.J., Merkle H., Yasukawa K., Devasahayam N., Suburamanian S., Mitchell J.B. and Krishna M.C. In vivo imaging of tumor physiological, metabolic, and redox changes in response to the anti-angiogenic agent sunitinib: Longitudinal assessment to identify transient vascular renormalization. *Antioxid Redox Signal* 2014; 21(8)**:** 1145-1155.

88.   Matthews T.J., Hand G.C., Rees J.L., Athanasou N.A. and Carr A.J. Pathology of the torn rotator cuff tendon. Reduction in potential for repair as tear size increases. *J Bone Joint Surg Br* 2006; 88(4)**:** 489-495.

89.   McCarthy M.M. and Hannafin J.A. The mature athlete: Aging tendon and ligament. *Sports Health* 2014; 6(1)**:** 41-48.

90.   Miller K.S., Connizzo B.K., Feeney E. and Soslowsky L.J. Characterizing local collagen fiber re-alignment and crimp behavior throughout mechanical testing in a mature mouse supraspinatus tendon model. *J Biomech* 2012; 45(12)**:** 2061-2065.

91.   Miller K.S., Edelstein L., Connizzo B.K. and Soslowsky L.J. Effect of preconditioning and stress relaxation on local collagen fiber re-alignment: Inhomogeneous properties of rat supraspinatus tendon. *J Biomech Eng* 2012; 134(3)**:** 031007.

92.   Mulvagh S.L. Myocardial perfusion by contrast echocardiography: Diagnosis of coronary

artery disease using contrast-enhanced stress echocardiography and assessment of coronary anatomy and flow reserve. *Coron Artery Dis* 2000; 11(3)**:** 243-251.

93.   Needles A., Arditi M., Rognin N.G., Mehi J., Coulthard T., Bilan-Tracey C., Gaud E., Frinking P., Hirson D. and Foster F.S. Nonlinear contrast imaging with an array-based micro-ultrasound system. *Ultrasound Med Biol* 2010; 36(12)**:** 2097-2106.

94.   Needles A., Heinmiller A., Sun J., Theodoropoulos C., Bates D., Hirson D., Yin M. and Foster F.S. Development and initial application of a fully integrated photoacoustic micro-ultrasound system. *IEEE Trans Ultrason Ferroelectr Freq Control* 2013; 60(5)**:** 888-897.

95.   Noce J.P. Fundamentals of diagnostic ultrasonography. *Biomed Instrum Technol* 1990; 24(6)**:** 456-459.

96.   Nourissat G., Houard X., Sellam J., Duprez D. and Berenbaum F. Use of autologous growth factors in aging tendon and chronic tendinopathy. *Front Biosci (Elite Ed)* 2013; 5**:** 911-921.

97.   O'Brien M. The anatomy of the achilles tendon. *Foot Ankle Clin* 2005; 10(2)**:** 225-238.

98.   Ohberg L. and Alfredson H. Ultrasound guided sclerosis of neovessels in painful chronic achilles tendinosis: Pilot study of a new treatment. *Br J Sports Med* 2002; 36(3)**:** 173-175; discussion 176-177.

99.   Ozcan A.A., Ciloglu E., Esen E. and Simdivar G.H. Use of topical bevacizumab for conjunctival intraepithelial neoplasia. *Cornea* 2014; 33(11)**:** 1205-1209.

100.   Pandya N.M., Dhalla N.S. and Santani D.D. Angiogenesis--a new target for future therapy. *Vascul Pharmacol* 2006; 44(5)**:** 265-274.

101.   Peltonen J., Cronin N.J., Stenroth L., Finni T. and Avela J. Viscoelastic properties of the achilles tendon in vivo. *Springerplus* 2013; 2(1)**:** 212.

102.   Petersen W., Pufe T., Zantop T., Tillmann B., Tsokos M. and Mentlein R. Expression of vegfr-1 and vegfr-2 in degenerative achilles tendons. *Clin Orthop Relat Res* 2004; (420)**:** 286-291.

103.   Plate J.F., Brown P.J., Walters J., Clark J.A., Smith T.L., Freehill M.T., Tuohy C.J., Stitzel J.D. and Mannava S. Advanced age diminishes tendon-to-bone healing in a rat model of rotator cuff repair. *Am J Sports Med* 2014; 42(4)**:** 859-868.

104.   Plate J.F., Wiggins W.F., Haubruck P., Scott A.T., Smith T.L., Saul K.R. and Mannava S. Normal aging alters in vivo passive biomechanical response of the rat gastrocnemius-achilles muscle-tendon unit. *J Biomech* 2013; 46(3)**:** 450-455.

105.   Pufe T., Petersen W., Kurz B., Tsokos M., Tillmann B. and Mentlein R. Mechanical factors influence the expression of endostatin--an inhibitor of angiogenesis--in tendons. *J Orthop*

Res 2003; 21(4)**:** 610-616.

106. Pufe T., Petersen W., Tillmann B. and Mentlein R. The angiogenic peptide vascular endothelial growth factor is expressed in foetal and ruptured tendons. *Virchows Arch* 2001; 439(4)**:** 579-585.

107. Pufe T., Petersen W.J., Mentlein R. and Tillmann B.N. The role of vasculature and angiogenesis for the pathogenesis of degenerative tendons disease. *Scand J Med Sci Sports* 2005; 15(4)**:** 211-222.

108. Rajian J.R., Girish G. and Wang X. Photoacoustic tomography to identify inflammatory arthritis. *J Biomed Opt* 2012; 17(9)**:** 96013-96011.

109. Rajian J.R., Shao X., Chamberland D.L. and Wang X. Characterization and treatment monitoring of inflammatory arthritis by photoacoustic imaging: A study on adjuvant-induced arthritis rat model. *Biomed Opt Express* 2013; 4(6)**:** 900-908.

110. Riggin C.N., Morris T.R. and Soslowsky L.J. Tendinopathy ii: Etiology, pathology, and healing of tendon injury and disease. In: Gomes M.E., Rodrigues M.T. andReis R.L. (eds). *Tendon regeneration*. Elsevier, 2015.

111. Riley G.P., Curry V., DeGroot J., van El B., Verzijl N., Hazleman B.L. and Bank R.A. Matrix metalloproteinase activities and their relationship with collagen remodelling in tendon pathology. *Matrix Biol* 2002; 21(2)**:** 185-195.

112. Robbins J.R., Evanko S.P. and Vogel K.G. Mechanical loading and tgf-beta regulate proteoglycan synthesis in tendon. *Arch Biochem Biophys* 1997; 342(2)**:** 203-211.

113. Rudzki J.R., Adler R.S., Warren R.F., Kadrmas W.R., Verma N., Pearle A.D., Lyman S. and Fealy S. Contrast-enhanced ultrasound characterization of the vascularity of the rotator cuff tendon: Age- and activity-related changes in the intact asymptomatic rotator cuff. *J Shoulder Elbow Surg* 2008; 17(1 Suppl)**:** 96S-100S.

114. Schiaffino S. and Reggiani C. Fiber types in mammalian skeletal muscles. *Physiol Rev* 2011; 91(4)**:** 1447-1531.

115. Schumacher B., Pecher P., von Specht B.U. and Stegmann T. Induction of neoangiogenesis in ischemic myocardium by human growth factors: First clinical results of a new treatment of coronary heart disease. *Circulation* 1998; 97(7)**:** 645-650.

116. Sehgal C.M., Arger P.H., Rowling S.E., Conant E.F., Reynolds C. and Patton J.A. Quantitative vascularity of breast masses by doppler imaging: Regional variations and diagnostic implications. *J Ultrasound Med* 2000; 19(7)**:** 427-440; quiz 441-422.

117. Sharma P. and Maffulli N. Tendon injury and tendinopathy: Healing and repair. *J Bone Joint Surg Am* 2005; 87(1)**:** 187-202.

118.   Skutek M., van Griensven M., Zeichen J., Brauer N. and Bosch U. Cyclic mechanical stretching modulates secretion pattern of growth factors in human tendon fibroblasts. *Eur J Appl Physiol* 2001; 86(1)**:** 48-52.

119.   Sultan L.R., Xiong H., Zafar H.M., Schultz S.M., Langer J.E. and Sehgal C.M. Vascularity assessment of thyroid nodules by quantitative color doppler ultrasound. *Ultrasound Med Biol* 2015; 41(5)**:** 1287-1293.

120.   Tallon C., Maffulli N. and Ewen S.W. Ruptured achilles tendons are significantly more degenerated than tendinopathic tendons. *Med Sci Sports Exerc* 2001; 33(12)**:** 1983-1990.

121.   Tempfer H. and Traweger A. Tendon vasculature in health and disease. *Front Physiol* 2015; 6**:** 330.

122.   Tham E.R., Briggs L. and Murrell G.A. Ultrasound changes after rotator cuff repair: Is supraspinatus tendon thickness related to pain? *J Shoulder Elbow Surg* 2013; 22(8)**:** e8-15.

123.   Tsai W.C., Chang H.N., Yu T.Y., Chien C.H., Fu L.F., Liang F.C. and Pang J.H. Decreased proliferation of aging tenocytes is associated with down-regulation of cellular senescence-inhibited gene and up-regulation of p27. *J Orthop Res* 2011; 29(10)**:** 1598-1603.

124.   Uefuji A., Matsumoto T., Matsushita T., Ueha T., Zhang S., Kurosaka M. and Kuroda R. Age-related differences in anterior cruciate ligament remnant vascular-derived cells. *Am J Sports Med* 2014; 42(6)**:** 1478-1486.

125.   Urwin M., Symmons D., Allison T., Brammah T., Busby H., Roxby M., Simmons A. and Williams G. Estimating the burden of musculoskeletal disorders in the community: The comparative prevalence of symptoms at different anatomical sites, and the relation to social deprivation. *Ann Rheum Dis* 1998; 57(11)**:** 649-655.

126.   VisualSonics. 700-series rmv scanhead selector. In. Toronto, Canada: VisualSonics, 2007.

127.   Voleti P.B., Buckley M.R. and Soslowsky L.J. Tendon healing: Repair and regeneration. *Annu Rev Biomed Eng* 2012; 14**:** 47-71.

128.   Wang B., Cheheltani R., Rosano J., Crabbe D.L. and Kiani M.F. Targeted delivery of vegf to treat myocardial infarction. *Adv Exp Med Biol* 2013; 765**:** 307-314.

129.   Wang J.H., Jia F., Yang G., Yang S., Campbell B.H., Stone D. and Woo S.L. Cyclic mechanical stretching of human tendon fibroblasts increases the production of prostaglandin e2 and levels of cyclooxygenase expression: A novel in vitro model study. *Connect Tissue Res* 2003; 44(3-4)**:** 128-133.

130.   Wang P.H., Luh J.J., Chen W.S. and Li M.L. In vivo photoacoustic micro-imaging of microvascular changes for achilles tendon injury on a mouse model. *Biomed Opt Express* 2011; 2(6)**:** 1462-1469.

131. Wang X., Chamberland D.L., Carson P.L., Fowlkes J.B., Bude R.O., Jamadar D.A. and Roessler B.J. Imaging of joints with laser-based photoacoustic tomography: An animal study. *Med Phys* 2006; 33(8)**:** 2691-2697.

132. Woo S.L., Debski R.E., Zeminski J., Abramowitch S.D., Saw S.S. and Fenwick J.A. Injury and repair of ligaments and tendons. *Annu Rev Biomed Eng* 2000; 2**:** 83-118.

133. Xia H.S., Wang X., Ding H., Wen J.X., Fan P.L. and Wang W.P. Papillary breast lesions on contrast-enhanced ultrasound: Morphological enhancement patterns and diagnostic strategy. *Eur Radiol* 2014; 24(12)**:** 3178-3190.

134. Yang X., Coleman D.P., Pugh N.D. and Nokes L.D. A novel 3-d power doppler ultrasound approach to the quantification of achilles tendon neovascularity. *Ultrasound Med Biol* 2011; 37(7)**:** 1046-1055.

135. Yang X., Coleman D.P., Pugh N.D. and Nokes L.D. The volume of the neovascularity and its clinical implications in achilles tendinopathy. *Ultrasound Med Biol* 2012; 38(11)**:** 1887-1895.

136. Yao J., Maslov K.I., Zhang Y., Xia Y. and Wang L.V. Label-free oxygen-metabolic photoacoustic microscopy in vivo. *J Biomed Opt* 2011; 16(7)**:** 076003.

137. Yoshikawa T., Tohyama H., Katsura T., Kondo E., Kotani Y., Matsumoto H., Toyama Y. and Yasuda K. Effects of local administration of vascular endothelial growth factor on mechanical characteristics of the semitendinosus tendon graft after anterior cruciate ligament reconstruction in sheep. *Am J Sports Med* 2006; 34(12)**:** 1918-1925.

138. Yu T.Y., Pang J.H., Wu K.P., Chen M.J., Chen C.H. and Tsai W.C. Aging is associated with increased activities of matrix metalloproteinase-2 and -9 in tenocytes. *BMC Musculoskelet Disord* 2013; 14**:** 2.

139. Zhang F., Liu H., Stile F., Lei M.P., Pang Y., Oswald T.M., Beck J., Dorsett-Martin W. and Lineaweaver W.C. Effect of vascular endothelial growth factor on rat achilles tendon healing. *Plast Reconstr Surg* 2003; 112(6)**:** 1613-1619.

140. Zhang T., Cui H., Fang C.Y., Cheng K., Yang X., Chang H.C. and Forrest M.L. Targeted nanodiamonds as phenotype-specific photoacoustic contrast agents for breast cancer. *Nanomedicine (Lond)* 2015; 10(4)**:** 573-587.

CHAPTER 2: ANALYSIS OF COLLAGEN ORGANIZATION IN MOUSE ACHILLES TENDON USING HIGH-FREQUENCY ULTRASOUND IMAGING

A. INTRODUCTION

This work was previously published by Riggin et al.[30] Achilles tendon ruptures are traumatic injuries that frequently occur in active individuals and result in significant medical expense. As many as 2.5 million individuals sustain Achilles tendon ruptures each year and the incidence is rising.[15, 25, 35] Healing of a ruptured Achilles tendon extends between months and years, and understanding the temporal changes in tendon properties (structural, biological, mechanical) are essential to successful healing.[20] However, common techniques for assessing outcomes of surgical repair and rehabilitation rely heavily on patient-based measures of pain and function. These measures include functional performance tests, such as the "hop" test or heel-raise endurance, ankle range of motion, and basic descriptive scoring measures.[6, 26, 31, 32, 34] While these measures can provide evidence for recovery of functional performance, they do not directly assess tendon healing, which, if insufficient, can lead to re-rupture. Additionally, those approaches are only semi-quantitative, and may be biased by confounding factors, such as strength, agility, and coordination. Consequently, there is an urgent need for a quantitative, in vivo measure of tendon properties to guide rehabilitation progression and return to activity criteria.

Tendon collagen alignment is an important structural tissue property that changes throughout the progression of tendon healing. It is known that changes in collagen organization precede and correlate with changes in mechanical properties in tendons, and

are affected by both load and injury.[7, 12, 18, 23, 24] Therefore, the clinical evaluation of collagen organization following Achilles tendon injury may provide a more appropriate measure of healing than traditional, functional performance tests. There are currently multiple techniques for measuring collagen alignment, such as crossed polarizer imaging,[18, 28, 29] quantitative polarized light microscopy,[9, 36] second-harmonic generation imaging,[1, 13, 19] and infrared spectroscopy.[38] However, these methods are typically destructive and are not easily clinically translatable. Ultrasound imaging, currently used clinically to evaluate injuries in tendon including the Achilles,[2, 21, 22, 27, 37] has recently been investigated as a quantitative tool to analyze tendon properties. It is an attractive alternative because it has the potential to provide the same organizational information as other methods, is relatively inexpensive and portable, is non-invasive, and is not limited to tendon size or thickness. Therefore, ultrasound could be used as diagnostic clinical tool for the evaluation of tendon health. A number of studies have quantitatively evaluated tendon structural properties using ultrasound. Specifically, it has been demonstrated that changes in tendon mechanical properties correlate with changes in ultrasound echogenicity in both rat Achilles and porcine digital flexor tendons.[4, 8] Additionally, it has been shown that tendinopathy in human Achilles and patellar tendons can be predicted by analyzing the degree of speckle patterning in ultrasound imaging using a Fourier analysis.[3, 17] Finally, quantitative shear wave elastography has been used for assessing the relative elasticity of injured and uninjured Achilles tendons.[5]

While these current techniques correlate ultrasound properties to tendon mechanical properties and are therefore important for the field, they do not evaluate

collagen alignment specifically (which directly relates to tendon strength), or establish a specific mechanism for the change in ultrasonic properties. The method described in this chapter advances previous research and utilizes the patterning seen in tendon ultrasound images to quantitatively describe organization, specifically the variation of collagen alignment. Collagen appears hyperechoic in ultrasound imaging, whereas the matrix between the collagen appears hypoechoic. This gives the appearance of "bands" in ultrasound images of tendons that corresponds to the collagen matrix. In the method presented in this paper, these fiber elements are identified, and the deviation of the fiber directions are quantified as a measure of structural organization.[33] Additionally, to further support that our results are consistent with actual changes in collagen organization, the analysis is also performed using standard organizational measure, cross polarizer (CP) imaging.

Therefore, the objective of this study was to perform an ex vivo experiment on mouse Achilles tendons to determine if high-frequency ultrasound (HFUS) imaging can capture changes in collagen alignment. We will confirm this method by using HFUS to analyze organizational changes due to applied load and injury (known cases that create changes in alignment), and then confirm these findings using the established CP imaging method. We hypothesize that because the bands seen in tendon ultrasound images are created by collagen bundles, the changes in collagen alignment that are measurable by CP will also be measurable by HFUS. Additionally, we hypothesize that the HFUS imaging method will be capable of detecting both an increase in alignment with increased loading, and a decrease in alignment with the presence of a defect.

B. METHODS

B-1. Study Design and Sample Preparation

Mouse Achilles tendons were selected for this experiment because their small size enabled analysis with our CP system, which will be used for validation of our novel HFUS analysis, and because their straight and superficial anatomical position makes this system a likely first step toward direct translation to future in vivo studies. This study was performed ex vivo with a high-frequency ultrasound transducer to enhance the spatial resolution of the tendon structure in our small animal model, and represents the first, necessary step toward developing a rigorous, non-invasive measure of tendon organization. Eighteen Achilles tendons were harvested and frozen (-20°C) from C57BL/6 type mice. Tendons were thawed and fine dissected to remove all surrounding tissue, leaving the insertion site intact on the calcaneus. Tendons were tested in custom fixtures and had an initial gauge length of 5 mm. Two experimental situations that are known to cause a change in tendon organization were performed to demonstrate that collagen alignment can be quantified with our ultrasound-based technique: (1) an increase in alignment with increasing load and (2) a decrease in alignment with injury. Eleven tendons were used to evaluate collagen alignment during loading, and seven were used to analyze the effect of excisional injury on collagen alignment (Figure 2.1). To account for variability between specimens, these experiments were performed paired, so that each tendon specimen could be compared against itself.
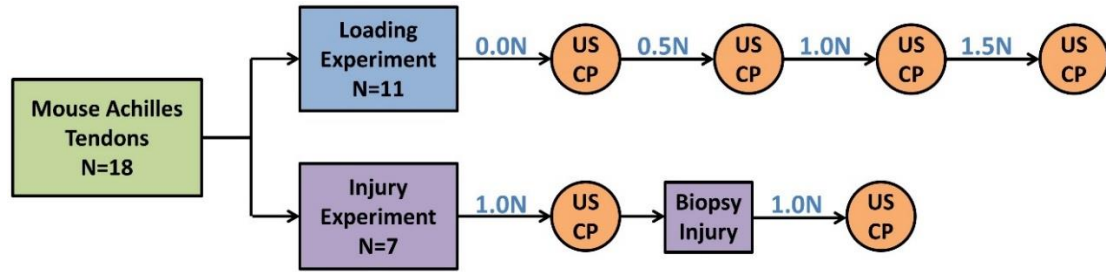
Figure 2.1: Study design. US and CP represent simultaneous ultrasound and cross-polarizer imaging after each loading or injury condition

B-2. Image Acquisition

For HFUS and CP image acquisition, tendons were secured in a custom fixture, submerged in a phosphate buffered saline (PBS) bath, and aligned so that the CP and HFUS would capture coronal cross-sectional images simultaneously (Figure 2.2). Ultrasound images were captured using a Vevo 770 scanner (VisualSonics, Toronto, Canada) and a 55 MHz transducer (RMV 708, VisualSonics, Toronto, Canada). A 55 MHz transducer was used in order to obtain sufficient resolution in the mouse tendon (note that a lower frequency transducer would be more appropriate for a larger model). A motorized scanner used for 3-D imaging was attached to the ultrasound transducer to allow for consecutive coronal images to be obtained (Figure 2.3). All ultrasound settings (i.e., frequency, gain) were kept constant during testing to standardize the images. The ultrasound transducer was manually positioned so that it was parallel and centered over the tendon. Consecutive cross-sectional coronal images were taken every 0.1 mm across the tendon thickness (<1 mm). The CP set-up consisted of a linear backlight (Dolan-Jenner, Boxborough, MA), 90°-offset rotating polarizer sheets (Edmund Optics, Barrington, NJ) on either side of the tendon, and a digital camera (Basler, Exton, PA). As described previously,[18] images were

acquired through the rotation of the polarizer sheets to obtain localized fiber alignment data. Prior to testing, the encoder in the stepper motor (Lin Engineering, Santa Clara, CA) that rotates the polarizer sheets was set at a position corresponding to 0 degrees of angular rotation. The tendon was secured in a fixture that was attached to a custom tensiometer[11] through a sliding shaft to allow for load control while the tendon is in the horizontal configuration required for ultrasound imaging (Figure 2.2).
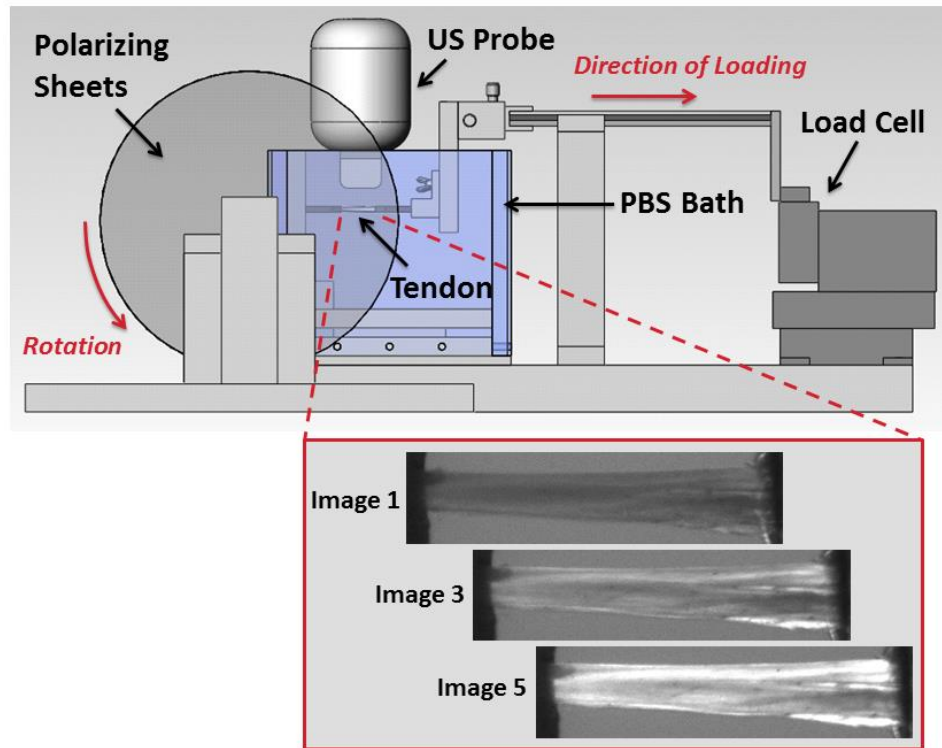
Figure 2.2: Schematic of setup for capturing CP and HFUS imaging simultaneously. The tendon is secured between two grips in a PBS tank, where the ultrasound probe can be centered over top of the tendon, submerged in the PBS. Two polarizing sheets are located on either side of the tank, with a linear backlight on one side and a camera on the other (not depicted in this image). A custom-built tensiometer is attached to a sliding shaft to allow for load control. Inset figure (below) shows representative images of a tendon as captured by the CP camera through one rotation cycle.
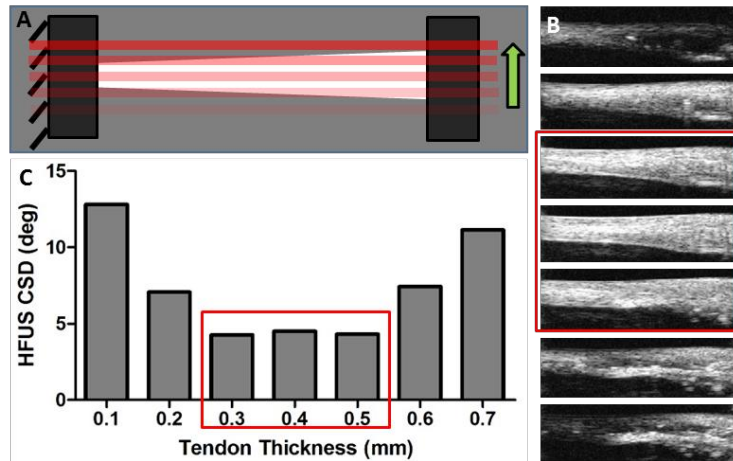
Figure 2.3: (A) Diagram depicting motorized scanning across the tendon width and the resulting (B) ultrasound images and (C) CSD calculations of each tendon image slice. Only the central images, where there is no edge artifact, are used for CSD calculations.

To examine the effect of fiber alignment during loading (n=11), loads of 0.0, 0.5, 1.0, and 1.5 N, previously determined to show changes in alignment, were applied consecutively through control of the tensiometer, making sure the tendon had sufficient time to creep at each steady load. HFUS and CP images were captured at each load. The experimenter ensured that the load was stable before acquiring images, and this waiting period was consistent from sample to sample ($\sim$ 15 seconds). Both the cross polarizer and the ultrasound only take $\sim$2-3 seconds to capture the series of images necessary for analysis, and they are captured simultaneously. Due to the speed of the image capture, and the small levels of relaxation that may occur after this point, any changes in alignment from these effects would be negligible. To examine changes in collagen alignment following excisional injury (n=7), uninjured tendons were loaded into the same custom fixture and imaged under 1.0N load. The tendons were then injured using a 0.5mm biopsy punch to create a standard defect and re-imaged using the same protocol.

B-3. Image Analysis

The analysis of the HFUS images was conducted using a custom MATLAB (Mathworks, Natick, MA) program, and followed an approach based on a previously described algorithm.[33] Using a 55 MHz transducer, the effective resolution of the ultrasound images were approximately 30 µm. Tendon collagen fascicles appear hyperechoic under HFUS, where the non-collagenous matrix between the fascicles appears hypoechoic, giving rise to the appearance of bands in the images (Figure 2.4).[10] These bands are analyzed to determine a quantitative measure of tendon organization. Briefly, the ultrasound images that comprised the center of the tendon (with no edge artifacts) were chosen for analysis (Figure 2.3). The ultrasound images were filtered to remove any small particles and reduce background noise. A matrix convolution was then used to apply a linear kernel over groups of pixels in the filtered image at varying angles (0-180 degrees in 5 degree increments). A power series function was then fit to the intensity versus angle data (least squares curve-fit) and used to determine the angle with maximum intensity and therefore the fiber direction.

$$Intensity = A\left[2^{\frac{-B}{1000}(Angle-C)^2}\right] + D$$

In addition, any regions in which the confidence intervals for the parameters of the power series fit were too high were masked. The circular standard deviation (CSD), a measure of the distribution of collagen alignment (increased CSD means increased disorganization), was calculated for the local fiber directions in each selected image segment in a specimen and averaged to obtain a value representative of the organization of the entire tendon thickness. A representative example of high and low CSD measures is depicted in

histograms for both injured and uninjured specimens (Figure 2.5). This method is novel because it translates a technology developed for identifying and quantifying properties of filaments to the collagen patterning in ultrasound images. Since this method is a post-image acquisition analysis, it can be applied to any ultrasound image, and no new equipment is necessary to during the image acquisition phase.
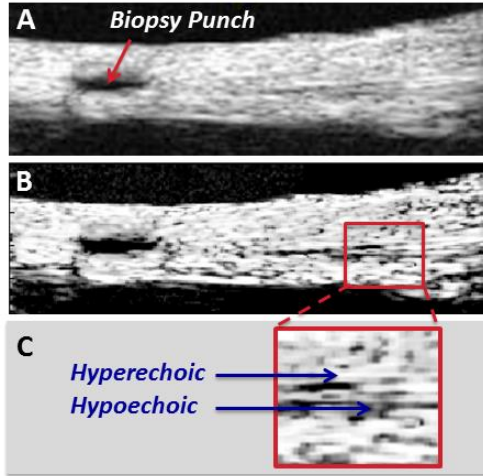
Figure 2.4: (a) HFUS image of Achilles tendon with excisional injury, (b) filtered HFUS image, (c) hyper- and hypoechoic regions that create the banded pattern that is quantified as the CSD of the fiber orientations.
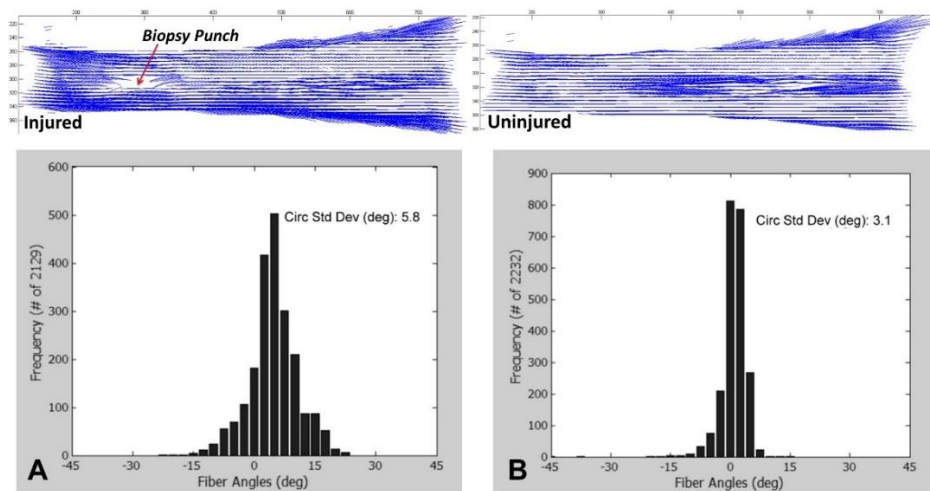
Figure 2.5: Alignment maps and histograms depicting the distribution of localized fiber directions throughout the tendon that were produced through CP analysis for (a) injured and (b) uninjured specimens.

For the analysis of the CP images, collagen fiber direction was determined across the tendon length and width. Collagen refracts polarized light by 90 degrees, thus the collagen fiber direction can be determined by collecting images at varying angles of polarization (0-140°). The images of the tendon are then divided into 2x2 bundles of pixels with 5 pixel spacing between bundles (effective resolution of approximately 50 µm, comparable to the HFUS), and the pixel intensities were summed in each pixel group for each angle of polarizer rotation. These intensity values were then plotted against the angle of polarizer rotation, and a $\sin^2$ wave was fit to the data to determine the angle corresponding to the minimum pixel intensity. This point represents the average localized collagen fiber direction. A compilation of these localized directions can be represented as an alignment map over the whole tendon (Figure 2.5). The CSD was calculated for each specimen in each experimental group to quantify collagen organization.

B-4. Statistics

For analyzing the change in alignment in response to load, significance was assessed using two 1-way repeated measures ANOVAs, one for each imaging modality. This was followed by paired t-test analyses with Holm-Bonferroni post hoc for multiple comparisons to determine specific differences due to load within each imaging modality. For analyzing the change in alignment in response to injury, a paired t-test was performed for each imaging modality. Finally, a regression analysis was performed on the CSD values comparing measurement techniques. In order to reflect the paired nature of the analysis, the regression was run on the change in CSD with respect to 0N (baseline) for

each load and uninjured (baseline) for the injury data. Significance was set at $p < 0.05$ and trends were set at $p < 0.1$.

C. RESULTS

We first evaluated the HFUS results to determine if the expected changes in alignment due to load and injury were able to be detected using this novel method. It was found that the HFUS analysis detected a significant decrease in CSD in response to increasing load, meaning the tendon became more organized with increasing load as expected (Figure 2.6A). Statistically, the 0.5, 1.0, and 1.5 N groups were all compared to the 0N group, and additionally, the 1.0 and 1.5 N groups were compared to the 0.5N group to demonstrate further incremental changes with load. For the injury study, CSD as measured by HFUS was significantly larger for the injured group, meaning the tendon became more disorganized with an injury also as expected (Figure 2.6B). This demonstrates that the HFUS technique is sensitive enough to detect the expected changes in organization caused by both increases in load, as well as infliction of injury.
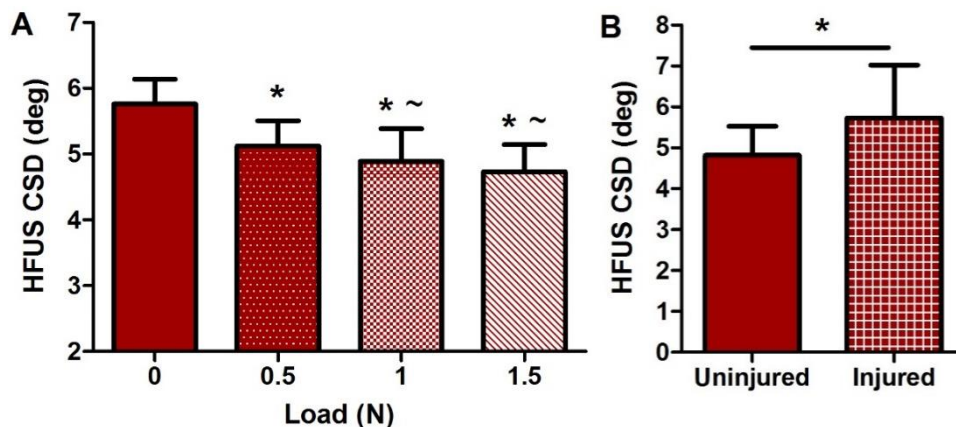
Figure 2.6: (a) Changes in CSD in response to load for the HFUS images. There is a significant decrease in CSD (increase in organization) with increased loading. Statistics for

each load compared to 0 N (*p < 0.05) and to 0.5 N (~p < 0.05). (b) CSD measures for HFUS images before and after a biopsy punch excisional injury (tendon loaded to 1.0N). There is a significant increase in CSD (decrease in organization) with injury (*p < 0.05).

To further support that our HFUS results are consistent with the actual changes in collagen alignment in these two conditions, we conducted the same experiment simultaneously on the same tendons using the established CP analysis. The CP method also was able to detect a consistent decrease in CSD with increased load (Figure 2.7A), and an increase in CSD with injury (Figure 2.7B), consistent with expected results, and with our HFUS results.
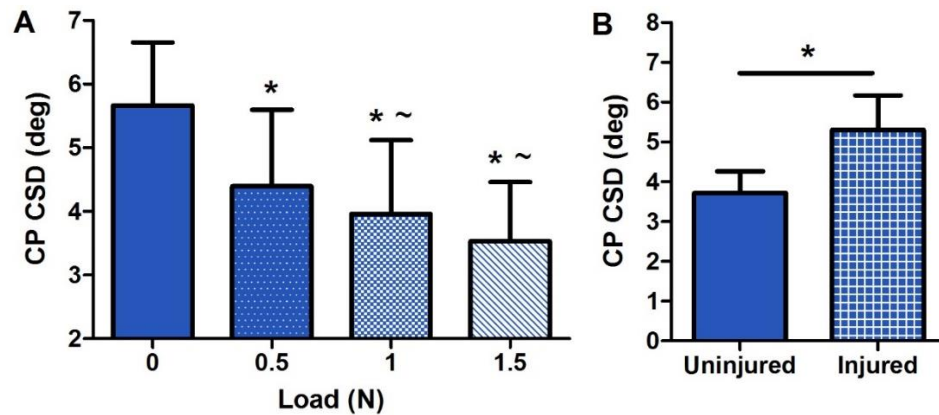
Figure 2.7: (a) Changes in CSD in response to load for the CP images. There is a significant decrease in CSD (increase in organization) with increased loading. Statistics for each load compared to 0 N (*p < 0.05) and to 0.5 N (~p < 0.05). (b) CSD measures for CP images before and after a biopsy punch excisional injury (tendon loaded to 1.0N). There is an increase in CSD (decrease in organization) with injury (*p < 0.05).

For the comparison of the CSD measures of each imaging technique, a regression was run on the change in CSD with respect to 0N (baseline) for each load, and uninjured (baseline) for the injury data, and a correlation was determined with $R^2 = 0.45$ and p<0.0001 (Figure 2.8).
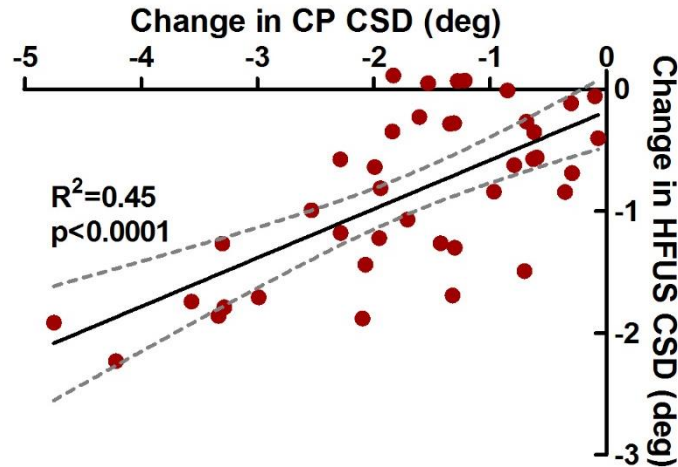
Figure 2.8: Regression analysis between HFUS and CP measurements, with the data presented as a difference from baseline. Solid line represents the linear regression and dotted lines represent the 95% confidence interval range.

D. DISCUSSION

In this study, a controlled ex vivo experiment was conducted to demonstrate the use of HFUS for detecting changes in collagen alignment, which is the first, necessary step toward developing a rigorous, non-invasive, in vivo measure of tendon organization. Our novel image analysis algorithm identifies the hyperechoic bands seen in tendon ultrasound images, which are created by the tendon collagen matrix, and quantifies the deviation in alignment of the collagen bands to produce a quantitative measure of collagen organization. The findings of this study support our hypothesis that because the bands seen in ultrasound images of tendon are collagen, changes in collagen organization measurable by CP imaging, an established technique, will also be measureable by HFUS. Specifically, our HFUS method can capture the alignment of tendon collagen fibers along the direction of loading, thereby increasing the level of organization in the tissue and decreasing the CSD of the collagen fibers. This result is consistent with previous work in our lab, which

demonstrated fiber re-alignment during tendon tensile mechanical testing.[18, 23, 24] Additionally, the injury data demonstrates that our HFUS method is able to detect a disruption to the collagen fibers, which causes a decrease in organization throughout the length of the tendon (not just in the defect region) likely due to unloading of collagen fibers proximal to the injury site. Since the image analysis algorithm filters out any non-fibrous data, including the excisional defect, the disorganization detected by these imaging modalities is a result of damage propagated through the intact regions of the tendon. Furthermore, since this is not a healing study, there is no scar formation, which would cause even further disorganization and a more drastic change in CSD in the injured tendon. Therefore, importantly, this experiment demonstrates that even this smallest possible change due to an injury, can be detected through HFUS. Since consistent responses to both load and injury were observed in both the HFUS and CP imaging modalities, it can be concluded that HFUS is an alternative to the established CP method. Additionally, and as a potential future advantage which motivated the current work, this HFUS method has the potential to be translated both to larger ex vivo specimens, as well as to in vivo imaging, neither of which can be done with CP imaging.

The regression analysis comparing imaging methods was highly significant. However, it was only a modest correlation. This is not surprising given that the two methods are measuring different phenomena. The ultrasound is detecting the impedance difference between the collagen fibers and the surrounding matrix to obtain a striated signal of echogenicity, where the cross polarizer is using the birefringence properties of the collagen. Due to differences in the physics of the image acquisition, each method has its

own bias and inaccuracies associated with the outcome measure. Since these biases are consistent within an imaging method, the same response to these different conditions was observed. However, when comparing between the two methods, the biases are not consistent, and therefore manifest as differences unrelated to the overall response of the methods. Since the aim of this study is to quantify a change in organization, and we have demonstrated that both methods detect the same response with significance, given these differences, this correlation is in support of our overall findings. Additionally, this is the first study to use this technique and prove its feasibility. Future studies, with a larger sample sizes and a greater range of data values, could be designed to more fully characterize the correlation between the measures.

While there are a number of previous studies that demonstrate the use of ultrasound for evaluating tendon health,[3, 4, 8, 17] they are designed to provide a correlation or statistical relationship between their measured ultrasound properties and tissue properties. In contrast, our method directly measures a tissue property, collagen organization. Therefore, this method can provide a more direct evaluation of tendon health. Additionally, the correlations determined through these other methods are susceptible to confounding factors such as density, tissue hydration, collagen fibril type, etc. Collagen organization can be measured independently of these factors, allowing for a more mechanistic evaluation that can give specific structural information about how organization contributes to healing. This mechanism also provides the opportunity to develop a targeted therapy (such as loading or rehabilitation protocols) to specifically address the changes seen in the ultrasound analysis. Finally, ultrasonic property changes found in other studies assume to

be influenced by collagen fiber organization. This study provides evidence that collagen organization is a contributing factor to the changes seen in ultrasound properties demonstrated in other groups.

This study is not without limitations. Only healthy tendons (from previously sacrificed animals) were evaluated, so even by applying a load or inflicting an injury, the range of achievable organization values is fairly small. Furthermore, a standardized, yet simple injury model was used for this validation study. While this injury is not clinically relevant, it provides a standard defect that alters the collagen alignment. Therefore, the changes observed, while significant, only represent a small range of values that are likely larger in healing tissues with more clinically relevant defects. However, this allows demonstration of the sensitivity and capability of this experimental technique. Future studies will evaluate a more extensive injury model to further demonstrate the range of organization values that can be achieved using HFUS. Additionally, while our tensiometer allowed us to apply a range of precise loading conditions, we were not able to perform more sophisticated mechanical testing, such as pre-conditioning or application of a constant strain rate. However, any variability in loading speed is likely to be nominal, since it was performed by the same operator (first author). Furthermore, we are using a 55 MHz ultrasound transducer, which, because of its high resolution, is ideal for small tendons (which was needed for this study in order to perform the CP analysis). However, the depth capabilities of this frequency transducer are limited, and so in order to translate this method in vivo and to larger tendons, it must be demonstrated using a lower frequency probe. In a rat or larger animal's Achilles tendon, since the collagen structure approximately scales

with size, a lower frequency transducer will be able to resolve the collagen structure while still penetrating through surrounding tissue layers. This can be demonstrated by looking at a clinical scan of a human Achilles tendon, where the striated pattern we are quantifying can be seen.[10, 16] Clinical scanners range from 2-18 MHz, and structures such as the Achilles tendon are commonly imaged at 15-18 MHz since they are superficial. A scanner of 17.5 MHz has an axial resolution of ~85 μm,[39] and given that human tendon fascicle structures have a diameter of approximately 300-400 μm,[14] this technique would be able to resolve, and therefore quantify, the fascicle structure. Additionally, while not commonly used clinically, a 25 MHz probe has an axial resolution of ~70 μm[39] and, in most cases, may still have an appropriate focal length for imaging the human Achilles, so it could potentially be used for this application. However, further investigation is needed to determine the sensitivity of this technique using a lower resolution scanner on a larger specimen. The current study provides evidence that such a study should be conducted since it is shown that the banded pattern and collagen orientation are related. One limitation of this is that it may not work as well for tendons that are less superficial (such as supraspinatus) when compared to more superficial tendons (such as Achilles as used here). Finally, this new technique shows significant differences that are scientifically relevant, however, it is difficult to determine how these measures will translate to the clinical situation to determine patient-to-patient differences in organization. Further analysis would be needed to obtain a normal in vivo range, as well as the degree of change between normal and injury, in order to provide a more clinically relevant comparison. Additionally, since this technique has the potential to become non-invasive, it could be used for

longitudinal studies, and therefore data would be compared within an individual over time, overcoming the potential variability between individuals in some studies.

This is the first study to directly quantify tendon collagen alignment from ultrasound images. Specifically, it has demonstrated that HFUS is capable of detecting changes in organization due to load and injury, and that these changes are consistent with both the established CP method, and expected results based on previous studies.[7, 12, 18, 23, 24] As such, this experiment validates the use of HFUS imaging for obtaining a quantitative measure of tendon organization, and provides critical data to continue to refine the technique for future in vivo applications requiring a non-invasive method. Such a method could eventually be used in clinical studies to monitor progress during treatment and ultimately improve patient outcomes.

E. REFERENCES

1.   Abraham T., Fong G. and Scott A. Second harmonic generation analysis of early achilles tendinosis in response to in vivo mechanical loading. *BMC Musculoskelet Disord* 2011; 12**:** 26.

2.   Alfredson H., Masci L. and Ohberg L. Partial mid-portion achilles tendon ruptures: New sonographic findings helpful for diagnosis. *Br J Sports Med* 2011; 45(5)**:** 429-432.

3.   Bashford G.R., Tomsen N., Arya S., Burnfield J.M. and Kulig K. Tendinopathy discrimination by use of spatial frequency parameters in ultrasound b-mode images. *IEEE Trans Med Imaging* 2008; 27(5)**:** 608-615.

4.   Chamberlain C.S., Duenwald-Kuehl S.E., Okotie G., Brounts S.H., Baer G.S. and Vanderby R. Temporal healing in rat achilles tendon: Ultrasound correlations. *Ann Biomed Eng* 2013; 41(3)**:** 477-487.

5.   Chen X.M., Cui L.G., He P., Shen W.W., Qian Y.J. and Wang J.R. Shear wave elastographic characterization of normal and torn achilles tendons: A pilot study. *J Ultrasound Med* 2013; 32(3)**:** 449-455.

6.   Chinn L. and Hertel J. Rehabilitation of ankle and foot injuries in athletes. *Clin Sports Med*

2010; 29(1)**:** 157-167, table of contents.

7. Dourte L.M., Perry S.M., Getz C.L. and Soslowsky L.J. Tendon properties remain altered in a chronic rat rotator cuff model. *Clin Orthop Relat Res* 2010; 468(6)**:** 1485-1492.

8. Duenwald-Kuehl S., Lakes R. and Vanderby R., Jr. Strain-induced damage reduces echo intensity changes in tendon during loading. *J Biomech* 2012; 45(9)**:** 1607-1611.

9. Franchi M., Torricelli P., Giavaresi G. and Fini M. Role of moderate exercising on achilles tendon collagen crimping patterns and proteoglycans. *Connect Tissue Res* 2013.

10. Garcia T., Hornof W.J. and Insana M.F. On the ultrasonic properties of tendon. *Ultrasound Med Biol* 2003; 29(12)**:** 1787-1797.

11. Gimbel J.A., Mehta S., Van Kleunen J.P., Williams G.R. and Soslowsky L.J. The tension required at repair to reappose the supraspinatus tendon to bone rapidly increases after injury. *Clin Orthop Relat Res* 2004; (426)**:** 258-265.

12. Gimbel J.A., Van Kleunen J.P., Mehta S., Perry S.M., Williams G.R. and Soslowsky L.J. Supraspinatus tendon organizational and mechanical properties in a chronic rotator cuff tear animal model. *J Biomech* 2004; 37(5)**:** 739-749.

13. Gusachenko I., Tran V., Houssen Y.G., Allain J.M. and Schanne-Klein M.C. Polarization-resolved second-harmonic generation in tendon upon mechanical stretching. *Biophys J* 2012; 102(9)**:** 2220-2229.

14. Hansen P., Haraldsson B.T., Aagaard P., Kovanen V., Avery N.C., Qvortrup K., Larsen J.O., Krogsgaard M., Kjaer M. and Peter Magnusson S. Lower strength of the human posterior patellar tendon seems unrelated to mature collagen cross-linking and fibril morphology. *J Appl Physiol (1985)* 2010; 108(1)**:** 47-52.

15. Houshian S., Tscherning T. and Riegels-Nielsen P. The epidemiology of achilles tendon rupture in a danish county. *Injury* 1998; 29(9)**:** 651-654.

16. Khoury V., Guillin R., Dhanju J. and Cardinal E. Ultrasound of ankle and foot: Overuse and sports injuries. *Semin Musculoskelet Radiol* 2007; 11(2)**:** 149-161.

17. Kulig K., Landel R., Chang Y.J., Hannanvash N., Reischl S.F., Song P. and Bashford G.R. Patellar tendon morphology in volleyball athletes with and without patellar tendinopathy. *Scand J Med Sci Sports* 2013; 23(2)**:** e81-88.

18. Lake S.P., Miller K.S., Elliott D.M. and Soslowsky L.J. Effect of fiber distribution and realignment on the nonlinear and inhomogeneous mechanical properties of human supraspinatus tendon under longitudinal tensile loading. *J Orthop Res* 2009; 27(12)**:** 1596-1602.

19. Lau T.Y., Ambekar R. and Toussaint K.C. Quantification of collagen fiber organization using three-dimensional fourier transform-second-harmonic generation imaging. *Opt

Express 2012; 20(19)**:** 21821-21832.

20. Lin T.W., Cardenas L. and Soslowsky L.J. Biomechanics of tendon injury and repair. *J Biomech* 2004; 37(6)**:** 865-877.

21. Mangat K.S., Kanwar R., Johnson K., Korah G. and Prem H. Ultrasonographic phases in gap healing following ponseti-type achilles tenotomy. *J Bone Joint Surg Am* 2010; 92(6)**:** 1462-1467.

22. Maranho D.A., Nogueira-Barbosa M.H., Simao M.N. and Volpon J.B. Ultrasonographic evaluation of achilles tendon repair after percutaneous sectioning for the correction of congenital clubfoot residual equinus. *J Pediatr Orthop* 2009; 29(7)**:** 804-810.

23. Miller K.S., Connizzo B.K., Feeney E. and Soslowsky L.J. Characterizing local collagen fiber re-alignment and crimp behavior throughout mechanical testing in a mature mouse supraspinatus tendon model. *J Biomech* 2012; 45(12)**:** 2061-2065.

24. Miller K.S., Edelstein L., Connizzo B.K. and Soslowsky L.J. Effect of preconditioning and stress relaxation on local collagen fiber re-alignment: Inhomogeneous properties of rat supraspinatus tendon. *J Biomech Eng* 2012; 134(3)**:** 031007.

25. Moller A., Astron M. and Westlin N. Increasing incidence of achilles tendon rupture. *Acta Orthop Scand* 1996; 67(5)**:** 479-481.

26. Mullaney M.J., McHugh M.P., Tyler T.F., Nicholas S.J. and Lee S.J. Weakness in end-range plantar flexion after achilles tendon repair. *Am J Sports Med* 2006; 34(7)**:** 1120-1125.

27. Poposka A., Georgieva D. and Dzoleva-Tolevska R. Significance of ultrasound in the diagnosis and treatment of achilles tendon rupture. *Prilozi* 2012; 33(1)**:** 209-216.

28. Quinn K.P., Bauman J.A., Crosby N.D. and Winkelstein B.A. Anomalous fiber realignment during tensile loading of the rat facet capsular ligament identifies mechanically induced damage and physiological dysfunction. *J Biomech* 2010; 43(10)**:** 1870-1875.

29. Quinn K.P. and Winkelstein B.A. Altered collagen fiber kinematics define the onset of localized ligament damage during loading. *J Appl Physiol* 2008; 105(6)**:** 1881-1888.

30. Riggin C.N., Sarver J.J., Freedman B.R., Thomas S.J. and Soslowsky L.J. Analysis of collagen organization in mouse achilles tendon using high-frequency ultrasound imaging. *J Biomech Eng* 2014; 136(2)**:** 021029.

31. Robinson J.M., Cook J.L., Purdam C., Visentini P.J., Ross J., Maffulli N., Taunton J.E. and Khan K.M. The visa-a questionnaire: A valid and reliable index of the clinical severity of achilles tendinopathy. *Br J Sports Med* 2001; 35(5)**:** 335-341.

32. Saxena A., Ewen B. and Maffulli N. Rehabilitation of the operated achilles tendon: Parameters for predicting return to activity. *J Foot Ankle Surg* 2011; 50(1)**:** 37-40.

33.   Shah S.A., Santago P. and Rubin B.K. Quantification of biopolymer filament structure. *Ultramicroscopy* 2005; 104(3-4)**:** 244-254.

34.   Silbernagel K.G., Nilsson-Helander K., Thomee R., Eriksson B.I. and Karlsson J. A new measurement of heel-rise endurance with the ability to detect functional deficits in patients with achilles tendon rupture. *Knee Surg Sports Traumatol Arthrosc* 2010; 18(2)**:** 258-264.

35.   Suchak A.A., Bostick G., Reid D., Blitz S. and Jomha N. The incidence of achilles tendon ruptures in edmonton, canada. *Foot Ankle Int* 2005; 26(11)**:** 932-936.

36.   Thomopoulos S., Williams G.R., Gimbel J.A., Favata M. and Soslowsky L.J. Variation of biomechanical, structural, and compositional properties along the tendon to bone insertion site. *J Orthop Res* 2003; 21(3)**:** 413-419.

37.   Vadala A., De Carli A., Vulpiani M.C., Iorio R., Vetrano M., Scapellato S., Suarez T., Di Salvo F. and Ferretti A. Clinical, functional and radiological results of achilles tenorraphy surgically treated with mini-open technique. *J Sports Med Phys Fitness* 2012; 52(6)**:** 616-621.

38.   Vidal Bde C. and Mello M.L. Collagen type i amide i band infrared spectroscopy. *Micron* 2011; 42(3)**:** 283-289.

39.   VisualSonics. 700-series rmv scanhead selector. In. Toronto, Canada: VisualSonics, 2007.

CHAPTER 3: METHODS FOR MODULATION OF VASCULAR RESPONSE AFTER INJURY

A. INTRODUCTION

Despite its strength, the Achilles tendon is commonly affected by spontaneous rupture. Once ruptured, the tendon undergoes a healing response initiated by the release of growth factors to facilitate extracellular matrix formation, cellular proliferation, and the formation of blood vessels. Later in healing, the tendon remodels the disorganized collagen type III that primarily makes up the scar tissue and replaces it with more organized collagen type I.[6, 25, 52] While this increased organization improves the tensile mechanical properties towards normal tendon, the repaired tissue remains fibrous scar, and will never completely regain its structural, compositional, or functional properties it had prior to injury. Unfortunately, this leads to a relatively high rate of re-rupture as well as tendon lengthening during healing, causing loss of calf muscle strength and ankle function.

Blood vessel formation, or angiogenesis, is an important part of the tendon healing process as it facilitates the delivery of nutrients and regulatory factors, removes waste, and helps control the immune response. Unlike many tissues, healthy tendons are relatively hypovascular and only become hypervascular during injury or degeneration. While vascular ingrowth is necessary for tendon healing, prolonged hypervascularization following tendon injury may not be beneficial.[50] An imbalance of pro- and anti-angiogenic factors could promote abnormal angiogenesis, creating vessels with structural

and functional deficits. [20] Conversely, it is possible that the angiogenic response is not sufficient to facilitate a robust healing response, and that increasing the vascular formation after injury could improve healing outcome.[56]

Angiogenic treatments have been studied in the context of many vascular diseases. Conditions with excess or uncontrolled vascular formation include diabetic nephropathy, arthritis, retinopathy, and tumor growth, among others.[20, 44] Whereas conditions such as myocardial infarction and ischemic injury are caused by inadequate angiogenic response to injury generating cell and tissue death.[44] Animal and human trials evaluating the delivery of pro- and anti-angiogenic factors to correct these vascular conditions have been shown to be effective in both altering the vascular response in the tissue as well as improving outcome measures.[4, 9, 13, 16, 18, 20-23, 31, 35, 37, 43, 48, 51] While these treatment strategies have been investigated extensively in these fields, there is very little evidence supporting their efficacy in tendon and ligament applications. The delivery of vascular endothelial growth factor (VEGF) or basic fibroblast growth factor (bFGF) increased ACL reconstruction vascularization, but had no positive effect on healing outcome.[27, 30, 55] Whereas, these factors were shown to improve the mechanical properties after an Achilles tendon rupture, but there was no evaluation of the resulting vascular response to treatment.[29, 56] Finally, treatment with bevacizumab, an anti-VEGF antibody drug, after a collagenase induced injury caused a reduction in neovessels and improved collagen organization, but no mechanical analysis was performed.[10] While this collective work demonstrates that translating angiogenic therapies to tendon and ligament applications is promising, there is still a lack of understanding of how these treatments

70

alter the vascular and compositional properties of a tendon, and further how those changes impact tendon healing outcome. Consequently, establishing reliable methods for both increasing and decreasing vascular response following tendon injury is a necessary first step to defining the effect of altered angiogenesis on tendon healing.

Therefore, the objective of this study was to evaluate how the delivery of both pro- and anti-angiogenic factors affect the rat Achilles tendon vascular response after injury using *in vivo* ultrasound imaging and *ex vivo* histological measures. We hypothesized that vessel properties measurable by both ultrasound and histology, such as vessel density, vessel size, and blood flow velocity, will be increased due to the pro-angiogenic factor and decreased due to the anti-angiogenic factor delivery. For the first study in this chapter, we chose a VEGF dosage previously found to induce changes in vascular and healing outcomes.[27, 56] However, we were also interested in the question of how the timing of delivery might play a role in the tendon response. VEGF is naturally expressed after the initial inflammatory phase of healing, peaking around 7 days. [34] Most studies evaluating angiogenic modification deliver VEGF immediately after injury, which would be earlier than the normal VEGF expression.[9, 27, 29, 55, 56] Therefore, we wanted to evaluate the effect of delivering exogenous VEGF both prior to (early) or during (late) the time of peak endogenous expression. For the second study, we were interested in blocking endogenous VEGF expression, so we chose to evaluate the effect of anti-VEGF antibody only during the late delivery time. The dosage for anti-VEGF antibody factors is not well characterized for direct injection, as it is primarily used as a systemic drug. Therefore, for this part of the study, we evaluated 3 different dosages of B20.4-1-1

(Genentech, San Francisco, CA), which is a murine-compatible variation of the anti-VEGF antibody Bevacizumab. Combined, these two studies can help to define the effect of pro- and anti-angiogenic factor delivery on vascular response to injury in the rat Achilles tendon.

B. METHODS

B-1. Study Design

All procedures were performed in accordance to the University of Pennsylvania Institutional Animal Care and Use Committee. 56 Sprague Dawley rats were divided into two studies: (1) the evaluation of VEGF injection and (2) the evaluation of anti-VEGF antibody (B20) injection after tendon injury.

For the first study, 24 rats underwent unilateral Achilles tendon incisional injury, followed by bilateral intratendinous injections with 5μg rat recombinant VEGF-165 (VEGF, Peprotech, Rocky Hill, NJ) on either 0-2 days (early) or 4-6 days (late) post-injury. Color Doppler ultrasound imaging was performed on both injured and uninjured tendons on days 3, 7, 10, and 14 after injury, and animals were sacrificed at either day 7 or 14 for histological evaluation (n=4 tendons/group) (Figure 3.1).

For the second study, 32 rats underwent bilateral Achilles tendon incisional injury, followed by bilateral intratendinous injection with 50 (low), 250 (mid), or 500 μg (high) anti-VEGF antibody (B20.4-1-1, Genentech, San Francisco, CA) on days 4-6 post-injury. Color Doppler ultrasound was performed on days 7, 10, and 14 post-injury. Additionally, photoacoustic imaging was performed on days 7 and 14 after injury.

Animals were sacrificed at either day 7 or 14 for histological analysis (n=8 tendons/group) (Figure 3.2).

Day	0	1	2	3	4	5	6	7	8	9	10	11	12	13	14
Surgery		SAL						O							
		U						U			U				U	O
		Early VEGF						O							
		U						U			U				U	O
					Late VEGF			O							
								U			U				U	O

Figure 3.1: Study Design for the evaluation of VEGF delivery on vascular response after injury. "U" represents ultrasound imaging time points and "O" represents sacrifice for histological evaluation.

Day	0	1	2	3	4	5	6	7	8	9	10	11	12	13	14
Surgery					SAL			O							
								U			U				U	O
					Low B20			O							
								U			U				U	O
					Mid B20			O							
								U			U				U	O
					High B20			O							
								U			U				U	O

Figure 3.2: Study Design for the evaluation of anti-VEGF antibody (B20) delivery on vascular response after injury. "U" represents ultrasound imaging time points and "O" represents sacrifice for histological evaluation.

B-2. Surgical Approach

Animals were anesthetized with isoflurane inhalation and using aseptic technique a skin incision was made on the medial side of the ankle to isolate the Achilles tendon. Using a 1.5mm flat scalpel blade (#61, MYCO Medical, Apex, NC), a partial-width, full-thickness incisional injury was made in the center of the tendon in the mid-substance

region (Figure 3.3). The tendon was left unrepaired and the skin was sutured closed.
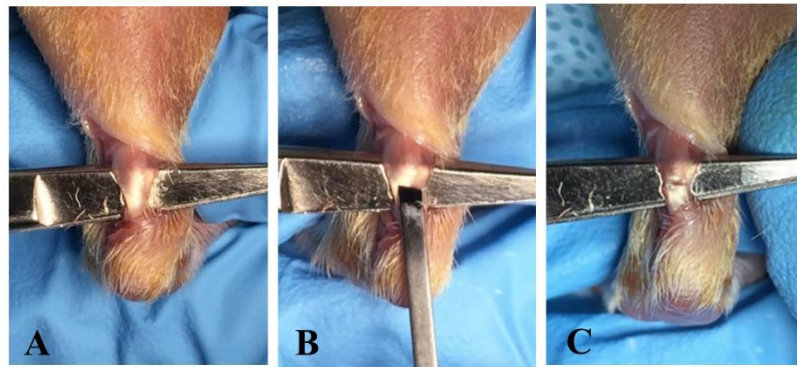
Figure 3.3: Surgical incisional injury of the rat Achilles tendon (A) during surgical exposure pre-injury, (B) with scalpel blade pictured, and (C) post-injury.

B-3. Angiogenic Injections

To evaluate pro-angiogenic factor delivery, 5µg VEGF in 20µl saline (or 20µl saline only as control) was injected bilaterally intratendinously on either days 0-2 (early) or 4-6 (late) after surgery. The dosage was determined based on previously reported results in tendon or ligament healing applications.[27, 56] To evaluate anti-angiogenic factor delivery, 50, 250, or 500µg B20 in 30µl saline was injected bilaterally intratendinously on days 4-6 after surgery (or 30µl saline as control). This range was determined based on the mid-range,[3, 15, 36, 42] lower,[1, 2, 14, 28, 32, 33, 46, 54] and upper[10-12, 24, 39, 53] limits for total systemic dosages found in the literature. All injections were administrated percutaneously in the coronal plane from the medial side of the tendon, with half of the solution injected above and half injected below the injury site.

B-4. Color Doppler Ultrasound Analysis

Imaging (n=4-8 tendons/group) was performed using a Vevo LAZR imaging

system (VisualSonics, Toronto, ON) with a 40 MHz center frequency transducer (LZ550). Following anesthetization using inhalation of isoflurane, all hair was removed from the left hind limb by shaving and hair removal cream to allow for ultrasound visualization. The animal was placed on a heated imaging table with the ankle secured at 90° flexion (Figure 3.4A). The transducer was placed to image the sagittal plane, ensuring that the tendon was parallel to the surface of the transducer, and the tendon length was in plane with the transducer length. The tendon was centered at a focal zone at 7mm image depth (Figure 3.4B). The mean color level (MCL: average blood flow velocity), the fractional area (FA: % area of Doppler signal), and the color weighted fractional area (CWFA: weighted average of blood flow velocity/unit area) were quantified over the entire tendon area and within a 3mm^2 rectangular area over the injury region (Figure 3.4B).[49] Image acquisition settings were held constant for all specimens. Measures for each image segment for a specimen were averaged to obtain a representative value of the entire tendon.
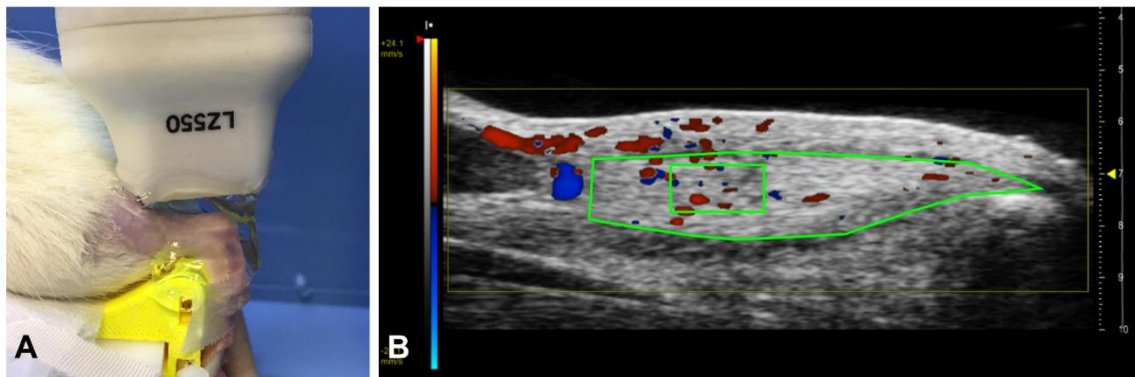
Figure 3.4: (A) Image of the ultrasound transducer positioned over the rat Achilles tendon. (B) Representative color Doppler image with tendon and injury regions of interest shown.

B-5. Photoacoustic Analysis

Photoacoustic imaging (n=6-8 tendons/group) was performed using the same transducer and positioning. Images were taken at two wavelengths (750 and 850 nm) based on the absorption spectrum of oxygenated (HbO_2) and deoxygenated hemoglobin (Hb), respectively (Figure 3.5A).[41] Three images were acquired within the center of the tendon (Figure 3.5B). Image acquisition settings were held constant for all specimens. Blood oxygenation (sO_2 Avg), average hemoglobin (HbT Avg), and relative tissue oxygenation (sO_2 Tot) were quantified over the entire tendon area and within a $3mm^2$ rectangular area over the injury region. Measures for all image segments for a specimen were averaged to obtain a representative value for the entire tendon.
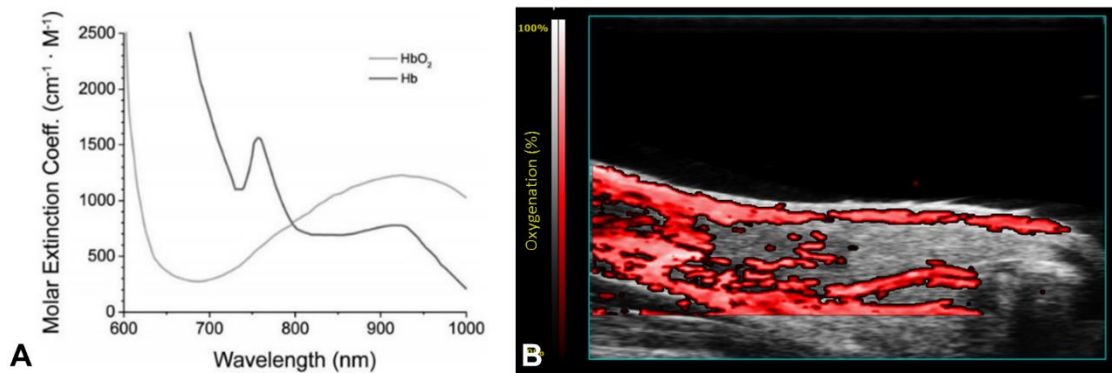
Figure 3.5: (A) Optical absorption spectra of oxygenated (HbO_2) and deoxygenated hemoglobin (Hb).[41] (B) Representative photoacoustics image of a rat Achilles tendon.

B-6. Tendon Histology

After sacrifice on days 7 and 14, Achilles tendons were dissected and processed (n=4-8 tendons/group. Sections were stained with hematoxylin-eosin (H&E) and graded by 3 blinded, independent graders for cell shape (1 = spindle to 3 = round) and cellularity

(1 = less cells to 3 = more cells). Additionally, sections underwent immunohistological staining for CD34, a vascular endothelial cell marker, and graded by 3 blinded, independent graders for vessel density (1 = less dense to 4 = more dense) and vessel size (1 = small diameter to 4 = large diameter).

B-7. Statistics

Ultrasound imaging measures were analyzed using Student's t-tests, and semi-quantitative histological measures were analyzed using Mann-Whitney t-tests. Significance was set at $p<0.05$ and trends at $p<0.1$, and all comparisons were made to saline control. Bar plots are displayed as mean and standard deviation and box plots are median and interquartile range.

C. RESULTS

C-1. Pro-Angiogenic Treatment

Color Doppler ultrasound for the uninjured tendon samples (Figure 3.6) was significantly increased for FA and CWFA at day 3 following VEGF injection. However, there were no changes to MCL, representing blood flow velocity, or changes at other time points.
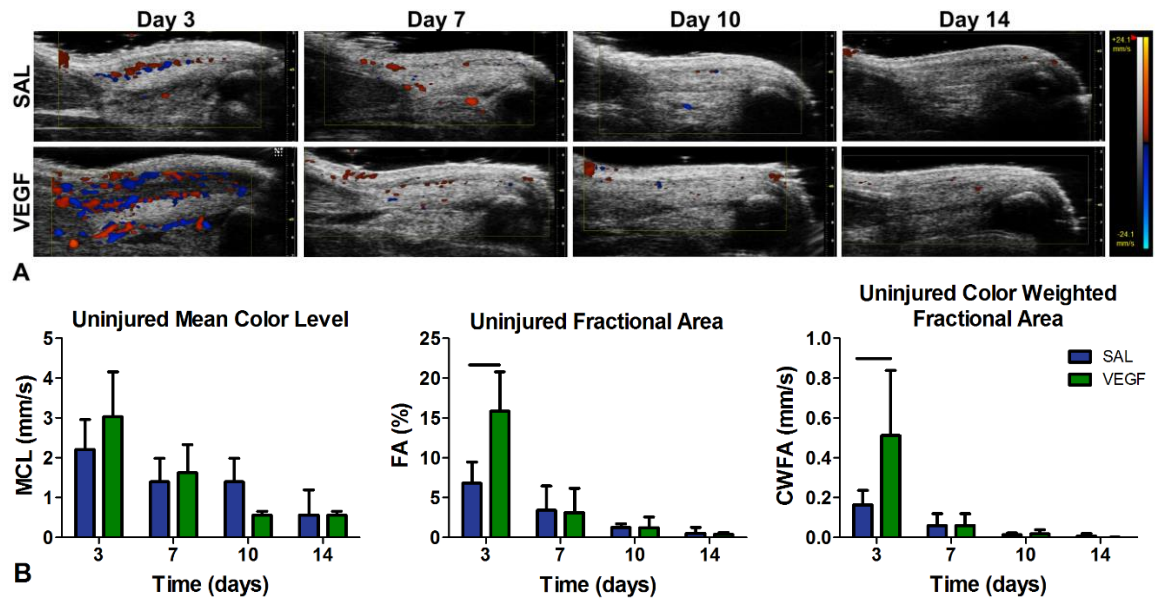
Figure 3.6: Color Doppler ultrasound for the uninjured Achilles tendon samples. (A) Representative images following VEGF injection. (B) Quantification of mean color level (MCL), fractional area (FA), and color weighted fractional area (CWFA) on days 3, 7, 10, and 14 after VEGF injection. FA and CWFA showed a significant increase in the VEGF group at day 3. Solid bars represent $p < 0.05$.

The injured tendons (Figure 3.7) also did not show a change in MCL, but showed significant increases in FA at days 7 and 14, and significant and trending increases in CWFA at days 7 and 14, respectively, in the late VEGF group. Additionally, there was a trend towards decreased FA and CWFA at day 14 in the early VEGF group.
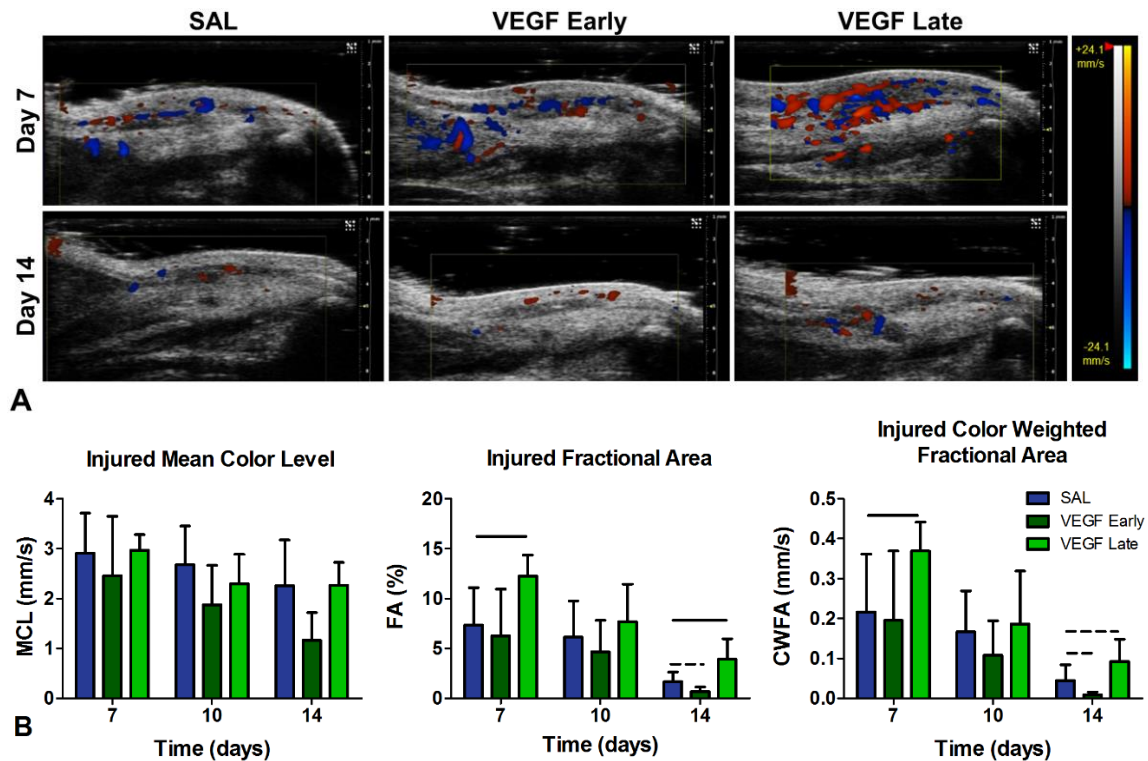
Figure 3.7: Color Doppler ultrasound for the injured Achilles tendon samples. (A) Representative images for days 7 and 14 following VEGF injection. (B) Quantification of mean color level (MCL), fractional area (FA), and color weighted fractional area (CWFA) on days 7, 10, and 14 after VEGF injection. FA and CWFA showed significant and trending increases in the late VEGF group at days 7 and 14. The early VEGF group had a trend towards decreased FA and CWFA at day 14. Solid bars represent $p<0.05$ and dashed bars represent $p<0.1$.

H&E histological evaluation (Figure 3.8) of early and late VEGF injection in the injured tendons had significantly more rounded cell shape in the late group at day 7, but no changes in cellularity. Neither measure had significant changes at day 14. For CD34 analysis of vascular structure (Figure 3.9), there was a trending increase in vessel density and a significant increase in vessel size in the late VEGF group at day 7. Similarly to H&E, these changes were not present by day 14.
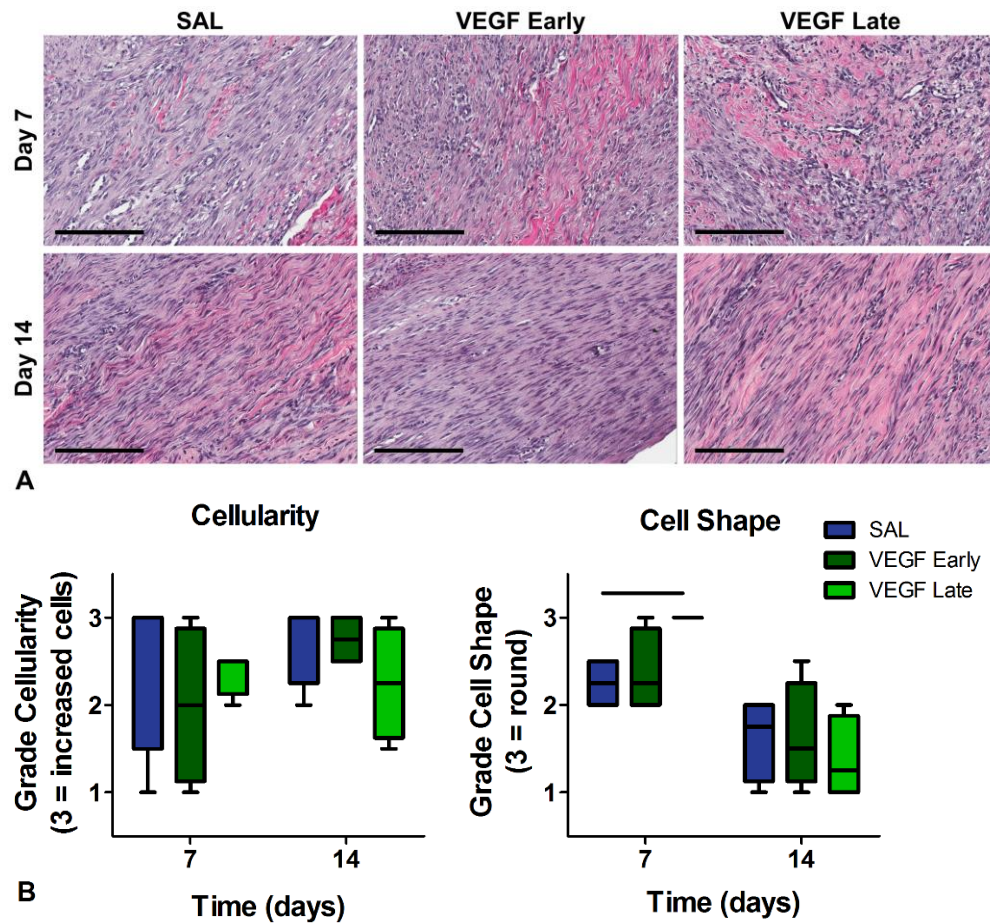
Figure 3.8: H&E staining for the VEGF study with (A) representative images for each group (scale bar 200µm) and (B) quantification of cellularity and cell shape. The late VEGF group had significantly more rounded cells at day 7. Solid bars represent $p < 0.05$.
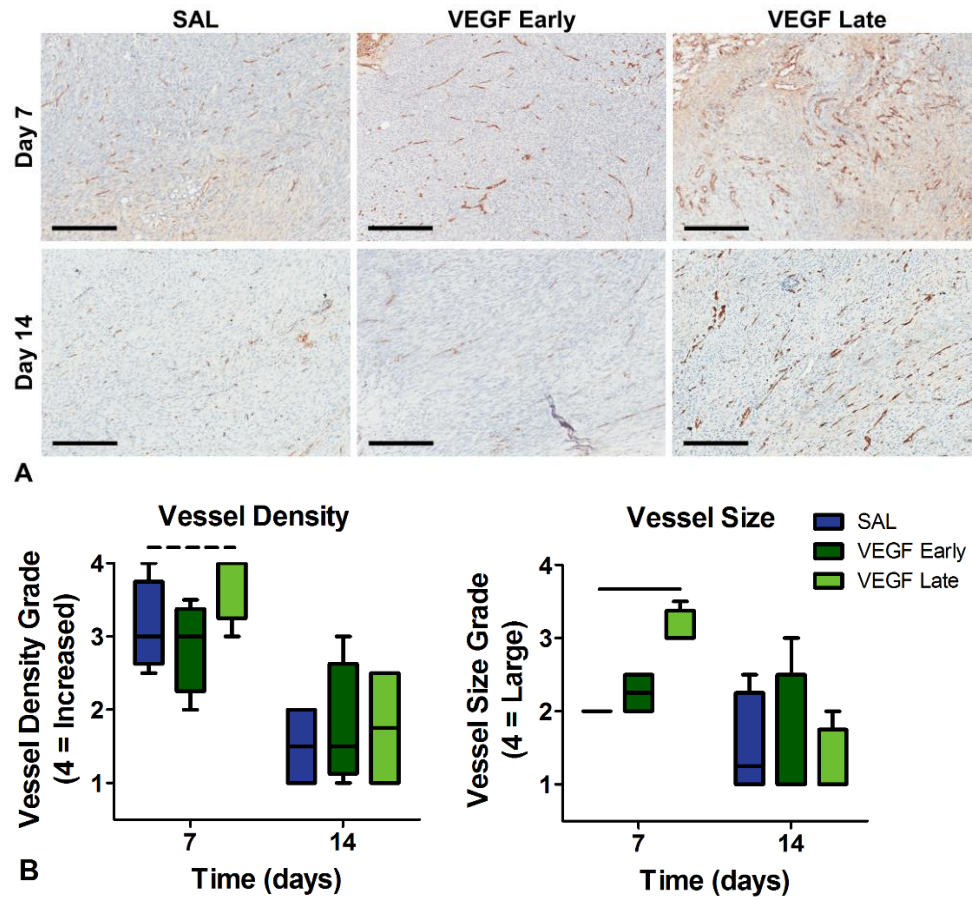
Figure 3.9: CD34 immunohistochemical staining for the VEGF study with (A) representative images for each group (scale bar 300μm) and (B) quantification of vessel density and size. The late VEGF group demonstrated a trending increase in vessel density and a significant increase in vessel size at day 7. Solid bars represent p<0.05 and dashed bars represent p<0.1.

C-2. Anti-Angiogenic Treatment

The evaluation of color Doppler ultrasound (Figure 3.10) revealed that the delivery of mid-dosage B20 caused a significant decrease in FA on days 7 and 10, and a trending and significant decrease in CWFA on days 7 and 10. Additionally, there was a significant increase in both FA and CWFA on day 14 in the low-dosage group. No differences were found in MCL for any group, and no differences were found for the high-dosage group.
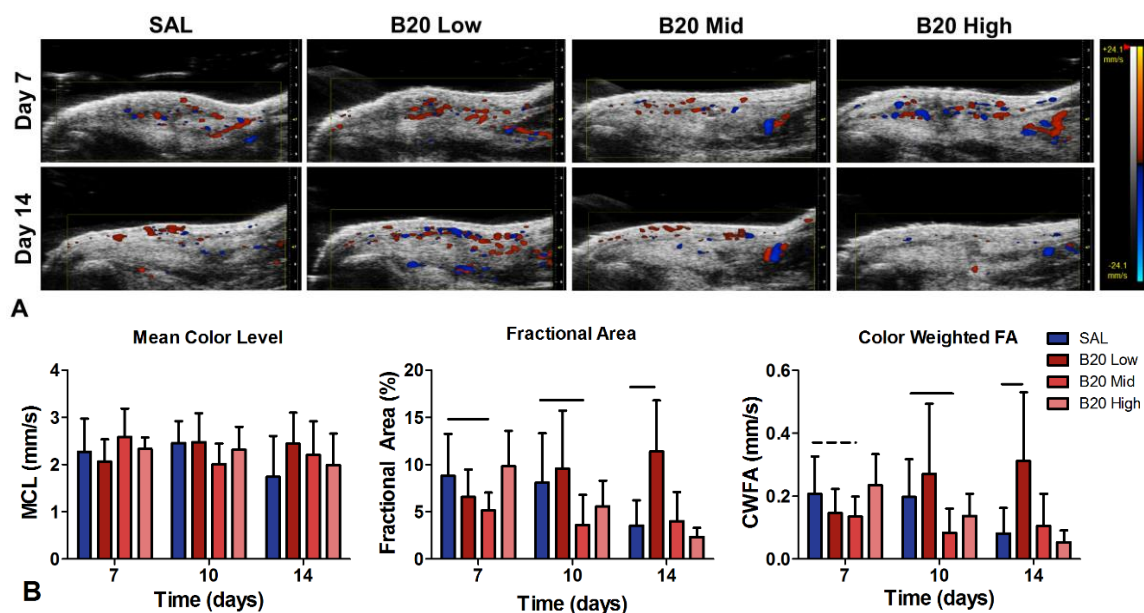
Figure 3.10: Color Doppler ultrasound of low (50μg), mid (250μg), and high (500μg) dose anti-VEGF antibody (B20). (A) Representative images at days 7 and 14 and (B) quantification of mean color level (MCL), fractional area (FA), and color weighted fractional area (CWFA). There were no differences in MCL, but significant and trending decreases in the mid group at days 7 and 10 in FA and CWFA. Also, there are significant increases in FA and CWFA with the low group at day 14. Solid bars represent $p<0.05$ and dashed bars represent $p<0.1$.

Photoacoustic imaging (Figure 3.11) demonstrated a significant decrease in both average hemoglobin (Hb Avg) and tissue oxygenation (sO_2 Total) at day 7 in the mid- and high-dosage groups. Additionally, the low-dosage group showed a trending decrease in Hb Avg at day 7. Conversely, on day 14 there was a significant increase in Hb Avg and sO_2 Total in the low- and mid-dosage groups. No groups showed changes in blood oxygenation (sO_2 Avg).
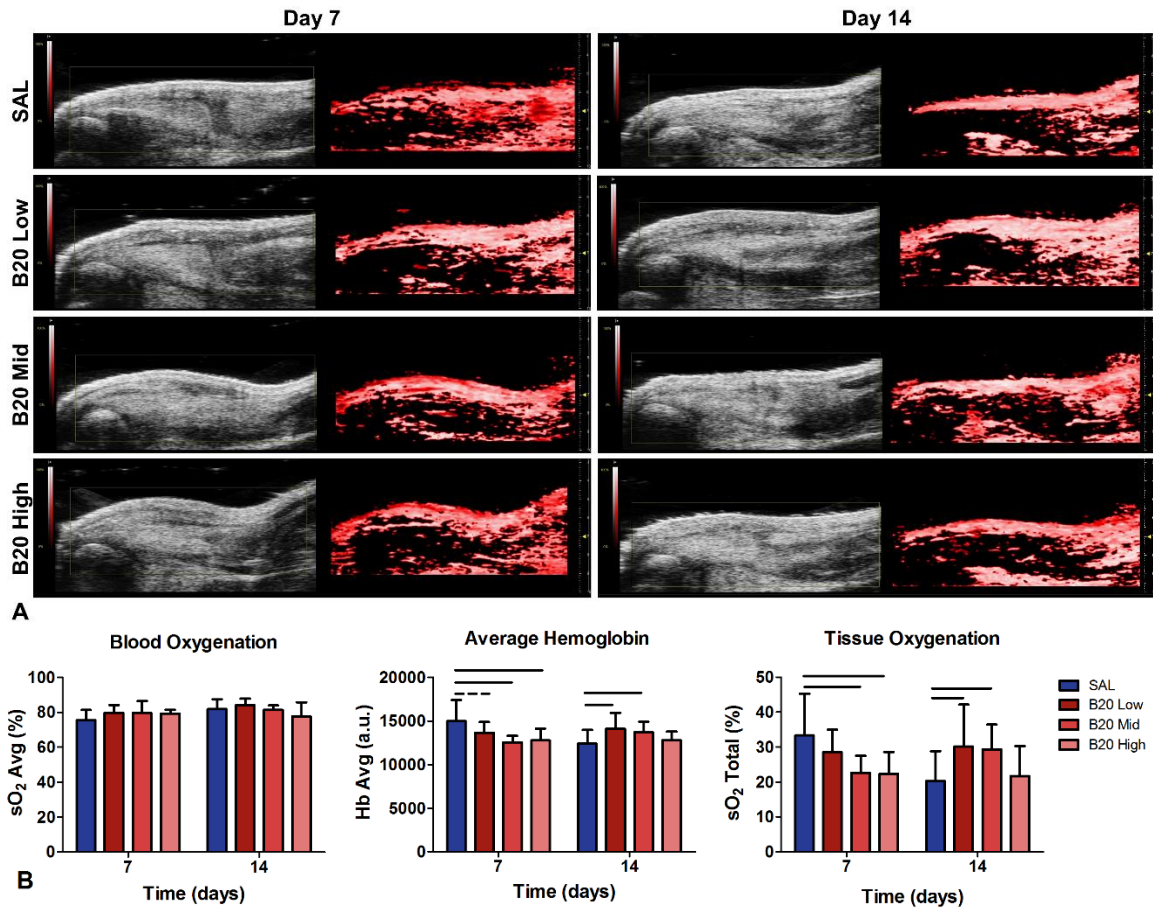
Figure 3.11: Photoacoustics imaging of low (50µg), medium (250µg), and high (500µg) dose anti-VEGF antibody (B20). (A) Representative images at days 7 and 14 and (B) quantification of blood oxygenation (sO$_2$ Avg), average hemoglobin (Hb Avg), and tissue oxygenation (sO$_2$ Total). There were no differences in sO$_2$ Avg, but significant decreases at day 7 in mid and high dosages and increases at day 14 in low and mid dosages for both Hb Avg and sO$_2$ Total. Solid bars represent $p < 0.05$ and dashed bars represent $p < 0.1$.

Finally, when evaluating histological measures of the mid-dosage group, there was no change in cell shape of cellularity at day 7 (Figure 3.12). However, there was a trending decrease in vessel size and a significant decrease in vessel density on day 7 in the mid-dosage group (Figure 3.13).
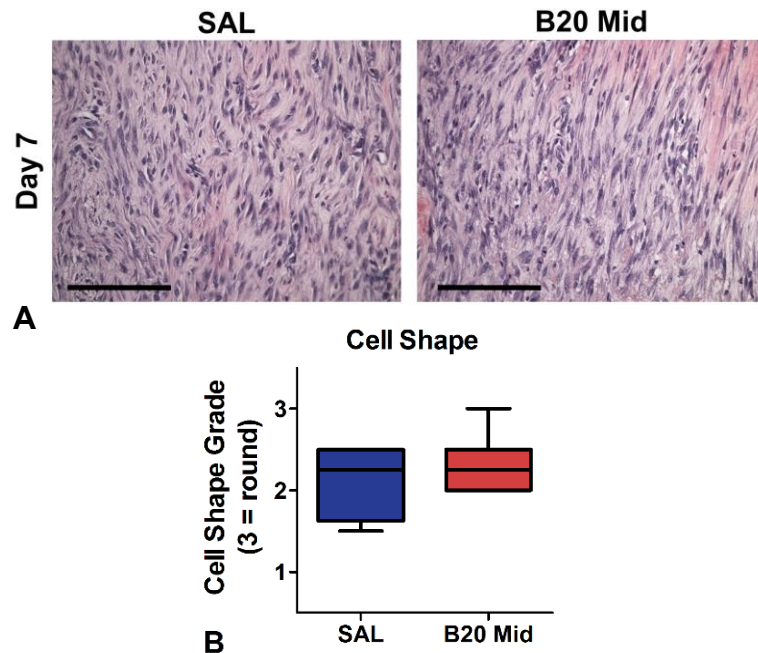
Figure 3.12: H&E histological analysis of B20 mid-dosage group. (A) Representative images at day 7 (scale bar 100µm) and (B) semi-quantification of cell shape (cellularity images too similar to form a grading scale). There were no significant differences in any group.
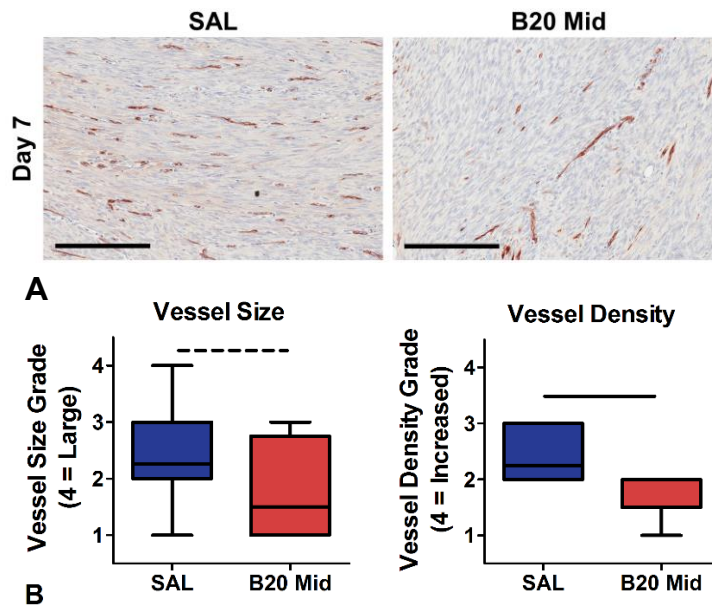
Figure 3.13: CD34 immunohistochemical analysis of B20 mid-dosage group. (A) Representative images of staining at day 7 (scale bar 200µm) and (B) semi-quantification of vessel size and vessel density. There was a trending decrease in vessel size and a significant decrease in vessel density. Solid bars represent $p<0.05$ and dashed bars represent $p<0.1$.

D. DISCUSSION

In this chapter, we investigated two studies evaluating the effect of VEGF and anti-VEGF antibody delivery on vascular response following injury. We demonstrated that the vascular response could be modulated through the delivery of these factors, and importantly that both dosage and timing of delivery had significant effects on the response.

In the first study, we chose a VEGF dosage previously found to induce vascular and healing outcome changes.[27, 56] To investigate the effect of VEGF delivery further, we evaluated how the timing of delivery might play a role in the tendon response. We first evaluated the effect of VEGF delivery on uninjured tendon, where there was a transient increase in vascularity at day 3 that recovered to control levels by day 7. When evaluating the injured tendons, the late VEGF group, with delivery during peak endogenous expression,[5] caused an increase in vessel size through histological analysis along with increased percent area of blood flow detected through Doppler ultrasound imaging. Additionally, this delivery time caused the cells to be more rounded, suggesting a more active cellular state. However, when VEGF was delivered early, prior to peak endogenous expression, there was no increase in vascular response and even a trend towards decreased vascularity by day 14 This suggests that the early delivery of VEGF could have shifted the VEGF expression, causing it to peak prior to our evaluation at day 7 and start to decline sooner, decreasing vascularity at later time points. While numerous studies have evaluated the effect of pro-angiogenic factor delivery on vascular response during healing, they all begin factor delivery immediately following injury, similar to our

early delivery group.[7-9, 16, 19, 27, 29, 30, 51, 55, 56] Although a subset of these studies have implemented an extended delivery duration for at least several days,[7, 8, 16, 19, 30, 51] to our knowledge there have been no studies evaluating the delayed delivery of pro-angiogenic factors in the context of wound healing. Additionally, the conclusions of this collective literature are not consistent regarding either the resulting vascular alterations induced through these angiogenic treatments, or their effect on healing capacity. Since we found that delaying the delivery of VEGF causes a more significant effect on vascular response than immediate delivery after injury, it is possible that the outcomes of this previous work could be altered with the implementation of different delivery times. The next two chapters in this dissertation will investigate this question for both early and late delivery times.

For the second study, we were interested in the effect of blocking naturally occurring VEGF expression, and so we decided to only evaluate the late delivery time for B20. The dosage for anti-angiogenic factors is not well characterized in the literature for direct injection, as they are primarily used as systemic drugs. Therefore, we chose to evaluate three different dosages of B20. We found that the dosage of B20 had a significant impact on the vascular response as measured by ultrasound and histological measures. It is worth noting that this is the first study to evaluate photoacoustic measures of vascularity in a tendon injury model, specifically at these wavelengths to measure oxygenation properties. Interestingly, the largest reduction in vascularity was achieved with the mid-dosage B20 group. Histological measures of vascular size and density at day 7 support the reduction in vascular signal seen in the ultrasound analyses. Surprisingly,

the high-dosage group had a minimal effect on altering vascularity, causing a decrease only in photoacoustic measures at day 7. Unlike the other dosage groups, the low-dosage group caused no significant changes at day 7 but a large increase in vascularity at day 14.

The reduced vascularity results of the mid-dosage group are similar to the responses described in tumor models with anti-VEGF antibody or tyrosine kinase inhibitor drug treatments.[13, 35, 45, 47] However, in this dosage group the vascular properties either return to baseline or increase compared to control by day 14. This could be explained by previous work where there was rapid vascular re-growth following reversal of VEGF inhibition in a tumor model.[35] This indicates that a decrease in vascularity may only be temporary, and that vascular density can recover after treatment stops. The data from the low dosage group could suggest that there may be a compensation effect, where a lower level of VEGF inhibition after injury may cause delayed or increased expression once the inhibitor is removed. Additionally, it appears that the degree to which the VEGF is blocked (dosage of B20) has an effect on the level of increased vascularity observed at the later time points, where the more it is blocked the less it is able to recover or increase after factor removal. Alternatively, it is possible that a temporary reduction in VEGF signaling could cause vascular normalization commonly observed in cancer research.[17, 26, 38, 45] Overexpression of VEGF can create abnormal vasculature that is leaky and tortuous,[40] and therefore blocking VEGF overexpression can cause remodeling of the vasculature so it is functionally and morphologically more normal and efficient, in effect increasing vascular perfusion properties.[26, 45] This effect could be dose dependent, and so it is possible that it may not occur with a larger dosage of VEGF inhibitor.

However, all of the literature describing this phenomenon is in the context of tumor growth and treatment, which likely has distinctly different characteristics from vascularity in tendon healing. There is a lack of research describing anti-angiogenic delivery in the context of tissue healing, and so further work needs to be completed to understand the mechanism for the immediate decrease and delayed increase in vascular response following delivery of anti-VEGF antibody.

This work is not without limitations. First, we only performed our saline injection for the VEGF group at the early delivery time. This decision was based on the assumption that, since saline is not bioactive, the effect of the needle puncture timing and saline delivery would be negligible compared to the magnitude of the surgical injury that would be performed. While the B20 study has a "late" saline control group, there are some differences between these two independent pilot studies that do not allow us to directly compare groups between the studies. The VEGF study implemented a unilateral injury with a bilateral injection, whereas the B20 study had a bilateral injury and injection. This was performed in order to evaluate the effect that VEGF had on uninjured tendons. While there was a transient effect at day 3, it was resolved by day 7 and therefore not further pursued in future studies. Also, since VEGF is not expressed in healthy tendons, the delivery of anti-VEGF antibody in uninjured tendons was not of interest. Therefore, to increase our sample size, we performed a bilateral injury for the B20 study. To address this issue of a proper late-group control, all experiments in the following chapters of this dissertation have associated control animals during each delivery time. Another limitation is that since our injury model is a central partial

rupture, it is not directly clinically relevant. However, this controlled injury model does not require surgical repair of the tendon or immobilization of the limb, which is important for the use of ultrasound imaging. Another limitation is the small sample size of both studies, and the use of bilateral limbs as separate specimens in the B20 study. These experiments were performed as a proof of principle that vascular response could be both increased and decreased with the delivery of angiogenic factors. We found significant changes with both of our studies, which means that the changes were large enough that we had sufficient power even with our small sample size to detect differences. Furthermore, in these studies, we did not perform mechanical evaluation of our tendons. This is because the goal was to first prove that we could induce vascular changes in our rat model of Achilles tendon injury. Mechanical evaluation requires a larger sample size and longer time points to fully evaluate healing outcome. Work described in the next chapters of this dissertation will evaluate the mechanical effect of the vascular changes induced here. An additional limitation is that only one dosage was evaluated with the VEGF delivery. This dosage was supported in the literature, and we found that it was able to induced changes in our late delivery model as well. However, since our sample size is small, we cannot conclude if the lack of changes observed in the early group is truly no change, or possibly just a smaller change not detected with these methods at this sample size. Since we are still interested in the question of timing of delivery, future work will continue to look into early and late delivery using more sensitive outcome measures and a larger sample size. Finally, we only evaluated H&E and CD34 in this study, and did not investigate extracellular matrix markers, inflammation, or structural

changes. This was because our goal was focused on evaluating vascular changes, but the following chapters of this dissertation will provide a more comprehensive histological evaluation.

Overall, this work provides a model system for altering the vascular response following injury in a rat Achilles tendon model. It also establishes that differences created through these pro- and anti- angiogenic modifications can be detected using both ultrasound and histological measures of vascularity. Work outlined in the next chapters will build on this study to comprehensively evaluate all of the functional, compositional, structural, and mechanical changes occurring due to this vascular modulation, as well as investigate the effect of vascular modulation on an aged population.

E. REFERENCES

1.   Abcouwer S.F., Lin C.M., Wolpert E.B., Shanmugam S., Schaefer E.W., Freeman W.M., Barber A.J. and Antonetti D.A. Effects of ischemic preconditioning and bevacizumab on apoptosis and vascular permeability following retinal ischemia-reperfusion injury. *Invest Ophthalmol Vis Sci* 2010; 51(11)**:** 5920-5933.

2.   Bakri S.J., Snyder M.R., Reid J.M., Pulido J.S. and Singh R.J. Pharmacokinetics of intravitreal bevacizumab (avastin). *Ophthalmology* 2007; 114(5)**:** 855-859.

3.   Barros L.F. and Belfort R., Jr. The effects of the subconjunctival injection of bevacizumab (avastin) on angiogenesis in the rat cornea. *An Acad Bras Cienc* 2007; 79(3)**:** 389-394.

4.   Battler A., Scheinowitz M., Bor A., Hasdai D., Vered Z., Di Segni E., Varda-Bloom N., Nass D., Engelberg S., Eldar M. and et al. Intracoronary injection of basic fibroblast growth factor enhances angiogenesis in infarcted swine myocardium. *J Am Coll Cardiol* 1993; 22(7)**:** 2001-2006.

5.   Boyer M.I., Watson J.T., Lou J., Manske P.R., Gelberman R.H. and Cai S.R. Quantitative variation in vascular endothelial growth factor mrna expression during early flexor tendon healing: An investigation in a canine model. *J Orthop Res* 2001; 19(5)**:** 869-872.

6.   Buckwalter J.A. and Hunziker E.B. Orthopaedics. Healing of bones, cartilages, tendons,

and ligaments: A new era. *Lancet* 1996; 348 Suppl 2**:** sII18.

7.   Chan B.P., Fu S., Qin L., Lee K., Rolf C.G. and Chan K. Effects of basic fibroblast growth factor (bfgf) on early stages of tendon healing: A rat patellar tendon model. *Acta Orthop Scand* 2000; 71(5)**:** 513-518.

8.   Chereddy K.K., Lopes A., Koussoroplis S., Payen V., Moia C., Zhu H., Sonveaux P., Carmeliet P., des Rieux A., Vandermeulen G. and Preat V. Combined effects of plga and vascular endothelial growth factor promote the healing of non-diabetic and diabetic wounds. *Nanomedicine* 2015; 11(8)**:** 1975-1984.

9.   Corral C.J., Siddiqui A., Wu L., Farrell C.L., Lyons D. and Mustoe T.A. Vascular endothelial growth factor is more important than basic fibroblastic growth factor during ischemic wound healing. *Arch Surg* 1999; 134(2)**:** 200-205.

10.   Dallaudiere B., Lempicki M., Pesquer L., Louedec L., Preux P.M., Meyer P., Hess A., Durieux M.H., Hummel V., Larbi A., Deschamps L., Benayoun Y., Journe C., Perozziello A., Schouman-Claeys E., Michel J.B. and Serfaty J.M. Acceleration of tendon healing using us guided intratendinous injection of bevacizumab: First pre-clinical study on a murine model. *Eur J Radiol* 2013; 82(12)**:** e823-828.

11.   Datta M., Via L.E., Kamoun W.S., Liu C., Chen W., Seano G., Weiner D.M., Schimel D., England K., Martin J.D., Gao X., Xu L., Barry C.E., 3rd and Jain R.K. Anti-vascular endothelial growth factor treatment normalizes tuberculosis granuloma vasculature and improves small molecule delivery. *Proc Natl Acad Sci U S A* 2015; 112(6)**:** 1827-1832.

12.   Davies S., Dai D., Pickett G., Thiel K.W., Korovkina V.P. and Leslie K.K. Effects of bevacizumab in mouse model of endometrial cancer: Defining the molecular basis for resistance. *Oncol Rep* 2011; 25(3)**:** 855-862.

13.   Denorme M., Yon L., Roux C., Gonzalez B.J., Baudin E., Anouar Y. and Dubessy C. Both sunitinib and sorafenib are effective treatments for pheochromocytoma in a xenograft model. *Cancer Lett* 2014; 352(2)**:** 236-244.

14.   Dinc E., Yildirim O., Necat Yilmaz S., Canacankatan N., Ayaz L., Ozcan T. and Temel G.O. Intravitreal bevacizumab effects on vegf levels in distant organs: An experimental study. *Cutan Ocul Toxicol* 2014; 33(4)**:** 275-282.

15.   Emami M.J., Jaberi F.M., Azarpira N., Vosoughi A.R. and Tanideh N. Prevention of arthrofibrosis by monoclonal antibody against vascular endothelial growth factor: A novel use of bevacizumab in rabbits. *Orthop Traumatol Surg Res* 2012; 98(7)**:** 759-764.

16.   Fayazzadeh E., Ahmadi S.H., Rabbani S., Boroumand M.A., Salavati A. and Anvari M.S. A comparative study of recombinant human basic fibroblast growth factor (bfgf) and erythropoietin (epo) in prevention of skin flap ischemic necrosis in rats. *Arch Iran Med* 2012; 15(9)**:** 553-556.

17.   Fukumura D. and Jain R.K. Tumor microvasculature and microenvironment: Targets for

anti-angiogenesis and normalization. *Microvasc Res* 2007; 74(2-3)**:** 72-84.

18.   Grenier N., Douws C., Perot V., Ferriere J.M. and Ravaud A. Combined radiofrequency ablation and antiangiogenic drug for the treatment of recurrent renal tumor. *Urology* 2009; 73(4)**:** 928 e911-922.

19.   Halici M., Karaoglu S., Canoz O., Kabak S. and Baktir A. Sodium hyaluronate regulating angiogenesis during achilles tendon healing. *Knee Surg Sports Traumatol Arthrosc* 2004; 12(6)**:** 562-567.

20.   Hall K. and Ran S. Regulation of tumor angiogenesis by the local environment. *Front Biosci (Landmark Ed)* 2010; 15**:** 195-212.

21.   Hendel R.C., Henry T.D., Rocha-Singh K., Isner J.M., Kereiakes D.J., Giordano F.J., Simons M. and Bonow R.O. Effect of intracoronary recombinant human vascular endothelial growth factor on myocardial perfusion: Evidence for a dose-dependent effect. *Circulation* 2000; 101(2)**:** 118-121.

22.   Henry T.D., Annex B.H., McKendall G.R., Azrin M.A., Lopez J.J., Giordano F.J., Shah P.K., Willerson J.T., Benza R.L., Berman D.S., Gibson C.M., Bajamonde A., Rundle A.C., Fine J. and McCluskey E.R. The viva trial: Vascular endothelial growth factor in ischemia for vascular angiogenesis. *Circulation* 2003; 107(10)**:** 1359-1365.

23.   Henry T.D., Rocha-Singh K., Isner J.M., Kereiakes D.J., Giordano F.J., Simons M., Losordo D.W., Hendel R.C., Bonow R.O., Eppler S.M., Zioncheck T.F., Holmgren E.B. and McCluskey E.R. Intracoronary administration of recombinant human vascular endothelial growth factor to patients with coronary artery disease. *Am Heart J* 2001; 142(5)**:** 872-880.

24.   Hollanders K., Van Bergen T., Van de Velde S., Sijnave D., Vandewalle E., Moons L. and Stalmans I. Bevacizumab revisited: Its use in different mouse models of ocular pathologies. *Curr Eye Res* 2015; 40(6)**:** 611-621.

25.   Hope M. and Saxby T.S. Tendon healing. *Foot Ankle Clin* 2007; 12(4)**:** 553-567, v.

26.   Jain R.K. Normalization of tumor vasculature: An emerging concept in antiangiogenic therapy. *Science* 2005; 307(5706)**:** 58-62.

27.   Ju Y.J., Tohyama H., Kondo E., Yoshikawa T., Muneta T., Shinomiya K. and Yasuda K. Effects of local administration of vascular endothelial growth factor on properties of the in situ frozen-thawed anterior cruciate ligament in rabbits. *Am J Sports Med* 2006; 34(1)**:** 84-91.

28.   Jung J.H., Lee J.H., Lee J.E. and Choi H.Y. Safety of bevacizumab on extraocular muscle in a rabbit model. *Korean J Ophthalmol* 2012; 26(4)**:** 290-296.

29.   Kaux J.F., Janssen L., Drion P., Nusgens B., Libertiaux V., Pascon F., Heyeres A., Hoffmann A., Lambert C., Le Goff C., Denoel V., Defraigne J.O., Rickert M., Crielaard

J.M. and Colige A. Vascular endothelial growth factor-111 (vegf-111) and tendon healing: Preliminary results in a rat model of tendon injury. *Muscles Ligaments Tendons J* 2014; 4(1)**:** 24-28.

30.   Kobayashi D., Kurosaka M., Yoshiya S. and Mizuno K. Effect of basic fibroblast growth factor on the healing of defects in the canine anterior cruciate ligament. *Knee Surg Sports Traumatol Arthrosc* 1997; 5(3)**:** 189-194.

31.   Kryger Z., Zhang F., Dogan T., Cheng C., Lineaweaver W.C. and Buncke H.J. The effects of vegf on survival of a random flap in the rat: Examination of various routes of administration. *Br J Plast Surg* 2000; 53(3)**:** 234-239.

32.   Lu F. and Adelman R.A. Are intravitreal bevacizumab and ranibizumab effective in a rat model of choroidal neovascularization? *Graefes Arch Clin Exp Ophthalmol* 2009; 247(2)**:** 171-177.

33.   Ma J., Zhu T., Tang X., Ye P. and Zhang Z. Effect of an intravitreal injection of bevacizumab on the expression of vegf and cd34 in the retina of diabetic rats. *Clin Exp Ophthalmol* 2010; 38(9)**:** 875-884.

34.   Magnan B., Bondi M., Pierantoni S. and Samaila E. The pathogenesis of achilles tendinopathy: A systematic review. *Foot Ankle Surg* 2014; 20(3)**:** 154-159.

35.   Mancuso M.R., Davis R., Norberg S.M., O'Brien S., Sennino B., Nakahara T., Yao V.J., Inai T., Brooks P., Freimark B., Shalinsky D.R., Hu-Lowe D.D. and McDonald D.M. Rapid vascular regrowth in tumors after reversal of vegf inhibition. *J Clin Invest* 2006; 116(10)**:** 2610-2621.

36.   Manzano R.P., Peyman G.A., Khan P. and Kivilcim M. Testing intravitreal toxicity of bevacizumab (avastin). *Retina* 2006; 26(3)**:** 257-261.

37.   Matsumoto S., Saito K., Takakusagi Y., Matsuo M., Munasinghe J.P., Morris H.D., Lizak M.J., Merkle H., Yasukawa K., Devasahayam N., Suburamanian S., Mitchell J.B. and Krishna M.C. In vivo imaging of tumor physiological, metabolic, and redox changes in response to the anti-angiogenic agent sunitinib: Longitudinal assessment to identify transient vascular renormalization. *Antioxid Redox Signal* 2014; 21(8)**:** 1145-1155.

38.   McGee M.C., Hamner J.B., Williams R.F., Rosati S.F., Sims T.L., Ng C.Y., Gaber M.W., Calabrese C., Wu J., Nathwani A.C., Duntsch C., Merchant T.E. and Davidoff A.M. Improved intratumoral oxygenation through vascular normalization increases glioma sensitivity to ionizing radiation. *Int J Radiat Oncol Biol Phys* 2010; 76(5)**:** 1537-1545.

39.   Nagai T., Sato M., Kobayashi M., Yokoyama M., Tani Y. and Mochida J. Bevacizumab, an anti-vascular endothelial growth factor antibody, inhibits osteoarthritis. *Arthritis Res Ther* 2014; 16(5)**:** 427.

40.   Nagy J.A., Vasile E., Feng D., Sundberg C., Brown L.F., Detmar M.J., Lawitts J.A., Benjamin L., Tan X., Manseau E.J., Dvorak A.M. and Dvorak H.F. Vascular

permeability factor/vascular endothelial growth factor induces lymphangiogenesis as well as angiogenesis. *J Exp Med* 2002; 196(11)**:** 1497-1506.

41.   Needles A., Heinmiller A., Sun J., Theodoropoulos C., Bates D., Hirson D., Yin M. and Foster F.S. Development and initial application of a fully integrated photoacoustic micro-ultrasound system. *IEEE Trans Ultrason Ferroelectr Freq Control* 2013; 60(5)**:** 888-897.

42.   Okada Y., Akisue T., Hara H., Kishimoto K., Kawamoto T., Imabori M., Kishimoto S., Fukase N., Onishi Y. and Kurosaka M. The effect of bevacizumab on tumour growth of malignant fibrous histiocytoma in an animal model. *Anticancer Res* 2010; 30(9)**:** 3391-3395.

43.   Ozcan A.A., Ciloglu E., Esen E. and Simdivar G.H. Use of topical bevacizumab for conjunctival intraepithelial neoplasia. *Cornea* 2014; 33(11)**:** 1205-1209.

44.   Pandya N.M., Dhalla N.S. and Santani D.D. Angiogenesis--a new target for future therapy. *Vascul Pharmacol* 2006; 44(5)**:** 265-274.

45.   Peng F., Xu Z., Wang J., Chen Y., Li Q., Zuo Y., Chen J., Hu X., Zhou Q., Wang Y., Ma H., Bao Y. and Chen M. Recombinant human endostatin normalizes tumor vasculature and enhances radiation response in xenografted human nasopharyngeal carcinoma models. *PLoS One* 2012; 7(4)**:** e34646.

46.   Romano M.R., Biagioni F., Besozzi G., Carrizzo A., Vecchione C., Fornai F. and Lograno M.D. Effects of bevacizumab on neuronal viability of retinal ganglion cells in rats. *Brain Res* 2012; 1478**:** 55-63.

47.   Scharf V.F., Farese J.P., Coomer A.R., Milner R.J., Taylor D.P., Salute M.E., Chang M.N., Neal D. and Siemann D.W. Effect of bevacizumab on angiogenesis and growth of canine osteosarcoma cells xenografted in athymic mice. *Am J Vet Res* 2013; 74(5)**:** 771-778.

48.   Schumacher B., Pecher P., von Specht B.U. and Stegmann T. Induction of neoangiogenesis in ischemic myocardium by human growth factors: First clinical results of a new treatment of coronary heart disease. *Circulation* 1998; 97(7)**:** 645-650.

49.   Sehgal C.M., Arger P.H., Silver A.C., Patton J.A., Saunders H.M., Bhattacharyya A. and Bell C.P. Renal blood flow changes induced with endothelin-1 and fenoldopam mesylate at quantitative doppler us: Initial results in a canine study. *Radiology* 2001; 219(2)**:** 419-426.

50.   Tempfer H. and Traweger A. Tendon vasculature in health and disease. *Front Physiol* 2015; 6**:** 330.

51.   Wang B., Cheheltani R., Rosano J., Crabbe D.L. and Kiani M.F. Targeted delivery of vegf to treat myocardial infarction. *Adv Exp Med Biol* 2013; 765**:** 307-314.

52.   Woo S.L., Debski R.E., Zeminski J., Abramowitch S.D., Saw S.S. and Fenwick J.A.

Injury and repair of ligaments and tendons. *Annu Rev Biomed Eng* 2000; 2**:** 83-118.

53.   Xiao L., Yan K., Yang Y., Chen N., Li Y., Deng X., Wang L., Liu Y., Mu L., Li R., Luo M., Ren M. and Wu J. Anti-vascular endothelial growth factor treatment induces blood flow recovery through vascular remodeling in high-fat diet induced diabetic mice. *Microvasc Res* 2016; 105**:** 70-76.

54.   Xu W., Wang H., Wang F., Jiang Y., Zhang X., Wang W., Qian J., Xu X. and Sun X. Testing toxicity of multiple intravitreal injections of bevacizumab in rabbit eyes. *Can J Ophthalmol* 2010; 45(4)**:** 386-392.

55.   Yoshikawa T., Tohyama H., Katsura T., Kondo E., Kotani Y., Matsumoto H., Toyama Y. and Yasuda K. Effects of local administration of vascular endothelial growth factor on mechanical characteristics of the semitendinosus tendon graft after anterior cruciate ligament reconstruction in sheep. *Am J Sports Med* 2006; 34(12)**:** 1918-1925.

56.   Zhang F., Liu H., Stile F., Lei M.P., Pang Y., Oswald T.M., Beck J., Dorsett-Martin W. and Lineaweaver W.C. Effect of vascular endothelial growth factor on rat achilles tendon healing. *Plast Reconstr Surg* 2003; 112(6)**:** 1613-1619.

CHAPTER 4: EFFECT OF VASCULAR MODULATION ON ACHILLES TENDON HEALING IN AN ADULT RAT INJURY MODEL

A. INTRODUCTION

Tendons are relatively hypovascular tissues that become hypervascular during both injury and degeneration. This is due to the angiogenic response, or the formation of new blood vessels, to tissue injury. Blood vessels have numerous roles within tissues to facilitate the healing process, including the delivery of oxygen and nutrients, the removal of waste products, the transport of regulatory factors, and the control of the immune response.[14] While angiogenesis is a necessary component to tendon healing, prolonged hypervascularization following tendon injury is not always believed to be beneficial.[36] As seen in various vascular diseases an imbalance of pro- and anti-angiogenic factors could promote abnormal angiogenesis creating vessels with structural and functional deficits. These deficits can cause inflammation, inefficient nutrient exchange, and potentially hypoxia despite increased vessel density.[14] Conversely, it is possible that the angiogenic response following tendon injury is not sufficient and that increasing vascular formation could promote a more robust healing response.[38] Therefore, there is uncertainty regarding the balance of angiogenic processes in the progression of tendon healing.[11]

There has been promising research investigating the use of angiogenic factor delivery for tendon or ligament applications. However, while these studies show distinct alterations in vascularity, the effect on healing outcome is unclear.[3, 6, 15, 16, 18, 37, 38] Additionally, in the previous chapter we found that the delivery of vascular endothelial

growth factor (VEGF) and anti-VEGF antibody (B20) can alter the vascular response after injury in a rat Achilles tendon model in a dose- and time-dependent manner.[31] Specifically, we found that the late delivery of VEGF (days 4-6 after injury) causes significant increases in Doppler ultrasound parameters and histological measures of vascularity, where no changes were detected with early (days 0-2 after injury) administration. Additionally, a mid-range dosage of B20 caused a decrease in vascular properties measured by Doppler ultrasound, photoacoustic imaging, and histological measures. While this work proves that tendon vascularity can be altered through the delivery of these factors, it does not comprehensively evaluate all of the vascular, compositional, functional, and mechanical changes that occur with this modification to the injury response. Additionally, since Doppler ultrasound is only capable of detecting relatively large vessels, it is possible that the early delivery group may undergo more subtle vascular changes that requre more sensitive measurements. Finally, this previous work did not evaluate the effect of altering timing of delivery for the B20 group. Therefore, since it is unknown how increasing or decreasing vascularity will affect healing outcome, we are interested in investigating both early and late delivery of both pro- and anti-angiogenic factors.

In order to fully understand how these angiogenic treatments are altering the vascular response after injury in the tendon, there is a need for imaging methodologies that can longitudinally evaluate multiple vascular characteristics. We have previously used color Doppler ultrasound and photoacoustics imaging, which are able to evaluate blood flow velocity, blood oxygenation, and percent area of detected blood flow. However, while these measures provide unique and important information they are only sensitive to larger

vascular changes. To overcome this limitation, non-linear contrast-enhanced ultrasound can be implemented to provide more sensitive measures of both time- and amplitude-based measures of tissue perfusion.[24]

Therefore, the objective of this study was to evaluate the effect of vascular modulation in rat Achilles tendons during healing using multiple *in vivo* ultrasound imaging modalities, *in vivo* functional assessment, and *ex vivo* measures of tendon compositional and mechanical properties. We hypothesize that reducing the vascular response will result in reduced scar tissue formation and reduced mechanical properties, while increasing the vascular response will result in the opposite. Further, we hypothesize that *in vivo* gait and joint functional measures will not be significantly impacted by vascular changes.

B. METHODS

B-1. Study Design

90 Fischer 344 rats (4 months old, IACUC approved) underwent a bilateral Achilles incisional injury, followed by local injections of vascular endothelial growth factor (VEGF) (Peprotech, Rocky Hill, NJ), anti-VEGF antibody (B20.4-1-1, Genentech, San Francisco, CA), or saline (SAL). *In vivo* functional assessments and ultrasound imaging were performed and animals were sacrificed at 7, 14, and 28 days after injury for histological and mechanical evaluation.

Week

Group			0	1	2	3	4
Adult	**Early**	Surgery	**B20**	O			
			F	F F	F X		
			U	U	U	U	U X
			SAL	O			
			F	F F	F X		
			U	U	U	U	U X
			VEGF	O			
			F	F F	F X		
			U	U	U	U	U X
	Late	Surgery	**B20**	O			
			F	F F X			
			U	U	U	U X	
			SAL	O			
			F	F F X			
			U	U	U	U X	
			VEGF	O			
			F	F F X			
			U	U	U	U X	

Figure 4.1: Study Design for the effect of vascular modulation on tendon healing in adult animals. "F" represents functional joint and ambulation measures, "U" represents ultrasound imaging, "O" represents sacrifice for histological and biological assays only, and "X" represents sacrifice for mechanical, histological, and biological assays.

B-2. Surgical Approach

All procedures were performed in accordance to the University of Pennsylvania Institutional Animal Care and Use Committee. Animals were anesthetized with isoflurane inhalation and using aseptic technique a full thickness, partial-width incisional injury was made in the center of the tendon width in the mid-substance region as described in Chapter 3 Section B-2.

B-3. Angiogenic injections

On days 0-2 (early) or 4-6 (late) after surgical injury, each animal received 5µg VEGF in 20µl saline, 250µg anti-VEGF antibody (B20) in 20µl saline, or 20µl saline only injected bilaterally intratendinously. These dosages were chosen based on literature values[1, 8, 15, 22, 26, 38] and the findings from Chapter 3 Sections C-1 and C-2. The injections were administrated percutaneously in the coronal plane from the medial side of the tendon, with 10µl of the solution injected above and 10µl injected below the injury site.

B-4. Ultrasound Imaging

Imaging was performed on days 3 (early only), 7, 14, 21, and 28 (n=12/group) post-injury using a Vevo LAZR ultrasound system (VisualSonics, Toronto, ON). Following anesthetization using inhalation of isoflurane, all hair was removed from the left hind limb by shaving and hair removal cream to allow for ultrasound visualization. The animal was placed on a heated imaging table with the ankle secured at 90° flexion. The transducer was placed to image the sagittal plane, ensuring that the tendon was parallel to the surface of the transducer and the tendon length was in plane with the transducer length. The tendon was centered at a focal zone at 7mm image depth.

<u>B-mode Alignment Analysis:</u> B-mode images were taken at a center frequency of 40MHz (MS550D transducer) with an effective resolution of 40µm for collagen alignment analysis as previously described in Chapter 2 Section B-3.[30] A motorized scanner used for 3D imaging was attached to the ultrasound transducer to allow for consecutive sagittal images to be taken every 0.1 mm over a range of 3.5 mm (tendon width < 3mm). Image

acquisition settings were held constant for all specimens. The central 5 images were analyzed using a custom Matlab program (Mathworks, Natick, MA). Briefly, tendon collagen fascicles appear hyperechoic, whereas the noncollagenous matrix between the fascicles appears hypoechoic, giving rise to the appearance of bands in the images.[13] These bands are analyzed to determine a quantitative measure of tendon organization by detecting the angles of the fibers throughout the region of interest and calculating the circular standard deviation of the angles (Figure 4.2). Specifically, the ultrasound images were first filtered to remove any small particles and reduce background noise. A matrix convolution was then used to apply a linear kernel over groups of pixels in the filtered image at varying angles (0 deg–180 deg in 5 deg increments). A power series function was fit to the intensity versus angle data (least squares curve-fit) and used to determine the angle with maximum intensity and therefore the fiber direction. In addition, any regions in which the confidence intervals for the parameters of the power series fit were too high were masked. The circular standard deviation (CSD), a measure of the distribution of collagen alignment, and echogenicity measures were calculated over the entire tendon area as well as within a 3mm^2 rectangular area over the injury region. Measures for each image segment for a specimen were averaged to obtain a value representative of the entire tendon thickness.
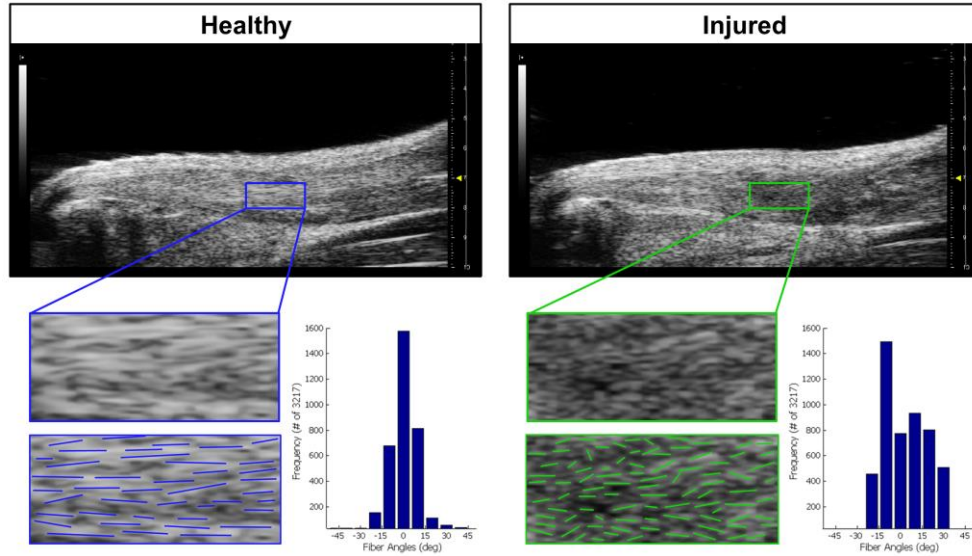
Figure 4.2: Schematic demonstrating differences in the striation patterning between healthy and injured tendon under ultrasound imaging. The image processing algorithm can detect the angle of the fibers and calculate the circular standard deviation of the fiber angles. Note that a lower circular standard deviation (as seen in the healthy tissue) indicates more aligned collagen fibers.

Color Doppler Ultrasound Analysis: Imaging and analysis were performed similar to what was described in Chapter 3 Section B-4. Spatially sequential color Doppler ultrasound images were acquired using the 3D motorized scanner every 0.1mm across the tendon over a range of 3.5mm. Image acquisition settings were held constant for all specimens, and imaging persistence was used to remove any motion artifact from the 3D motorized scanner. The central 8-10 tendon images were analyzed using a custom IDL program (Harris Geospatial Solutions, Herndon, VA). The mean color level (average blood flow velocity), fractional area (% area of Doppler signal), and color weighted fractional area (weighted average of blood flow velocity/unit area) were quantified over the entire tendon area and within a 3mm^2 rectangular area over the injury region.[34] Measures for

each image segment for a specimen were averaged to obtain a representative value for the entire tendon.

Photoacoustic analysis: As described in Chapter 3 Section B-5, images were taken at two wavelengths (750 and 850 nm)[25] within the center of each tendon. Blood oxygenation (sO$_2$ Avg), average hemoglobin (HbT Avg), and relative tissue oxygenation (sO$_2$ Tot) were quantified over the entire tendon area and within a 3mm^2 rectangular area over the injury region. Measures for all image segments for a specimen were averaged to obtain a representative value for the entire tendon.

Contrast-Enhanced Ultrasound analysis: Following anesthetization a tail vein catheter was inserted and secured. The Achilles tendon was visualized in non-linear contrast mode using the MS250 transducer (18MHz center frequency). The ultrasound video clip was initiated at start of the bolus injection of 100µl of Definity (Lantheus Medical Imaging, Billerica, MA) microbubble contrast agent, followed immediately by a bolus injection of 200µl of saline. The video clip was taken for 200 seconds to capture the wash-in and wash-out of the contrast in the tissue (Figure 4.3A).

The nonlinear contrast ultrasound clip was loaded into a contrast analysis program, VevoCQ (VisualSonics, Toronto, ON).[24] A region of interest ROI was traced around the entire tendon area and any motion artifact was removed using the VevoCQ motion stabilization tool. Perfusion of the contrast agent was quantified for each frame of the clip. Briefly, the video data was converted into echo-power data (linearization), which is a quantity directly proportional to the instantaneous concentration of contrast agent at each

location in the ROI. This echo-power data as a function of time is processed using a curve-fitting algorithm (eq. 1) for a parametric perfusion model (Figure 4.3B, Table 4.1).[24]
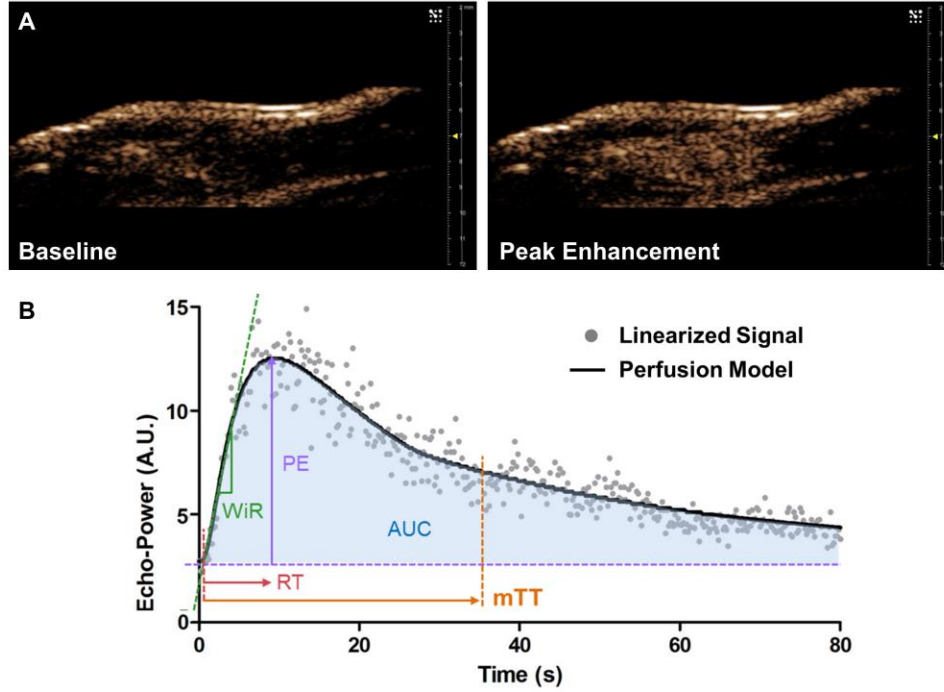
Figure 4.3: (A) Representative images of baseline and peak enhancement frames from the non-linear contrast-enhanced ultrasound clip. (B) Schematic of the echo-power vs time plot from contrast data and associated parameters derived from the perfusion model fitted curve.

$$f(t) = 0 + AUC \frac{1}{st\sqrt{2\pi}} e^{-\frac{(\ln(t)-m)^2}{2s^2}} \tag{1}$$

Where

$$m = \ln(mTT) - \frac{s^2}{2} \tag{2}$$

Table 4.1: Description of variables in the perfusion model

Variable	Definition	Unit
f(t)	Best-fit function of echo-power	[a.u., dB]
t	Time variable	[s]
m	Mean of logarithm of t	[s]
s	Standard deviation of logarithm of t	[s]
AUC	Area under the curve to infinite time	[a.u.]
mTT	Mean transit time	[s]
O	Offset amplitude	[a.u.]

Perfusion parameters can then be derived from this model as defined by Table 4.2.[24] They can be divided into three general categories: amplitude, time, and a combination of amplitude and time. All amplitude-based parameters are expressed as relative echo-power measures, such as peak enhancement. Time-based parameters are expressed in seconds and define the kinetics of the contrast flowing through the tissue, such as rise time or mean transit time. Finally, combined amplitude- and time-based parameters can describe measurements related to blood flow, such as perfusion index.

Table 4.2: Perfusion parameters derived from the fitted curve model

Abbreviation	Parameter Name	Definition	Unit
PE	Peak Enhancement	Difference between maximum amplitude and offset baseline (proportional to relative blood volume)	[a.u.]
AUC	Area Under the Curve	Area under the curve to infinite time	[a.u.]
mTT	Mean Transit Time	Average amount of time for blood to pass through a region of tissue	[s]
WiAUC	Wash-in Area Under the Curve	Area under the curve up to the point that PE is reached	[a.u.]
RT	Rise Time	Time to go from baseline to PE	[s]
WiR	Wash-in Rate	Maximum slope of the fitted bolus function (proportional to local blood flow rate)	[a.u.]
WiPI	Wash-in Perfusion Index	WiAUC/RT	[a.u.]
PI	Perfusion Index	AUC/mTT	[a.u.]

B-5. Gait Analysis

Hindlimb gait distances and ground reaction forces were measured in the day 14 animals (n=12/group) using an instrumented walkway[32] before injury and at 3 (early only), 7, 10, and 14 days post-injury. For each measurement, ground reaction force data

(medial/lateral, braking, propulsion, and vertical forces), paw placement data (stride width and length), and ambulation timing data (speed, rate of loading, and stance time) were acquired (Figure 4.4). All parameters were averaged across walks on a given day for each animal, and all force data was normalized to the body weight of each animal at each time point. Data was collected using a custom LabVIEW program (National Instruments, Austin, TX) and parameters of ankle function were analyzed using a custom MATLAB program (MathWorks, Inc., Natick, MA).
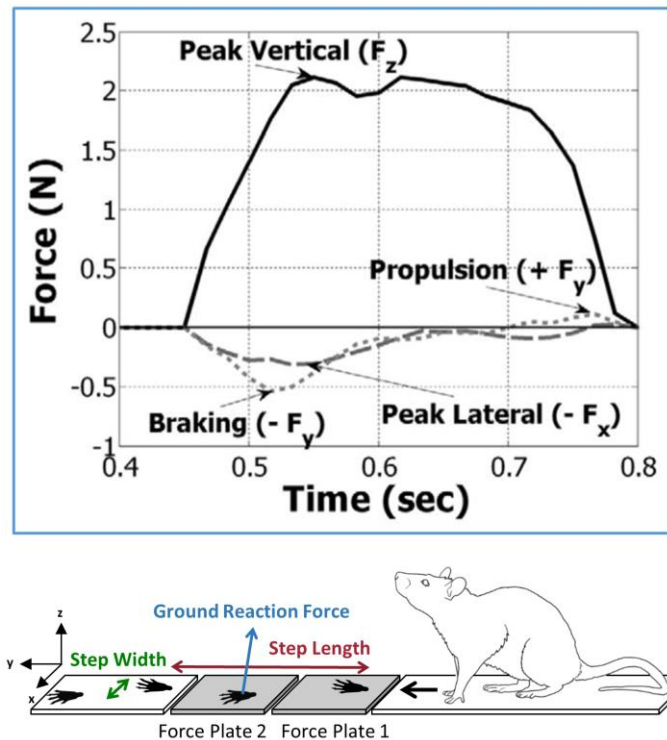
Figure 4.4: Diagram of gait analysis set-up with a representative ground reaction force curve. The force plates have 6-degrees of freedom, to measure the vertical (z), propulsion/breaking (y), and medial/lateral (x) forces for an isolated hindlimb step. The step width, step length, and stride length can also be measured. This figure was modified from Sarver et al.[32]

B-6. Passive Ankle Mechanics

Passive functional ankle joint properties[33] (n = 12/group) were measured before injury and at 3 (early only), 7, 10 and 14 days after injury. Animals were anesthetized and their hind leg placed in a rotating clamp with their ankle at 90 degrees flexion. A torque was applied to the ankle for four plantar- and dorsi-flexion rotation cycles. Torque cutoffs (plantar flexion, 25 N·mm; dorsiflexion, 35 N·mm) were employed to ensure that a consistent range of torques was analyzed for all animals. Range of motion was determined by averaging the difference between the minimum and maximum angles. To calculate joint stiffness, the data from the last three cycles of each animal was pooled and the toe and linear regions of a bilinear fit of the torque-angle data were defined for both dorsiflexion and plantar flexion (Figure 4.5). All analyses were performed using custom MATLAB software (MathWorks, Inc., Natick, MA).
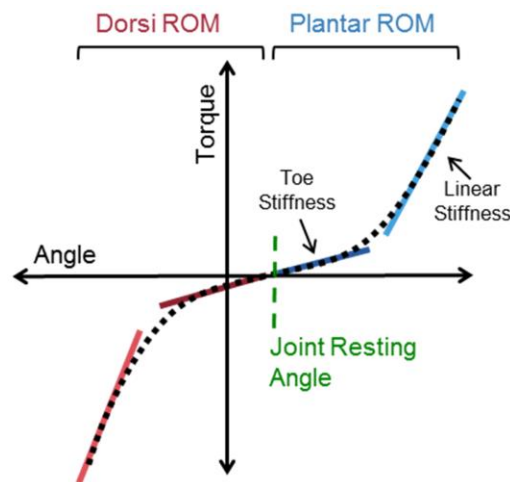
Figure 4.5: Representative curve depicting the full ankle range of motion (ROM) through dorsi- and plantarflexion. The joint resting angle is defined at the zero torque point, and the toe and linear stiffness can be calculated through a bilinear fit of each segment of the curve.

B-7. Tendon Histology

Tendon samples from 7, 14, and 28 days post-injury (n=6/group) were dissected, paraffin processed, and sectioned at 5μm in the sagittal plane. Sections were stained with hematoxylin-eosin (H&E) and immunohistochemical (IHC) staining for vascular endothelial cell marker (CD34), angiopoietin-1 (Ang-1), vascular endothelial growth factor (VEGF), collagen type III (Col III), tumor necrosis factor alpha (TNFα), and matrix metallopeptidase-13 (MMP-13). Processing protocol details are outlined in Table 4.3.

Table 4.3: Immunohistochemistry Protocols

Primary Antibody	Antigen Retrieval	Secondary Ab/Amplification
Rabbit **Anti-CD34** (Abcam, ab81289)	Heat Induced at 75°C for 20min in 1mM EDTA, pH 8.0	Vectastain Elite ABC HRP Kit (Vector Laboratories, PK-6200)
Rabbit **Anti-Ang1** (Abcam, ab102015)	Heat Induced at 95°C for 10min in 10mM Sodium Citrate, pH 6.0	Vectastain Elite ABC HRP Kit (Vector Laboratories, PK-6200)
Rabbit **Anti-VEGF** (Abcam, ab46154)	Digestion in 0.5mg/mL Hyaluronidase for 60min at 37°C	EnVision+ HRP labelled polymer solution (Dako, K4002)
Mouse **Anti-Col III** (Sigma-Aldrich, C7805)	Digestion in 0.4mg/mL protease K in 30mM Tris HCl for 4 min at RT, 0.5mg/mL Hyaluronidase for 60 min at 37°C, and 0.5N acetic acid for 4hr at 4°C	Secondary (BD Biosciences, 550331), ABC amplification (Vector Laboratories, PK-6200)
Rabbit **Anti-TNFα** (Novus Biologics, NBP1-19532)	Digestion in 0.5 mg/ml Pepsin in 0.1N HCl for 20 min at RT	Secondary (Jackson Co. 111-035-003)
Rabbit **Anti-MMP13** (Abcam, ab39012)	Digestion in 0.5mg/mL Hyaluronidase for 60min at 37°C	Secondary (BD Sciences, 550338), ABC amplification (vector laboratories, PK-6200).

Histology images were taken in the injury region of the tendon at 50x magnification for CD34 (in order to better view vascular structure) and 100x magnification for all other stains. H&E and CD34 were semi-quantitatively graded by three blinded investigators.

H&E was graded for cell shape (1=spindle to 3=round shape) and cellularity (1=less cells to 3=more cells), and CD34 was graded for vessel density (1=less to 4=more dense) and vessel size (1=small to 4=large diameter). All other IHC stains were quantitatively analyzed for percent area of positive stain using a custom MATLAB program (Mathworks, Natick, MA). Briefly, the image is first cropped to remove any sectioning or staining artifact that should not be included in the analysis. Then a cluster analysis is performed to separate out blue (hematoxylin cell nuclei), white (slide or tissue background), and brown (DAB positive stain) colors. The threshold values can be adjusted for each of these three clusters in order to include only positive brown DAB staining. The percent area of positive stain is then calculated based on the total area of the region of interest selected in the image.

B-8. Tendon Mechanics

Tendons from 14 and 28 days post-injury (n=12/group) were prepared for tensile testing. The Achilles tendon was removed with the muscle and foot attached. The tendon was fine dissected to remove all connective tissue leaving the calcaneus insertion and foot intact. Verhoeff stain lines were applied at the insertion, 12mm from the insertion to mark the grip length, and bordering the top and bottom of the injury region. Verhoeff stain dots were applied to the rest of the tendon for optical strain measurement. Tendon cross-sectional area was measured using a custom laser-based device.[12] The proximal side of the tendon was fixed between two layers of sandpaper using cyanoacrylate adhesive at the 12mm stain line. The entire foot was secured in polymethylmethacrylate up to the base of the calcaneal insertion. The specimen was attached between two fixtures so that the foot

and the tendon were oriented perpendicular, and submerged in a 37°C phosphate-buffered saline bath. The tendon was tested in tension using an ElectroPuls E3000 (Instron, Norwood, MA) with a 250N load cell. The mechanical protocol consisted of (1) preloading (0.15N), (2) preconditioning (0.5% to 1.5% strain at 0.25Hz for 30 cycles), (3) stress-relaxation (6% strain for 10 minutes), (4) a dynamic frequency sweep (0.125% strain amplitude at 0.1, 1, 5, and 10 Hz, for 10 cycles each), and (5) ramp to failure (0.1% strain/sec) (Figure 4.6).
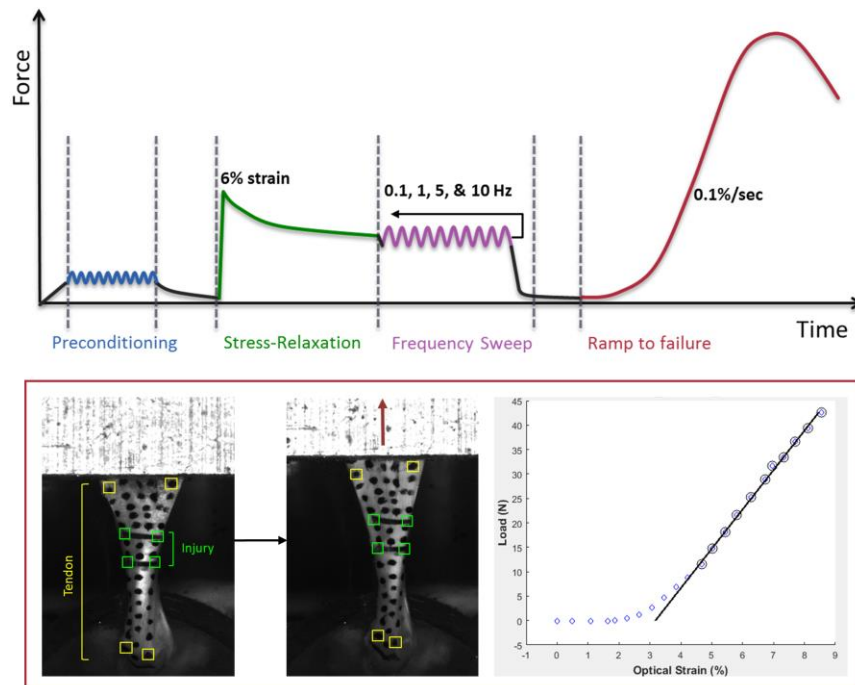
Figure 4.6: Schematic of the mechanical testing protocol with preconditioning (30 cycles), stress-relaxation (6% strain), frequency sweep (10 cycles at 0.1, 1, 5, & 10 Hz), and ramp to failure (0.1%/sec). The lower panel shows a representative image of the stained Achilles tendon with stain lines bordering the injury site and examples of 4 points used for tendon and injury region tracking. Finally, an example curve created from optical tracking where the linear region can be defined.

Images for optical strain measures were captured. Tendon viscoelastic and dynamic properties of percent relaxation, dynamic modulus ($|E^*|$), and the tangent of the phase shift

between stress and strain (tan(δ)) were computed. Quasi-static properties were determined

from the slope of the linear region of the force vs. displacement (stiffness) or stress vs.

strain (elastic modulus) curves, as well as from failure properties (max force, displacement,

and stress).

B-9. Statistics

Normally distributed data was analyzed using a 1-way ANOVA followed by

Bonferroni multiple comparisons post-hoc tests with all comparisons made to saline control

within a time point. Non-normally distributed data was analyzed using Kruskal-Wallis 1-

way ANOVA followed by Dunn's multiple comparison post-hoc tests with comparisons

made to saline control within a time point. To adjust for multiple comparisons, significance

was set at $p \leq 0.025$ (indicated by solid bars) and trends at $p \leq 0.05$ (indicated by dashed bars).

Bar plots are displayed as mean and standard deviation and box plots represent median and

interquartile range.

C. RESULTS

C-1. Late Delivery of Angiogenic Factors

A subset of this work was previously published in a conference abstract for the

2018 Orthopaedic Research Society annual meeting in New Orleans, LA.[29]

Ultrasound Analysis: For the color Doppler ultrasound imaging (Figure 4.7A), we

evaluated the mean color level (MCL) representing blood flow velocity, fractional area

(FA) which is the percent area of signal in the region of interest (ROI), and color weighted

fractional area (CWFA) which is the blood flow velocity weighted by the percent area of signal. All parameters were evaluated in the entire tendon and injury region ROIs. The B20 group had a decrease in MCL at day 14 in the full tendon and injury site (Figure 4.7B,E), but an increase in the tendon at day 21 (Figure 4.7B). Similarly, there was a decrease in FA (Figure 4.7C,F) and CWFA (Figure 4.7D,G) in the this group in both ROIs at 7 days and the tendon at 14 days, but an increase in these properties at day 21 in the whole tendon (Figure 4.7C,D).

For the VEGF group, FA was significantly decreased at day 7 in the injury region (Figure 4.7F). Additionally, the MCL (in both ROIs) and FA and CWFA (in the full tendon) had significant and trending increases at day 21 (Figure 4.7B-D), as well as increases in the injury site FA and CWFA at day 28 (Figure 4.7F,G).

Photoacoustics imaging revealed a trending increase in blood oxygenation in the B20 group at day 21 in the tendon and day 28 in the injury region (Figure 4.8B,E). There were no significant changes in average hemoglobin in either region (Figure 4.8C,F). Finally, there was a trending increase in the full tendon tissue oxygenation level at day 28 in the B20 group (Figure 4.8D).
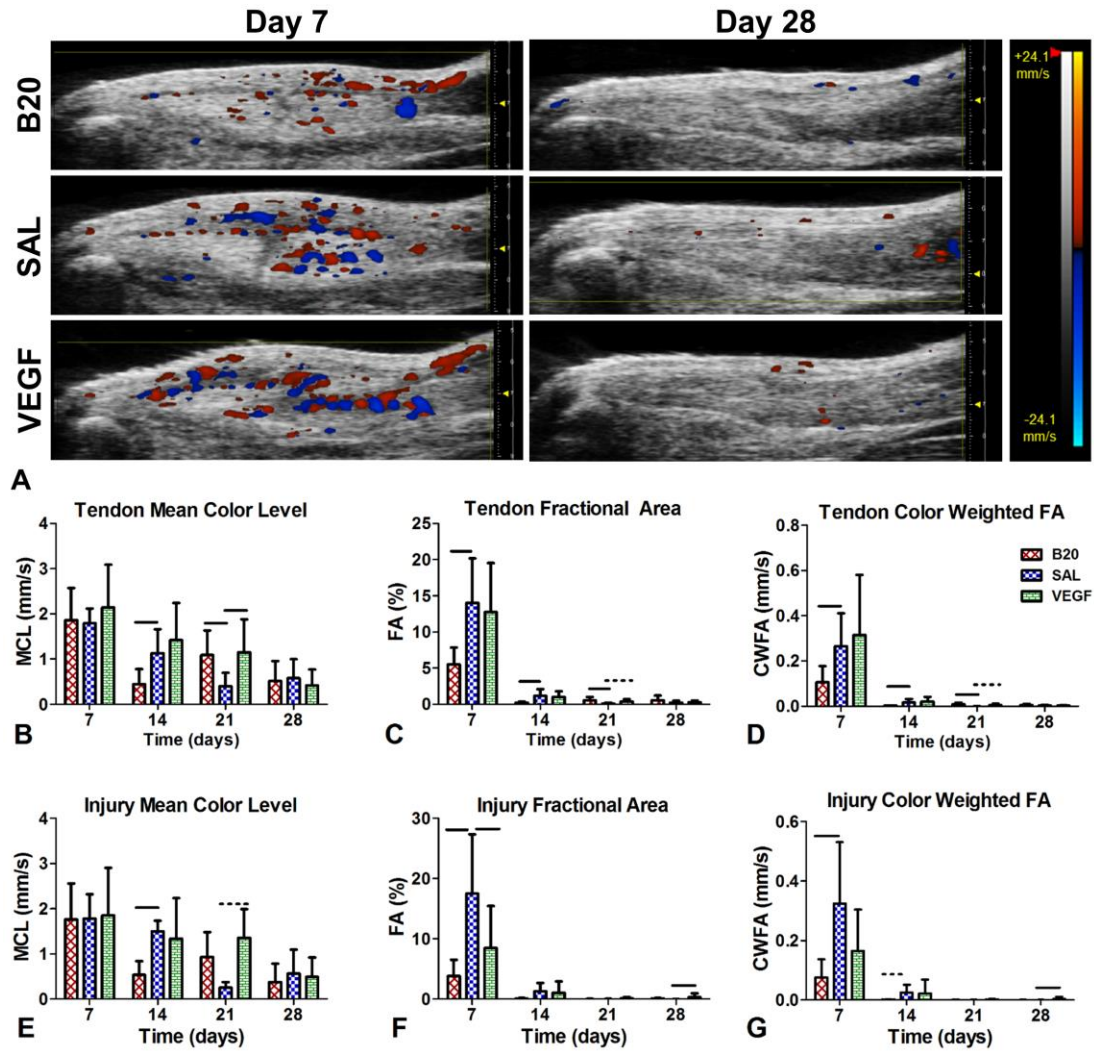
Figure 4.7: (A) Representative images for late delivery color Doppler ultrasound results and quantification of the (B-D) tendon ROI and the (E-G) injury ROI. (B,E) Mean color level (MCL) represents blood flow velocity, (C,F) fractional area (FA) represents the percent area of the ROI where blood flow was detected, and (D,G) color weighted fractional area (CWFA) is the weighted average of the blood flow velocity by the percent area of signal (MCL*FA). The delivery of B20 generally causes decreases in vascular properties at early time points, with increases at later time points. VEGF shows the largest increase at day 21.
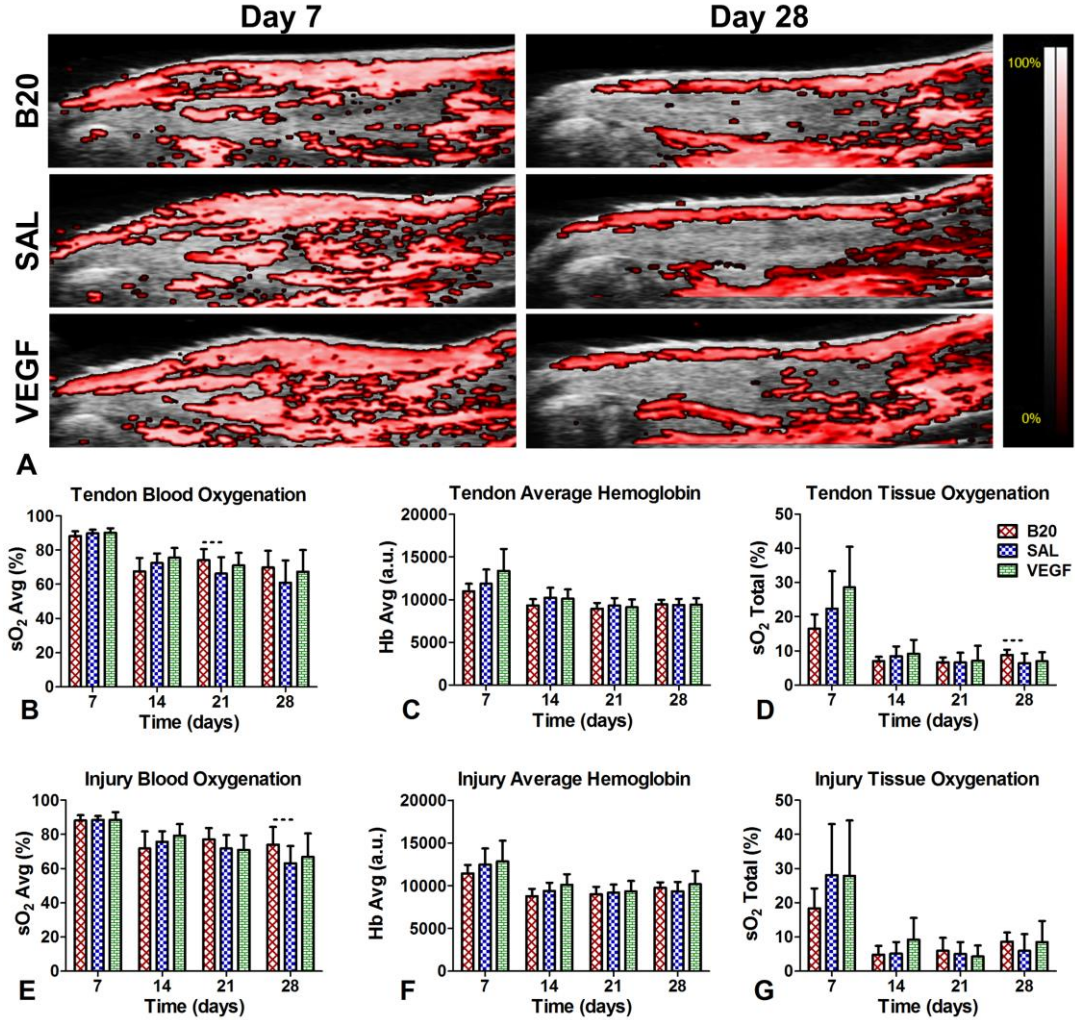
Figure 4.8: (A) Representative images for late delivery photoacoustics imaging results and quantification of the (B-D) tendon ROI and the (E-G) injury ROI. (B,D) Blood oxygenation (sO_2 Avg) represents the oxygenation level of the hemoglobin that is detected, (C,F) average hemoglobin (Hb Avg) represents the average amount of hemoglobin detected total weighted by the ROI area, and (D,G) tissue oxygenation (sO_2 Total) represents the oxygenation weighted by the percent of the ROI area where hemoglobin was detected. While there were no significant differences, B20 shows trending increases in oxygenation level.

For the evaluation of non-linear contrast-enhanced ultrasound imaging, the parameters can be divided into amplitude-based, time-based, and a combination of amplitude and time. The amplitude-based are peak enhancement (PE) and full curve and

wash-in area under the curve (AUC, WiAUC). The time-based parameters are rise time

(RT), mean transit time (mTT), and wash-in rate (WiR).   Finally, the combination

parameters are full curve and wash-in perfusion index (PI, WiPI).
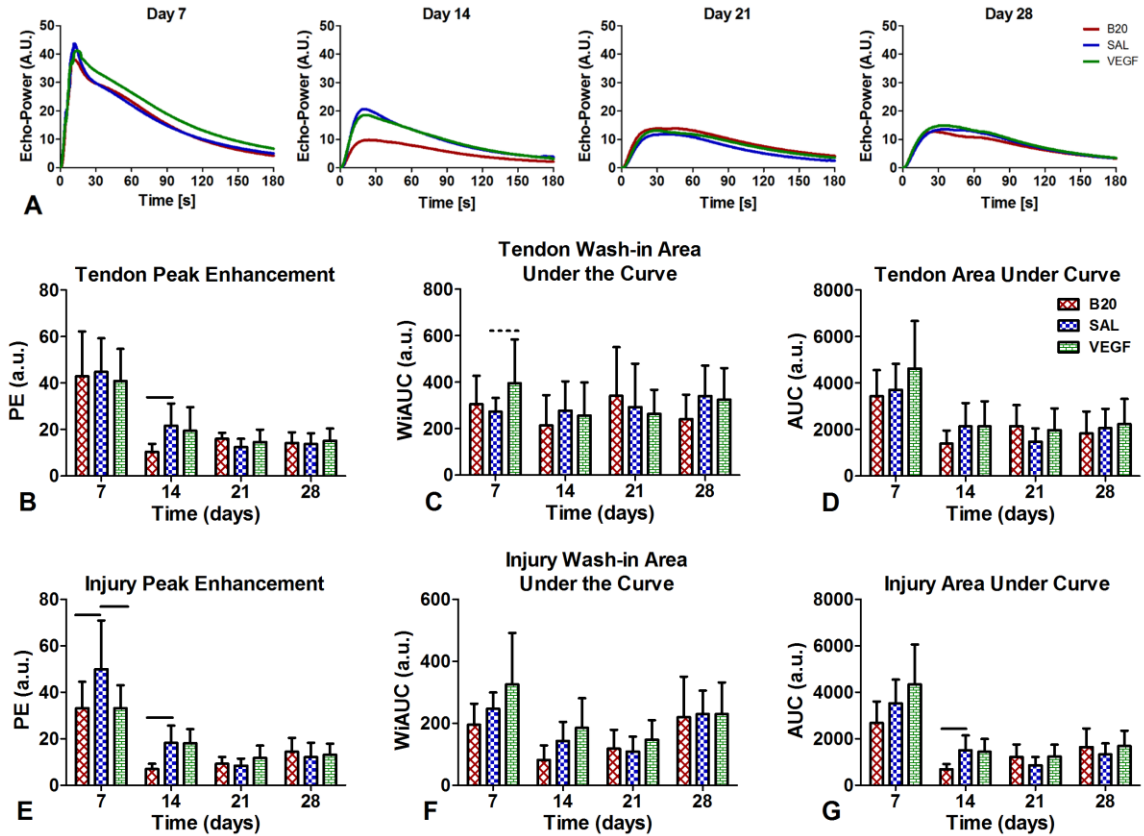
Figure 4.9: (A) Averaged curves for echo-power vs time contrast-enhanced ultrasound late-delivery group data. Amplitude-based parameters measured in the tendon (B-D) and injury (E-G) ROIs. (B,E) Peak enhancement (PE), (C,F) wash-in area under the curve (WiAUC), (D,G) area under the curve (AUC). Delivery of B20 causes the largest reduction in vascular parameters at day 14, which can also be visualized in the average curves in panel A.

All parameters were evaluated for the whole tendon and the injury region. For the

amplitude-based parameters, the B20 group demonstrated a decrease in PE at day 14 in

both ROIs (Figure 4.9B,E), and a decrease at day 7 in the injury ROI (Figure 4.9E).

Additionally, there was a decrease in injury site AUC at day 14 (Figure 4.9G). The VEGF group had decreased PE in the injury ROI (Figure 4.9E) and a trend towards increased WiAUC in the tendon ROI (Figure 4.9C) at day 7.

When evaluating time-based contrast parameters, there was an increase in RT in the VEGF group at days 7 and 14 in the injury (Figure 4.10D), and a trending increase at day 7 in the tendon (Figure 4.10A). Additionally, there was a significant increase in mTT at day 21 in both ROIs (Figure 4.10B,E), but in contrast, a decrease in mTT at day 14 in the injury ROI (Figure 4.10E). Finally, VEGF had a decrease in WiR in the injury at day 7 (Figure 4.10F).

The B20 group RT increased at day 14 and then decreased at day 28 in the injury ROI, with a trending decrease at day 28 in the full tendon (Figure 4.10A,D). Finally, there was a trending and significant decrease in WiR at day 7 and 28, respectively, in the injury region, and a significant decrease at day 14 in both ROIs (Figure 4.10C,F).

Contrast-enhanced ultrasound combined amplitude and time parameters demonstrated significant or trending decreases in both WiPI and PI in the B20 group at day 14 in both ROIs (Figure 4.11), with the injury site also demonstrating a decrease at day 7 in WiPI (Figure 4.11C). There was also a trending decrease in the VEGF group at day 7 in the injury region (Figure 4.11C).

116
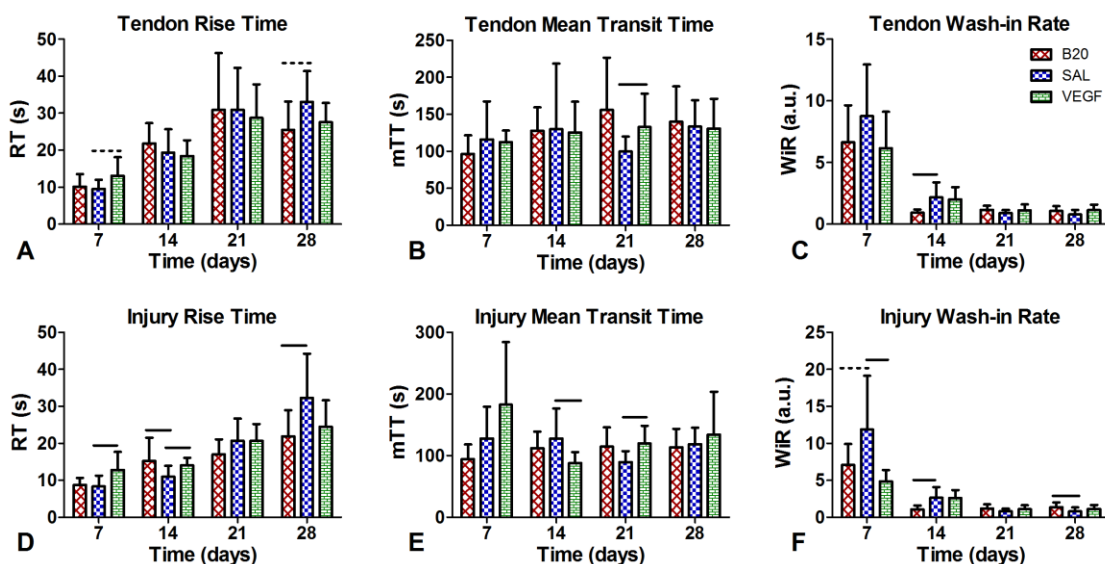
Figure 4.10: Late delivery contrast-enhanced ultrasound time-based parameters measured in the tendon (A-C) and injury (D-F) ROIs. (A,D) Rise time (RT), (B,E) mean transit time (mTT), (C,D) wash-in rate (WiR). Overall, the VEGF group generally increased perfusion time, while the B20 group decreased the wash-in rate at early time points.
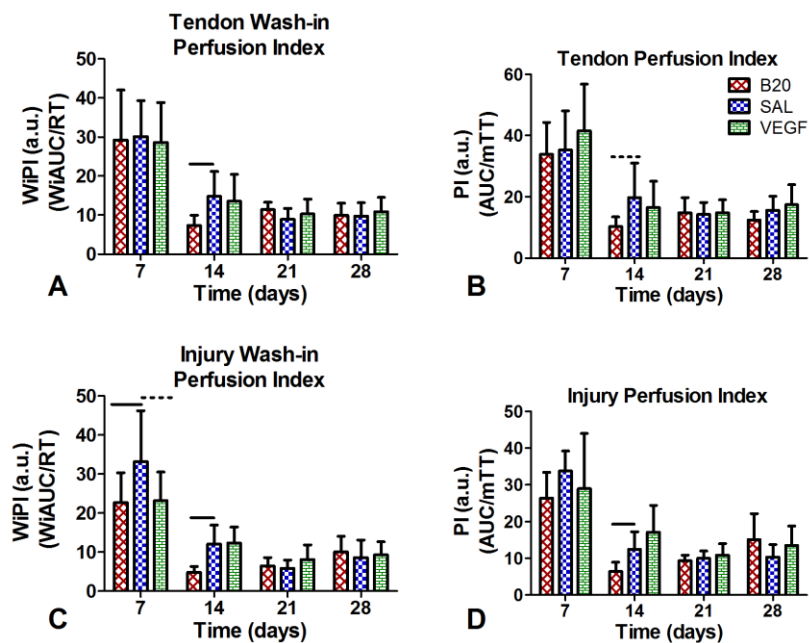
Figure 4.11: Late delivery contrast combination amplitude and time parameters measured in the tendon (A-B) and injury (C-D) ROIs. (A,D) Wash-in perfusion index (WiPI = WiAUC/RT) and (B,D) perfusion index (PI = AUC/mTT). Significant differences (p<0.05) indicated by the solid bar and trends (p<0.1) indicated by the dashed bar. The B20 group decreased vascular properties at early time points.

B-mode ultrasound alignment analysis showed decreased circular standard deviation (CSD) of collagen fiber orientation, indicating more aligned tissue, at day 14 in the B20 group injury region (Figure 4.12D). Additionally, B20 increased echogenicity at days 7, 14, and 28 in the injury region (Figure 4.12E), and at day 28 in the tendon ROI (Figure 4.12C). VEGF had a trending decrease in echogenicity at days 14 and 21 (Figure 4.12C).
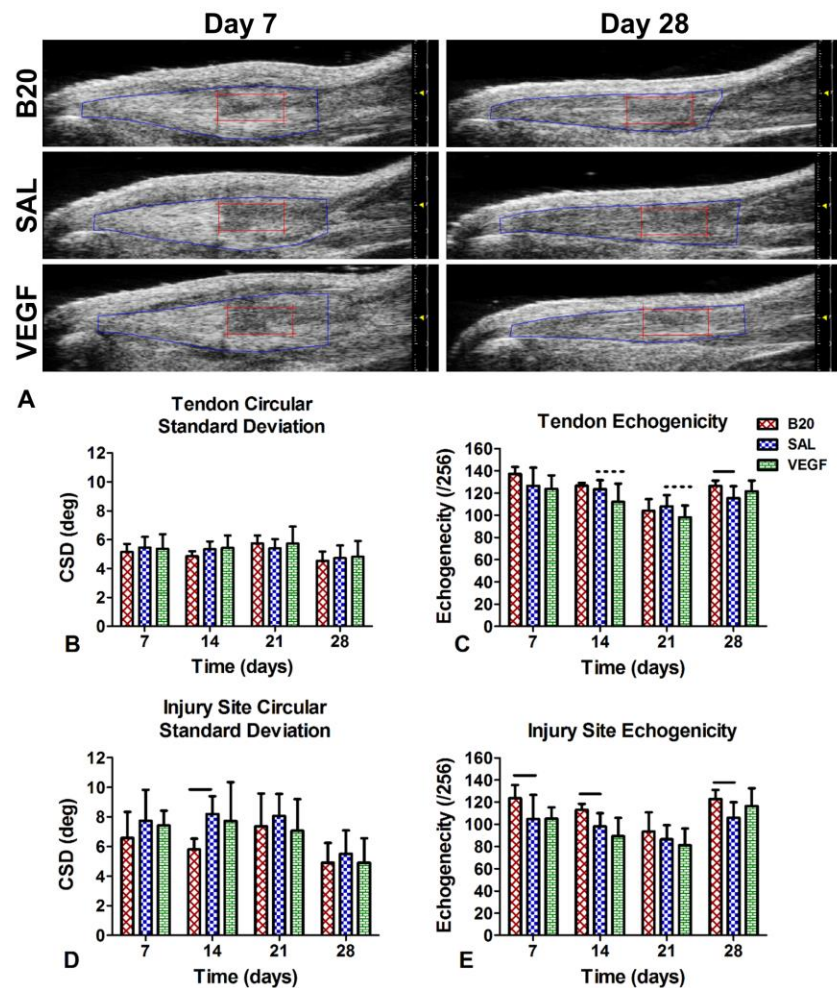
Figure 4.12: (A) Representative b-mode ultrasound images. (B,D) Circular standard deviation and (C,E) echogenicity measures for (B,C) full tendon and (D,E) injury ROIs. The B20 group showed improvements in tendon organization with decreased CSD and increased echogenicity.

Gait Analysis: None of the ground reaction force (Figure 4.13) or paw placement (Figure 4.14) parameters showed any differences between treatment groups at any time point.
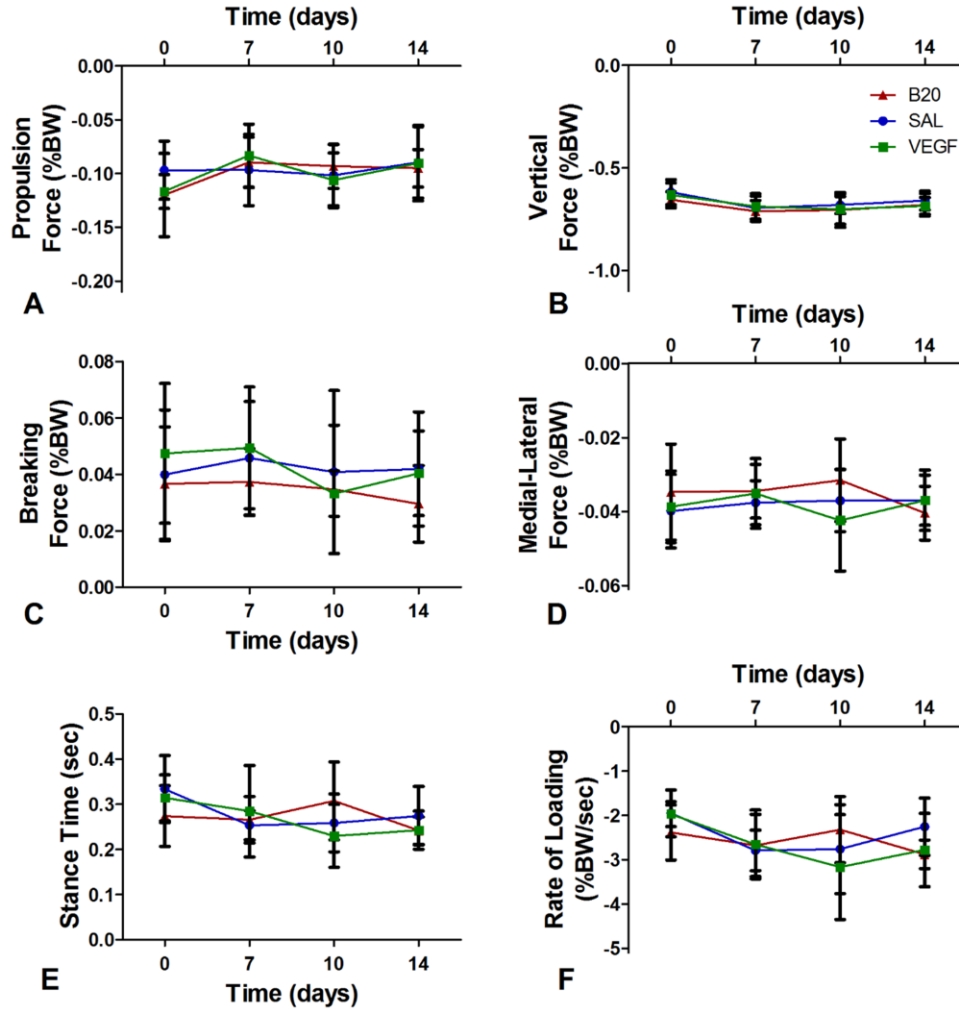
Figure 4.13: Late delivery ground reaction force and timing measures of rat ambulation pre-injury (day 0) and 7, 10, and 14 days post-injury for (A) propulsion, (B) vertical, (C) breaking, and (D) medial-lateral forces, along with (E) stance time and (F) rate of loading measures. There were no significant changes between groups for any parameters.
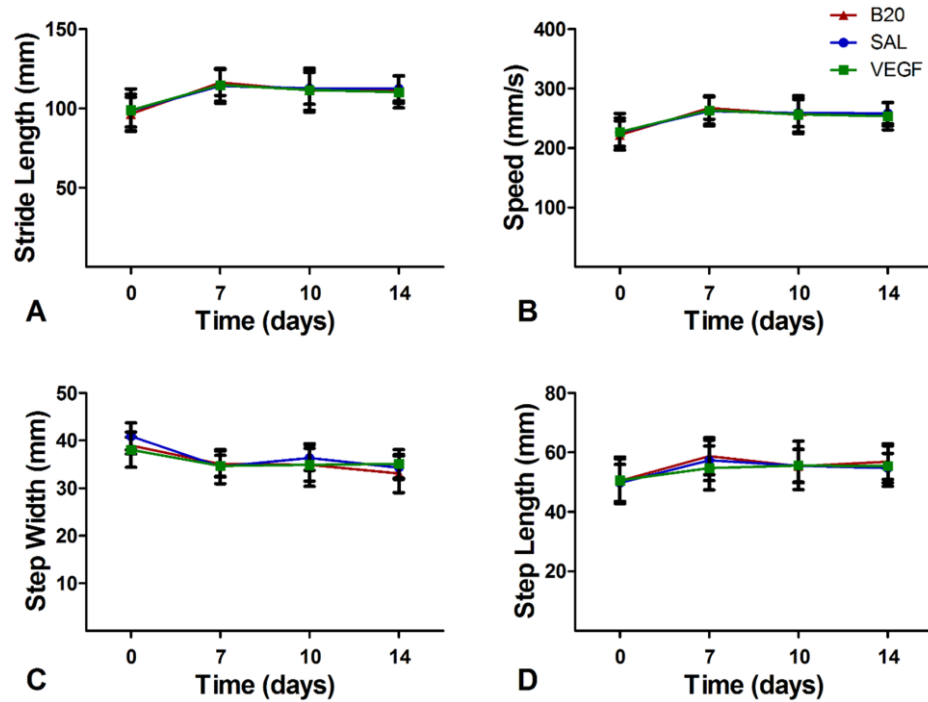
Figure 4.14: Late delivery paw placement measures of rat ambulation pre-injury (day 0) and 7, 10, and 14 days post-injury for (A) stride length, (B) speed, (C) step width, (D) and step length. There were no significant changes between groups for any parameters.

Passive Ankle Mechanics: Range of motion (ROM) measures showed a trending decrease in plantarflexion ROM in the B20 group at day 7 (Figure 4.15A). No other differences were found in either group.
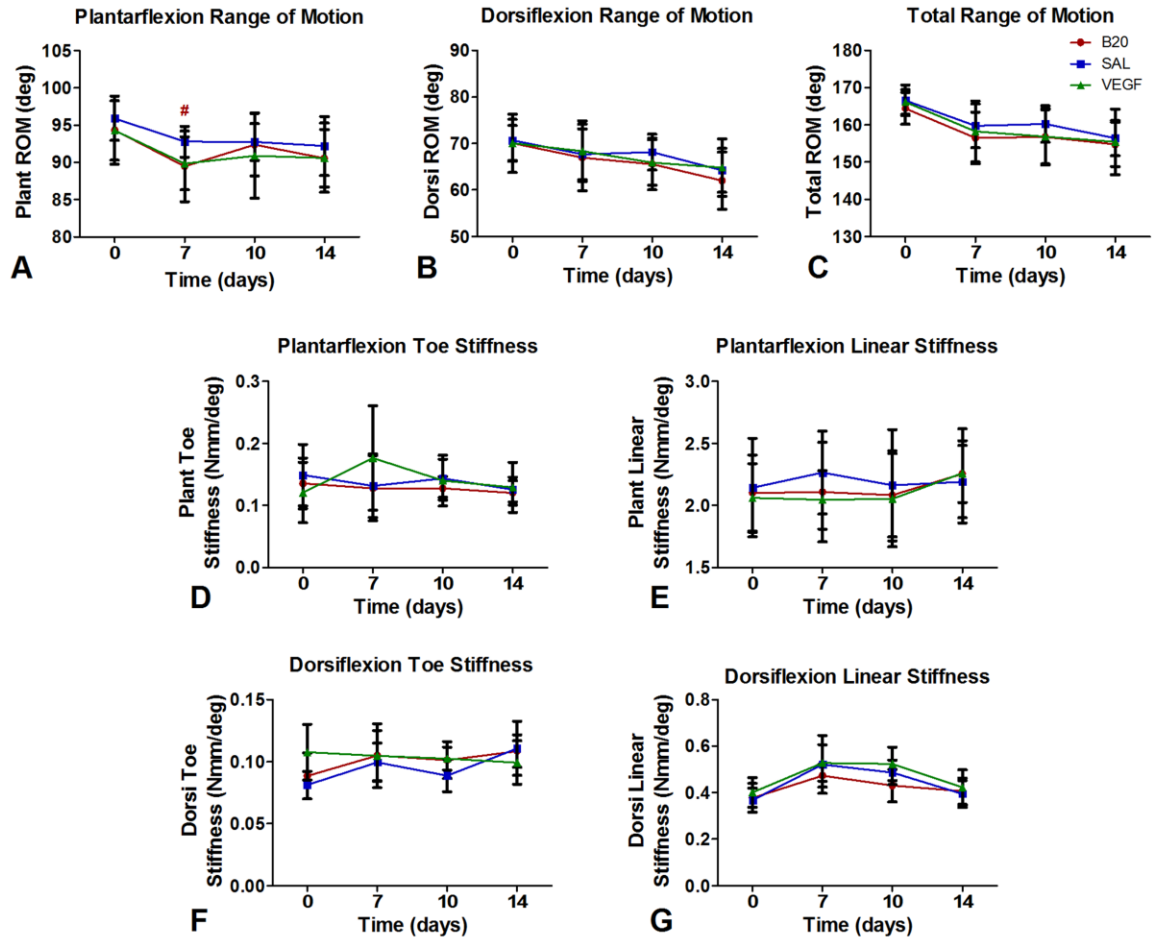
Figure 4.15: Late delivery passive ankle mechanics measures of (A) plantarflexion, (B) dorsiflexion, and (C) total range of motion (ROM), as well as (D,E) plantarflexion and (F,G) dorsiflexion toe and linear stiffness. Significant (*$p<0.025$) and trending (#$p<0.05$) differences indicated in red for B20 and green for VEGF compared to saline.

Histology: There are no significant changes in H&E stained histology. However, there was a trending increase in more rounded cell shape in the VEGF group at day 7 (Figure 4.16A,C).
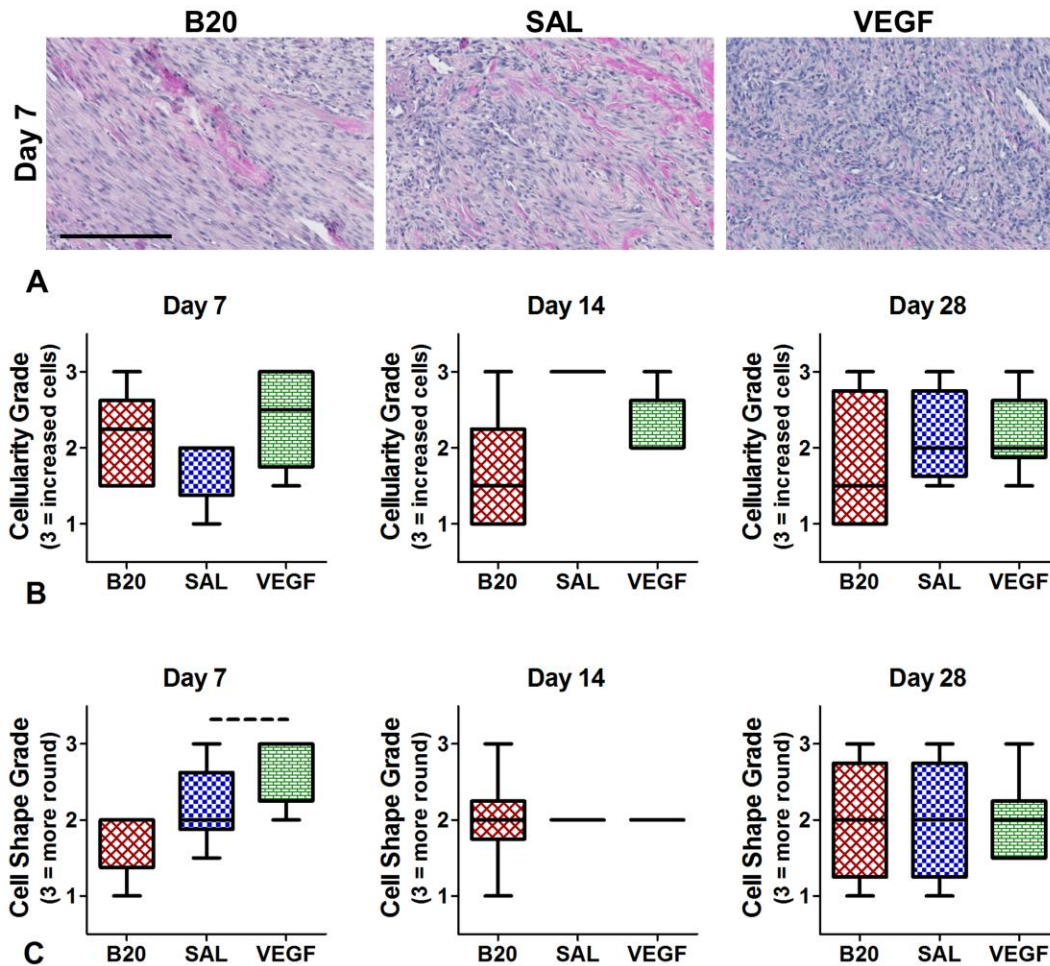
Figure 4.16: Late delivery hematoxylin and eosin (H&E) staining. (A) Representative images of the three treatment groups at day 7 (scale bar 200µm). Semi-quantitative measures of (B) cellularity and (C) cell shape for each treatment at days 7, 14, and 28. Note that each time point was graded separately, so the grading scales are not comparable across time points.

CD34 staining for vascular endothelial cells demonstrated a trending and significant decrease in vascular density in the B20 group at days 7 and 14 (Figure 4.17B). Additionally, there was an increase in vascular size in the VEGF group at day 7 (Figure 4.17C). Finally, a trending decrease in vessel size in the B20 group at day 28 (Figure 4.17C).
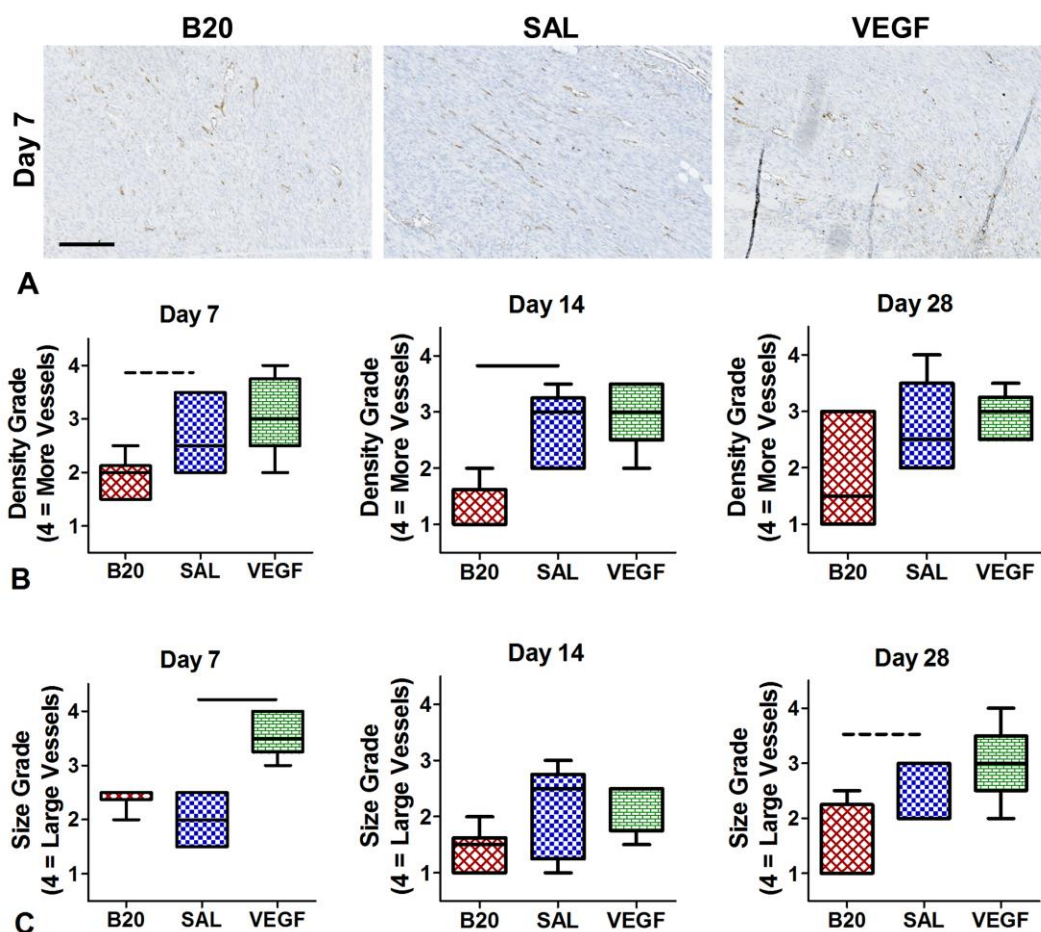
Figure 4.17: Late delivery CD34 immunohistochemical staining. (A) Representative images of each treatment at day 7 (scale bar 200μm). Semi-quantitative measures of (B) vessel density and (C) vessel size for each group at days 7, 14, and 28. Note that each time point was graded separately, so the grading scales are not comparable across time points. B20 delivery decreased vessel density, while VEGF delivery increased vessel size.

Immunohistochemical quantitative analysis revealed that B20 delivery caused a trending decrease in VEGF at day 14 (Figure 4.18B, 20), a trending increase in MMP13 at day 7 (Figure 4.18D, 22).
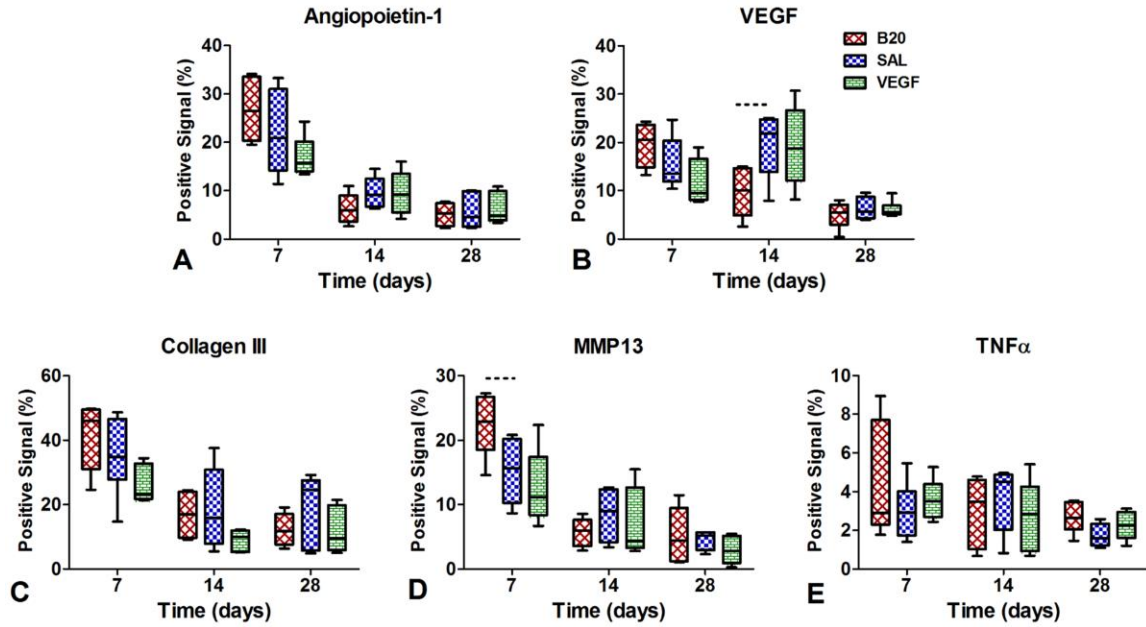
Figure 4.18: Quantification of percent positive staining for angiopoietin-1 (Ang-1), vascular endothelial growth factor (VEGF), type III collagen (Col III), matrix metallopeptidase 13 (MMP-13), and tumor necrosis factor alpha (TNFα). The B20 group showed a trending decrease in VEGF at day 14, and a trending increase in MMP13 at day 7.
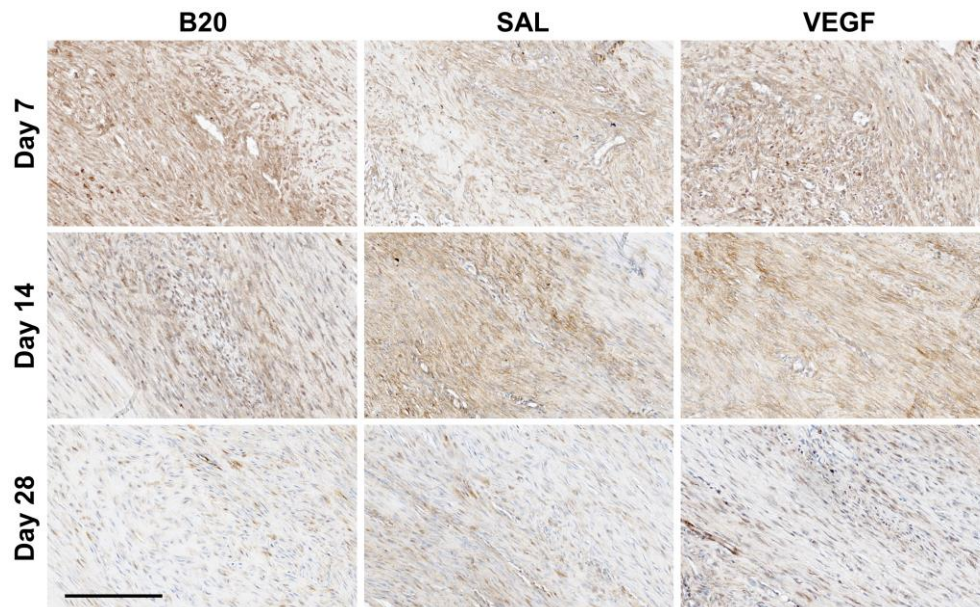
Figure 4.19: Vascular endothelial growth factor (VEGF) IHC representative images for B20, SAL, and VEGF at days 7, 14, and 28 (scale bar 200µm). Brown is positive staining for the antibody and blue is hematoxylin counterstain.

124
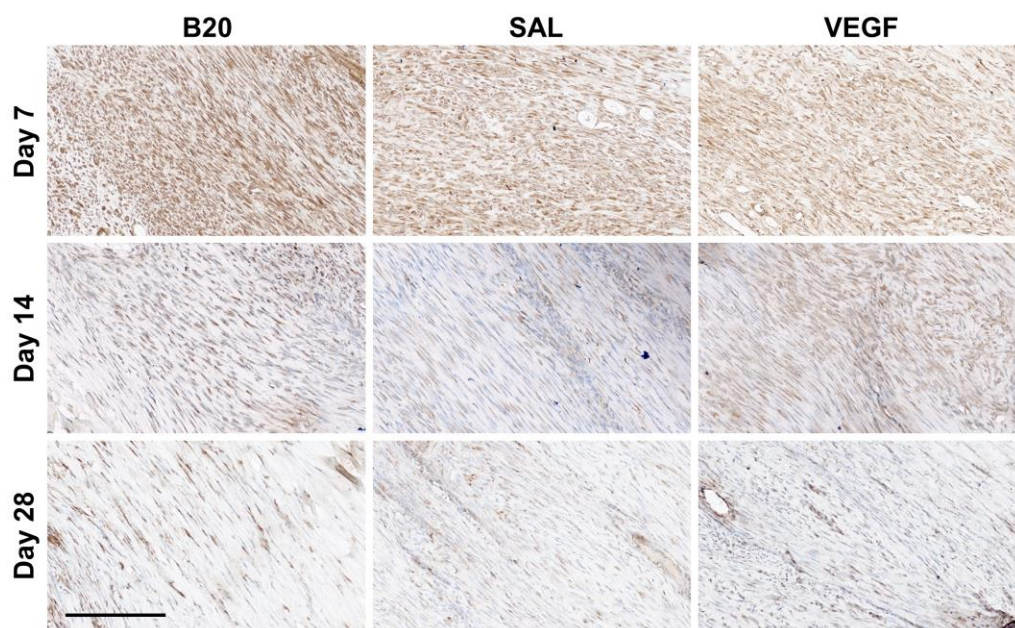
Figure 4.20: Angiopoietin-1 (Ang-1) IHC representative images for B20, SAL, and VEGF at days 7, 14, and 28 (scale bar 200μm). Brown is positive staining for the antibody and blue is hematoxylin counterstain.
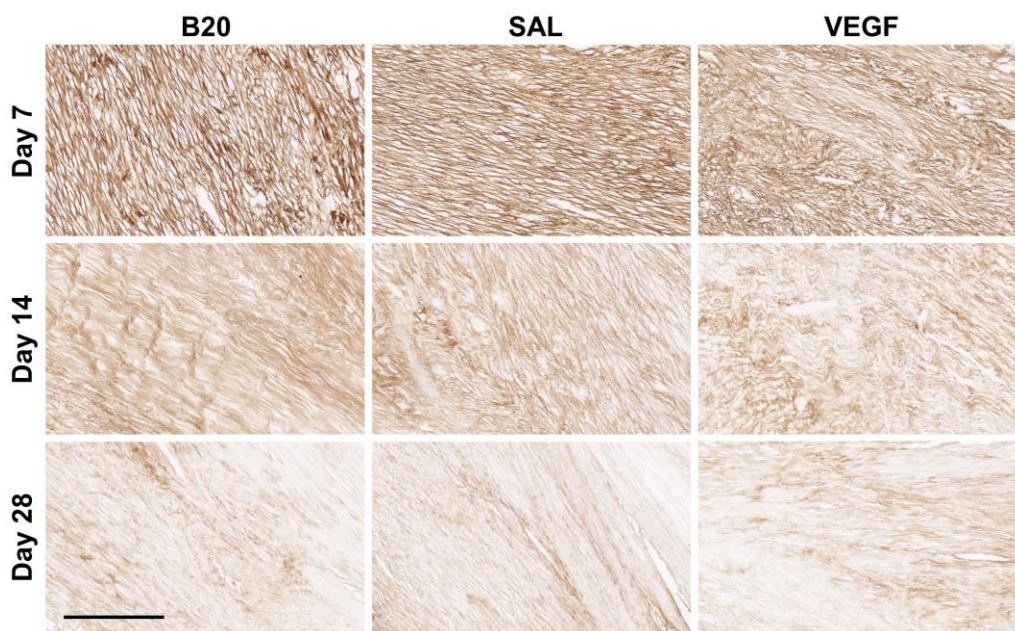
Figure 4.21: Type III collagen (Col III) representative images for B20, SAL, and VEGF at days 7, 14, and 28 (scale bar 200μm). Brown is positive staining for the antibody.

125
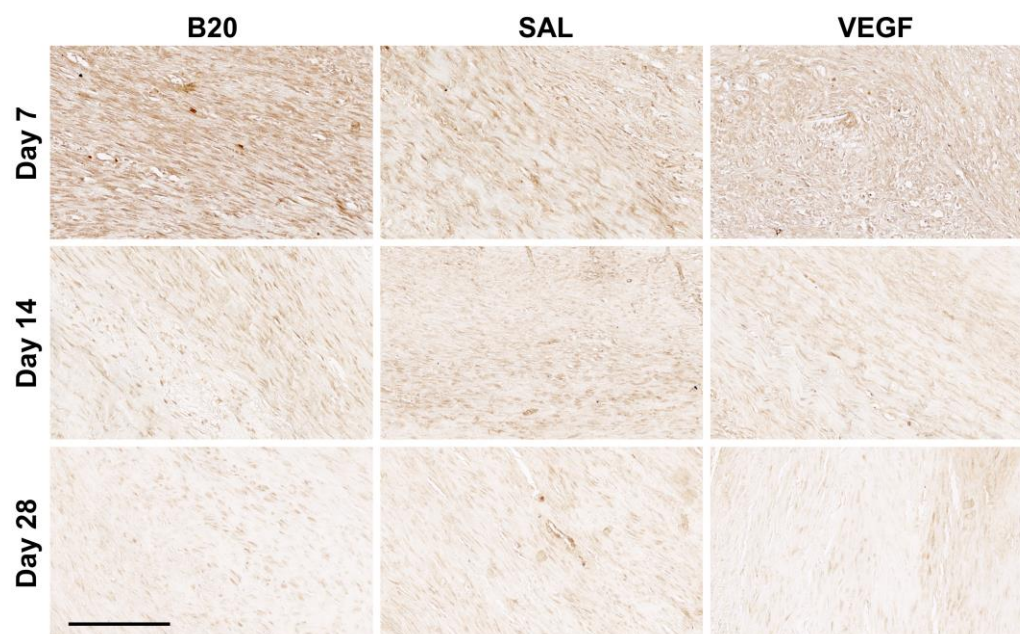
Figure 4.22: Matrix metallopeptidase 13 (MMP-13) representative images for B20, SAL, and VEGF at days 7, 14, and 28 (scale bar 200µm). Brown is positive staining for the antibody.
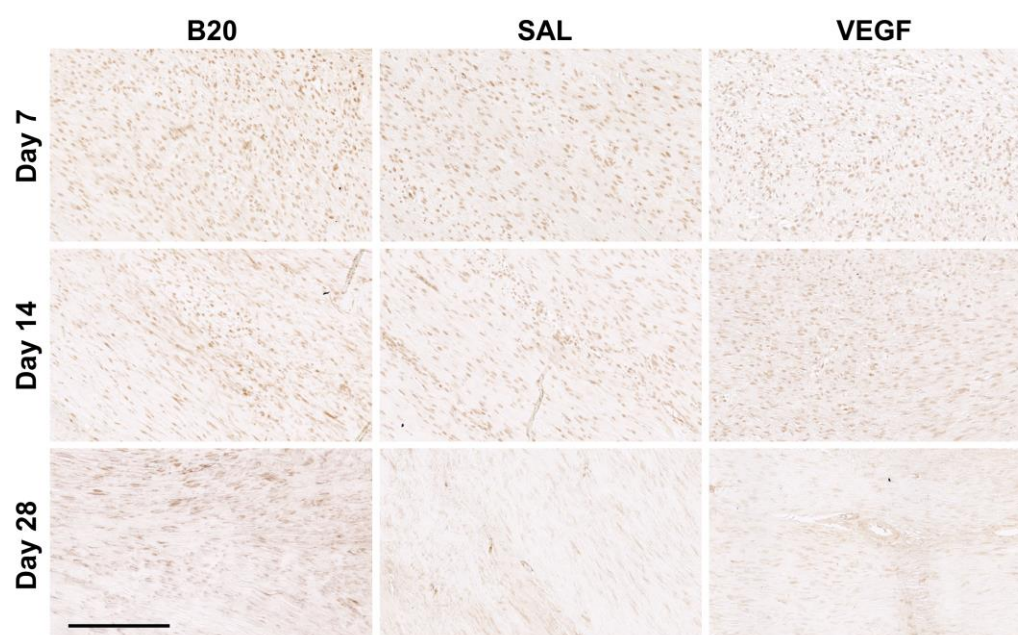
Figure 4.23: Tumor necrosis factor alpha (TNFα) representative images for B20, SAL, and VEGF at days 7, 14, and 28 (scale bar 200µm). Brown is positive staining for the antibody.

Mechanics: When evaluating the geometric and structural properties of the tendons from mechanical testing, there was a trending decrease in percent relaxation in the VEGF group at day 14 (Figure 4.24B). The B20 group had a trending decrease in stiffness and a significant decrease in failure load at day 14 (Figure 4.24C,F). There were no significant changes at day 28 in any parameter, or in tendon or injury cross sectional area or max displacement measures at either time point.
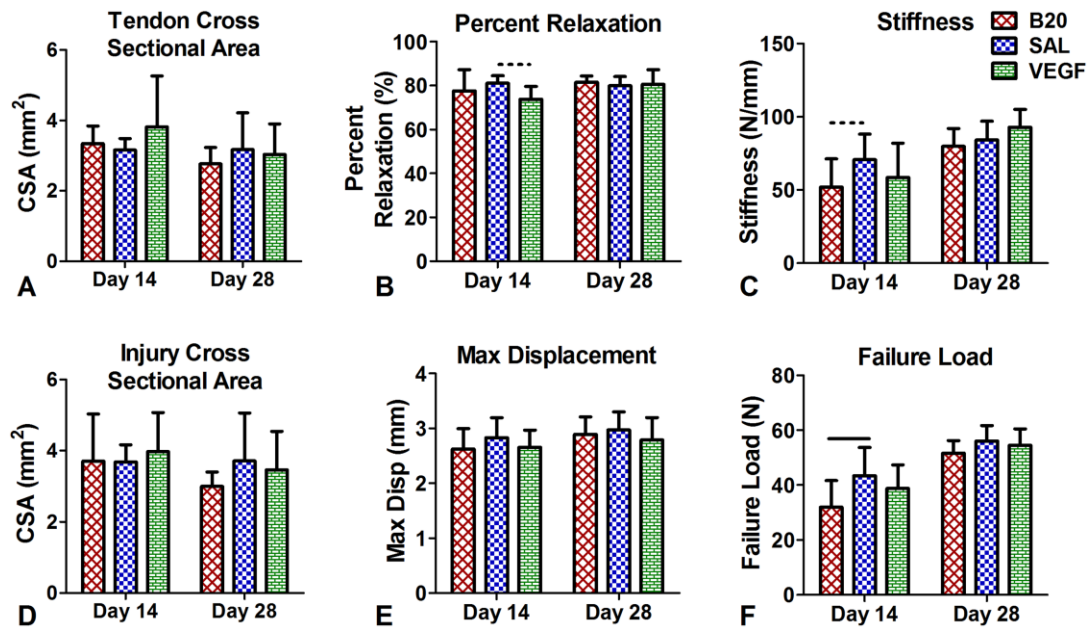
Figure 4.24: Late delivery Achilles tendon geometric and structural mechanical properties. (A) Tendon cross sectional area (CSA), (B) percent relaxation, (C) stiffness, (D) injury CSA, (E) max displacement, and (F) failure load are all shown for day 14 and 28 post-injury. The B20 group reduced structural properties at day 14.

Evaluation of material properties demonstrated a decrease in max stress (Figure 4.25A) and tendon modulus (Figure 4.25B) in the B20 group at day 14. However, there was an increase in injury site modulus in the B20 group at day 28 (Figure 4.25C). No other differences were found in the VEGF group.
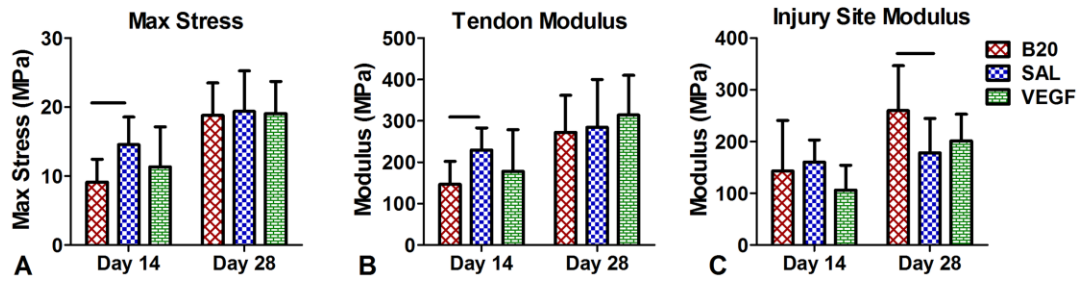
Figure 4.25: Late delivery Achilles tendon material mechanical properties. (A) Max stress and (B) tendon and (C) injury modulus parameters at days 14 and 28.

Finally, dynamic mechanical properties were not significantly different between groups at any time point (Figure 4.26).
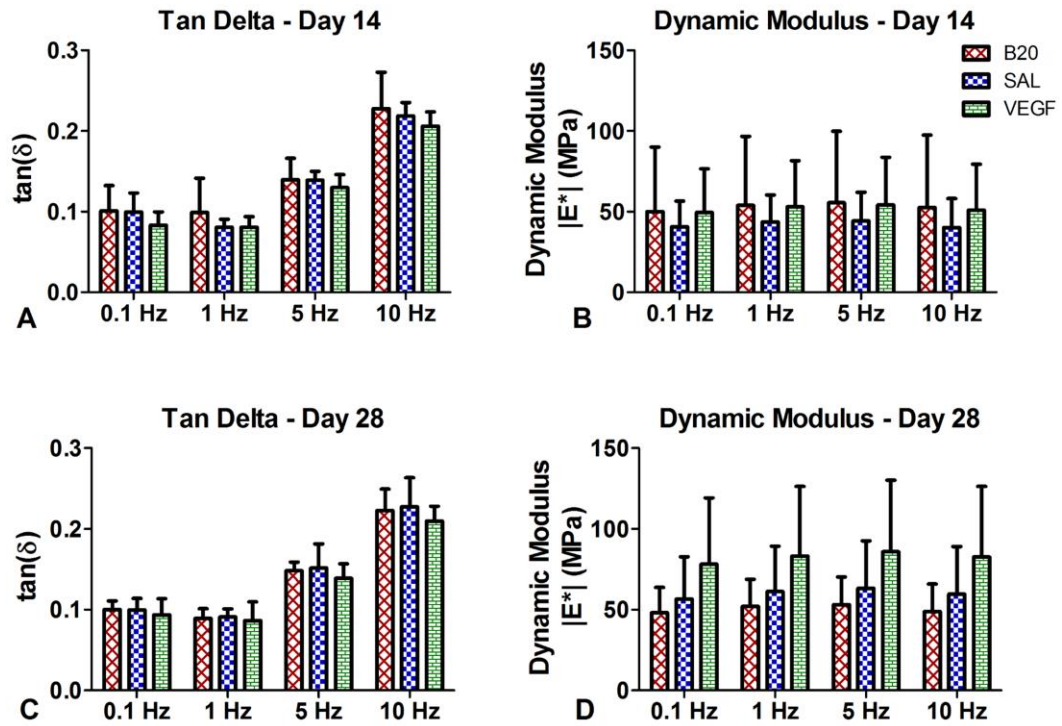
Figure 4.26: Late delivery Achilles tendon dynamic mechanical properties. (A,C) Tangent delta and (B, C) dynamic modulus at (A,B) day 14 and (C,D) day 28. There were no significant difference between groups.

C-2. Early Delivery of Angiogenic Factors

Ultrasound: Color Doppler analysis of tendons with the early delivery group had no significant changes in MCL in either ROI (Figure 4.27B,E). There was a decrease in FA and CWFA at day 7 in the B20 group for both ROIs (Figure 4.27C,D,F,G). There was a trending increase in CWFA in the B20 group at day 14 in the tendon (Figure 4.27D). Finally, there were significant and trending decreases in FA and CWFA in the VEGF group at day 7 in the injury region (Figure 4.27F,G).
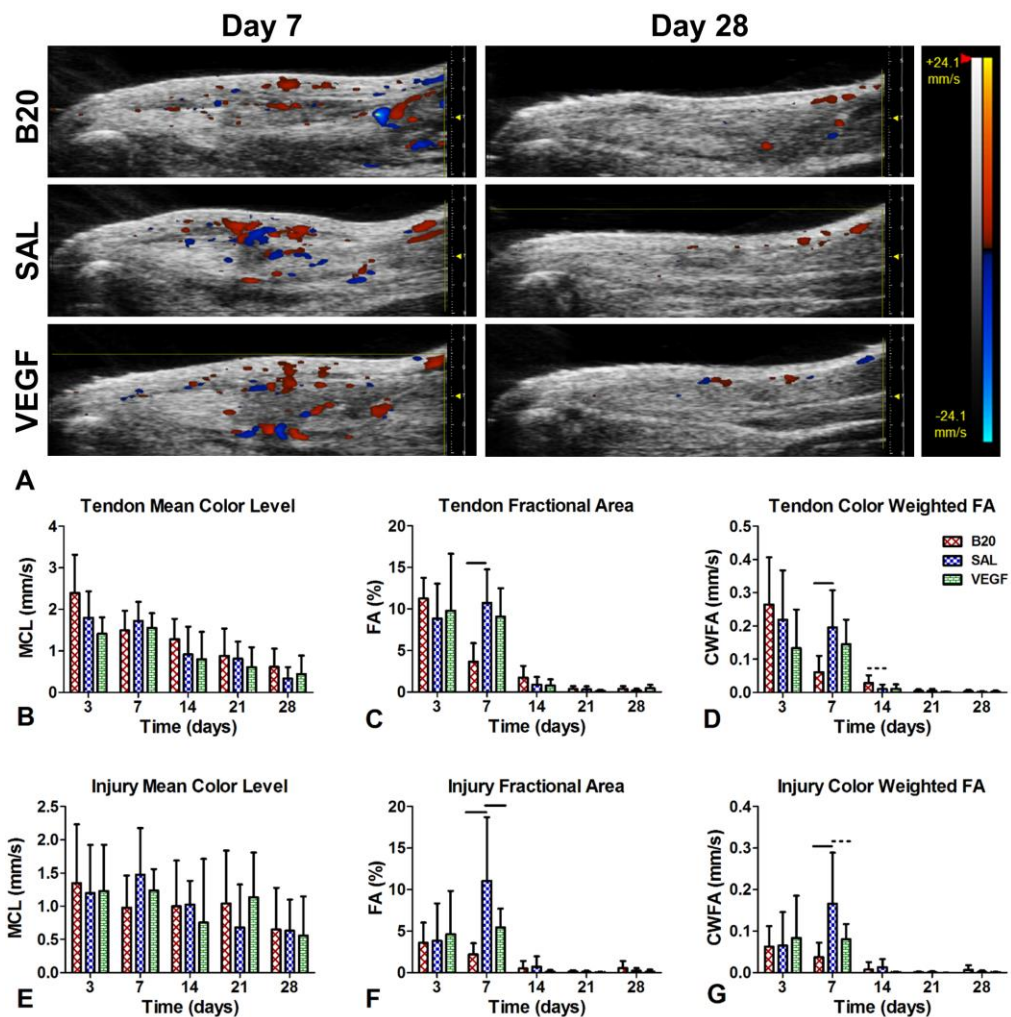
Figure 4.27: Early delivery color Doppler ultrasound (A) representative images and quantification for the (B-D) tendon ROI and the (E-G) injury ROI. (B,E) Mean color level (MCL) represents blood flow velocity, (C,F) fractional area (FA) represents the percent

area of the ROI where blood flow was detected, and (D,F) color weighted fractional area (CWFA) is the weighted average of the blood flow velocity by the percent area of signal (MCL*FA). The B20 group showed consistent decreases in FA and CWFA at day 7.

Photoacoustic imaging measurements showed a decrease in blood oxygenation in the VEGF group at day 3 in both ROIs and a trending decrease at day 21 in the injury region (Figure 4.28B,E).

For the B20 group, there were trending and significant decreases in blood oxygenation at days 3 and 7 that transitioned to an increase at day 14 in both ROIs (Figure 4.28B,E). There were trending and significant increases in average hemoglobin at days 21 and 28, respectively, in the injury region (Figure 4.28F). Finally, there was a trending decrease in tissue oxygenation at day 7 in the tendon ROI, and a subsequent increase at day 28 in the tendon, with a trending increase at day 21 in the injury (Figure 4.28D,G).
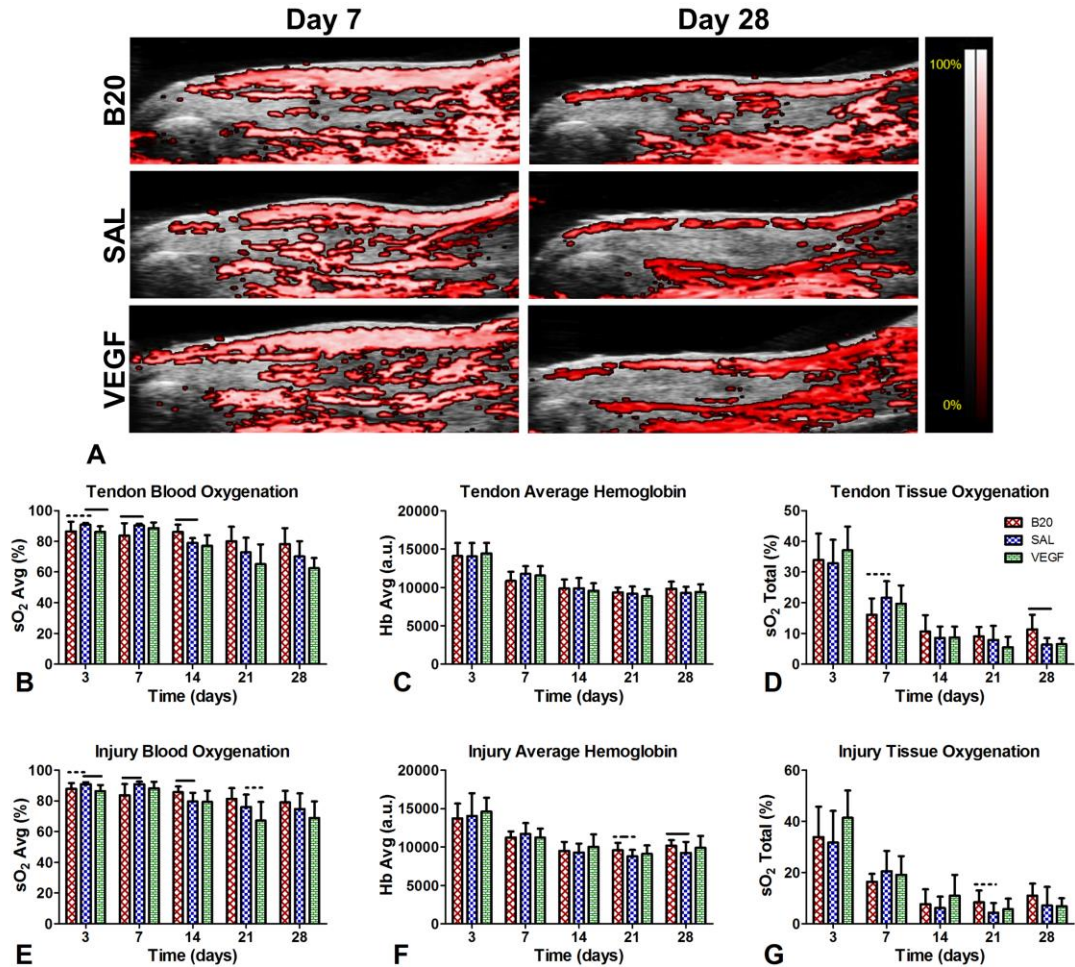
Figure 4.28: Early delivery photoacoustics imaging (A) representative images for days 7 and 28 and quantification of results for the (B-D) tendon ROI and the (E-G) injury ROI. (B,E) Blood oxygenation (sO_2 Avg) represents the oxygenation level of the hemoglobin that is detected, (C,F) average hemoglobin (Hb Avg) represents the average amount of hemoglobin detected total weighted by the ROI area, and (D,G) tissue oxygenation (sO_2 Total) represents the oxygenation weighted by the percent of the ROI area where hemoglobin was detected. The B20 group showed decreased oxygenation properties at early time points and increased properties at later time points.

When evaluating the contrast-enhanced ultrasound analysis of amplitude-based parameters, the B20 group showed an increase in PE at day 3 in both ROIs, with a trending decrease at day 7 in the injury and a trending increase at day 21 in the tendon (Figure

4.29B,E). The VEGF group showed increases in PE (tendon only), WiAUC, and AUC at day 3 in both ROIs (Figure 4.29B-D, F-G).
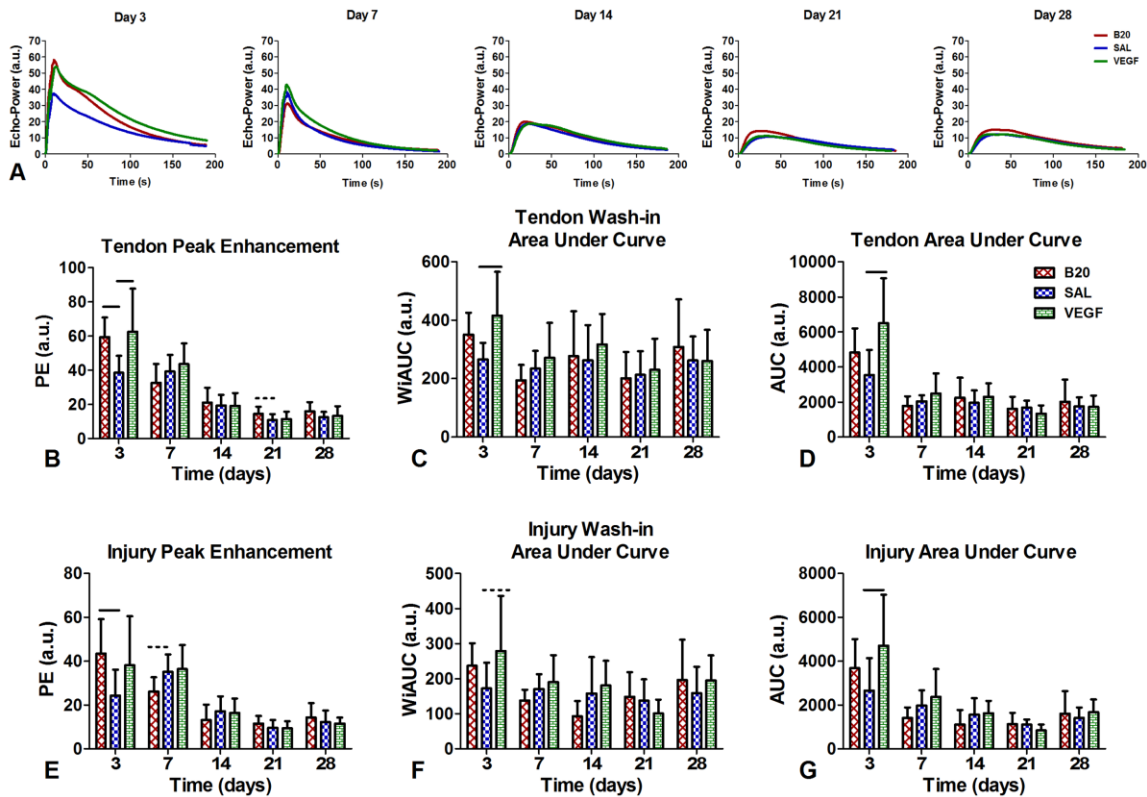
Figure 4.29: (A) Early delivery contrast-enhanced ultrasound averaged curves. Quantification of amplitude-based parameters measured in the (B-D) tendon and (E-G) injury ROIs. (B,E) Peak enhancement (PE), (C,F) wash-in area under the curve (WiAUC), (D,G) area under the curve (AUC). The VEGF group showed consistent increases in these parameters at day 3.

For the time-based contrast parameters, the VEGF group showed trending increases in RT at day 14 and WiR at day 3 in the full tendon (Figure 4.30A,C). The B20 group had a trending decrease in RT at day 21 and mTT at day 3 in the tendon (Figure 4.30A,B). Additionally, there were significant increases in WiR at day 3, a trending decrease at day

7 in the injury, and significant and trending increases at days 21 and 28 in the tendon and injury regions, respectively (Figure 4.30C,F).
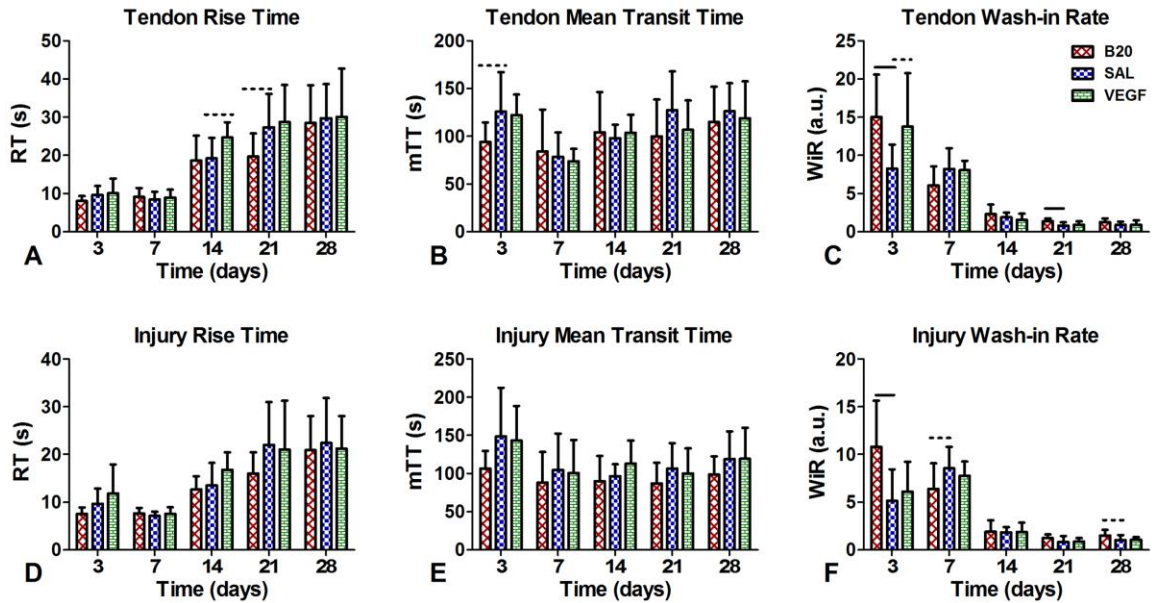
Figure 4.30: Early delivery contrast-enhanced ultrasound time-based parameters measured in the tendon (A-C) and injury (D-F) ROIs. (A,D) Rise time (RT), (B,E) mean transit time (mTT), (C,D) wash-in rate (WiR). The B20 group increased the WiR at early and late time points.

Finally, for the combined amplitude-time parameters, the VEGF group increased WiPI and PI in the tendon ROI at day 3 (Figure 4.31A,B). The B20 group increased both the WiPI and PI at day 3 (Figure 4.31), followed by a trending decrease at day 7 in the injury for WiPI (Figure 4.31C) and significant and trending increases at day 21 in both parameters (Figure 4.31A,B,D).
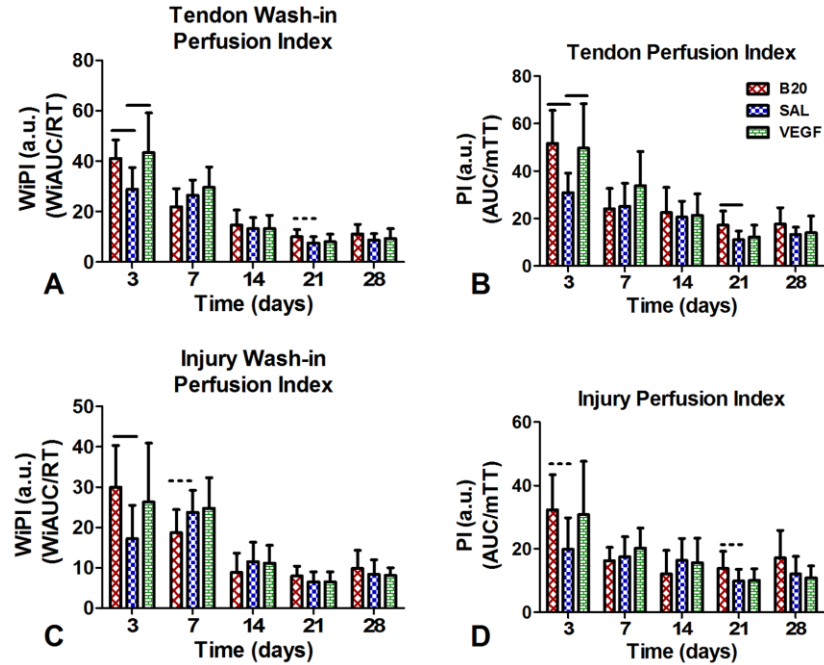
Figure 4.31: Early delivery contrast combination amplitude and time parameters measured in the tendon (A-B) and injury (C-D) ROIs. (A,D) Wash-in perfusion index (WiPI = WiAUC/RT) and (B,D) perfusion index (PI = AUC/mTT). Both groups caused significant increases in these parameters at day 3.

B-mode ultrasound alignment showed a significant decrease in circular standard deviation (CSD) of collagen fiber orientation in the B20 group on days 14-28 in the injury site, and days 7 and 28 in the tendon (with trends on day 21 in the tendon and 7 in the injury) (Figure 4.32B,D), indicating that the tissue has more aligned collagen than the saline group. This group also showed an increase in echogenicity at day 7 and 14 in both ROIs, and additionally a trend on day 28 in the injury region (Figure 4.32C,E).
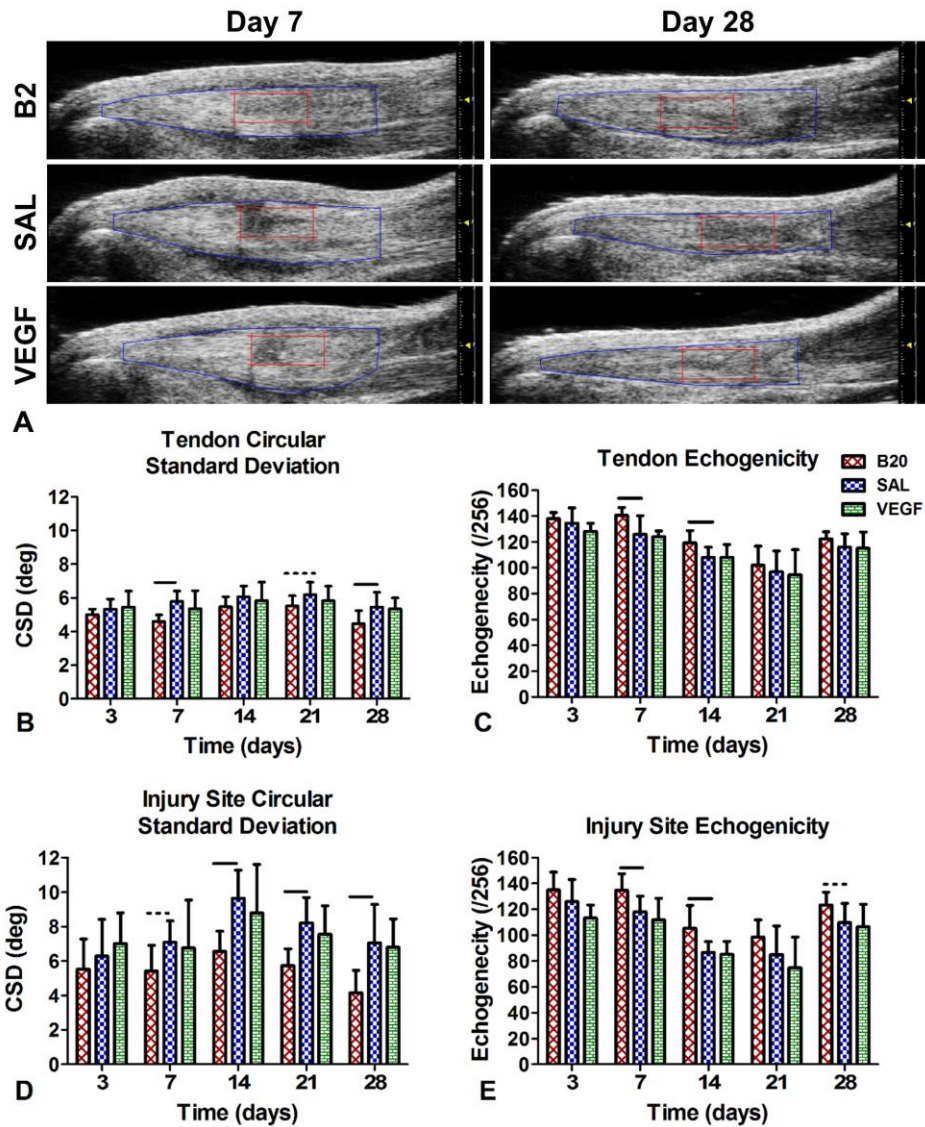
Figure 4.32: Early delivery ultrasound alignment. (A) Representative b-mode ultrasound images with ROIs shown. (B,D) Circular standard deviation and (C,E) echogenicity measures for (B,C) full tendon and (D,E) injury ROIs. The B20 group decreased circular standard deviation and increased echogenicity, indicating improved tissue organization across multiple time points.

Gait Analysis: All animals sacrificed at 2 weeks following injury underwent analysis of ground reaction force and paw placement ambulation parameters. For the ground reaction force analysis, there was a significant and trending decrease in breaking

force in the B20 and VEGF groups, respectively, at day 3 (Figure 4.33C). No other parameters showed significant changes with treatment.
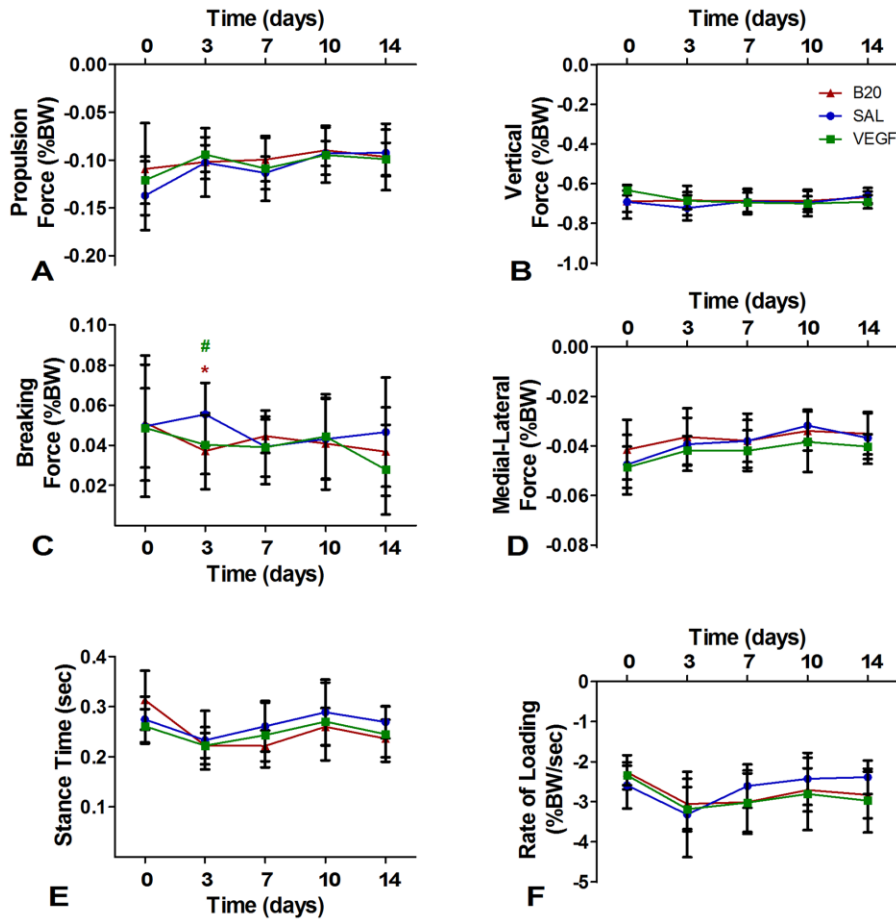
Figure 4.33: Early delivery ground reaction force and timing measures of rat ambulation pre-injury (day 0) and 7, 10, and 14 days post-injury for (A) propulsion, (B) vertical, (C) breaking, and (D) medial-lateral forces, along with (E) stance time and (F) rate of loading measures. The B20 group showed a decrease in breaking force at day 3, but there were no other significant changes. Trending (#p<0.05) and significant (*p<0.025) differences indicated in red for B20 and green for VEGF compared to saline.
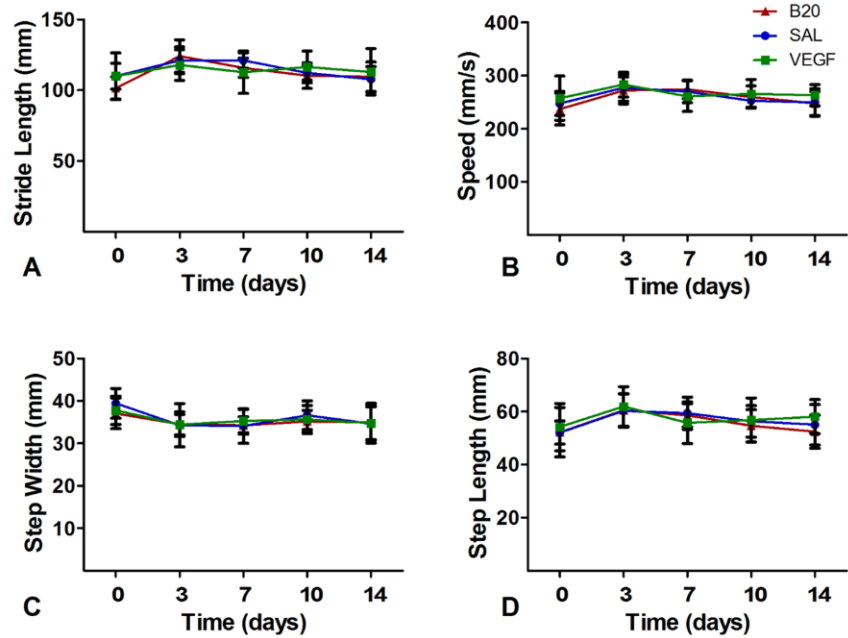
Figure 4.34: : Early delivery paw placement measures of rat ambulation pre-injury (day 0) and 7, 10, and 14 days post-injury for (A) stride length, (B) speed, (C) step width, (D) and step length. There were no significant changes between groups for any parameters.

Passive Ankle Mechanics: The B20 group had a trending increase in dorsiflexion range of motion at day 7 (Figure 4.35B). Both treatment groups had decreased plantarflexion linear stiffness at day 10 (Figure 4.35E). There were no other differences seen between groups.
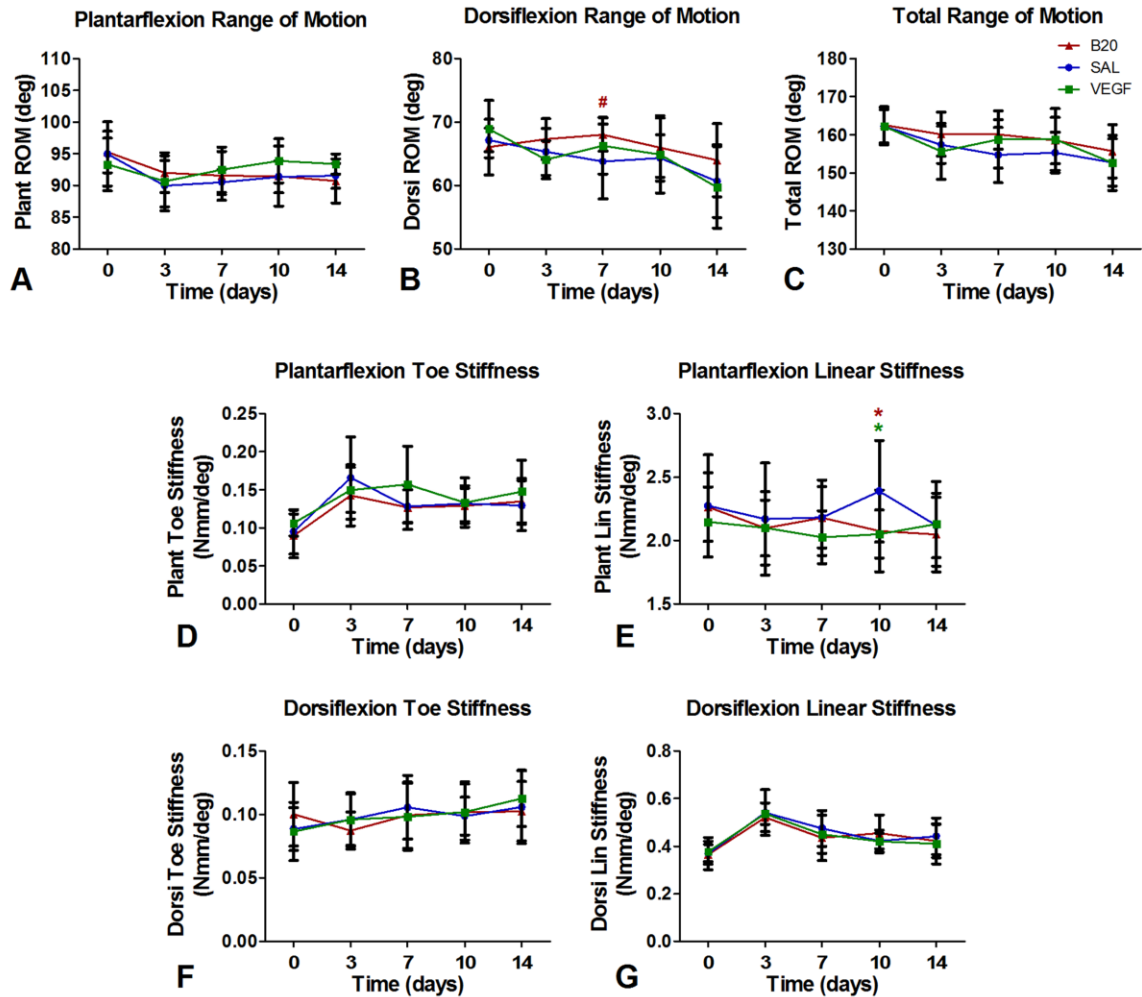
Figure 4.35: Early delivery passive ankle mechanics measures of (A) plantarflexion, (B) dorsiflexion, and (C) total range of motion (ROM), as well as (D,E) plantarflexion and (F,G) dorsiflexion toe and linear stiffness. Both treatments decreased plantarflexion linear stiffness at day 10. Significant (*$p<0.05$) and trending (#$p<0.1$) differences indicated in red for B20 and green for VEGF compared to saline.

Histology: There were no significant changes in H&E measures of cellularity or cell shape for any group at any time point (Figure 4.36).
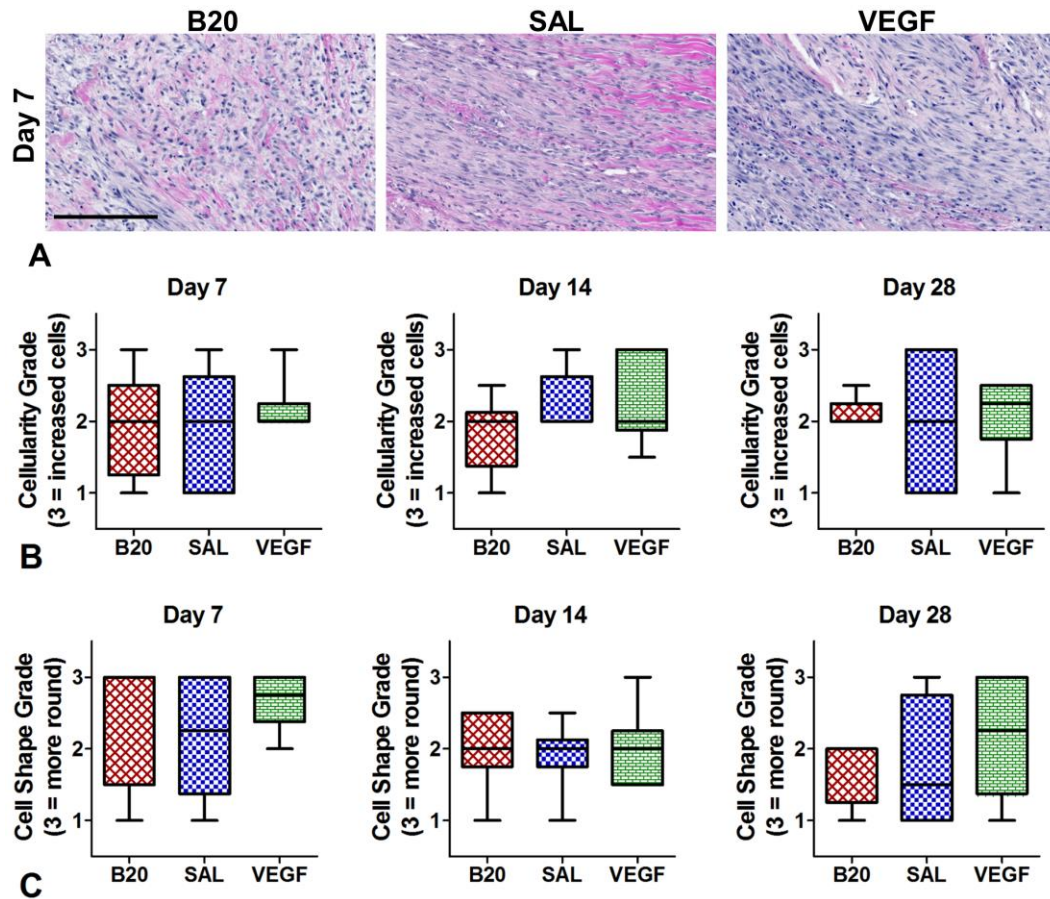
Figure 4.36: Early delivery hematoxylin and eosin (H&E) staining. (A) Representative images of the three treatment groups at day 7 (scale bar 200µm). Semi-quantitative measures of (B) cellularity and (C) cell shape for each treatment at days 7, 14, and 28. Note that each time point was graded separately, so the grading scales are not comparable across time points. There were no differences found in either group.

CD34 staining for vascular endothelial cells demonstrated trending decreases in vessel density at day 14 (Figure 4.37A,B) and vessel size at day 7 (Figure 4.37A,C) in the B20 group. The VEGF group did not show any significant changes.
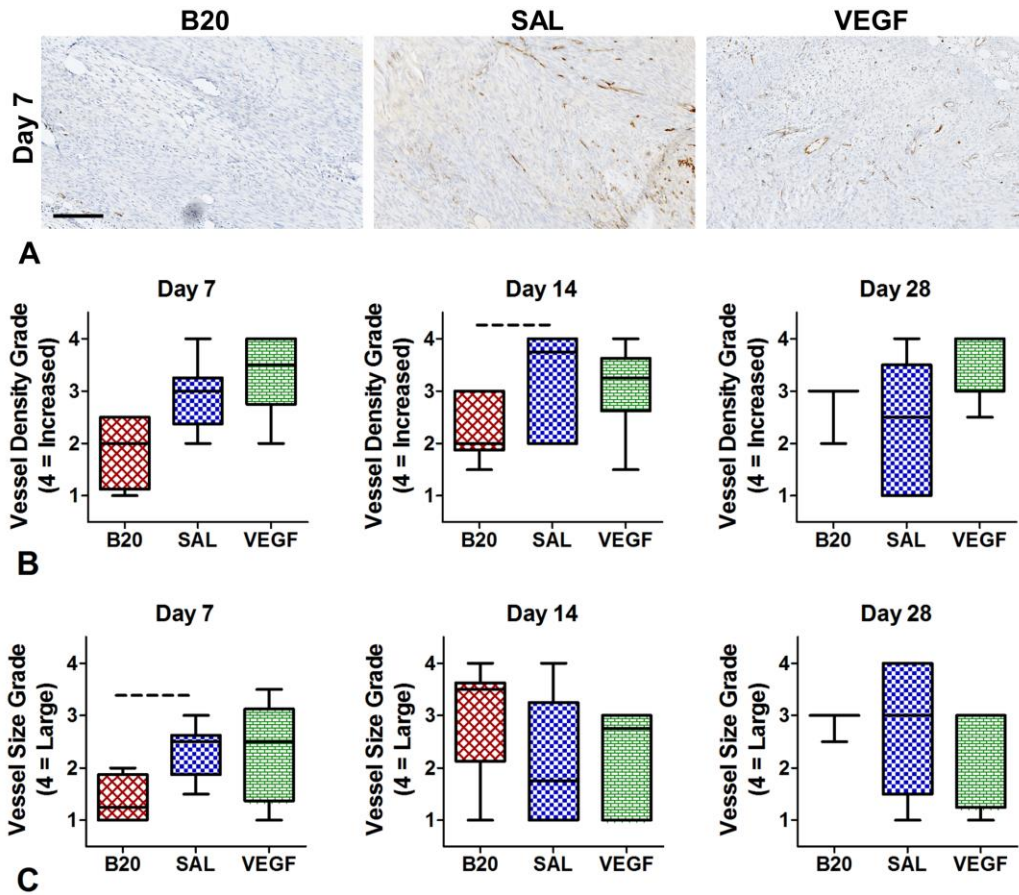
Figure 4.37: Early delivery CD34 immunohistochemical staining. (A) Representative images of each treatment at day 7 (scale bar 200µm). Semi-quantitative measures of (B) vessel density and (C) vessel size for each group at days 7, 14, and 28. Note that each time point was graded separately, so the grading scales are not comparable across time points. The B20 group showed trending decreases in vessel density at day 14 and vessel size at day 7.

Immunohistochemical quantitative analysis showed a trending decrease in MMP13 at day 28 (Figure 4.38D, 42) and a significant increase in TNFα in the B20 group at day 14 (Figure 4.38E, 43) in the B20 group.
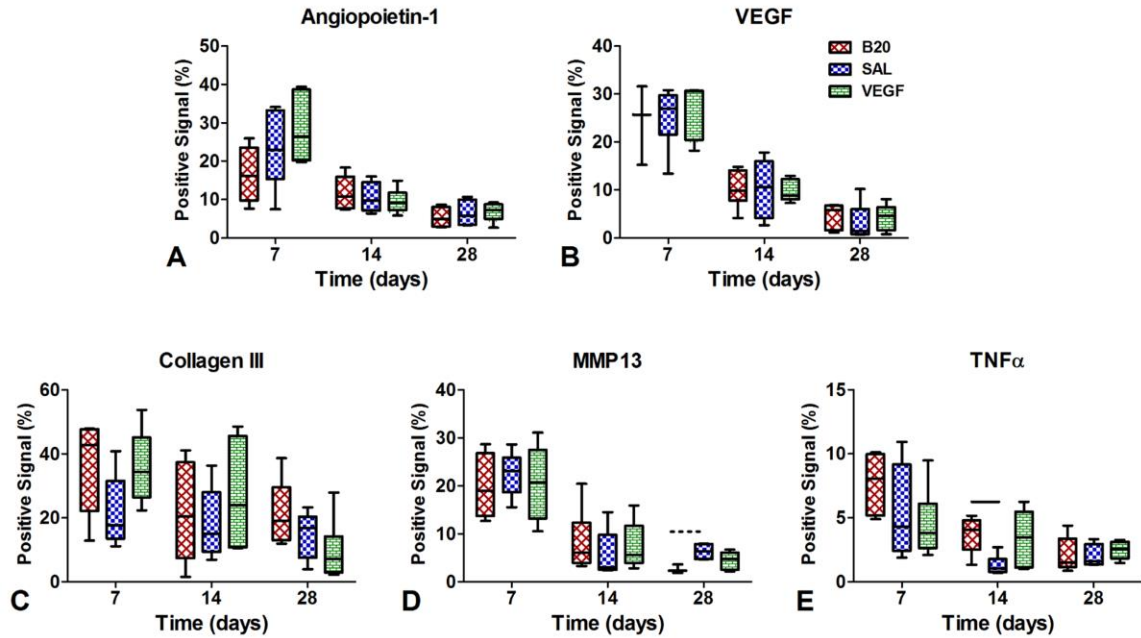
Figure 4.38: Quantification of percent positive staining for angiopoietin-1 (Ang-1), vascular endothelial growth factor (VEGF), type III collagen (Col III), matrix metallopeptidase 13 (MMP-13), and tumor necrosis factor alpha (TNFα). The B20 group had increased TNFα staining at day 14 and decreased MMP13 staining at day 28.
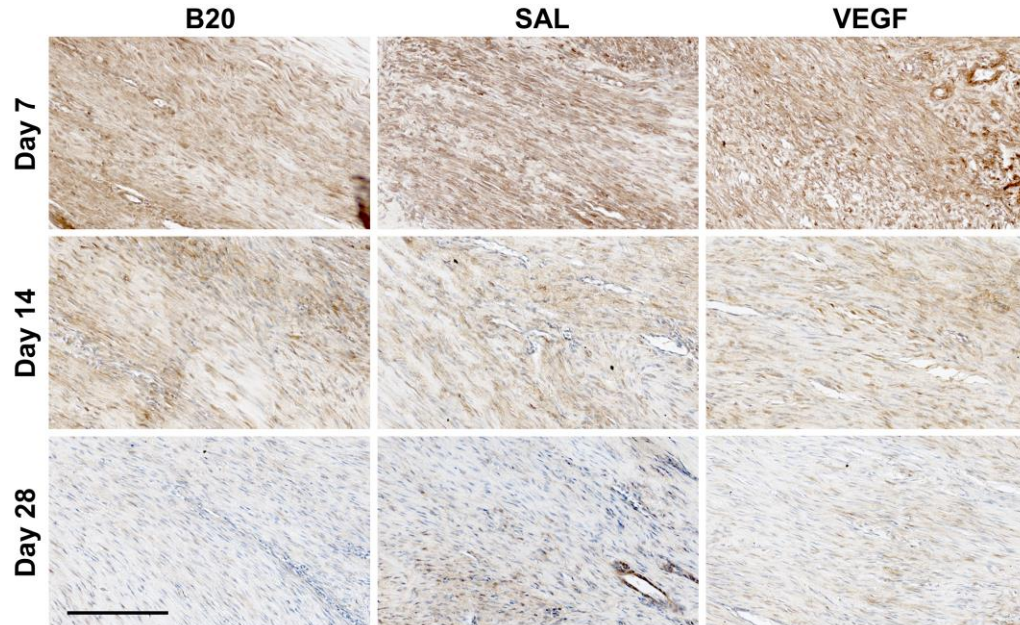
Figure 4.39: Vascular endothelial growth factor (VEGF) IHC representative images for B20, SAL, and VEGF at days 7, 14, and 28 (scale bar 200µm). Brown is positive staining for the antibody and blue is hematoxylin counterstain.
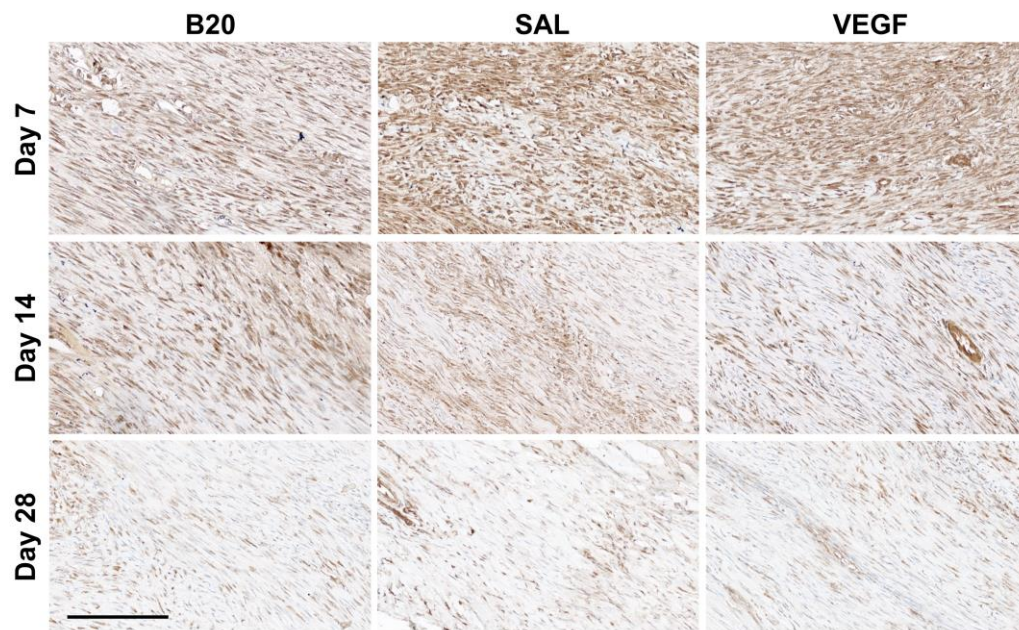
Figure 4.40: Angiopoietin-1 (Ang-1) IHC representative images for B20, SAL, and VEGF at days 7, 14, and 28 (scale bar 200µm). Brown is positive staining for the antibody and blue is hematoxylin counterstain.
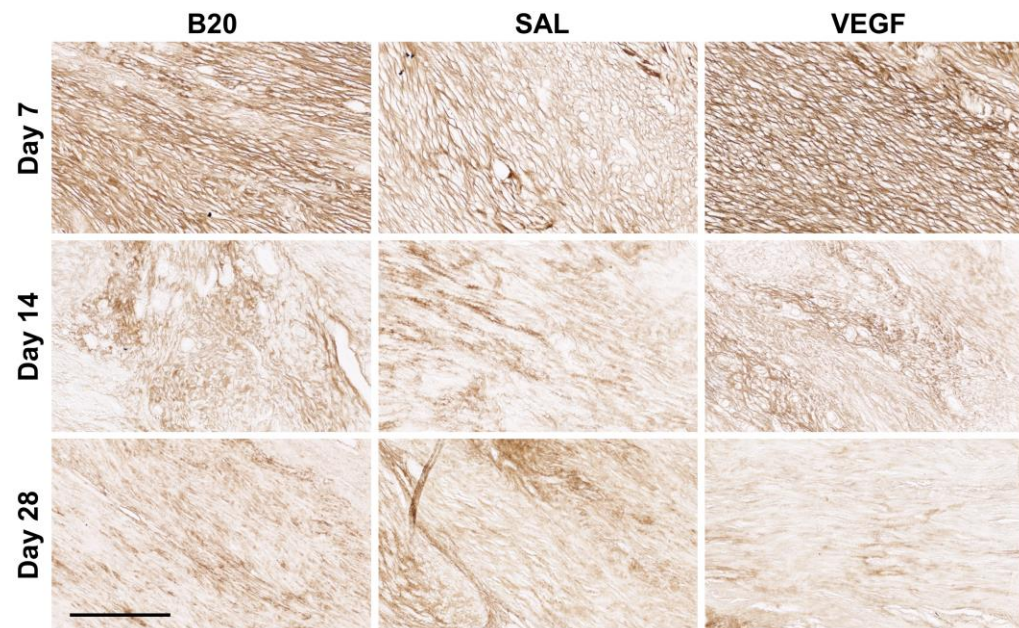
Figure 4.41: Type III collagen (Col III) IHC representative images for B20, SAL, and VEGF at days 7, 14, and 28 (scale bar 200µm). Brown is positive staining for the antibody.
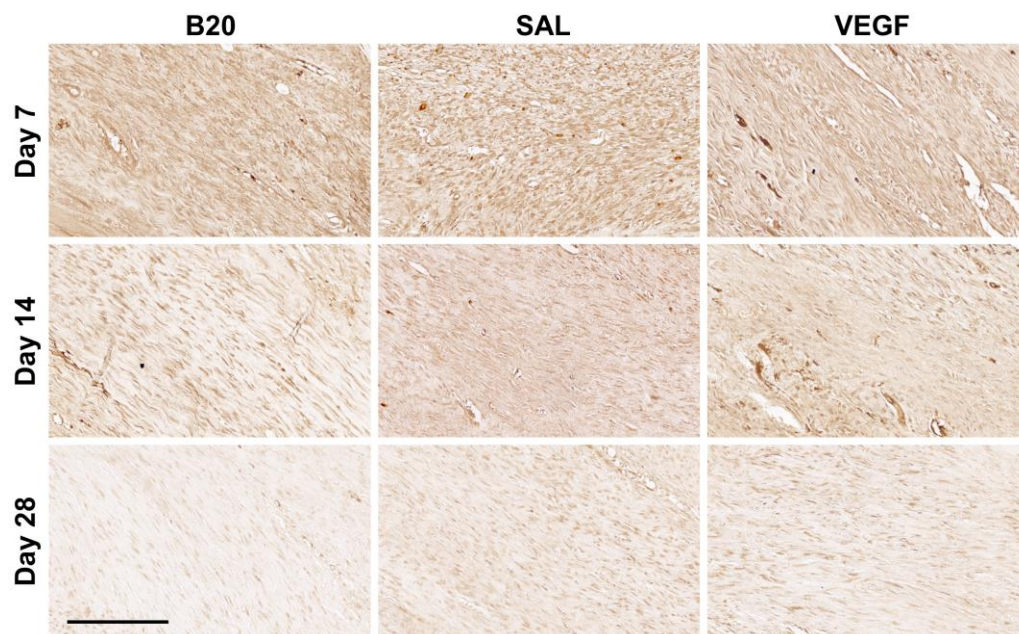
Figure 4.42: Matrix metallopeptidase 13 (MMP13) IHC representative images for B20, SAL, and VEGF at days 7, 14, and 28 (scale bar 200µm). Brown is positive staining for the antibody.
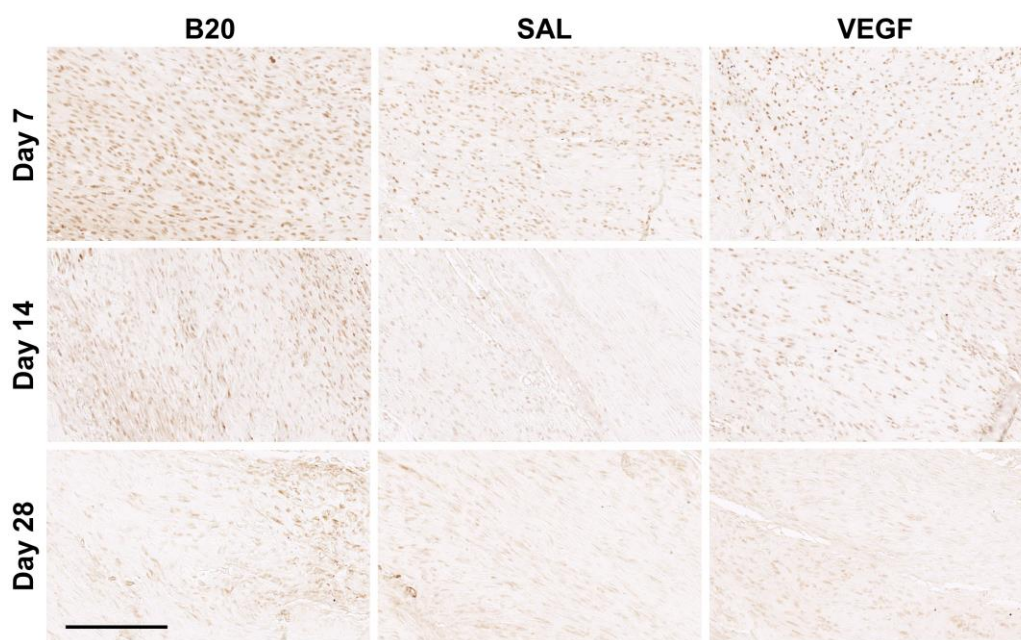
Figure 4.43: Tumor necrosis factor alpha (TNFα) IHC representative images for B20, SAL, and VEGF at days 7, 14, and 28 (scale bar 200µm). Brown is positive staining for the antibody.

Mechanics: When evaluating the early delivery group Achilles tendon mechanics, the only significant difference found was a decrease in percent relaxation in the VEGF group at day 28 (Figure 4.44B). All other parameters were not changed with treatment (Figures 46-48).
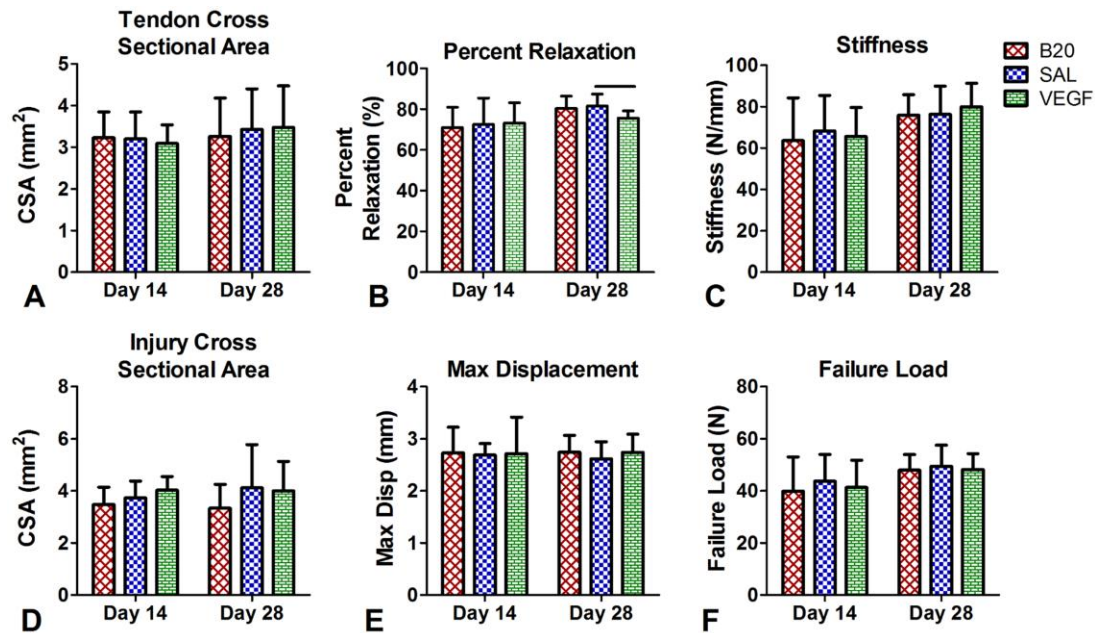
Figure 4.44: Early delivery Achilles tendon geometric and structural mechanical properties. (A) Tendon cross sectional area (CSA), (B) percent relaxation, (C) stiffness, (D) injury CSA, (E) max displacement, and (F) failure load are all shown for day 14 and 28 post-injury. The VEGF group percent relaxation was significantly decreased at day 28.
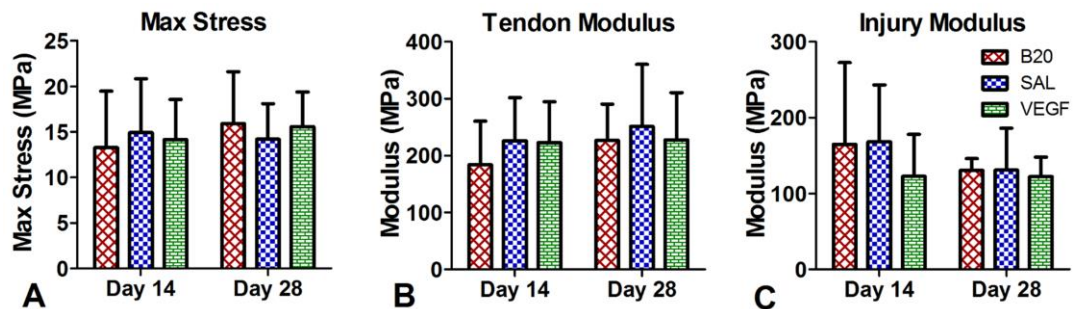
Figure 4.45: Early delivery Achilles tendon material mechanical properties. (A) Max stress and (B) tendon and (C) injury modulus parameters at days 14 and 28. There were no significant changes between groups.
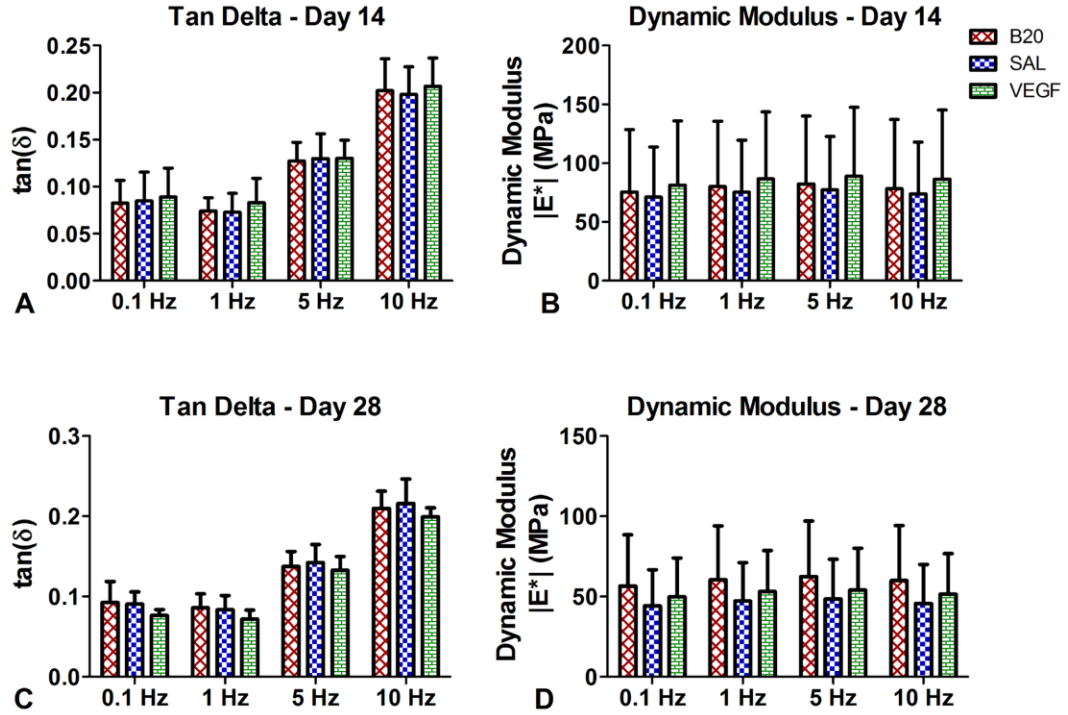
Figure 4.46: Early delivery Achilles tendon dynamic mechanical properties. (A,C) Tangent delta and (B, C) dynamic modulus at (A,B) day 14 and (C,D) day 28. There were no significant difference between groups.

D. DISCUSSION

In this chapter, we demonstrated that alterations in vascular response after injury impact tendon healing outcomes (Figure 4.47). The late delivery of anti-VEGF antibody, B20, caused a temporary reduction in healing capacity during a time point where vascularity was also decreased, and then an improvement during a later time point were vascularity was increased relative to control. However, the early delivery of B20 did not cause any changes to mechanical properties, and VEGF delivery also had a minimal impact on healing and vascular changes with both early and late delivery times (Figure 4.47).

A

LATE DELIVERY		B20					VEGF				
		3	7	14	21	28	3	7	14	21	28
Vascularity	Blood Flow Velocity		↓↓	↓↓	↑↑	↑		↓	—	↑↑	—
	Oxygenation		↓	↑↑	↑↑			↑	—	—	—
	Tissue Perfusion		↓	↓↓	↑	↑		↓	—	↑	—
Structure	Organization		—	↑↑	—	—		—	—	—	—
	Tissue Density		↑↑	↑↑	—	↑↑		—	—	—	—
Function	Gait Analysis		—	—				—	—		
	Passive Motion		—	—				—	—		
Histology	Cellularity		—	—		—		↑	—		—
	Vascularity		↓	↓↓		↓		↑↑	—		—
	Matrix Production		—	—		—		—	—		—
	Inflammation		—	—		—		—	—		—
	Matrix Degradation		↑	—		—		—	—		—
Mechanics	Geometric			—		—			—		—
	Viscoelastic			—		—			↓		—
	Structural			↓↓		—			—		—
	Material			↓↓		↑↑			—		—
	Dynamic			—		—			—		—

B

EARLY DELIVERY		B20					VEGF				
		3	7	14	21	28	3	7	14	21	28
Vascularity	Blood Flow Velocity	—	↓↓	↑	—	—	—	↓	—	—	—
	Oxygenation	↓	↓↓	↑↑	↑	↑↑	↓↓	↓	—	—	—
	Tissue Perfusion	↑↑	↓	—	↑↑	—	↑↑	—	—	—	—
Structure	Organization	—	↑	↑↑	↑↑	↑↑	—	—	—	—	—
	Tissue Density	—	↑↑	↑↑	—	↑	—	—	—	—	—
Function	Gait Analysis	—	—	—			—	—	—		
	Passive Motion	—	—	—			—	—	—		
Histology	Cellularity		—	—		—		—	—		—
	Vascularity		↓	↓		—		—	—		—
	Matrix Production		—	—		—		—	—		—
	Inflammation		—	↑↑		—		—	—		—
	Matrix Degradation		—	—		↓		—	—		—
Mechanics	Geometric			—		—			—		—
	Viscoelastic			—		—			—		↓↓
	Structural			—		—			—		—
	Material			—		—			—		—
	Dynamic			—		—			—		—

Figure 4.47: Summary of results for the (A) late and (B) early delivery group studies. B20 and VEGF columns indicate changes relative to SAL control. The findings for each analysis category are displayed with double arrows for a large (overall significant) change, and single arrows for a small (overall trending) change. Arrows are pointing up for increasing values and down for decreasing values. Arrows are colored green to indicate either increased vascularity or improved properties, and colored red to indicate either decreased vascularity or worsened properties.

There were more drastic changes observed with the delivery of B20 than the delivery of VEGF in both the early and late groups. As hypothesized B20 delivery significantly decreased vascularity at early time points, which is supported by numerous studies of anti-VEGF treatments in tumor literature.[7, 9, 21, 23, 28] However, contrary to our hypothesis, the B20 group did not induce a simple decrease in vascularity across time points but caused significant increases at later time points. Furthermore, in the early group B20 caused an increase in vascularity immediately after treatment at day 3, a decrease at day 7, and then an increase again at later time points as seen in the late group. The averaged curves for each angiogenic group demonstrates that the peak vascular response with B20 was around day 3, whereas the peak was around day 7 for the other two groups. This shift in peak vascularity earlier in the B20 group, followed by a quick reduction only 4 days later, can explain the switching of increased and decreased vascular response observed. The vascularity decrease in the late delivery group was sustained through day 14, which is the same time point where mechanical properties were reduced. This decrease in mechanical properties is supported by previous studies. In an ACL healing study, the expression of a VEGF agonist caused a significant reduction in biomechanical strength.[35] Additionally, the delivery of an anti-VEGF drug caused slowed cellular proliferation and delayed epithelial healing in the cornea.[17] However, for the early delivery group, the reduction in vascularity was already recovered by day 14 and there were no changes in mechanical properties at this time point. Because that is the first time point evaluated, it is possible that the mechanical properties could have been reduced earlier along with the decreased vascular properties but recovered by day 14 along with the vascular recovery.

147

Additionally, the early delivery B20 group had significant improvements in collagen alignment in all time points except for day 3. This finding is supported by a tendinopathy study where an anti-VEGF antibody drug resulted in more organized collagen, however no mechanical evaluation was performed.[6] In the late delivery group, there was surprisingly also an improvement in alignment but only at day 14. This data suggests that B20 changes the way that the tissue is remodeling in response to the injury. While it is counter intuitive that the collagen alignment would be improved in tissues with decreased mechanical properties, we do not see any negative changes in mechanics in the early group where there is a more significant improvement in tissue organization. Therefore, it is possible that these organizational changes are countering other mechanisms induced by the decrease in vascularity that are contributing to the reduction in mechanical properties in the late group. Unfortunately, our histological results do not provide additional insight into the mechanism causing these structural and mechanical alterations.

While the VEGF treatment did cause multiple significant changes relative to saline control, they were observed in fewer parameters and at less time points than the B20 treatment. Specifically, in the late delivery group, the largest vascular increases manifested at later time points (day 21) for ultrasound. Additionally, VEGF caused a reduction in the speed of perfusion of the tissue at early time points. However, in the early group there was also an increase in amplitude-based contrast-enhanced ultrasound parameters at early time points, but a decrease in blood oxygenation. Histologically, we found that VEGF caused an increase in vessel size but not an increase in vessel density. These findings evaluated together could indicate that VEGF is causing more structural changes to the forming

vessels than increasing the density of new vessels. During angiogenesis, VEGF expression causes vessels to become more unstable and leaky to allow for branching and vessel growth. Therefore, larger but possibly more leaky or disorganized vessels could cause a slower perfusion of the tissue with a decreased blood oxygenation. However, because the vessels are also larger, that could account for the increases in area under the curve and peak enhancement at early time points. This finding is also supported by a study evaluating how the dosage of VEGF effects the morphology of the vessels. Specifically, lower dosages of VEGF induce increased vessel density, whereas higher doses increase vessel size.[27] It is possible that adding more VEGF to a system with an already robust vascular response is acting as a "higher" dosage that is inducing structural changes to the vessels that are not beneficial to tendon healing.

In the previous chapter we demonstrated more significant increases in vascularity with VEGF delivery after injury than observed in this work. These smaller changes observed in this chapter could be due to the use of younger animals potentially with a more robust vascular response to injury. Interestingly, the only significant mechanical change observed with this treatment group is a decrease in percent relaxation, which would be considered less viscous and more similar to healthy tendon values. Since there are no significant alterations to mechanical properties, it is not surprising that there are no changes in collagen organization or histological properties. When comparing to previous literature, there is support for increased vascular response with VEGF delivery during tissue healing,[2, 4, 15, 20, 35, 37] including in tendon injury models. However, the majority of these studies only evaluate vascular changes only using histological measures, where we were able to perform

a comprehensive vascular analysis using *in vivo* ultrasound imaging in the tendon. Contrary to our results, many of the tendon or ligament studies evaluating VEGF delivery found significant improvements in mechanical properties.[16, 35, 38] However, none of the tendon or ligament studies with mechanical evaluation directly measured what vascular changes occurred with their treatment, so it is difficult to compare our angiogenic treatment to these models. However, skin healing models have also consistently reported improved healing outcomes and increased vascularity with VEGF treatment. [2, 4, 5, 20] It is possible that our VEGF delivery model did not cause a large enough vascular change to induce the improvements in healing that is observed in these models.

In addition to mechanical outcomes, we also evaluated *in vivo* measures of joint function. While there were a few transient changes seen due to treatment, a majority of the parameters did not have significant changes at any time point. Therefore, we conclude that there are insignificant alterations to animal ambulation and ankle function with the administration of these treatments. This is information is beneficial because even though we did not find improvements in healing properties with these groups, we know that this level of vascular modulation does not also create significant detriments to joint function, which could be promising for future studies in other tendon models.

In this work, we were able to implement color Doppler, photoacoustics, and non-linear contrast-enhanced ultrasound imaging to provide multiple metrics for evaluating vascular alterations, including vessel density, blood flow velocity, blood oxygenation, and time- and amplitude-based perfusion parameters. This is the first time that all of these *in vivo* vascular properties have been evaluated in the context of tendon healing.

Interestingly, we found that Doppler ultrasound and photoacoustics are just as sensitive to detecting changes in vascularity due to these treatments as contrast-enhanced ultrasound. This is surprising given that contrast is able to detect perfusion through much smaller vessels. It is possible that it is the larger vessels that are undergoing more of the changes due to these treatments, particularly in the case of VEGF delivery, allowing these less sensitive ultrasound measures to also detect alterations due to treatment and injury. Finally, we found that these imaging parameters were more consistent at detecting vascular changes than the more commonly used histological staining methods.

This work is not without limitations. In this chapter, we only evaluated one dosage for each angiogenic factor. While we previously tested multiple dosages of B20 in Chapter 3, we did not evaluate multiple dosages of VEGF due to the literature support for the dosage we selected, as well as our positive results in Chapter 3. However, we found only mild vascular changes with this VEGF dosage and subsequently no major differences in healing outcome. It is possible that we need to implement a higher VEGF dosage to induce a more significant vascular change for this particular rat strain and age. However, it is unknown if a higher dose of VEGF would be beneficial in this model even though anti-VEGF was shown to decreased mechanical properties. Another limitation is that we did not evaluate other angiogenic factors in addition to VEGF and anti-VEGF. Both bFGF and PDGF-BB have also been shown in the literature to induce vascular changes during wound healing,[10, 18, 19] and there are a variety of other anti-angiogenic therapies that have different mechanisms of action that could be implemented.[7, 9, 28] However, the factors evaluated in this work were chosen because there was the most support in the literature to induce the

desired vascular changes. Additionally, we only evaluated mechanical outcomes at days 14 and 28. It is possible that mechanical changes existed in the early delivery group at earlier time points when B20 induced a reduced vascular response, but this would be very transient since there were no changes by day 14. We also do not perform other biological assays besides immunohistochemistry. These methods were chosen to evaluate the localized deposition of proteins, but the sensitivity for quantifying immunohistochemistry is limited. However, proteomics or mRNA analysis could provide more insight about how different processes, such as inflammation, matrix production, and angiogenesis, are impacted by the vascular modulation. However, tissue within and adjacent to the injury site were harvested for future protein or mRNA analysis.

This study was the first to evaluate vascular changes using both *in vivo* imaging methods and *ex vivo* histological methods, as well as functional and mechanical outcomes associated with these vascular changes. We demonstrated that reducing the vascular response following injury impairs healing potential at early time points, but increasing vascular response does not improve healing potential in adult animals. This work is also the first to substantially use new imaging methods, such as photoacoustics, to evaluate blood oxygenation alterations during tendon healing. In the next chapter, we will evaluate the delivery of these pro- and anti-angiogenic factors in an aged model to determine if the vascular modulation could aid healing in a model of impaired healing and reduced vascular response.

E. REFERENCES

1.	Barros L.F. and Belfort R., Jr. The effects of the subconjunctival injection of bevacizumab (avastin) on angiogenesis in the rat cornea. *An Acad Bras Cienc* 2007; 79(3)**:** 389-394.

2.	Basu G., Downey H., Guo S., Israel A., Asmar A., Hargrave B. and Heller R. Prevention of distal flap necrosis in a rat random skin flap model by gene electro transfer delivering vegf(165) plasmid. *J Gene Med* 2014; 16(3-4)**:** 55-65.

3.	Chan B.P., Fu S., Qin L., Lee K., Rolf C.G. and Chan K. Effects of basic fibroblast growth factor (bfgf) on early stages of tendon healing: A rat patellar tendon model. *Acta Orthop Scand* 2000; 71(5)**:** 513-518.

4.	Chereddy K.K., Lopes A., Koussoroplis S., Payen V., Moia C., Zhu H., Sonveaux P., Carmeliet P., des Rieux A., Vandermeulen G. and Preat V. Combined effects of plga and vascular endothelial growth factor promote the healing of non-diabetic and diabetic wounds. *Nanomedicine* 2015; 11(8)**:** 1975-1984.

5.	Corral C.J., Siddiqui A., Wu L., Farrell C.L., Lyons D. and Mustoe T.A. Vascular endothelial growth factor is more important than basic fibroblastic growth factor during ischemic wound healing. *Arch Surg* 1999; 134(2)**:** 200-205.

6.	Dallaudiere B., Lempicki M., Pesquer L., Louedec L., Preux P.M., Meyer P., Hess A., Durieux M.H., Hummel V., Larbi A., Deschamps L., Benayoun Y., Journe C., Perozziello A., Schouman-Claeys E., Michel J.B. and Serfaty J.M. Acceleration of tendon healing using us guided intratendinous injection of bevacizumab: First pre-clinical study on a murine model. *Eur J Radiol* 2013; 82(12)**:** e823-828.

7.	Denorme M., Yon L., Roux C., Gonzalez B.J., Baudin E., Anouar Y. and Dubessy C. Both sunitinib and sorafenib are effective treatments for pheochromocytoma in a xenograft model. *Cancer Lett* 2014; 352(2)**:** 236-244.

8.	Emami M.J., Jaberi F.M., Azarpira N., Vosoughi A.R. and Tanideh N. Prevention of arthrofibrosis by monoclonal antibody against vascular endothelial growth factor: A novel use of bevacizumab in rabbits. *Orthop Traumatol Surg Res* 2012; 98(7)**:** 759-764.

9.	Falcon B.L., Hashizume H., Koumoutsakos P., Chou J., Bready J.V., Coxon A., Oliner J.D. and McDonald D.M. Contrasting actions of selective inhibitors of angiopoietin-1 and angiopoietin-2 on the normalization of tumor blood vessels. *Am J Pathol* 2009; 175(5)**:** 2159-2170.

10.	Fayazzadeh E., Ahmadi S.H., Rabbani S., Boroumand M.A., Salavati A. and Anvari M.S. A comparative study of recombinant human basic fibroblast growth factor (bfgf) and erythropoietin (epo) in prevention of skin flap ischemic necrosis in rats. *Arch Iran Med* 2012; 15(9)**:** 553-556.

11.   Fenwick S.A., Hazleman B.L. and Riley G.P. The vasculature and its role in the damaged and healing tendon. *Arthritis Res* 2002; 4(4)**:** 252-260.

12.   Fevata M. Scarless healing in the fetus: Implications and strategies for postnatal tendon repair. University of Pennsylvania, Philadelphia, PA, 2006.

13.   Garcia T., Hornof W.J. and Insana M.F. On the ultrasonic properties of tendon. *Ultrasound Med Biol* 2003; 29(12)**:** 1787-1797.

14.   Hall K. and Ran S. Regulation of tumor angiogenesis by the local environment. *Front Biosci (Landmark Ed)* 2010; 15**:** 195-212.

15.   Ju Y.J., Tohyama H., Kondo E., Yoshikawa T., Muneta T., Shinomiya K. and Yasuda K. Effects of local administration of vascular endothelial growth factor on properties of the in situ frozen-thawed anterior cruciate ligament in rabbits. *Am J Sports Med* 2006; 34(1)**:** 84-91.

16.   Kaux J.F., Janssen L., Drion P., Nusgens B., Libertiaux V., Pascon F., Heyeres A., Hoffmann A., Lambert C., Le Goff C., Denoel V., Defraigne J.O., Rickert M., Crielaard J.M. and Colige A. Vascular endothelial growth factor-111 (vegf-111) and tendon healing: Preliminary results in a rat model of tendon injury. *Muscles Ligaments Tendons J* 2014; 4(1)**:** 24-28.

17.   Kim T.I., Chung J.L., Hong J.P., Min K., Seo K.Y. and Kim E.K. Bevacizumab application delays epithelial healing in rabbit cornea. *Invest Ophthalmol Vis Sci* 2009; 50(10)**:** 4653-4659.

18.   Kobayashi D., Kurosaka M., Yoshiya S. and Mizuno K. Effect of basic fibroblast growth factor on the healing of defects in the canine anterior cruciate ligament. *Knee Surg Sports Traumatol Arthrosc* 1997; 5(3)**:** 189-194.

19.   Kovacevic D., Gulotta L.V., Ying L., Ehteshami J.R., Deng X.H. and Rodeo S.A. Rhpdgf-bb promotes early healing in a rat rotator cuff repair model. *Clin Orthop Relat Res* 2015; 473(5)**:** 1644-1654.

20.   Kryger Z., Zhang F., Dogan T., Cheng C., Lineaweaver W.C. and Buncke H.J. The effects of vegf on survival of a random flap in the rat: Examination of various routes of administration. *Br J Plast Surg* 2000; 53(3)**:** 234-239.

21.   Mancuso M.R., Davis R., Norberg S.M., O'Brien S., Sennino B., Nakahara T., Yao V.J., Inai T., Brooks P., Freimark B., Shalinsky D.R., Hu-Lowe D.D. and McDonald D.M. Rapid vascular regrowth in tumors after reversal of vegf inhibition. *J Clin Invest* 2006; 116(10)**:** 2610-2621.

22.   Manzano R.P., Peyman G.A., Khan P. and Kivilcim M. Testing intravitreal toxicity of bevacizumab (avastin). *Retina* 2006; 26(3)**:** 257-261.

23. Matsumoto S., Saito K., Takakusagi Y., Matsuo M., Munasinghe J.P., Morris H.D., Lizak M.J., Merkle H., Yasukawa K., Devasahayam N., Suburamanian S., Mitchell J.B. and Krishna M.C. In vivo imaging of tumor physiological, metabolic, and redox changes in response to the anti-angiogenic agent sunitinib: Longitudinal assessment to identify transient vascular renormalization. *Antioxid Redox Signal* 2014; 21(8)**:** 1145-1155.

24. Needles A., Arditi M., Rognin N.G., Mehi J., Coulthard T., Bilan-Tracey C., Gaud E., Frinking P., Hirson D. and Foster F.S. Nonlinear contrast imaging with an array-based micro-ultrasound system. *Ultrasound Med Biol* 2010; 36(12)**:** 2097-2106.

25. Needles A., Heinmiller A., Sun J., Theodoropoulos C., Bates D., Hirson D., Yin M. and Foster F.S. Development and initial application of a fully integrated photoacoustic micro-ultrasound system. *IEEE Trans Ultrason Ferroelectr Freq Control* 2013; 60(5)**:** 888-897.

26. Okada Y., Akisue T., Hara H., Kishimoto K., Kawamoto T., Imabori M., Kishimoto S., Fukase N., Onishi Y. and Kurosaka M. The effect of bevacizumab on tumour growth of malignant fibrous histiocytoma in an animal model. *Anticancer Res* 2010; 30(9)**:** 3391-3395.

27. Parsons-Wingerter P., Chandrasekharan U.M., McKay T.L., Radhakrishnan K., DiCorleto P.E., Albarran B. and Farr A.G. A vegf165-induced phenotypic switch from increased vessel density to increased vessel diameter and increased endothelial nos activity. *Microvasc Res* 2006; 72(3)**:** 91-100.

28. Peng F., Xu Z., Wang J., Chen Y., Li Q., Zuo Y., Chen J., Hu X., Zhou Q., Wang Y., Ma H., Bao Y. and Chen M. Recombinant human endostatin normalizes tumor vasculature and enhances radiation response in xenografted human nasopharyngeal carcinoma models. *PLoS One* 2012; 7(4)**:** e34646.

29. Riggin C.N., Rodrigues A.B., Weiss S.N., Raja H.A., Chen M., Schultz S.M., Sehgal C.M. and Soslowsky L.J. Modulation of vascular response after injury in the rat achilles tendon alters healing capacity. *Orthopaedic Research Society*. San Diego, CA. 2018. 0567.

30. Riggin C.N., Sarver J.J., Freedman B.R., Thomas S.J. and Soslowsky L.J. Analysis of collagen organization in mouse achilles tendon using high-frequency ultrasound imaging. *J Biomech Eng* 2014; 136(2)**:** 021029.

31. Riggin C.N., Schultz S.M., Sehgal C.M. and Soslowsky L.J. Effect of pro- and anti-angiogenic factors on vascular response in the rat achilles tendon after injury. *Orthopaedic Research Society*. San Diego, CA 2017. 1580.

32. Sarver J.J., Dishowitz M.I., Kim S.Y. and Soslowsky L.J. Transient decreases in forelimb gait and ground reaction forces following rotator cuff injury and repair in a rat model. *J Biomech* 2010; 43(4)**:** 778-782.

33. Sarver J.J., Peltz C.D., Dourte L., Reddy S., Williams G.R. and Soslowsky L.J. After rotator cuff repair, stiffness--but not the loss in range of motion--increased transiently for

immobilized shoulders in a rat model. *J Shoulder Elbow Surg* 2008; 17(1 Suppl)**:** 108S-113S.

34. Sehgal C.M., Arger P.H., Silver A.C., Patton J.A., Saunders H.M., Bhattacharyya A. and Bell C.P. Renal blood flow changes induced with endothelin-1 and fenoldopam mesylate at quantitative doppler us: Initial results in a canine study. *Radiology* 2001; 219(2)**:** 419-426.

35. Takayama K., Kawakami Y., Mifune Y., Matsumoto T., Tang Y., Cummins J.H., Greco N., Kuroda R., Kurosaka M., Wang B., Fu F.H. and Huard J. The effect of blocking angiogenesis on anterior cruciate ligament healing following stem cell transplantation. *Biomaterials* 2015; 60**:** 9-19.

36. Tempfer H. and Traweger A. Tendon vasculature in health and disease. *Front Physiol* 2015; 6**:** 330.

37. Yoshikawa T., Tohyama H., Katsura T., Kondo E., Kotani Y., Matsumoto H., Toyama Y. and Yasuda K. Effects of local administration of vascular endothelial growth factor on mechanical characteristics of the semitendinosus tendon graft after anterior cruciate ligament reconstruction in sheep. *Am J Sports Med* 2006; 34(12)**:** 1918-1925.

38. Zhang F., Liu H., Stile F., Lei M.P., Pang Y., Oswald T.M., Beck J., Dorsett-Martin W. and Lineaweaver W.C. Effect of vascular endothelial growth factor on rat achilles tendon healing. *Plast Reconstr Surg* 2003; 112(6)**:** 1613-1619.

CHAPTER 5: EFFECT OF VASCULAR MODULATION ON ACHILLES TENDON HEALING WITH AGING

A. INTRODUCTION

The frequency of musculoskeletal injury is expected to increase greatly in the coming decades with both increased life expectancy and a sustained higher level of activity with aging. It is expected that the number of people older than 60 years will exceed 1 billion by the year 2025.[1, 13] There are many challenges associated with advanced age, namely the development of multiple impairments, alterations in physiological functions, decline in functional capacity, and ultimately loss of independence.[13] Many of the contributors to these challenges and disabilities are due to structural and functional changes to the musculoskeletal system with aging.[13]

Tendon injuries in particular positively correlate with patient age, as aging has significant effects on both tendon homeostatic maintenance as well as tendon healing potential after injury.[25] Mechanical evaluations have demonstrated impaired structural and material properties with aging including alterations in elastic modulus, viscoelastic properties, and stiffness.[20, 30, 41] Additionally, this decline in mechanical properties has been shown to correlate with a reduction in collagen content.[10, 11] When investigating aging on a cellular level, aged tenocytes have been found to be less viable with a lower proliferation rate, motility, density, and organization within the tissue.[2, 4, 40, 44] This could indicate a reduced potential for the cells to perform maintenance or reparative tasks, which may lead to tendon degeneration. Protein and mRNA expression is significantly altered, with

decreased expression of extracellular matrix proteins such as proteoglycans, elastin, aggrecan, and collagens I, III, and V, as well as increased levels of matrix metallopeptidase (MMP)-2 and -9 indicating increased matrix degradation.[18, 23, 40, 44] When evaluating tendons after injury, aging causes significant reductions in max load and stiffness of the healing tendon along with less organized fiber organization and a reduction in matrix production at the injury site.[2, 29] All of this data suggests that aging has major effects on the tendon's ability to maintain homeostasis, increasing susceptibility to rupture, as well as impairing the ability to recover from an injury.

Tendon vascularity is also altered with aging. Clinical ultrasound studies have demonstrated reduced blood flow[14, 21, 36] and histological studies show decreased vessel density in uninjured tendons with aging.[23, 24] Cellular studies have demonstrated reduced vascular endothelial cell expansion and differentiation potential in tendon cell populations harvested from older age groups.[42] This suggests that aged tendons are less capable of forming or maintaining the necessary vascular structure, and these changes in vasculature could alter their cellular responses, contributing to reduced healing capacity in the aged population.

While aging affects tendon maintenance, vascular structure, and healing potential, it is unknown how aging affects the vascular response following injury in the tendon. Additionally, we have shown that delivery of VEGF and anti-VEGF antibody locally to tendons can increase and decrease the vascular response after injury in young animals, respectively.[33] However, the effect of altering the vascular response after injury in the aged population is also unknown. Therefore, the objective of this study is to evaluate the

vascular response following Achilles tendon injury in adult and aged rats, and to define the alterations to tendon healing in an aged model following injection of angiogenic factors. We hypothesize that when compared to adult rats, aged rats will demonstrate a decrease in blood flow parameters as well as a decrease in vascular density following injury. Additionally, we hypothesize that increasing the vascular response through the administration of a pro-angiogenic treatment will improve healing capacity as shown by increased mechanical properties.

B. METHODS

B-1. Study Design

Study 1 – Vascular Response to Injury with Aging: We investigated 5 adult (4 months old) and 5 aged (16 months old) Sprague Dawley rats. All animals underwent a bilateral Achilles incisional injury followed by bilateral color Doppler ultrasound imaging on day 7 post-injury and sacrifice on the same day for histological evaluation (n = 8-9 tendons/group) (Figure 5.1).

Figure 5.1: Study Design to evaluate the effect of age on vascular response after injury. "U" represents ultrasound imaging, and "O" represents sacrifice for histological evaluation.

159

Study 2 – Vascular Modulation with Aging: 36 Fischer 344 rats (19-20 months old) underwent a bilateral Achilles incisional injury, followed by local injections of vascular endothelial growth factor (VEGF) (Peprotech, Rocky Hill, NJ), anti-VEGF antibody (B20.4-1-1, Genentech, San Francisco, CA), or saline (SAL). *In vivo* ultrasound imaging (b-mode, color Doppler, photoacoustics, and contrast-enhanced ultrasound) was performed and animals were sacrificed 14 days after injury for histological and mechanical evaluation (Figure 5.2).

Figure 5.2: Study Design for the effect of vascular modulation on tendon healing in aged animals. "U" represents ultrasound imaging and "X" represents sacrifice for mechanical, histological, and biological assays.

B-2. Surgical Approach

All procedures were performed in accordance with the University of Pennsylvania Institutional Animal Care and Use Committee. Animals were anesthetized with isoflurane inhalation, and using aseptic technique, a full thickness incisional injury was made in the center of the tendon width in the mid-substance region as described in Chapter 3 Section B-2.

B-3. Angiogenic Injections

For Study 2 only, each animal received either 5μg VEGF or 250μg anti-VEGF antibody (B20) in 20μl saline, or 20μl saline only, injected bilaterally intratendinously on days 4-6 after surgical injury. These dosages were chosen based on literature values[5, 10, 16, 22, 28, 45] and the findings from Chapter 3 Sections C-1 and C-2.[33] The injections were administrated percutaneously in the coronal plane from the medial side of the tendon, with 10μl of the solution injected above and 10μl injected below the injury site.

B-4. Ultrasound Imaging

Imaging was performed on day 7 (Study 1 and 2) and 14 (Study 2 only) using a Vevo LAZR ultrasound system (VisualSonics, Toronto, ON). Only color Doppler imaging was performed for Study 1. Following anesthetization using inhalation of isoflurane, all hair was removed from the hind limb by shaving and hair removal cream to allow for ultrasound visualization. The animal was placed on a heated imaging table with the ankle secured at 90° flexion. The transducer was placed to image the sagittal plane ensuring that the tendon was parallel to the surface of the transducer and the tendon length was in plane with the transducer length. The tendon was centered at a focal zone at 7mm image depth.

Color Doppler Ultrasound: Image acquisition, animal positioning, and image analysis was performed as described in Chapter 3 Section B-4. Briefly, the central 8-10 tendon images were analyzed using a custom IDL program (Harris Geospatial Solutions, Herndon, VA). The mean color level (average blood flow velocity), fractional area (% area of Doppler signal), and color weighted fractional area (weighted average of blood flow

velocity/unit area) were quantified[38] over the entire tendon area and within a 3mm^2 rectangular area over the injury region. Measures for each image segment for a specimen were averaged to obtain a representative value of the entire tendon.

Photoacoustic Imaging: As described in Chapter 3 Section B-5, images were taken at two wavelengths (750 and 850 nm)[27] within the center of each tendon. Blood oxygenation (sO$_2$ Avg), average hemoglobin (HbT Avg), and relative tissue oxygenation (sO$_2$ Tot) were quantified over the entire tendon area and within a 3mm^2 rectangular area over the injury region. Measures for all image segments for a specimen were averaged to obtain a representative value for the entire tendon.

Contrast-Enhanced Ultrasound: Image acquisition and analysis was performed as described in Chapter 4 Section B-4. Briefly, the Achilles tendon was visualized in non-linear contrast mode using the MS250 transducer (18MHz center frequency). A 200 sec ultrasound video clip was initiated at the start of the bolus injection of 100µl of Definity (Lantheus Medical Imaging, Billerica, MA) microbubble contrast agent followed immediately by a bolus injection of 200µl of saline. The ultrasound clip was analyzed using contrast analysis program VevoCQ (VisualSonics, Toronto, ON),[26] where perfusion of the contrast agent was quantified for each frame of the clip and a curve-fitting algorithm was applied to the echo-power data as a function of time. Amplitude- and time-based perfusion parameters were then derived from this model.[26]

B-mode Ultrasound Alignment Analysis: Images were taken at a center frequency of 40MHz (LZ550 transducer), with an effective resolution of 40 µm, for collagen alignment analysis as previously described in Chapter 2 Section B-3.[32] Image acquisition

and animal positioning was performed as described in Chapter 4 Section B-4. The circular standard deviation (CSD), a measure of the distribution of collagen alignment, and echogenicity measures were calculated over the entire tendon area and within a $3mm^2$ rectangular area over the injury region. Measures for each image segment in a specimen were averaged to obtain a value representative of the entire tendon thickness.

B-5. Tendon Histology

Study 1 – Vascular response to injury with aging: Bilateral tendon samples from 7 days post-injury (n=8-9 tendons/group) were dissected, paraffin processed, and sectioned at 5µm in the sagittal plane. Sections were stained with hematoxylin-eosin (H&E) and immunohistochemical (IHC) staining for vascular endothelial cell marker (CD34). Histology images were taken in the injury region of the tendon at 50x magnification for CD34 (in order to better view vascular structure) and 100x magnification for H&E, and images were semi-quantitatively graded by three blinded investigators.

Study 2 – Vascular modulation with aging: Histological samples were processed, stained, and analyzed as described in Chapter 4 Section B-7. Briefly, tendon samples from 7 and 14 days post-injury (n=6/group) were dissected, paraffin processed, and sectioned at 5µm in the sagittal plane. Sections were stained with hematoxylin-eosin (H&E) and immunohistochemical (IHC) staining for vascular endothelial cell marker (CD34), vascular endothelial growth factor (VEGF), angiopoietin-1 (Ang-1), collagen type III (Col III), matrix metallopeptidase-13 (MMP-13), and tumor necrosis factor alpha (TNFα).

163

Histology images were taken in the injury region of the tendon at 50x magnification for CD34 (in order to better view vascular structure) and 100x magnification for all other stains. H&E and CD34 were semi-quantitatively graded by three blinded investigators. All other IHC stains were quantitatively analyzed for percent area of positive stain using a custom MATLAB program (Mathworks, Natick, MA).

B-6. Tendon Mechanics

Mechanical testing was performed as described in Chapter 4 Section B-8. Briefly, tendons from 14 days after injury (n=12/group) in Study 2 were prepared for tensile testing. The Achilles tendon was removed and fine dissected. Verhoeff stain was applied for optical tracking. Tendon cross-sectional area was measured using a custom laser-based device.[12] The tendon was tested in tension using an ElectroPuls E3000 (Instron, Norwood, MA) with a 250N load cell. The mechanical protocol consisted of (1) preloading (0.15N), (2) preconditioning (0.5% to 1.5% strain at 0.25Hz for 30 cycles), (3) stress-relaxation (6% strain for 10 minutes), (4) a dynamic frequency sweep (0.125% strain amplitude at 0.1, 1, 5, and 10 Hz, for 10 cycles each), and (5) ramp to failure (0.1% strain/sec). Tendon viscoelastic and dynamic properties of percent relaxation, dynamic modulus ($|E^*|$), and the tangent of the phase shift between stress and strain ($\tan(\delta)$) were computed. Quasi-static properties were determined from the slope of the linear region of the force vs. displacement (stiffness) or stress vs. strain (elastic modulus) curves, as well as from failure properties (max force, displacement, and stress).

B-7. Statistics

Normally distributed data was analyzed using a 1-way ANOVA followed by Bonferroni multiple comparisons post-hoc tests with all comparisons made to saline control within a time point. Non-normally distributed data was analyzed using Kruskal-Wallis 1-way ANOVA followed by Dunn's multiple comparison post-hoc tests with comparisons made to saline control within a time point. To adjust for multiple comparisons, significance was set at p≤0.025 (indicated by solid bars) and trends at p≤0.05 (indicated by dashed bars). Bar plots are displayed as mean and standard deviation and box plots represent median and interquartile range.

C. RESULTS

C-1. Study 1: Vascular Response to Injury with Aging

Color Doppler Ultrasound: For the analysis of color Doppler ultrasound (Figure 5.3), there was a significant decrease in mean color level (MCL), fractional area (FA), and color weighted fractional (CWFA) area following injury in the aged group at 7 days post-injury.
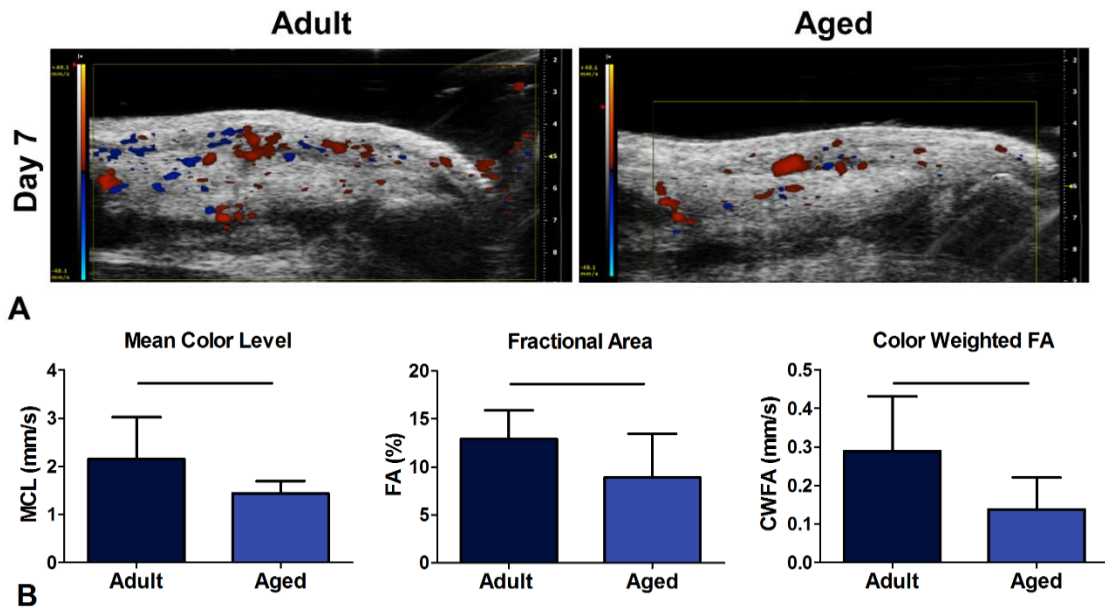
Figure 5.3: (A) Representative images for color Doppler ultrasound analysis. (B) Quantification of mean color level (MCL), fractional area (FA), and color weighted fractional area (CWFA). Solid bars indicate $p<0.05$.

Histological Analysis: H&E analysis of cell number and cell shape did not demonstrate differences between groups (Figure 5.4). Immunohistochemical evaluation of CD34 (Figure 5.5), a marker of vascular endothelial cells, showed a significant decrease in vessel density but no change in vessel size following injury in the aged group.
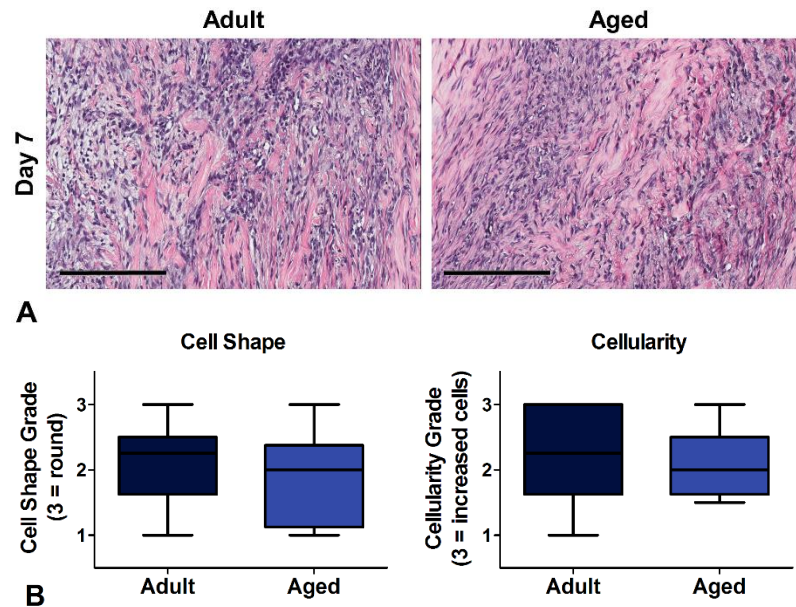
Figure 5.4: H&E histological analysis. (A) Representative images (scale bar 200μm) and (B) semi-quantitative analysis of cell shape and cellularity. Images taken at 100x magnification.
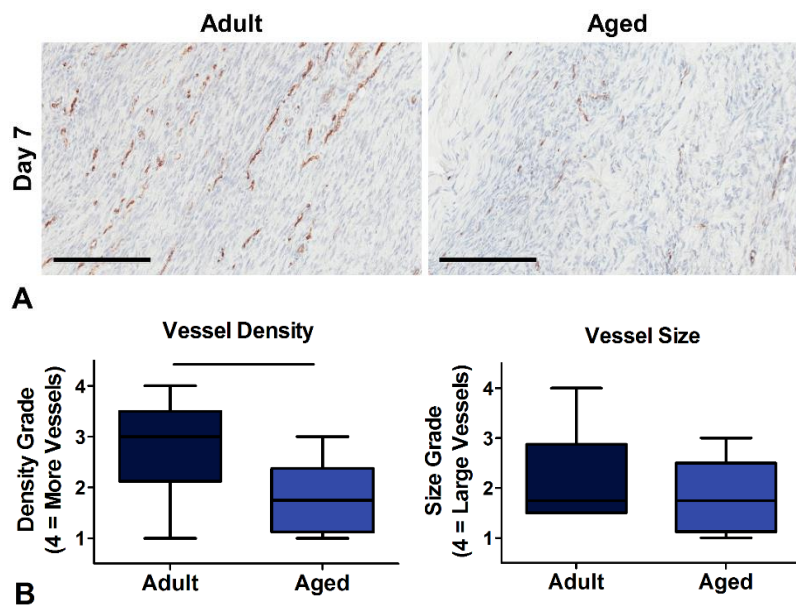
Figure 5.5: CD34 immunohistological analysis. (A) Representative images (scale bar 200μm) and (B) semi-quantitative analysis of vessel density and vessel size. Aged animals had a significantly reduced vessel density compared to adult animals. Solid bars indicate $p < 0.05$.

C-2. Study 2: Vascular Modulation with Aging

<u>Color Doppler Ultrasound</u>: There was a significant increase in MCL, representing increased blood flow velocity, in the VEGF group tendon ROI at day 7 after injury (Figure 5.6B). The B20 group had a trending decrease in MCL at day 7 in the tendon and day 14 in both ROIs (Figure 5.6B,E). Additionally, this group significant decreased FA and CWFA for both ROIs at both time points except CWFA day 14 in the injury region (Figure 5.6C,D,F,G).

<u>Photoacoustic Imaging</u>: The VEGF group had a trending increase in blood oxygenation at day 14 in both ROIs (Figure 5.7B,E). Additionally, this group had a significant increase in average hemoglobin (Figure 5.7C,F) and tissue oxygenation (Figure 5.7D,G) on day 7 in both ROIs and day 14 in the injury ROI. The B20 group average hemoglobin and tissue oxygenation was significantly decreased on day 7 in the tendon ROI (Figure 5.7C,D).
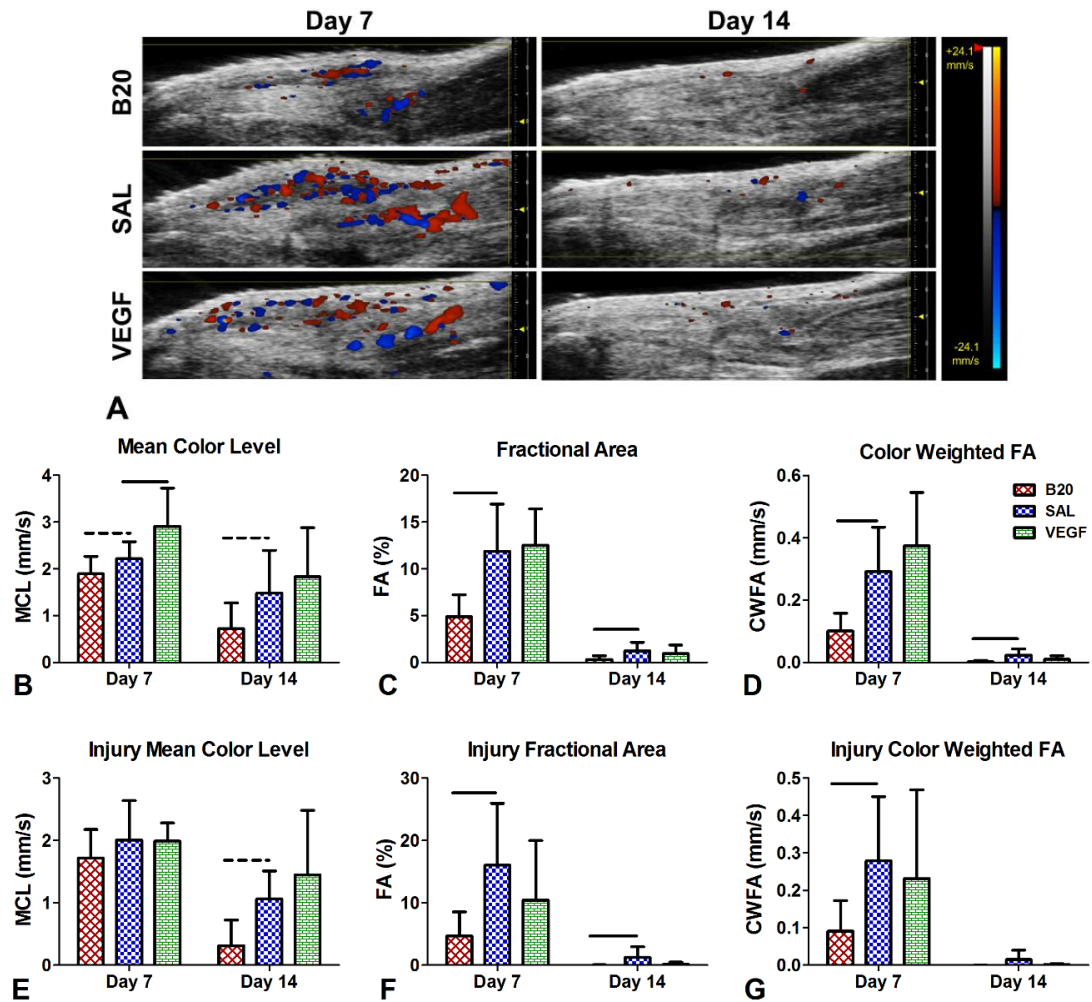
Figure 5.6: (A) Representative images of color Doppler ultrasound, where the red and blue color scale represents blood flow velocity towards and away from the transducer, respectively. Quantification of (B,E) mean color level (MCL), (C,F) fractional area (FA), and (D,G) color weighted fractional area (CWFA) in both the (B-D) tendon and (E-G) injury regions of interest (ROIs). VEGF caused a significant increase in MCL at day 7, where B20 caused a trending or significant decreases in all three properties at multiple time points.
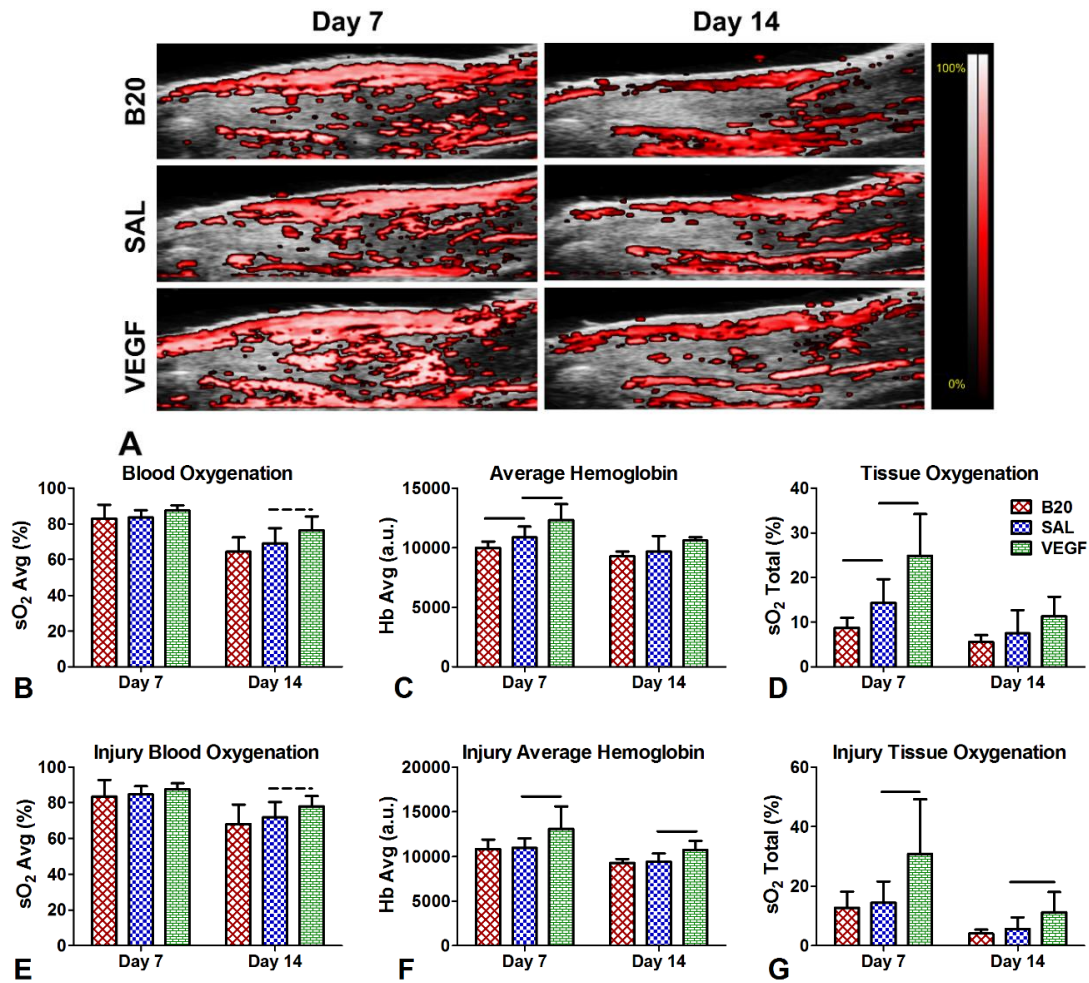
Figure 5.7: (A) Representative images of photoacoustic ultrasound, where the overlaid color scale indicates oxygen saturation of the detected hemoglobin. Quantification of (B,E) blood oxygenation (sO_2 Avg), (C,F) average hemoglobin (Hb Avg), and (D,G) tissue oxygenation (sO_2 Total) for (B-D) tendon and (E-G) injury ROIs. VEGF caused significant or trending increases in all three parameters at multiple time points, where B20 caused significant decreases in Hb Avg and sO_2 Total in the tendon at day 7.

Contrast-Enhanced Ultrasound: For the amplitude-based contrast parameters, the B20 group significantly decreased peak enhancement (PE) in the injury ROI for both time points and had a trending decrease in the tendon ROI at day 14 (Figure 5.8B,E). Additionally, this group had trending and significant decreases in wash-in area under the curve (WiAUC) in the tendon and injury ROIs, respectively, at both time points (Figure

170

5.8C,F). Finally, this group caused a significantly decreased area under the curve (AUC) at day 7, and had a trending decrease at day 14, in the injury region. (Figure 5.8G). There were no significant changes in the VEGF group in any amplitude-based parameter.
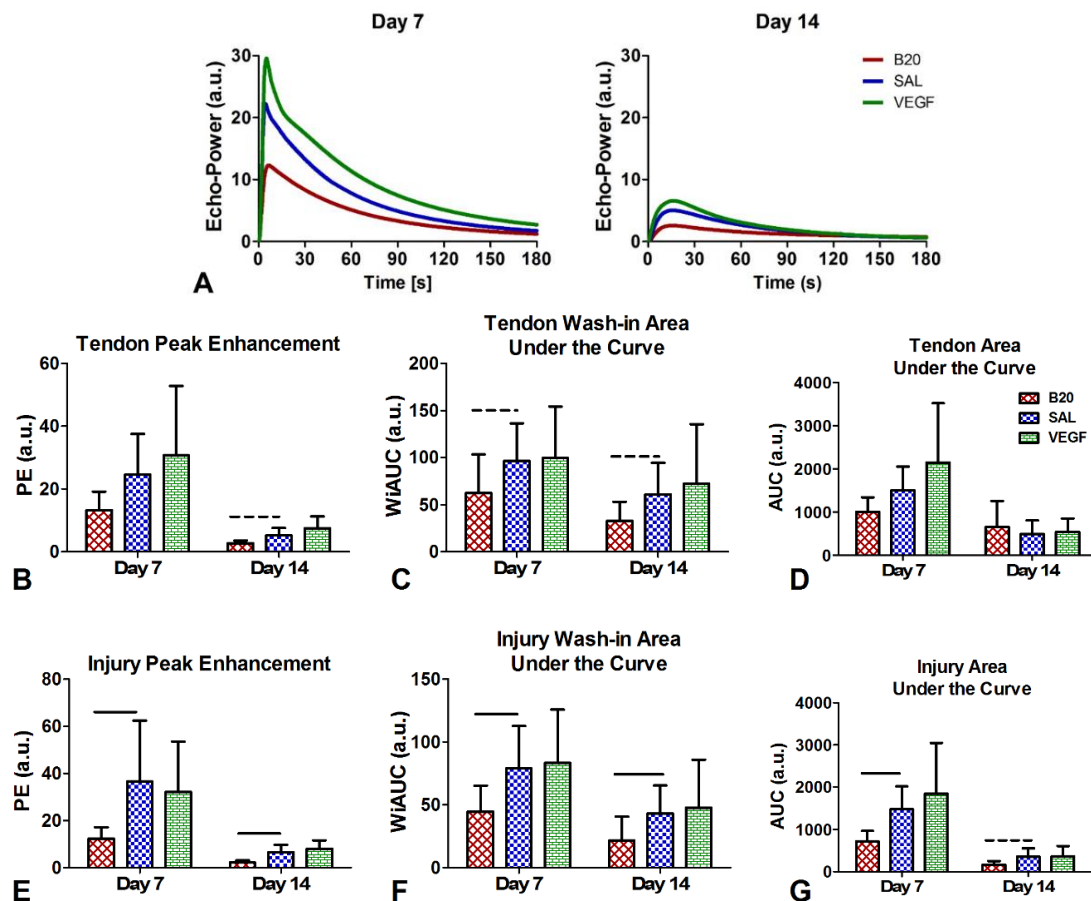
Figure 5.8: Amplitude-based contrast-enhanced ultrasound parameters. (A) Average echo-power vs. time curves for each treatment on days 7 and 14. Quantification of (B,E) peak enhancement (PE), (C,F) wash-in area under the curve (WiAUC), and (D,G) area under the curve (AUC) for the (B-D) tendon and (E-G) injury ROIs. B20 was decreased in all parameters at multiple time points, where VEGF caused no change compared to saline.

For the time-based contrast enhanced parameters, there were no changes in rise time (RT) (Figure 5.9A,D). The B20 group increased mean transit time (mTT) in the

tendon ROI at day 14 (Figure 5.9B). Finally, the B20 group had significant and trending decreases in the wash-in rate (WiR) at both time points in both ROIs (Figure 5.9C,F).
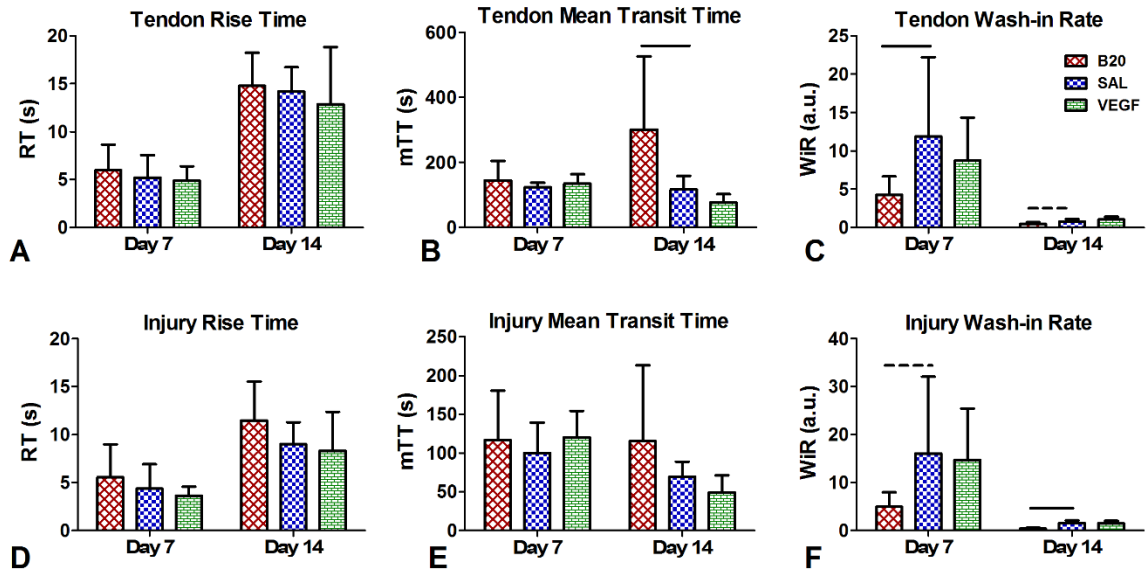
Figure 5.9: Time-based contrast-enhanced ultrasound parameters. Quantification of (A,D) rise time (RT), (B,E) mean transit time (mTT), and (C,F) wash-in rate (WiR) for the (A-C) tendon and (D-F) injury ROIs. The B20 group showed an overall decrease in WiR.

For the combined amplitude and time-based parameters, there were no changes in the VEGF group. In the B20 tendon ROI there was a significant decrease in wash-in perfusion index (WiPI) at day 7 and trending decreases in WiPI and perfusion index (PI) at day 14 (Figure 5.10A,B). Additionally, there were significant decreases at both time points in the injury site ROI for both WiPI and PI (Figure 5.10C,D).
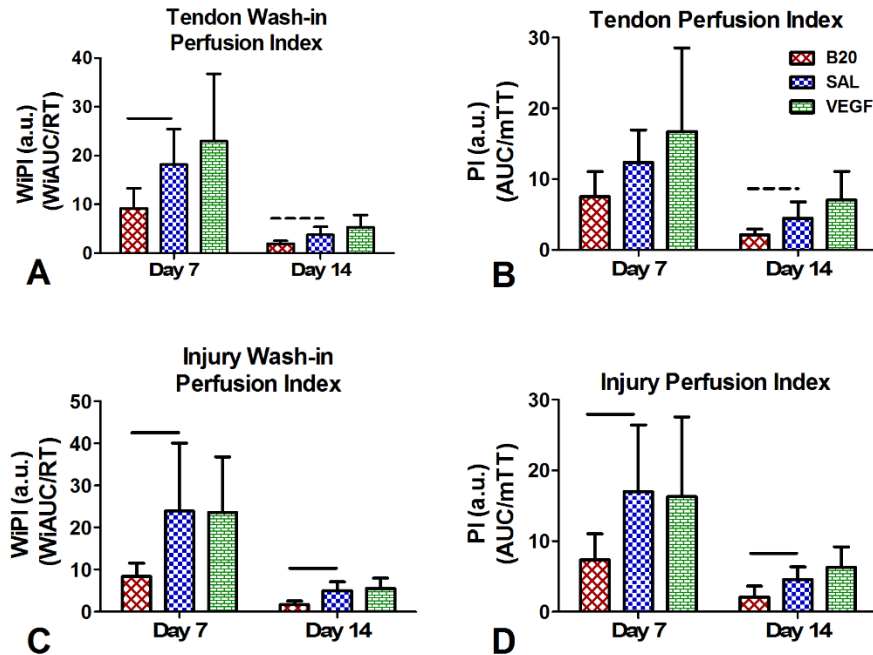
Figure 5.10: Combined amplitude-time based contrast-enhanced ultrasound parameters. Quantification of (A,C) wash-in perfusion index (WiPI) and (B,D) perfusion index (PI) for (A,B) tendon and (C,D) injury ROIs. The B20 group was decreased for both parameters at both time points.

B-Mode Ultrasound Alignment Analysis: There was no significant change in either circular standard deviation (CSD) or echogenicity in either group when evaluating the full tendon ROI (Figure 5.11B,C). However, when evaluating the injury ROI, there was a significant decrease in CSD, indicating an increase in collagen alignment, on day 14 in the B20 group (Figure 5.11D). Additionally, the VEGF group had a trending increase in echogenicity on day 7 (Figure 5.11E) in the injury ROI.
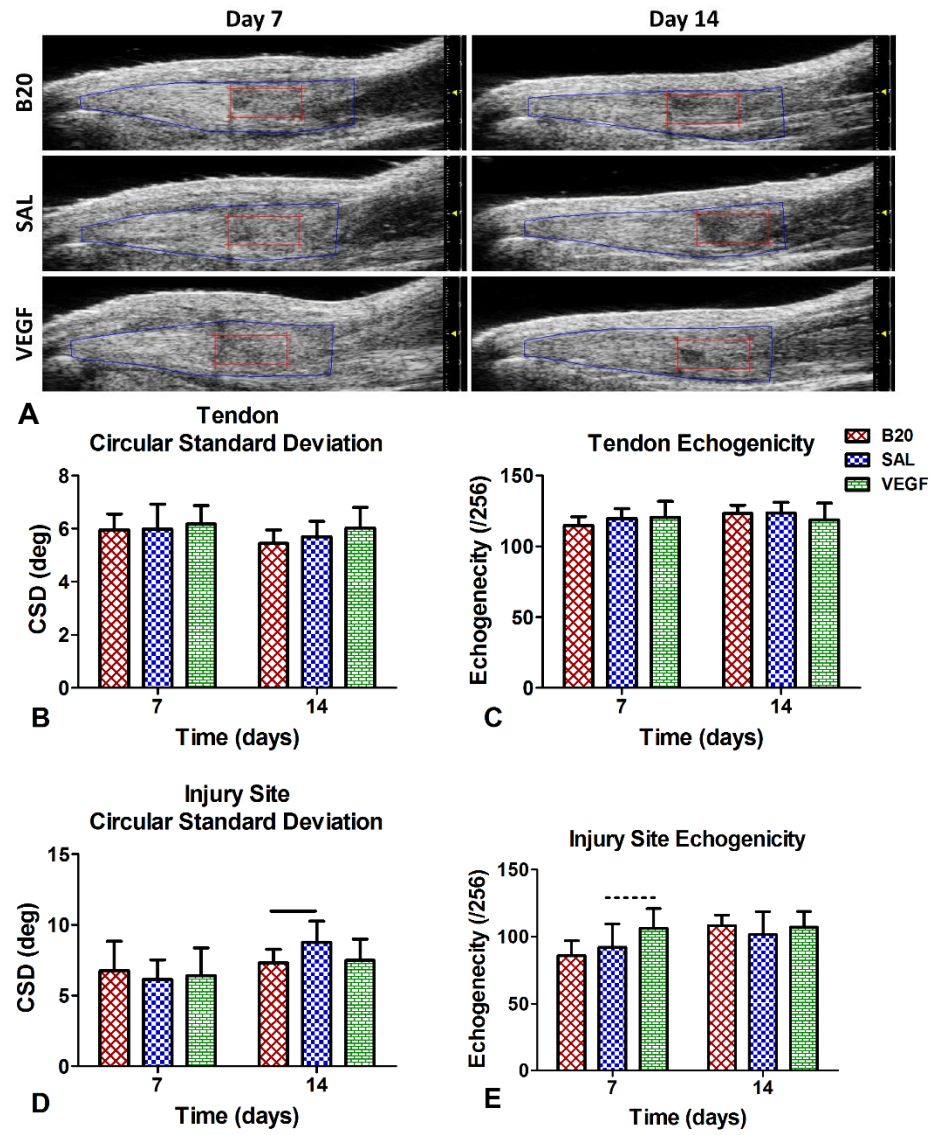
Figure 5.11: (A) Representative b-mode ultrasound images showing the full tendon (blue) and injury (red) ROIs. Quantification of (B,D) circular standard deviation (CSD) and (C,E) echogenicity in the (B,C) full tendon and (D,E) injury site ROIs.

Histological Analysis: H&E histological analysis showed no changes in cell shape or cellularity in either group (Figure 5.12A,B). CD34 immunohistochemical staining also showed no changes in vessel density or vessel size in either group (Figure 5.12A,C).
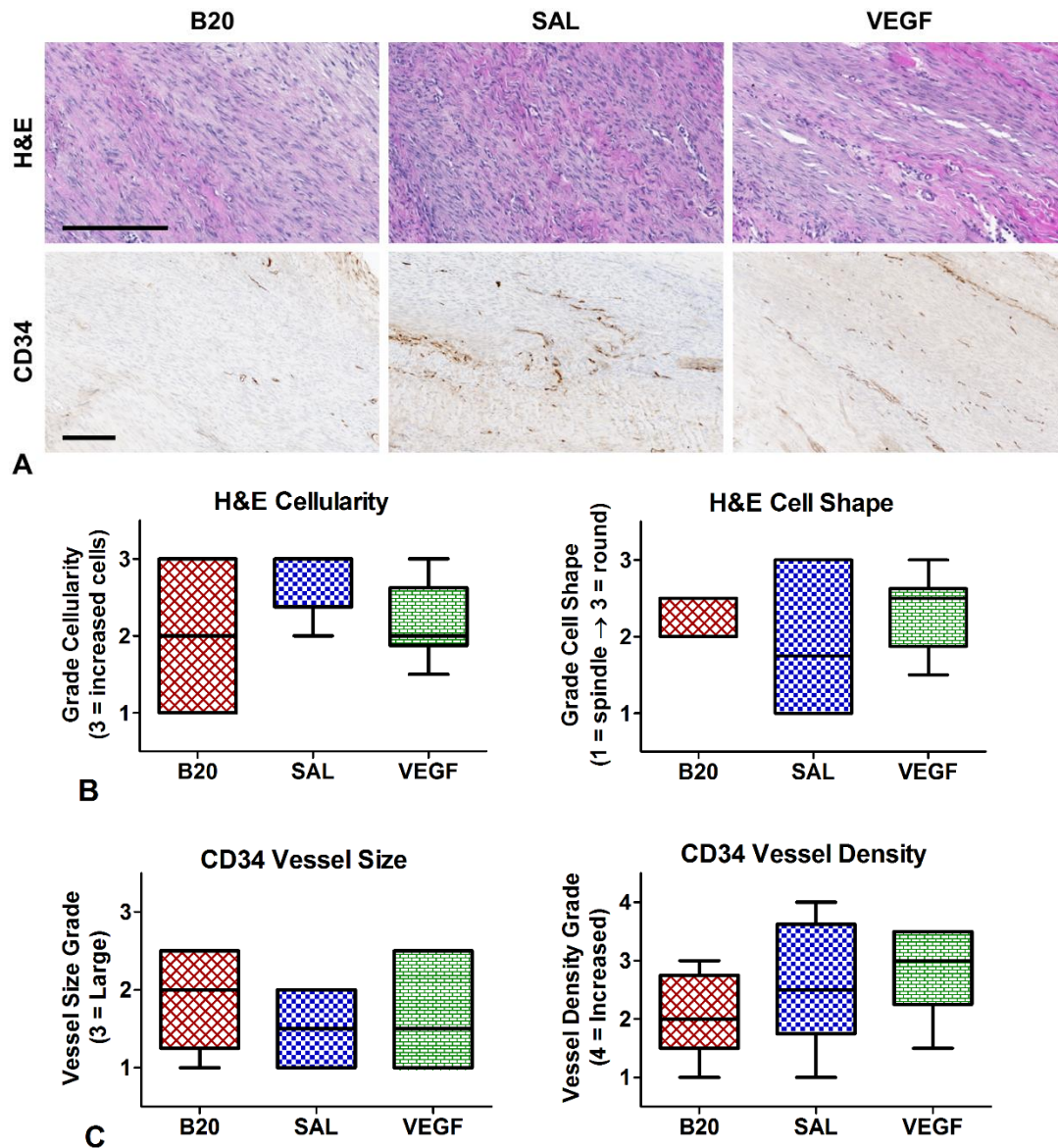
Figure 5.12: (A) Representative images of H&E (100x magnification) and immunohistochemical staining for CD34 (50x magnification) (scale bar 200µm). Semi-quantitative evaluation of (B) H&E cell shape and (C) cellularity, and (D) CD34 vessel density and (E) vessel size.

Representative images for immunohistochemistry are shown in Figure 5.13. Quantification of IHC staining showed that the delivery of B20 caused a significant

increase in angiopoietin-1 (Figure 5.14B). No other stains showed significant differences between groups.
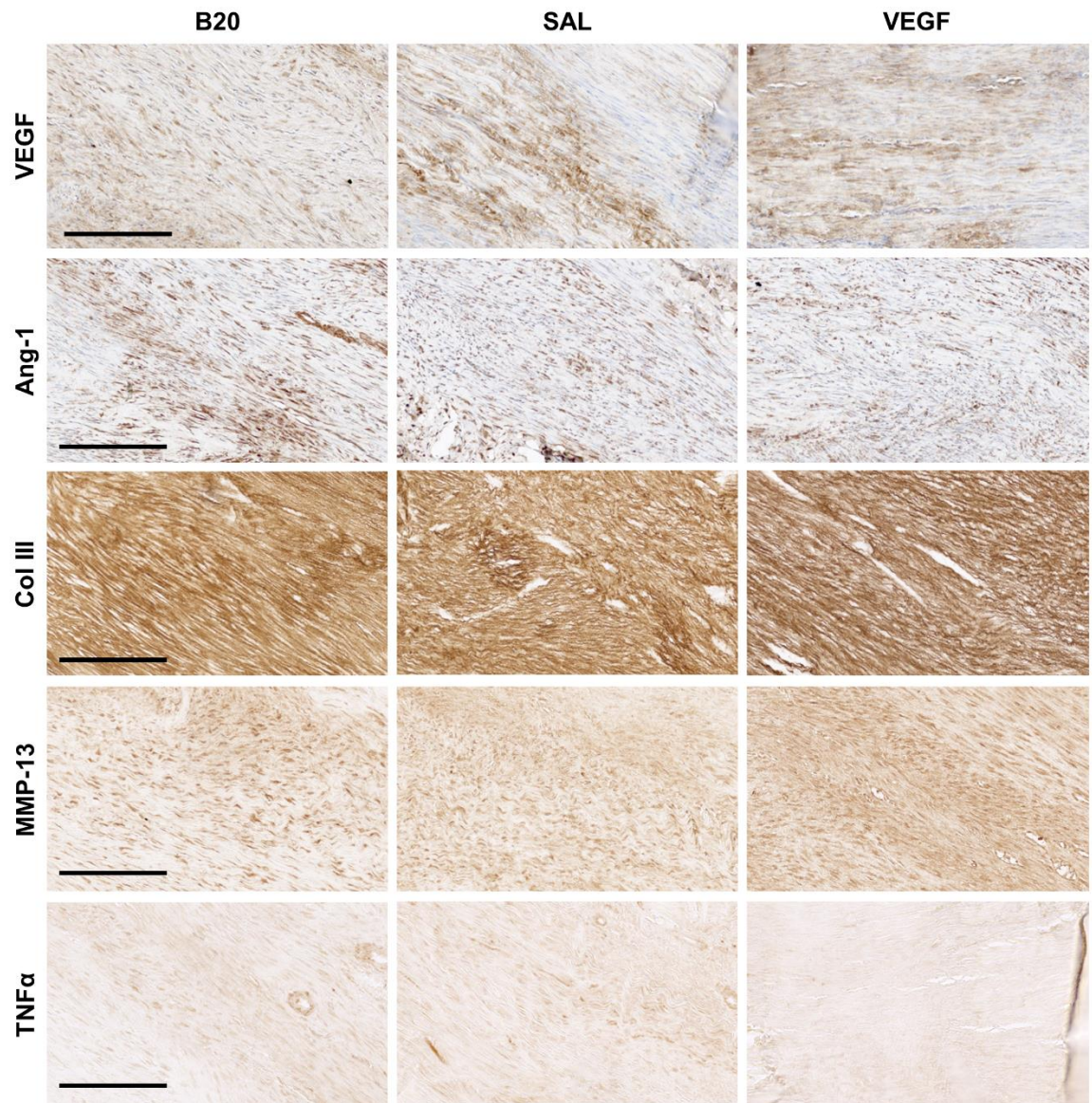
Figure 5.13: Representative images of immunohistochemical staining (100x magnification, scale bar 200µm) of vascular endothelial growth factor (VEGF), angiopoietin-1 (Ang-1), type III collagen (Col III), matrix metallopeptidase 13 (MMP-13), and tumor necrosis factor alpha (TNFα).
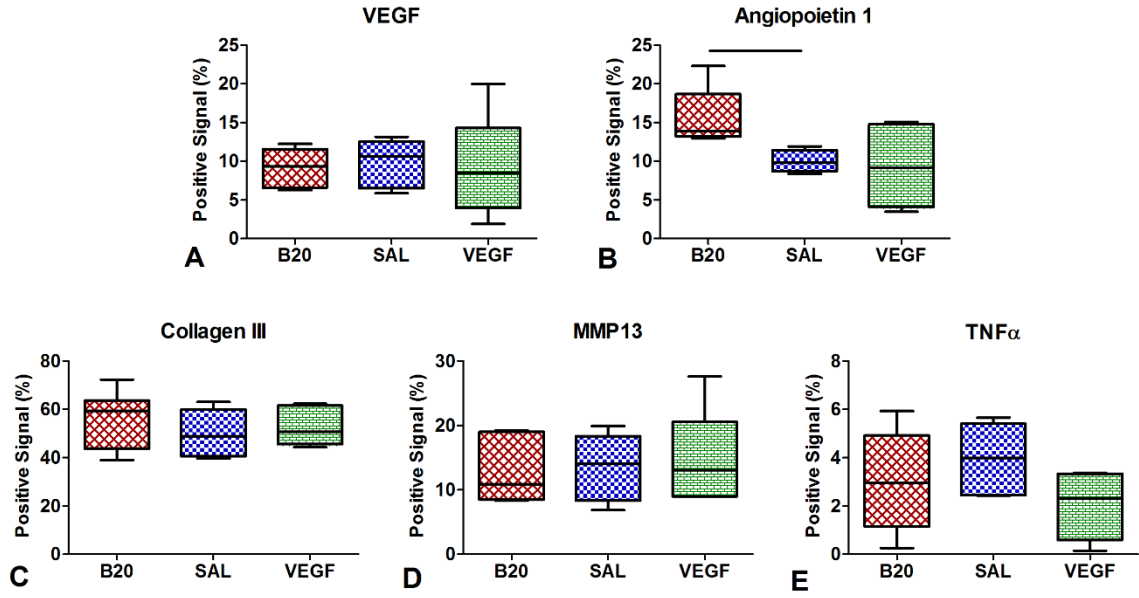
Figure 5.14: Quantification of percent positive staining for vascular endothelial growth factor (VEGF), angiopoietin-1 (Ang-1), type III collagen (Col III), matrix metallopeptidase 13 (MMP-13), and tumor necrosis factor alpha (TNFα). There is a significant increase in Ang1 in the B20 group and no other differences.

Mechanical Analysis: When evaluating structural mechanical changes, there was no change in full tendon or injury site cross-sectional area (Figure 5.15A,D), max displacement (Figure 5.15E), or stiffness (Figure 5.15F) for either group. However, the VEGF group had a significant decrease in percent relaxation (Figure 5.15B) and a significant increase in max load (Figure 5.15C). The B20 group also had a trending increase in max load (Figure 5.15C).
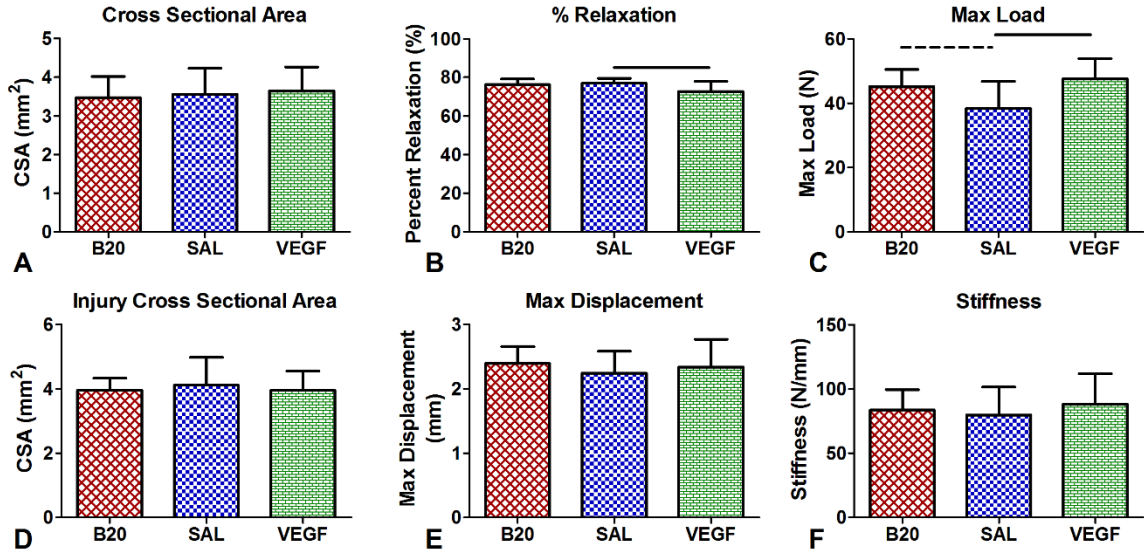
Figure 5.15: Geometric and structural mechanical properties. (A) Full tendon and (D) injury site cross-sectional area, (B) percent relaxation, (C) max load, (E) max displacement, and (F) stiffness. The VEGF group percent relaxation was decreased and max load increased compared to the saline control.

Analysis of material mechanical properties revealed no change in the max stress or full tendon modulus (Figure 5.16A,B), but there was a significant increase in injury site modulus in the VEGF group, and a trending increase in the B20 group (Figure 5.16C). Additionally, the dynamic mechanical analysis showed no changes in tangent of delta, but a trending but consistent increase in dynamic modulus in the VEGF group at all 4 frequencies (Figure 5.16D,E).
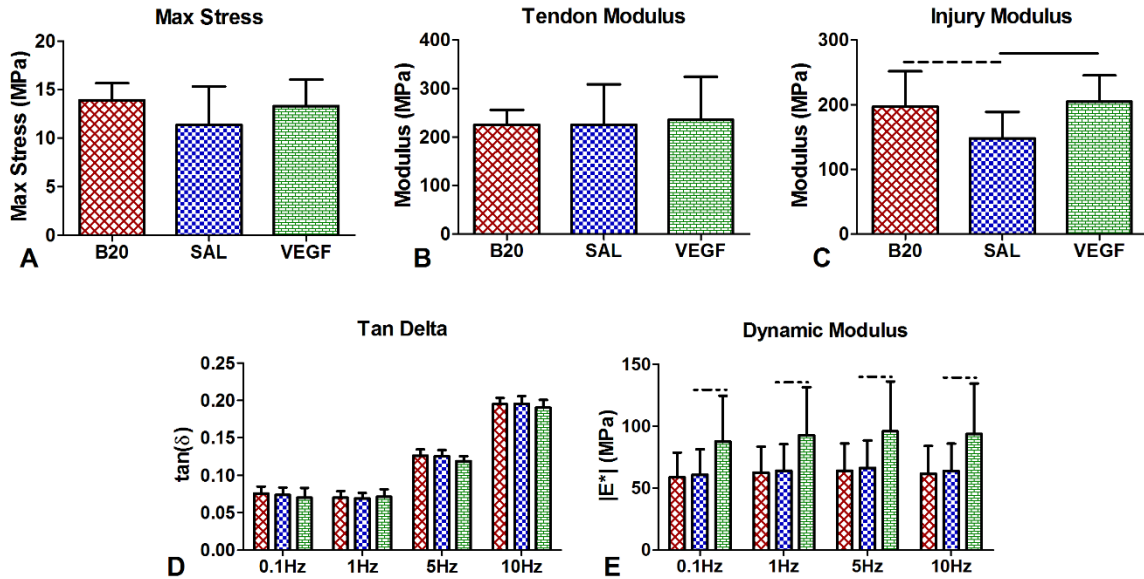
Figure 5.16: Material and dynamic mechanical properties. (A) Max stress and (B) tendon modulus showed no changes, but (C) injury site modulus was significantly increased in the VEGF group. There were no significant changes in either (D) tan delta or (E) dynamic modulus.

D. DISCUSSION

The first study discussed in this chapter evaluated the effect of aging on vascular response to injury. We demonstrated that aging causes significant decreases in both blood flow, as shown by the decreased mean color level and color weighted fractional area measures, as well as vascular density, as shown by the ultrasound fractional area and histological vessel density measures. This data supports previous human ultrasound studies,[21, 36] showing decreased blood flow in elderly patients in both the uninjured Achilles and supraspinatus tendons.

In the second study in this chapter, we evaluated how the delivery of both pro- and anti-angiogenic factors altered vascular response and healing outcomes in aged animals. There were significant changes to the vascular response after injury in the aged animals

similar to the response seen in the adult animals in Chapter 4.[31, 33] However, there were larger changes with the VEGF delivery in the aged animals compared to previous data in the adults (Figure 5.17).[31] We previously found that in adult animals, decreasing the vascular response following injury impaired the healing, but increasing vascularity did not alter healing outcome.[31] In the aged animals, increasing the vascular response following injury caused an improvement in mechanical properties. Additionally, decreasing the vascular response did not impair healing outcome but surprisingly resulted in a trending improvement (Figure 5.17). These results could be because the aged animals naturally exhibit a reduced vascular response following injury, as described in the first study in this chapter, so the stimulus for increasing angiogenesis may have more effect than in the case of adults that already have a robust vascular response. This VEGF treatment could therefore be counter-acting the inherent reduction of vascularity with aging, and therefore restoring some of the lost healing potential. Additionally, we see more pronounced changes in blood flow velocity and oxygenation with VEGF delivery in this aging population. In the adult animals in the previous chapter we found reductions in oxygenation and slower tissue perfusion properties, indicating VEGF is having a distinctly different effect in this age group where there is an altered angiogenic environment. Once again, we find that with VEGF delivery in particular color Doppler and photoacoustic vascular measures are as good, if not better, at detecting differences in vascular parameters as contrast-enhanced ultrasound. This is surprising given that contrast-enhanced ultrasound can detect perfusion through much smaller vessels. However, it suggests that the density of capillaries may not be the most impactful changes occuring, and larger vessels may be undergoing structural

changes that induce increased blood flow and oxygenation levels more easily detected using these less-sensitive ultrasound imaging techniques. This is promising given that color Doppler imaging is already used clinically in the evaluation of tendinopathy and so these methods could be more easily translated.

Similarly, since these aged animals already have a reduced vascular and healing response, a further reduction in vascularity does not seem to cause a significant change in healing outcome as we have seen in the adult animals. Additionally, in both the adult and aged animals, the reduction in vascularity through the delivery of B20 causes the tendons to have improved alignment properties. So while the reduction in vascularity may hinder healing the resulting improvements in collagen organization could explain the improved mechanics observed 4 weeks following injury in the adults and the trending improvement seen at 2 weeks in the aged animals. Finally, histologically there was a significant increase in Angiopoietin 1 (Ang1) in the B20 group. While VEGF and Angiopoietin 2 have roles in vessel destabilization and sprouting, the role of Ang1 is to initiate vascular stabilization and endothelial protection.[7, 11] It is possible that with the blocked VEGF signaling in addition to the already reduced vascular response with aging, this increase in Ang1 is normalizing the vessels and allowing them to be more efficient than the leaky vasculature normally formed at the start of angiogenesis. This could be a mechanism for why there are trending increases in mechanical properties in this group as well.

AGING		B20		VEGF	
		7	14	7	14
Vascularity	Blood Flow Velocity	↓↓	↓↓	↑↑	—
	Oxygenation	↓↓	—	↑↑	↑↑
	Tissue Perfusion	↓↓	↓↓	—	—
Structure	Organization	—	↑↑	—	—
	Tissue Density	—	—	↑	—
Histology	Cellularity		—		—
	Vascularity		—		—
	Vessel Normalization		↑↑		—
	Matrix Production		—		—
	Inflammation		—		—
	Matrix Degradation		—		—
Mechanics	Geometric		—		—
	Viscoelastic		—		↓
	Structural		↑		↑↑
	Material		↑		↑↑
	Dynamic		—		↑

Figure 5.17: Overview of results for Study 2: The effect of vascular modulation on aged Achilles tendons. The findings for each analysis category are displayed with double arrows for a large (overall significant) change, and single arrows for a small (overall trending) change. Arrows are pointing up for increasing values and down for decreasing values. Arrows are colored green to indicate either increased vascularity or improved properties, or colored red to indicate either decreased vascularity or worsened properties. While both B20 and VEGF induced significant decreases and increases in vascular properties after injury, respectively, only the VEGF group caused significant changes in mechanical properties, demonstrating improvements in tendon healing.

Aging has been shown to have significant impacts on tendon compositional, mechanical, and vascular properties. Aging causes reduced collagen and elastin production, as well as increased MMP and decreased TIMP activity.[18, 37, 44] Given these compositional changes, it is no surprise that aged tendons exhibit inferior mechanical properties.[20, 30, 41] Additionally, clinical studies have reported alterations in vascularity with aging, including reduced blood flow in and around tendons, [14, 21] as well as a reduced

vascular endothelial cell population, decreased cell expansion, and diminished angiogenic-lineage differentiation potential in ligament-based cell populations from aged patients.[42] This data supports the findings from our first study, that aging decreased vessel density as well as decreased blood flow velocity. However, there is no previous data reporting changes to tendon vascularity following tendon injury, so this is the first study to report this finding in an Achilles tendon injury model.

While there is limited data regarding vascularity tendons, it is well established that there are aging-related impairments in angiogenesis in other tissues. An arterial injury model demonstrated that aging impaired the ability for re-endothelialization.[15] Additionally, vascular ingrowth models show decreased endothelial cell proliferation and function with aging.[35, 43] There are numerous accounts of a decline in production of pro-angiogenic growth factors and cytokines, including VEGF, basic fibroblast growth factor (bFGF), and transforming growth factor beta 1 (TGF-β1), with the induction of angiogenesis in aged tissues.[3, 15, 34, 35, 37, 43] Specifically, there is a decrease in VEGF upregulation in response to hypoxia[34] as well as a reduction in hypoxia induced factor-1α (HIF-1α) DNA binding[34] and downregulation of importin-α expression.[3] HIF-1α is a transcription factor for VEGF and importin-α is necessary for HIF-1α to translocate to the nucleus to activate VEGF transcription. Therefore decreases to these factors all cause a decrease in VEGF expression. Additionally, there was an increase in angiogenic inhibitor, thrombospondin-2 (TSP-2), with aging.[37] These alterations in angiogenic factors caused a reduction in angiogenic invasion and capillary density in aged tissues.[3, 35, 37, 43] This

phenomenon was not only observed in these other tissue vascular models, but was also in our tendon studies in this chapter as a clear reduction in vascularity in our aged model.

The effect of angiogenic factor delivery on vascular response and healing outcome has been described in multiple injury models, as well as our studies described in Chapter 4.[33] In particular, VEGF delivery increased vascular response after injury and caused improvements in healing potential in some studies.[6, 8, 9, 16, 17, 19, 39, 45] However, there is very little research related to aiding tissue healing in aged specimens through the delivery of angiogenic factors. In this chapter, the delivery of VEGF not only increased angiogenic response to injury, but also improved the healing outcome in the aged Achilles tendon. While there is no previous work assessing angiogenic therapies in aging tendon models, how the impaired angiogenic response in other aged tissues can be rescued through the delivery of VEGF has been evaluated. The local delivery of adenoviral VEGF to injured iliac arteries in aged rabbits significantly improved re-endothelialization of the damaged arteries.[15] Additionally, VEGF delivery following femoral artery resection in aged rats improved blood pressure ratio, angiographic score, and capillary density.[35] Finally, VEGF 121 gene transfer enhanced the blood vessel formation, fibrovascular tissue ingrowth, and endothelial cell proliferation in a subcutaneous vascular ingrowth model in aged rats.[43] Interestingly, this same study also found that their VEGF treatment failed to further stimulate the already more robust angiogenesis in young animals.[43] This body of work demonstrates the ability to rescue the impaired angiogenic response in aged tissue, and supports the improved healing outcomes that we observed in our studies. Additionally, it supports that improvements to angiogenic response are frequently only possible in models

where there is a natural vascular impairment, such as with aging, but not in models of robust vascular response, such as with adult or young populations.

This study is not without limitations. First, histological and mechanical properties were only evaluated at day 14. This was primarily due to the limited availability of aged animals and so we chose the time point where we saw the most significant mechanical changes in the adult groups, as described in Chapter 4. However, it would be beneficial to have histological samples at earlier time points to evaluate early extracellular matrix and inflammatory changes. Additionally, future work could evaluate mechanical properties at later time points to see if this improvement due to VEGF administration is transient or persists over time. Another limitation is that this injury model does not have a direct clinical parallel since it is a central partial rupture. However, this controlled injury model does not require surgical repair of the tendon or immobilization of the limb, which is important for the use of ultrasound imaging. Additionally, central patellar tendon injuries are common for ACL reconstruction, so healing in this type of defect could be translated to that application. Finally, we did not perform any ankle functional evaluation as we did in Chapter 4. This was because we did not see any major differences in the adult animal studies, and we wanted to limit the anesthesia exposure and stress level for these more fragile aged animals.

In this work, aging caused a significant reduction in vascular response to injury. This is most likely due to the impaired capacity for angiogenesis and reduced VEGF expression in aged tissues, as described in previous work. This reduction in angiogenic potential could alter cellular responses and healing capacity after injury, and could help

explain the reduced tendon healing potential of the aged population. While VEGF treatment did not cause any significant improvements in healing in the adult groups where there is a relatively normal vascular response (Chapter 4), it did cause an improvement in healing outcome in the aged groups. Additionally, while anti-angiogenic treatments decreased healing properties in adult animals, it caused trending improvements in the aged animals. This demonstrates that an aged population not only has inherently different vascular properties, but also responds differently to vascular modulation after injury. Additionally, the delivery of VEGF can restore some of the lost angiogenic potential occurring with age. While angiogenesis in aging tissues has been studied before, to our knowledge there have been no studies demonstrating a recovery of vascularity and consequently an improvement in healing in an aged tendon injury model. This study was also the first to evaluate changes in vascular response in an aged model using *in vivo* measures of blood perfusion and relate them to alterations in healing properties.

E. REFERENCES

1. *World report on ageing and health*. World Health Organization: Geneva, Switzerland, 2015.

2. Ackerman J.E., Bah I., Jonason J.H., Buckley M.R. and Loiselle A.E. Aging does not alter tendon mechanical properties during homeostasis, but does impair flexor tendon healing. *J Orthop Res* 2017.

3. Ahluwalia A., Narula J., Jones M.K., Deng X. and Tarnawski A.S. Impaired angiogenesis in aging myocardial microvascular endothelial cells is associated with reduced importin alpha and decreased nuclear transport of hif1 alpha: Mechanistic implications. *J Physiol Pharmacol* 2010; 61(2)**:** 133-139.

4. Arnesen S.M. and Lawson M.A. Age-related changes in focal adhesions lead to altered cell behavior in tendon fibroblasts. *Mech Ageing Dev* 2006; 127(9)**:** 726-732.

5.   Barros L.F. and Belfort R., Jr. The effects of the subconjunctival injection of bevacizumab (avastin) on angiogenesis in the rat cornea. *An Acad Bras Cienc* 2007; 79(3)**:** 389-394.

6.   Basu G., Downey H., Guo S., Israel A., Asmar A., Hargrave B. and Heller R. Prevention of distal flap necrosis in a rat random skin flap model by gene electro transfer delivering vegf(165) plasmid. *J Gene Med* 2014; 16(3-4)**:** 55-65.

7.   Bouis D., Kusumanto Y., Meijer C., Mulder N.H. and Hospers G.A. A review on pro- and anti-angiogenic factors as targets of clinical intervention. *Pharmacol Res* 2006; 53(2)**:** 89-103.

8.   Chereddy K.K., Lopes A., Koussoroplis S., Payen V., Moia C., Zhu H., Sonveaux P., Carmeliet P., des Rieux A., Vandermeulen G. and Preat V. Combined effects of plga and vascular endothelial growth factor promote the healing of non-diabetic and diabetic wounds. *Nanomedicine* 2015; 11(8)**:** 1975-1984.

9.   Corral C.J., Siddiqui A., Wu L., Farrell C.L., Lyons D. and Mustoe T.A. Vascular endothelial growth factor is more important than basic fibroblastic growth factor during ischemic wound healing. *Arch Surg* 1999; 134(2)**:** 200-205.

10.   Emami M.J., Jaberi F.M., Azarpira N., Vosoughi A.R. and Tanideh N. Prevention of arthrofibrosis by monoclonal antibody against vascular endothelial growth factor: A novel use of bevacizumab in rabbits. *Orthop Traumatol Surg Res* 2012; 98(7)**:** 759-764.

11.   Falcon B.L., Hashizume H., Koumoutsakos P., Chou J., Bready J.V., Coxon A., Oliner J.D. and McDonald D.M. Contrasting actions of selective inhibitors of angiopoietin-1 and angiopoietin-2 on the normalization of tumor blood vessels. *Am J Pathol* 2009; 175(5)**:** 2159-2170.

12.   Fevata M. Scarless healing in the fetus: Implications and strategies for postnatal tendon repair. University of Pennsylvania, Philadelphia, PA, 2006.

13.   Frontera W.R. Physiologic changes of the musculoskeletal system with aging: A brief review. *Phys Med Rehabil Clin N Am* 2017; 28(4)**:** 705-711.

14.   Funakoshi T., Iwasaki N., Kamishima T., Nishida M., Ito Y., Kondo M. and Minami A. In vivo visualization of vascular patterns of rotator cuff tears using contrast-enhanced ultrasound. *Am J Sports Med* 2010; 38(12)**:** 2464-2471.

15.   Gennaro G., Menard C., Michaud S.E. and Rivard A. Age-dependent impairment of reendothelialization after arterial injury: Role of vascular endothelial growth factor. *Circulation* 2003; 107(2)**:** 230-233.

16.   Ju Y.J., Tohyama H., Kondo E., Yoshikawa T., Muneta T., Shinomiya K. and Yasuda K. Effects of local administration of vascular endothelial growth factor on properties of the in situ frozen-thawed anterior cruciate ligament in rabbits. *Am J Sports Med* 2006; 34(1)**:** 84-91.

17. Kaux J.F., Janssen L., Drion P., Nusgens B., Libertiaux V., Pascon F., Heyeres A., Hoffmann A., Lambert C., Le Goff C., Denoel V., Defraigne J.O., Rickert M., Crielaard J.M. and Colige A. Vascular endothelial growth factor-111 (vegf-111) and tendon healing: Preliminary results in a rat model of tendon injury. *Muscles Ligaments Tendons J* 2014; 4(1)**:** 24-28.

18. Kostrominova T.Y. and Brooks S.V. Age-related changes in structure and extracellular matrix protein expression levels in rat tendons. *Age (Dordr)* 2013; 35(6)**:** 2203-2214.

19. Kryger Z., Zhang F., Dogan T., Cheng C., Lineaweaver W.C. and Buncke H.J. The effects of vegf on survival of a random flap in the rat: Examination of various routes of administration. *Br J Plast Surg* 2000; 53(3)**:** 234-239.

20. LaCroix A.S., Duenwald-Kuehl S.E., Brickson S., Akins T.L., Diffee G., Aiken J., Vanderby R., Jr. and Lakes R.S. Effect of age and exercise on the viscoelastic properties of rat tail tendon. *Ann Biomed Eng* 2013; 41(6)**:** 1120-1128.

21. Langberg H., Olesen J., Skovgaard D. and Kjaer M. Age related blood flow around the achilles tendon during exercise in humans. *Eur J Appl Physiol* 2001; 84(3)**:** 246-248.

22. Manzano R.P., Peyman G.A., Khan P. and Kivilcim M. Testing intravitreal toxicity of bevacizumab (avastin). *Retina* 2006; 26(3)**:** 257-261.

23. Marqueti R.C., Durigan J.L.Q., Oliveira A.J.S., Mekaro M.S., Guzzoni V., Aro A.A., Pimentel E.R. and Selistre-de-Araujo H.S. Effects of aging and resistance training in rat tendon remodeling. *FASEB J* 2017.

24. Marquez-Arabia W.H., Gomez-Hoyos J., Gomez M., Florez I., Gallo J.A., Monsalve F., Arias L.F. and Martin H.D. Influence of aging on microvascular supply of the gluteus medius tendon: A cadaveric and histologic study. *Arthroscopy* 2017; 33(7)**:** 1354-1360.

25. McCarthy M.M. and Hannafin J.A. The mature athlete: Aging tendon and ligament. *Sports Health* 2014; 6(1)**:** 41-48.

26. Needles A., Arditi M., Rognin N.G., Mehi J., Coulthard T., Bilan-Tracey C., Gaud E., Frinking P., Hirson D. and Foster F.S. Nonlinear contrast imaging with an array-based micro-ultrasound system. *Ultrasound Med Biol* 2010; 36(12)**:** 2097-2106.

27. Needles A., Heinmiller A., Sun J., Theodoropoulos C., Bates D., Hirson D., Yin M. and Foster F.S. Development and initial application of a fully integrated photoacoustic micro-ultrasound system. *IEEE Trans Ultrason Ferroelectr Freq Control* 2013; 60(5)**:** 888-897.

28. Okada Y., Akisue T., Hara H., Kishimoto K., Kawamoto T., Imabori M., Kishimoto S., Fukase N., Onishi Y. and Kurosaka M. The effect of bevacizumab on tumour growth of malignant fibrous histiocytoma in an animal model. *Anticancer Res* 2010; 30(9)**:** 3391-3395.

29.   Plate J.F., Brown P.J., Walters J., Clark J.A., Smith T.L., Freehill M.T., Tuohy C.J., Stitzel J.D. and Mannava S. Advanced age diminishes tendon-to-bone healing in a rat model of rotator cuff repair. *Am J Sports Med* 2014; 42(4)**:** 859-868.

30.   Plate J.F., Wiggins W.F., Haubruck P., Scott A.T., Smith T.L., Saul K.R. and Mannava S. Normal aging alters in vivo passive biomechanical response of the rat gastrocnemius-achilles muscle-tendon unit. *J Biomech* 2013; 46(3)**:** 450-455.

31.   Riggin C.N., Rodriguez A.B., Weiss S.N., Raja H.A., Chen M., Schultz S.M., Sehgal C.M. and Soslowsky L.J. Modulation of vascular response after injury in the rat achilles tendon alters healing capacity. *Orthopaedic Research Society*. New Orleans, LA 2018. 0567.

32.   Riggin C.N., Sarver J.J., Freedman B.R., Thomas S.J. and Soslowsky L.J. Analysis of collagen organization in mouse achilles tendon using high-frequency ultrasound imaging. *J Biomech Eng* 2014; 136(2)**:** 021029.

33.   Riggin C.N., Schultz S.M., Sehgal C.M. and Soslowsky L.J. Effect of pro- and anti-angiogenic factors on vascular response in the rat achilles tendon after injury. *Orthopaedic Research Society*. San Diego, CA 2017. 1580.

34.   Rivard A., Berthou-Soulie L., Principe N., Kearney M., Curry C., Branellec D., Semenza G.L. and Isner J.M. Age-dependent defect in vascular endothelial growth factor expression is associated with reduced hypoxia-inducible factor 1 activity. *J Biol Chem* 2000; 275(38)**:** 29643-29647.

35.   Rivard A., Fabre J.E., Silver M., Chen D., Murohara T., Kearney M., Magner M., Asahara T. and Isner J.M. Age-dependent impairment of angiogenesis. *Circulation* 1999; 99(1)**:** 111-120.

36.   Rudzki J.R., Adler R.S., Warren R.F., Kadrmas W.R., Verma N., Pearle A.D., Lyman S. and Fealy S. Contrast-enhanced ultrasound characterization of the vascularity of the rotator cuff tendon: Age- and activity-related changes in the intact asymptomatic rotator cuff. *J Shoulder Elbow Surg* 2008; 17(1 Suppl)**:** 96S-100S.

37.   Sadoun E. and Reed M.J. Impaired angiogenesis in aging is associated with alterations in vessel density, matrix composition, inflammatory response, and growth factor expression. *J Histochem Cytochem* 2003; 51(9)**:** 1119-1130.

38.   Sehgal C.M., Arger P.H., Silver A.C., Patton J.A., Saunders H.M., Bhattacharyya A. and Bell C.P. Renal blood flow changes induced with endothelin-1 and fenoldopam mesylate at quantitative doppler us: Initial results in a canine study. *Radiology* 2001; 219(2)**:** 419-426.

39.   Takayama K., Kawakami Y., Mifune Y., Matsumoto T., Tang Y., Cummins J.H., Greco N., Kuroda R., Kurosaka M., Wang B., Fu F.H. and Huard J. The effect of blocking angiogenesis on anterior cruciate ligament healing following stem cell transplantation. *Biomaterials* 2015; 60**:** 9-19.

40. Torricelli P., Veronesi F., Pagani S., Maffulli N., Masiero S., Frizziero A. and Fini M. In vitro tenocyte metabolism in aging and oestrogen deficiency. *Age (Dordr)* 2013; 35(6)**:** 2125-2136.

41. Turan A., Teber M.A., Yakut Z.I., Unlu H.A. and Hekimoglu B. Sonoelastographic assessment of the age-related changes of the achilles tendon. *Med Ultrason* 2015; 17(1)**:** 58-61.

42. Uefuji A., Matsumoto T., Matsushita T., Ueha T., Zhang S., Kurosaka M. and Kuroda R. Age-related differences in anterior cruciate ligament remnant vascular-derived cells. *Am J Sports Med* 2014; 42(6)**:** 1478-1486.

43. Wang H., Keiser J.A., Olszewski B., Rosebury W., Robertson A., Kovesdi I. and Gordon D. Delayed angiogenesis in aging rats and therapeutic effect of adenoviral gene transfer of vegf. *Int J Mol Med* 2004; 13(4)**:** 581-587.

44. Yu T.Y., Pang J.H., Wu K.P., Chen M.J., Chen C.H. and Tsai W.C. Aging is associated with increased activities of matrix metalloproteinase-2 and -9 in tenocytes. *BMC Musculoskelet Disord* 2013; 14**:** 2.

45. Zhang F., Liu H., Stile F., Lei M.P., Pang Y., Oswald T.M., Beck J., Dorsett-Martin W. and Lineaweaver W.C. Effect of vascular endothelial growth factor on rat achilles tendon healing. *Plast Reconstr Surg* 2003; 112(6)**:** 1613-1619.

CHAPTER 6: CONCLUSIONS AND FUTURE DIRECTIONS

A. INTRODUCTION

In this dissertation, the role of angiogenesis in tendon healing was explored through the modulation of vascularity in both adult and aged rat Achilles tendons. Ultrasound imaging techniques were developed and translated from other applications to be used to evaluate tendon vascular and structural properties. In Chapter 2, we presented the development and validation of a method for quantifying collagen alignment using high-frequency ultrasound images. Chapter 3 outlined the preliminary studies necessary to demonstrate efficacy of administering both pro- and anti-angiogenic factors locally to the Achilles tendon after injury. This work developed our model of angiogenic modulation following injury that was used in the next two chapters. Chapter 4 evaluated the effect of vascular modulation on tendon healing in adult animals using *in vivo* ultrasound measures of structure and vascularity, *in vivo* functional measures of joint motion and ambulatory properties, *ex vivo* histological measures of tendon composition, and *ex vivo* mechanical evaluation. Finally, Chapter 5 explored the effect of vascular modulation on tendon healing in aged animals, where vascular response and healing outcome are impaired. The main findings and conclusions from these chapters, as well as proposed future directions, are discussed in this final chapter.

B. CHAPTER 2: USE OF B-MODE ULTRASOUND TO QUANTITATIVELY DETERMINE COLLAGEN ALIGNMENT IN THE ACHILLES TENDON

Collagen fibers appear as hyperechoic bands under ultrasound imaging. While there have been multiple methods developed to quantitatively evaluate the patterning or brightness of an ultrasound image, prior to this work, there had been no direct evaluation of collagen alignment specifically. Since changes in collagen organization relate to tendon mechanical properties, the development of an *in vivo* method to quantify organization would provide a sensitive metric to evaluate the degree of tendon injury or healing. Therefore, the objective of this study was to perform an *ex vivo* experiment on mouse Achilles tendons to determine if high-frequency ultrasound imaging can capture changes in collagen alignment as compared to standard cross-polarizer imaging. We hypothesized that because the bands seen in the tendon ultrasound images are created by collagen bundles, the changes in collagen alignment that are measurable by cross-polarizer would also be measurable by high-frequency ultrasound.

Consistent with our hypothesis, increases in collagen organization created through incremental loading of the tendon were detected by both the established cross-polarizer method as well as our new ultrasound method. Additionally, decreases in collagen organization created by disrupting the collagen fibers using a biopsy punch defect were also detected using both imaging methods.

However, while the regression analysis comparing the change in ultrasound and cross-polarizer alignment measurements with treatment was highly significant, it showed only a modest correlation. While this correlation is weaker than initially expected, it is not

altogether surprising given that these two methods are measuring different phenomena: the ultrasound is detecting the impedance difference between the collagen fibers and surrounding matrix, whereas the cross polarizer is using the birefringence properties of collagen.

In summary, this is the first study to directly quantify tendon collagen alignment from ultrasound images. Specifically, it demonstrated that ultrasound is capable of detecting a change in collagen organization due to load and injury, and that these changes are consistent with both the established cross-polarizer method and with previous studies.[18, 26, 37, 43, 44] As such, this experiment validates the use of high-frequency ultrasound imaging for obtaining a quantitative measure of tendon organization, and provides critical data to continue to refine the technique for future *in vivo* applications. Such a method could eventually be used in clinical studies to monitor progress during treatment and ultimately improve patient outcomes.

C. CHAPTER 3: MODULATION OF VASCULAR RESPONSE TO INJURY

While tendons undergo a typical wound healing response to injury, they never fully regain their pre-injury properties, pre-disposing them to re-rupture. Blood vessel formation, or angiogenesis, is an important part of the tendon healing process as it facilitates the delivery of nutrients and chemical factors as well as helps control the injury inflammatory response. While vascular ingrowth is necessary for tendon healing, an imbalance of angiogenic factors could produce either abnormal or insufficient angiogenesis, ultimately impacting the healing potential of the tissue. Altering the vascular

formation after injury could potentially improve healing outcome. Therefore, the objective of this chapter was to evaluate how the delivery of both pro- and anti-angiogenic factors effects the rat Achilles tendon vascular response after injury. We hypothesized that vessel properties measurable by both ultrasound and histological methods will be increased due to pro-angiogenic factor delivery and decreased due to anti-angiogenic factor delivery.

As hypothesized, we found that the delivery the pro-angiogenic factor, vascular endothelial growth factor (VEGF), caused an increase in ultrasound vascular properties as determined through color Doppler imaging and an increase in vessel size as determined through immunohistochemical staining of vascular endothelial cells. Similarly, the delivery of the anti-angiogenic factor, anti-VEGF antibody (B20), caused a decrease in both vascular properties determined through ultrasound imaging, as well as histological measures of vascular density.

However, these changes were not universally observed in all of our pro- and anti-angiogenic groups. We found that the increase in vascularity was only observed when VEGF was delivered delayed following injury and that the immediate delivery did not cause significant changes in any parameters. This could be due to the fact that the natural peak of VEGF after tendon injury is around 1 week,[8] and so delivering VEGF during that time window was more effective than delivering prior to VEGF endogenous expression. Additionally, only our mid-dosage B20 group demonstrated consistent decreases in vascular parameters. The low-dosage group had only increased parameters at later time points and the high-dosage group showed minimal changes at either time point. This demonstrates that the effects of anti-VEGF delivery are highly dose-dependent.

Additionally, the delayed increase in vascular measures with the delivery of this anti-angiogenic response could potentially be due to a compensation effect or increased normalization of the vasculature.[23, 33, 42, 47]

Overall, this work provides a model system for altering the vascular response following injury in a rat Achilles tendon model. It also establishes that the vascular changes created in this model can be detected using both ultrasound and histological measures of vascularity.

D. CHAPTER 4: EFFECT OF VASCULAR MODULATION ON ACHILLES TENDON HEALING IN AN ADULT RAT INJURY MODEL

In the previous chapter, we found that Achilles tendon vascular response to injury can be modified through the injection of pro- and anti-angiogenic factors. However, the effect of this altered angiogenesis on tendon healing outcome is unknown. Therefore, the objective of this chapter was to evaluate the effect of vascular modulation in rat Achilles tendons during healing using multiple *in vivo* ultrasound imaging modalities, *in vivo* functional assessment, and *ex vivo* measures of tendon compositional and mechanical properties. Our hypothesis was that reducing the vascular response would result in reduced mechanical properties, while increasing the vascular response will result in the opposite.

Consistent with our hypothesis, late administration of anti-VEGF antibody, B20, caused a reduction in failure load, max stress, and full tendon modulus. Surprisingly, this was accompanied by an improvement in tissue organization, as shown through our circular standard deviation and echogenicity measures in our ultrasound images. These changes

occurred at the same time point where decreases in vascular properties were still present. However, at later time points when the vascular changes had either leveled out to control levels or even increased in some parameters, there was no longer a reduction in these mechanical properties, and the in injury site modulus was significantly increased in this group. Decreasing VEGF signaling can inhibit the ability to undergo normal angiogenesis, and therefore impair the normal healing response. However, these changes only appear to be transient and it is possible that there is a delayed angiogenic response that causes both increased vascularity and the increased injury site modulus at late time points.

Contrary to our hypothesis, late administration of VEGF did not cause any improvements in material or structural properties. However, VEGF did cause a reduction in percent relaxation, which indicates a decrease in viscoelasticity closer to pre-injury tendon values. Therefore, while there is not a clear benefit to VEGF administration in this group, it does not appear to be harmful. Additionally, over-expression of VEGF can have pathophysiological consequences, including vascular permeability, edema, formation of tortuous vascular structure, and the inability for vessels to normalize. Since there were only minor changes with the administration of VEGF it is possible that the adult vascular response to injury is already at an optimal level. However, in contrast to our results in Chapter 3, the vascular changes with VEGF delivery were very mild, so it is possible that this treatment did not cause a large enough change to alter mechanical properties.

While the early delivery B20 group demonstrated vascular changes, they were for a shorter duration than observed in the late group, primarily at 7 days post-injury. Similar to our findings in Chapter 3, our early VEGF group only had minimal changes, primarily

in the contrast analysis. In both the VEGF and B20 groups, there were no mechanical changes, indicating that this delivery time did not alter the tissue to the same extent that the late delivery group did, despite some changes in vascularity. However, tissue organization improved with B20 in our early delivery group to a greater extent than in the late delivery group. This consistency demonstrates that the reductions in vascularity caused by the anti-angiogenic therapy are also altering the tissue structure. It is possible that this increased collagen alignment observed in the early group could be countering any detrimental effects of the decreased vascularity that reduced mechanical properties in the late group.

E. CHAPTER 5: EFFECT OF VASCULAR MODULATION ON ACHILLES TENDON HEALING WITH AGING

In Chapter 4, we found that the administration of anti-angiogenic factor, B20, causes the adult tendon healing capacity to be impaired, while pro-angiogenic factor, VEGF, does not change healing outcome. Aged tissues, however, have a reduced capacity for both angiogenesis and healing potential. Consequently, it is not known how these same angiogenic factors will effect healing in aged tissues. Therefore, the objective of this chapter was to evaluate the vascular response following Achilles tendon injury in adult and aged rats, and to define the alterations to tendon healing in an aged model following injection of pro- and anti-angiogenic factors. We hypothesized that when compared to adult rats, aged rats would demonstrate a decrease in blood flow parameters, as well as a decrease in vascular density following injury. Additionally, we hypothesized that increasing the

197

vascular response through the administration of a pro-angiogenic treatment would improve healing capacity as shown by increased mechanical properties.

Consistent with our hypothesis, the aged animals had a reduced vascular response to Achilles tendon injury as observed with both Doppler ultrasound and histological measures of blood flow and vessel density. Additionally, VEGF administration to the aged population caused an improvement in percent relaxation, max load, and injury site modulus, as well as a trending increase in dynamic modulus. It has been found that aged tissues have a reduced capacity to undergo angiogenesis due to decreased VEGF expression, reduced HIF-1α translocation into the nucleus to promote VEGF transcription, and reduced proliferation and migration of endothelial cells.[2, 24, 50, 51, 53, 61] Therefore, the exogenous delivery of VEGF may be able to compensate for some of those alterations in angiogenesis due to aging, partially returning the healing response to adult levels. While the literature indicates the increases in VEGF can lead to increases in collagen III production,[11, 13, 57] our immunohistochemistry results did not find significant changes in collagen III. However, it is possible that evaluating mRNA expression of collagen production, or evaluating a ratio of collagen I to collagen III could provide more insight into the reason for the improvements in mechanics.

Surprisingly, there were trending increases in max load and injury site modulus with the delivery of B20 as well. This is contrary to our findings in the adult animals, where anti-angiogenic treatment impaired healing potential at this same time point. It is possible that because aged animals already have reduced VEGF signaling, this further inhibition could be causing a vascular normalization effect. There was an increase in

angiopoietin-1 expression in our B20 group, which is a protein that regulates vascular normalization and endothelial cell protection. Therefore, while the delivery of anti-VEGF antibody clearly caused reduced vascular density compared to control, it may have increased normalization of the newly formed vessels and improved vessel efficiency. Additionally, the collagen alignment analysis for this group demonstrated increased tissue organization at this same time point, which could also contribute to the trending improvements in mechanical properties. Overall, this work indicates that aging affects the vascular response to injury, and also that vascular modulation has distinctly different effects on adult and aged populations.

F. FINAL CONCLUSIONS

In this dissertation, we developed new methodologies for using ultrasound imaging to quantify vascular properties *in vivo*. We also developed a model to alter the angiogenic response to injury in the rat Achilles tendon. Finally, we used this model to evaluate the effect of vascular modulation on healing in both adult and aged animals using ultrasound quantification of collagen alignment as well as histological and mechanical evaluation. Our results demonstrate that the delivery of anti-angiogenic factor caused impaired early healing in the adult animals, whereas the delivery of pro-angiogenic factor caused improved healing in the aged animals.

We conclude that angiogenic modulation has a profound effect on tendon healing properties, and importantly, that age effects the outcome of the modulation. Since there was no clear benefit found in the adult animals we conclude that these animals already have

a robust vascular response, and so additional vascular perturbations to this system in this manner is not beneficial to tendon healing. However, in the case of the aged animals, both their angiogenic and healing capacity is limited due to effects of aging, and so providing exogenous angiogenic signaling is able to partially correct these impairments.

This work is the first to evaluate tendon healing using multiple *in vivo* ultrasound imaging modalities alongside with functional, histological, and mechanical properties. We were able to translate imaging methods used in other research fields to extract distinct vascular properties that are not measurable using *ex vivo* methods, such as blood flow velocity, blood oxygenation, and time- and amplitude-based perfusion parameters. Photoacoustics, for example, has never before been used to evaluate blood oxygenation levels during tendon healing, and provided us with key information about the structure and efficacy of the vessels forming during healing. Because we were able to measure such a breadth of vascular properties, we found that our ultrasound imaging was more reliable for detecting changes in vascularity than commonly used histological methods. Additionally, these measures can be made longitudinally *in vivo*, which reduces the number of animals needed for future studies and provides the opportunity for the translation of these techniques to clinical practice.

G. FUTURE DIRECTIONS

G-1. Additional IHC Targets

In this study, we focused on immunohistochemical analysis in order to evaluate localized biological and matrix alterations caused by angiogenic modulations. These

include cellularity and cell shape (H&E), vascular markers (CD34, VEGF, Ang-1), matrix formation and degradation markers (Col III, MMP-13), and inflammatory markers (TNF-α). Unfortunately, we observed very few significant alterations with these targets. However, there are many more markers that would be beneficial to investigate in order to better characterize the tissue and explain the vascular and mechanical changes occuring. Specifically, a full analysis of factors that are present during the different phases of angiogenesis would give a better evaluation of temporal and expression level changes that occur due to these vascular perturbations. For example, Ang-2 is expressed with VEGF at the initiation of angiogenesis and responsible for vessel destabilization and induces MMP expression. Additionally, bFGF is expressed during endothelial sprouting and PDGF is expressed during endothelial stabilization. Finally, performing immunofluorescence could allow for the co-localization of targets, such as vascular endothelial cells and pericytes to evaluate pericyte detachment or vessel normalization. Also, the evaluation of HIF-1α could provide information about how the tissue is responding to the injury in the presence of these angiogenic factors. Alternatively, the use of a Hypoxyprobe kit, where the active solution is delivered to the animal prior to sacrifice and then immunostained, can detect cell and tissue hypoxia through immunofluorescent staining. In addition to vascular markers, a more thorough analysis of extracellular matrix proteins and MMPs could provide insight into how the matrix is degrading or remodeling in response to these angiogenic changes. Evaluation of other collagens, specifically collagen I, as well as proteoglycans or glycosaminoglycans could indicate if normal or abnormal healing is occurring, or if the speed of matrix production or remodeling is changing. Finally, a more

thorough evaluation of inflammatory cytokines (i.e., interleukins) and immune cells (i.e., macrophages, leukocytes) would provide a comprehensive evaluation of the inflammatory environment after injury, which can significantly impact healing outcome.

G-2. Additional Biologic Assays

Our immunohistochemical analysis provides information about the localized protein content in our tissue. However, it only provides a small snapshot of the biological changes occurring with the alterations in angiogenesis in the tissue and does not give information about which biological pathways are most involved, protein activity levels, or mRNA expression. And while we were able to quantify the area of staining, this assay does not allow for rigorous quantification of protein expression or deposition, so there may be more subtle changes that may not be detectable using IHC. Therefore, further biological assays should be conducted to supply a comprehensive evaluation of the biological mechanisms at play in this vascular modulation model system, as well as more quantitatively evaluate protein content. Specifically, VEGF expression is directly linked to increased MMP activity.[7, 25, 29, 40, 49, 54, 60] It would therefore be beneficial to explore the activity levels of MMPs and their inhibitors, TIMPs, to elucidate the level of matrix degradation occurring. While a certain level of degradation is necessary in order to facilitate vessel infiltration and matrix remodeling, heightened or extended MMP activity could inhibit normal tissue remodeling and impair mechanical properties.

Additionally, more quantitative measures of protein content, such as ELISAs or proteomics analyses, within the injury tissue could allow for more sensitive measures of

protein production changes. For example, it is beneficial to analyze collagen I/III ratio to determine how much scar formation vs. tissue remodeling is occurring in the injury site. This could be particularly relevant since VEGF expression has been shown to increase collagen III production,[11, 13, 57] which could be contributing to the alterations in mechanical properties. However, we were unable to detect any changes with IHC. Likewise, quantitative analysis of mRNA could help reveal how different signaling pathways are changing in these experimental groups.

Additionally, an evaluation of cell types and cell activity within the tissue should be evaluated. During the inflammatory stage of healing, there is the infiltration of inflammatory cells that release cytokines and other factors that can affect the activity of other cells including fibroblasts and endothelial cells. Metabolic and proliferation assays could be used to evaluate cellular activity, which is particularly important when looking at differences with aging.

While these biological assays were not conducted in this dissertation, tissue samples (n=6/group) were collected from both the adult and aged studies for use in future biological assays.

G-3. Additional Mechanical Testing Assays

Results from our study demonstrated that modulating the vascular response during tendon healing altered the quasi-static tendon mechanical properties (i.e., modulus, failure load, stiffness). We also investigated dynamic loading measurements (i.e., dynamic modulus, $\tan(\delta)$) and found trends in our aging group. However, in addition to these

properties, the analysis of fatigue properties (i.e., cycles to failure, tangent modulus, tangent stiffness) could provide more information that would be directly clinically relevant to the Achilles tendon. The Achilles tendon undergoes rigorous cyclic loading during normal daily activity, and due to the poor healing potential is susceptible to re-rupture during the healing process. Fatigue testing could allow for the detection of sub-rupture damage accumulation and elucidate the mechanisms governing fatigue induced tendon failure.[22] This information could inform which treatments reduce risk of re-rupture during tendon healing.

G-4. 3D Ultrasound Analysis

In this study, all of the ultrasound analyses were performed on a stack of sequential 2-dimensional images across the tendon width, with the average taken between all of the images to determine the measurement for a single specimen. However, with recent improvements in the VisualSonics software, the photoacoustic measurements can be calculated from a 3D scan. Essentially, a 3D volume can be created through interpolation of ROIs drawn in the b-mode images, and then oxygenation and hemoglobin measurements can be calculated as volumetric parameters. This would allow for a much more representative value of the entire tendon instead of just a sampling 2D images throughout the tendon. While VisualSonics does not currently have an analysis protocol for color Doppler imaging as presented in this dissertation, this may be included within future software updates and could be utilized in 2D and 3D analyses. A 3D scan was taken for all imaging modalities, except for contrast-enhanced ultrasound, so this evaluation could

be performed on the samples from this study once the technology is available.

G-5. Timing and Dosing of Angiogenic Factors

We found that both timing of factor administration as well as dosage has significant effects on both the resulting vascular changes as well as healing outcome. However, we only chose to fully evaluate two different administration times and one dose for each treatment. It is possible that altering either the timing or dosing of the groups could alter the changes observed. For example, while the VEGF treatment was shown to have only minor effects on altering vascularity, it proved to be beneficial for the aged group but did not alter the adult group healing outcomes. A study could be completed where an increased dose or extended administration time is implemented for the VEGF group to see if further improvements could be achieved. Additionally, no mechanical changes were seen to persist through to day 28 after injury. Administering angiogenic factors much later in the healing process could alter the long-term healing potential of the tissue. Finally, a combination of deliveries could prove to be useful, since it is possible that a heightened angiogenic response is beneficial early in the healing process, but angiogenic suppression is needed later in order to facilitate enhanced remodeling of the tissue.

G-6. Additional Angiogenic Factors

In this dissertation, we focused on evaluating the enhancement or removal of VEGF signaling for our angiogenic modification. While VEGF is considered the main regulator of angiogenesis, there are many factors at play during different stages of healing and

angiogenesis that could be altered to achieve different effects on vascularity and tendon healing. Both PDGF and bFGF are involved in the angiogenic process and have been investigated in altering vascularity in multiple models.[11, 21, 35, 36, 65] Additionally, angiopoietin-2 and bFGF play a role in vessel destabilization, while angiopoietin-1 and PDGF initiate endothelial stabilization and vessel maturation.[10, 20, 28] These factors could be used in combination to very specifically alter the stages of angiogenesis during healing. Finally, regulators of angiogenic factors, such as HIF-1α, could be altered in order to alter the endogenous expression of VEGF.

G-7. Other Tendon and Injury Models

The Achilles tendon provided a convenient model for this dissertation due to its large size, which enabled consistent injuries and percutaneous injections, as well as its straight and superficial anatomy, which enabled reliable ultrasound imaging and alignment quantification. However, there are many tendons within the body that serve different functions and would therefore likely respond differently to angiogenic alterations. The supraspinatus tendon is also commonly ruptured and is frequently preceded with tendinopathic degeneration. The hypervascularity commonly observed in tendinopathy[63] could alter the healing environment as compared to an acute rupture model that is hypovascular prior to injury. This tendon is one of the only tendons to have an established overuse-induced tendinopathy model that could be implemented in this research. The supraspinatus also most commonly ruptures at the insertion site, meaning it undergoes tendon-to-bone healing as opposed to tendon-to-tendon healing in the Achilles. This could

alter the way that the supraspinatus responds to angiogenic modulation compared to what we observe in the Achilles. A different example would be the flexor tendon. These sheathed tendons typically have complications with adhesion formation at the healing site limiting the gliding of the tendon and therefore reducing function of the injured digit.[9] Since VEGF has been shown to induce increased collagen III production in other healing models,[11, 13, 57] it is possible that the benefits observed from increased VEGF in other tissues would be a detriment in flexor tendons, and a reduced vascular response with more increased collagen alignment could be more beneficial to improve functional outcome, especially if healing impairments are only transient in this group.

In addition to other tendon models, these analyses could be performed on other injury models within the Achilles tendon. This dissertation investigated a relatively small injury so that the use of suture could be avoided, which causes ultrasound imaging artifact. However, with the use of limb immobilization we could investigate full thickness Achilles tendon injuries without the use of suture repair. It would be interesting to see how the size of the injury affects the vascular response, and how the delivery of angiogenic factors alters healing in different injury models. Additionally, the effect of limb immobilization itself could have effects on vascular formation, and would also be worth investigating.

G-8. Systemic Treatments

Many angiogenic treatments for other vascular conditions, such as limb ischemia or tumor growth, are delivered systemically. While a local administration allows for a higher concentration of the drug at the site of interest, it also requires daily injections into

the tissue for the duration of the treatment administration. The evaluation of both healing efficacy as well as potential side effects of systemic delivery would provide evidence to support if angiogenic treatments for tendon injuries could be developed into systemically administered drug. This could allow these treatment strategies to be more translatable for clinical use.

G-9. Sustained Release Drug Carriers

Based on the results of this dissertation, we can conclude that both dosage and timing of angiogenic factor delivery can alter the vascular and healing outcome. Additionally, we found that many of our results were only transient and did not persist to long-term improvements or detriments to healing. Therefore, it is possible that a sustained release of an angiogenic factor would provide longer-term changes to healing. However, repeated local injections for an extended duration is not only impractical but it can cause the accumulation of tissue damage from repeated needle puncture. The development of a drug carrier that would allow for the sustained release of the factor could provide a solution to this problem. The idea of sustained-release angiogenic treatment has been investigated in other fields. For example, the encapsulation of VEGF into a selectively targeted liposomes, as well as incorporation into a self-assembling peptide delivery system, was shown to improve vascularization following cardiac infarction.[27, 59] Additionally, incorporating heparin-binding into a scaffold system to facilitate sustained release of VEGF and other growth factors demonstrated improved wound healing.[41, 62] Finally, protease-mediated VEGF release from nanocapsules enhanced angiogenesis both *in vitro*

208

and *in vivo*.[68] In addition to the sustained release possibilities, a scaffold system could be implemented to allow for more complex delivery that can be tailored for the particular application. For example, a dual layer electrospun system with temporally independent delivery of VEGF and PDGF was shown to aid vascular regeneration.[67] These are only a few examples of sustained-release delivery systems that could be implemented in this model system to evaluate the effect of prolonged administration of angiogenic factors on tendon healing.

G-10. Cell or Genetic Therapy

In this dissertation, the alteration to angiogenic response was achieved through protein delivery. This was because protein delivery methods allow for a high level of temporal and dosage control as well as easy administration. However, the half-life of these factors is very short, so in order to achieve a more sustained expression repeat administrations are needed. As an alternative to developing a sustained release system for proteomic delivery, cell or genetic therapy could allow for sustained production of factors for more prolonged exposure. In addition, the use of cell delivery could provide a combined effect of providing angiogenic modulation as well as beneficial exogenous cells, such as tenocytes[32] or stem cells,[52] which could aid in tendon healing. However, these options do introduce the risk of viral vectors, inflammation, and do not allow for precise modulation of expression,[5] so the methodologies would have to be fine-tuned for the application.

G-11. Larger Animal Model

All of our ultrasound methods have been developed for *in vivo*, longitudinal evaluation, which could be translated for clinical use. However, because our methods are using a small rat model, we used a high-frequency ultrasound in order to obtain the necessary resolution to detect differences between our experimental groups. This high-frequency equipment cannot be used clinically because of low depth-penetration of imaging. Therefore, the use of a larger animal model would be beneficial to determine if these methods could be translated to a lower frequency probe and used in larger tissue samples.

G-12. Clinical Use of Ultrasound Imaging

While ultrasound imaging is currently used clinically, particularly for the evaluation of chronic tendinopathy, its use is not standard practice for all tendon injuries. Only a small number of patients receive any imaging for Achilles tendon injuries for diagnosis, and an even smaller percentage receive any follow-up imaging throughout the course of healing. While our current work provides information about how the structure and vascular properties of the tendon change over the course of healing using ultrasound imaging, this information is difficult to directly translate to human tendon properties without characterizing the human condition using these imaging techniques along with functional outcome measures. Additionally, imaging the contralateral tendon can also provide a relative baseline for the patients' vascular or structural parameters, which can be used to determine treatment strategies. Given the depth and breadth of information about

tendon properties that can be gained through this non-invasive imaging technique, there is support to include ultrasound imaging as part of the standard procedure in order to collect the necessary data to ultimately translate these findings to clinical practice.

G-13. Effects on Tendinopathy Models

Clinically, tendinopathy is associated with hypervascularity that correlates to increased pain scores.[63] Since the mechanisms governing tendinopathy and injury are distinct, we could use the methods from this dissertation to see how vascular modulation effects tendinopathy recovery. Only a few studies have tried investigating this question. However, the animal model studies of tendinopathy used collagenase injection as a tendinopathy model,[15] which could arguably be considered more of an acute injury model. Clinical studies have evaluated the delivery of sclerosing agents, which have reduced vascularity and improved pain scores in patients.[30, 31, 46] However, because of the nature of clinical studies, the effect of this vascularity removal on the mechanical properties of the tendon are unknown.

In order to properly address this question in a clinically relevant manner, an overuse or altered loading tendinopathy model would need to be used. While there is currently no overuse tendinopathy model for the rat Achilles tendon, the supraspinatus tendon overuse model could be investigated in this context. Alternatively, animal models with naturally occurring cases of tendinopathy, such as a horse superficial digital flexor tendon, could provide useful insight on the effect of vascular modulation on tendinopathy progression. Finally, clinical use of ultrasound elastography to measure tendon mechanical properties

in cases of tendinopathy with sclerosing agent injections could provide information about the safety of these treatments.

G-14. Association of Vascularity and Innervation

In addition to having low vascular density, the Achilles tendon midsubstance is also poorly innervated with the majority of the nerve fibers located within the paratenon.[1] Like many tissues in the body, nerves can grow into degenerated or ruptured tendons along with the ingrowth of vasculature. This nerve growth can correlate to tendon pain, especially in cases of tendinopathy where there is the prolonged presence of blood vessels and nerves that do not resolve due to the non-healing state of the tissue. The use of sclerosing agents for the clinical treatment of tendinopathy is likely to reduce blood vessel density so that there is regression of the associated nerves in the tissue.

In this dissertation, we did not evaluate the presence of nerves within the tissue, or how our angiogenic alterations change the innervation of the healing tissue. While we did not find any changes in our ambulation parameters that could have demonstrated differences due to pain, the association of vascularity and pain is still an important and clinically relevant question. In future work, especially related to larger injury or degeneration models, it would be beneficial to develop assays to measure the innervation of the tendon tissue, its association with vascularity, and if these changes cause painful or functional changes within these models.

G-15. Transgenic Models of Altered Angiogenesis

To further understand how angiogenic response alters the healing capacity in tendons, we could also explore the possibility of studying tendon healing in a transgenic mouse model. There are multiple transgenic strains that can be induced to knockout or overexpress angiogenic factors such as VEGF or PDGF. These models can be used to study exactly how these factors influence angiogenesis in various injury scenarios, and provide a high level of control over what factors are being altered. While all of our previous work performed ultrasound imaging in a rat model, there is support in other fields of research for the use of high-frequency ultrasound imaging in mouse models as well, especially at the highest frequency probe of 50 MHz. Therefore many of the same imaging techniques could be used in this smaller animal model.

G-16. Microbubble Delivery of Factors

In this work, we provided a local administration of our drug or factor through direct tissue injections. However, this method can be potentially inconsistent because there is no guarantee that the factor is distributed evenly through the tissue or fully reaching the injury region. The use of microbubble targeted delivery has been investigated for other applications of drug delivery, and could be applied to this work. Essentially, this delivery system would provide a non-invasive method for local drug delivery using ultrasound-activated destruction of microbubbles containing the drug or factor. The factor can be incorporated into the microbubble by binding to the albumin or phospholipid microbubble shell, which has high affinity for proteins, genetic material, and certain drugs.[58]

Ultrasound-activated cavitation of microbubbles can not only release the drug locally at the site of ultrasound imaging, but creates extravasation points in capillaries, allowing the deposit of protein or genetic material directly into the tissues.[58] This method would also deliver the factor locally at the site of existing vasculature, where signaling is needed for initiation or inhibition of angiogenesis.

A future study could be performed that develops methodologies for delivering angiogenic factors using ultrasound-activated microbubble destruction. We would hypothesize that compared to direct injections, microbubble delivery would allow for a more even and efficient distribution of factor delivery within the tendon tissue, and therefore have a larger effect on both the vascular properties and healing outcomes. The first aim of the study would be to develop the microbubble system and test the carrying capacity and delivery of factors using a phantom model. Specifically, the quantity of drug/factor that can be loaded into the microbubbles would be evaluated. Then, the quantity of factor released through normal circulation of microbubbles at non-specific sites could be tested, as well as the quantity of factor released at the site of ultrasound cavitation. Finally, the ideal loading density, concentration of microbubbles, and ultrasound power and duration to achieve the appropriate dosage of the factor can be determined. For the second aim, the microbubble delivery system would be tested in an *in vivo* model using tagged factors to evaluate the efficiency of delivery into the tissue. To achieve this aim, the factor of interest would be tagged prior to incorporation into the delivery system, and then delivered intravenously using ultrasound to perform the targeted delivery. The animals would then be sacrificed at targeted time points after delivery to evaluate the factor

incorporation into the tissue of interest, surrounding tissues, and tissues outside of the activation area. Finally, the third aim would perform a study evaluating the effect of factor delivery using this system on vascular and healing outcomes. Ultrasound imaging modalities would be used to measure vascular changes and biological and mechanical analyses to determine healing outcome. This delivery system would be compared to both local injection of factors, as completed in this dissertation, as well as to systemic delivery of factors to control for the possibility that the systemic injection of microbubbles is not causing the alterations, but the local activation of factor release. This work would be significant because it would provide a more clinically translatable, non-invasive local delivery mechanism for angiogenic modulation treatments that could also be translated to other treatments and factors.

G-17. Effects of Gender

While angiogenesis is a critical process during tissue development, it is virtually absent in adult tissues except for cases of wound healing and reproductive organ function. Due to this function, sex steroids play a role in angiogenesis regulation. Specifically, there is an estrogen responsive element in the gene for VEGF.[14, 39] Additionally, androgens, such as testosterone, have been shown to enhance angiogenesis in males.[55, 64] The regulation of angiogenesis through these sex hormones can induce gender-related differences in vascularity. For example, heightened estrogen expression in the breast tissue can lead to increased risk of breast cancer due to both increased cellular proliferation and angiogenesis from increased expression of VEGF.[14] Additionally, menstrual cycle hormonal

fluctuations influence endothelial progenitor cell regulation and mobilization, which has been hypothesized to contribute to lower cardiovascular risk in pre-menopausal women compared to men of the same age.[19, 38] Conversely, females were shown to have an impaired angiogenic response compared to males, including less vessel formation and endothelial cell proliferation *in vitro*, as well as lower blood flow and vasodilation response.[48] Interestingly, exogenous administration of androgens enhanced angiogenic processes, such as endothelial cell migration, proliferation, tubulogenesis, and *in vivo* limb ischemia, in males only. The same androgen administration to female cells did not have any effect.[55] Knocking out androgen receptors also significantly reduced angiogenic capacity, despite normal increases in HIF-1α and VEGF expression.[64] Since there are established gender differences in the prevalence and healing capacity of various tendon and ligament injuries, it would be interesting to study how gender-specific vascular differences contribute to these alterations in injury and healing.

A future study could be performed to evaluate the effects of gender and sex hormone expression on vascular response to injury and tendon healing. We would hypothesize that there would be gender differences in vascular response to tendon injury, and that altering the sex hormone exposure would alter the vascularity and have an impact on tendon healing. The first aim would evaluate the effect of gender on vascular response to injury. Both male and female rats would undergo a tendon injury, and be evaluated for changes in vascular properties using ultrasound measures and healing properties using histology and mechanical outcomes. The second aim would determine if hormonal alterations impacted vascularity and/or healing properties. For this study there would be

two additional groups that would be compared to the groups in aim 1: (1) female rats that have undergone ovarectomy to reduce estrogen expression and (2) male rats that have undergone castration to lower testosterone expression. After these hormonal alterations, these animals would undergo the same study design as defined in aim 1 to determine how the absence of sex hormones influences vascularity and tendon healing. Finally, the last aim would determine if angiogenic modulations could alter the results found in Aim 2 for tendon healing. This study would use the same groups in aim 2, but would additionally administer local injections of VEGF to the healing tendon to determine if angiogenic factor delivery effects the vascular and healing outcomes of animals with reduced hormonal expression. This work would help explain some of the mechanisms for altered tendon healing between males and females and altered healing in different phases of life when hormonal differences occur. Additionally, it would evaluate if there is a potential treatment strategy for recovering lost angiogenic potential due to reduced hormonal expression.

G-18. Angiogenic Treatment for Diabetic Tendon Healing

In this study, we chose aging as a model of naturally impaired healing and decreased vascular response. However, there are other systemic diseases that cause alterations to angiogenesis and vascular structure, one of which is diabetes. There is significant evidence demonstrating changes in inflammation and angiogenesis after tendon injury,[3, 12, 17] and also significant evidence of impaired healing, [4, 6, 16, 45, 66] in both animal and human studies of diabetes. Therefore, it is possible that, similar to our aging group, vascular modulation could be beneficial in a diseased model such as this. Previous research

has been conducted evaluating the delivery of angiogenic factors to treat tissues impaired due to diabetes. For example, the delivery of HIF-1α adenovirus in a diabetic model of hindlimb ischemia improved re-perfusion of the limb and decreased vascular leakiness.[34] Additionally, anti-VEGF therapy has been investigated to treat diabetic retinopathy due to the pathogenic role of VEGF in this condition.[56] The investigation of vascular modulation in diabetic tendon healing could provide a potential therapeutic for this condition.

A future study could be performed to evaluate how diabetes alters vascular response to tendon injury as well as tendon healing, and determine if vascular modulation would impact healing outcome. We would hypothesize that diabetes would limit both the angiogenic and healing potential of a tendon after injury, and that similar to what we see in aged animals, the delivery of VEGF would improve healing outcome. The first aim of this study would be to determine the effect of diabetes on vascular and mechanical properties during tendon healing. The study groups would include diabetic rats as well as aged and weight matched control rats all undergoing an Achilles tendon injury. These animals would be evaluated for vascular changes using ultrasound imaging as well as healing outcomes using histological and mechanical analyses. The second aim would be to determine if local administration of angiogenic factors could improve the healing response in diabetic tendons. This study would have the same groups as Aim 1, but would be administered local injections of angiogenic factors following injury. This study would provide insight into the role that altered vascularity plays in tendon healing with diabetes, and provide a potential therapeutic to improve healing outcome in this patient population.

G-19. Final Conclusions

In this chapter, we have proposed multiple future directions that would further investigate the role of vascularity in various tendon pathologies. This includes both additional assays in the context of this dissertation, as well as possible tangential studies using the methods and models developed in this work to further explore different injuries, model systems, treatments, and evaluation methods to investigate tendon vascularity. These future studies would provide a comprehensive evaluation of the ideal vascular response to tendon injury or disease, which could ultimately lead to the development of precision medicine strategies for tendon treatment.

H. REFERENCES

1.   Ackermann P.W., Li J., Finn A., Ahmed M. and Kreicbergs A. Autonomic innervation of tendons, ligaments and joint capsules. A morphologic and quantitative study in the rat. *J Orthop Res* 2001; 19(3)**:** 372-378.

2.   Ahluwalia A., Narula J., Jones M.K., Deng X. and Tarnawski A.S. Impaired angiogenesis in aging myocardial microvascular endothelial cells is associated with reduced importin alpha and decreased nuclear transport of hif1 alpha: Mechanistic implications. *J Physiol Pharmacol* 2010; 61(2)**:** 133-139.

3.   Ahmed A.S., Li J., Schizas N., Ahmed M., Ostenson C.G., Salo P., Hewitt C., Hart D.A. and Ackermann P.W. Expressional changes in growth and inflammatory mediators during achilles tendon repair in diabetic rats: New insights into a possible basis for compromised healing. *Cell Tissue Res* 2014; 357(1)**:** 109-117.

4.   Ahmed A.S., Schizas N., Li J., Ahmed M., Ostenson C.G., Salo P., Hewitt C., Hart D.A. and Ackermann P.W. Type 2 diabetes impairs tendon repair after injury in a rat model. *J Appl Physiol (1985)* 2012; 113(11)**:** 1784-1791.

5.   Al Sabti H. Therapeutic angiogenesis in cardiovascular disease. *J Cardiothorac Surg* 2007; 2**:** 49.

6.   Bedi A., Fox A.J., Harris P.E., Deng X.H., Ying L., Warren R.F. and Rodeo S.A. Diabetes mellitus impairs tendon-bone healing after rotator cuff repair. *J Shoulder Elbow Surg* 2010; 19(7)**:** 978-988.

7.   Berglund M.E., Hart D.A., Reno C. and Wiig M. Growth factor and protease expression during different phases of healing after rabbit deep flexor tendon repair. *J Orthop Res* 2011; 29(6)**:** 886-892.

8.   Boyer M.I., Watson J.T., Lou J., Manske P.R., Gelberman R.H. and Cai S.R. Quantitative variation in vascular endothelial growth factor mrna expression during early flexor tendon healing: An investigation in a canine model. *J Orthop Res* 2001; 19(5)**:** 869-872.

9.   Branford O.A., Klass B.R., Grobbelaar A.O. and Rolfe K.J. The growth factors involved in flexor tendon repair and adhesion formation. *J Hand Surg Eur Vol* 2014; 39(1)**:** 60-70.

10.   Brudno Y., Ennett-Shepard A.B., Chen R.R., Aizenberg M. and Mooney D.J. Enhancing microvascular formation and vessel maturation through temporal control over multiple pro-angiogenic and pro-maturation factors. *Biomaterials* 2013; 34(36)**:** 9201-9209.

11.   Chan B.P., Fu S., Qin L., Lee K., Rolf C.G. and Chan K. Effects of basic fibroblast growth factor (bfgf) on early stages of tendon healing: A rat patellar tendon model. *Acta Orthop Scand* 2000; 71(5)**:** 513-518.

12.   Chbinou N. and Frenette J. Insulin-dependent diabetes impairs the inflammatory response and delays angiogenesis following achilles tendon injury. *Am J Physiol Regul Integr Comp Physiol* 2004; 286(5)**:** R952-957.

13.   Chereddy K.K., Lopes A., Koussoroplis S., Payen V., Moia C., Zhu H., Sonveaux P., Carmeliet P., des Rieux A., Vandermeulen G. and Preat V. Combined effects of plga and vascular endothelial growth factor promote the healing of non-diabetic and diabetic wounds. *Nanomedicine* 2015; 11(8)**:** 1975-1984.

14.   Dabrosin C. Sex steroid regulation of angiogenesis in breast tissue. *Angiogenesis* 2005; 8(2)**:** 127-136.

15.   Dallaudiere B., Lempicki M., Pesquer L., Louedec L., Preux P.M., Meyer P., Hess A., Durieux M.H., Hummel V., Larbi A., Deschamps L., Benayoun Y., Journe C., Perozziello A., Schouman-Claeys E., Michel J.B. and Serfaty J.M. Acceleration of tendon healing using us guided intratendinous injection of bevacizumab: First pre-clinical study on a murine model. *Eur J Radiol* 2013; 82(12)**:** e823-828.

16.   David M.A., Jones K.H., Inzana J.A., Zuscik M.J., Awad H.A. and Mooney R.A. Tendon repair is compromised in a high fat diet-induced mouse model of obesity and type 2 diabetes. *PLoS One* 2014; 9(3)**:** e91234.

17.   de Oliveira R.R., Martins C.S., Rocha Y.R., Braga A.B., Mattos R.M., Hecht F., Brito G.A. and Nasciutti L.E. Experimental diabetes induces structural, inflammatory and vascular changes of achilles tendons. *PLoS One* 2013; 8(10)**:** e74942.

18.   Dourte L.M., Perry S.M., Getz C.L. and Soslowsky L.J. Tendon properties remain altered

in a chronic rat rotator cuff model. *Clin Orthop Relat Res* 2010; 468(6)**:** 1485-1492.

19. Fadini G.P., de Kreutzenberg S., Albiero M., Coracina A., Pagnin E., Baesso I., Cignarella A., Bolego C., Plebani M., Nardelli G.B., Sartore S., Agostini C. and Avogaro A. Gender differences in endothelial progenitor cells and cardiovascular risk profile: The role of female estrogens. *Arterioscler Thromb Vasc Biol* 2008; 28(5)**:** 997-1004.

20. Falcon B.L., Hashizume H., Koumoutsakos P., Chou J., Bready J.V., Coxon A., Oliner J.D. and McDonald D.M. Contrasting actions of selective inhibitors of angiopoietin-1 and angiopoietin-2 on the normalization of tumor blood vessels. *Am J Pathol* 2009; 175(5)**:** 2159-2170.

21. Fayazzadeh E., Ahmadi S.H., Rabbani S., Boroumand M.A., Salavati A. and Anvari M.S. A comparative study of recombinant human basic fibroblast growth factor (bfgf) and erythropoietin (epo) in prevention of skin flap ischemic necrosis in rats. *Arch Iran Med* 2012; 15(9)**:** 553-556.

22. Freedman B.R., Sarver J.J., Buckley M.R., Voleti P.B. and Soslowsky L.J. Biomechanical and structural response of healing achilles tendon to fatigue loading following acute injury. *J Biomech* 2014; 47(9)**:** 2028-2034.

23. Fukumura D. and Jain R.K. Tumor microvasculature and microenvironment: Targets for anti-angiogenesis and normalization. *Microvasc Res* 2007; 74(2-3)**:** 72-84.

24. Gennaro G., Menard C., Michaud S.E. and Rivard A. Age-dependent impairment of reendothelialization after arterial injury: Role of vascular endothelial growth factor. *Circulation* 2003; 107(2)**:** 230-233.

25. Ghosh S., Basu M. and Roy S.S. Ets-1 protein regulates vascular endothelial growth factor-induced matrix metalloproteinase-9 and matrix metalloproteinase-13 expression in human ovarian carcinoma cell line skov-3. *J Biol Chem* 2012; 287(18)**:** 15001-15015.

26. Gimbel J.A., Van Kleunen J.P., Mehta S., Perry S.M., Williams G.R. and Soslowsky L.J. Supraspinatus tendon organizational and mechanical properties in a chronic rotator cuff tear animal model. *J Biomech* 2004; 37(5)**:** 739-749.

27. Guo H.D., Cui G.H., Yang J.J., Wang C., Zhu J., Zhang L.S., Jiang J. and Shao S.J. Sustained delivery of vegf from designer self-assembling peptides improves cardiac function after myocardial infarction. *Biochem Biophys Res Commun* 2012; 424(1)**:** 105-111.

28. Hall K. and Ran S. Regulation of tumor angiogenesis by the local environment. *Front Biosci (Landmark Ed)* 2010; 15**:** 195-212.

29. Heo S.H., Choi Y.J., Ryoo H.M. and Cho J.Y. Expression profiling of ets and mmp factors in vegf-activated endothelial cells: Role of mmp-10 in vegf-induced angiogenesis. *J Cell Physiol* 2010; 224(3)**:** 734-742.

30. Hoksrud A., Ohberg L., Alfredson H. and Bahr R. Ultrasound-guided sclerosis of neovessels in painful chronic patellar tendinopathy: A randomized controlled trial. *Am J Sports Med* 2006; 34(11)**:** 1738-1746.

31. Hoksrud A., Torgalsen T., Harstad H., Haugen S., Andersen T.E., Risberg M.A. and Bahr R. Ultrasound-guided sclerosis of neovessels in patellar tendinopathy: A prospective study of 101 patients. *Am J Sports Med* 2012; 40(3)**:** 542-547.

32. Huegel J., Kim D.H., Cirone J.M., Pardes A.M., Morris T.R., Nuss C.A., Mauck R.L., Soslowsky L.J. and Kuntz A.F. Autologous tendon-derived cell-seeded nanofibrous scaffolds improve rotator cuff repair in an age-dependent fashion. *J Orthop Res* 2017; 35(6)**:** 1250-1257.

33. Jain R.K. Normalization of tumor vasculature: An emerging concept in antiangiogenic therapy. *Science* 2005; 307(5706)**:** 58-62.

34. Kajiwara H., Luo Z., Belanger A.J., Urabe A., Vincent K.A., Akita G.Y., Cheng S.H., Mochizuki S., Gregory R.J. and Jiang C. A hypoxic inducible factor-1 alpha hybrid enhances collateral development and reduces vascular leakage in diabetic rats. *J Gene Med* 2009; 11(5)**:** 390-400.

35. Kobayashi D., Kurosaka M., Yoshiya S. and Mizuno K. Effect of basic fibroblast growth factor on the healing of defects in the canine anterior cruciate ligament. *Knee Surg Sports Traumatol Arthrosc* 1997; 5(3)**:** 189-194.

36. Kovacevic D., Gulotta L.V., Ying L., Ehteshami J.R., Deng X.H. and Rodeo S.A. Rhpdgf-bb promotes early healing in a rat rotator cuff repair model. *Clin Orthop Relat Res* 2015; 473(5)**:** 1644-1654.

37. Lake S.P., Miller K.S., Elliott D.M. and Soslowsky L.J. Effect of fiber distribution and realignment on the nonlinear and inhomogeneous mechanical properties of human supraspinatus tendon under longitudinal tensile loading. *J Orthop Res* 2009; 27(12)**:** 1596-1602.

38. Lemieux C., Cloutier I. and Tanguay J.F. Menstrual cycle influences endothelial progenitor cell regulation: A link to gender differences in vascular protection? *Int J Cardiol* 2009; 136(2)**:** 200-210.

39. Liu H.X., Wang Y., Lu Q., Yang M.Z., Fan G.W., Karas R.H., Gao X.M. and Zhu Y. Bidirectional regulation of angiogenesis by phytoestrogens through estrogen receptor-mediated signaling networks. *Chin J Nat Med* 2016; 14(4)**:** 241-254.

40. Magnan B., Bondi M., Pierantoni S. and Samaila E. The pathogenesis of achilles tendinopathy: A systematic review. *Foot Ankle Surg* 2014; 20(3)**:** 154-159.

41. Martino M.M., Briquez P.S., Ranga A., Lutolf M.P. and Hubbell J.A. Heparin-binding

domain of fibrin(ogen) binds growth factors and promotes tissue repair when incorporated within a synthetic matrix. *Proc Natl Acad Sci U S A* 2013; 110(12)**:** 4563-4568.

42. McGee M.C., Hamner J.B., Williams R.F., Rosati S.F., Sims T.L., Ng C.Y., Gaber M.W., Calabrese C., Wu J., Nathwani A.C., Duntsch C., Merchant T.E. and Davidoff A.M. Improved intratumoral oxygenation through vascular normalization increases glioma sensitivity to ionizing radiation. *Int J Radiat Oncol Biol Phys* 2010; 76(5)**:** 1537-1545.

43. Miller K.S., Connizzo B.K., Feeney E. and Soslowsky L.J. Characterizing local collagen fiber re-alignment and crimp behavior throughout mechanical testing in a mature mouse supraspinatus tendon model. *J Biomech* 2012; 45(12)**:** 2061-2065.

44. Miller K.S., Edelstein L., Connizzo B.K. and Soslowsky L.J. Effect of preconditioning and stress relaxation on local collagen fiber re-alignment: Inhomogeneous properties of rat supraspinatus tendon. *J Biomech Eng* 2012; 134(3)**:** 031007.

45. Mohsenifar Z., Feridoni M.J., Bayat M., Masteri Farahani R., Bayat S. and Khoshvaghti A. Histological and biomechanical analysis of the effects of streptozotocin-induced type one diabetes mellitus on healing of tenotomised achilles tendons in rats. *Foot Ankle Surg* 2014; 20(3)**:** 186-191.

46. Ohberg L. and Alfredson H. Ultrasound guided sclerosis of neovessels in painful chronic achilles tendinosis: Pilot study of a new treatment. *Br J Sports Med* 2002; 36(3)**:** 173-175; discussion 176-177.

47. Peng F., Xu Z., Wang J., Chen Y., Li Q., Zuo Y., Chen J., Hu X., Zhou Q., Wang Y., Ma H., Bao Y. and Chen M. Recombinant human endostatin normalizes tumor vasculature and enhances radiation response in xenografted human nasopharyngeal carcinoma models. *PLoS One* 2012; 7(4)**:** e34646.

48. Peng X., Wang J., Lassance-Soares R.M., Najafi A.H., Sood S., Aghili N., Alderman L.O., Panza J.A., Faber J.E., Wang S., Epstein S.E. and Burnett M.S. Gender differences affect blood flow recovery in a mouse model of hindlimb ischemia. *Am J Physiol Heart Circ Physiol* 2011; 300(6)**:** H2027-2034.

49. Pufe T., Petersen W.J., Mentlein R. and Tillmann B.N. The role of vasculature and angiogenesis for the pathogenesis of degenerative tendons disease. *Scand J Med Sci Sports* 2005; 15(4)**:** 211-222.

50. Rivard A., Berthou-Soulie L., Principe N., Kearney M., Curry C., Branellec D., Semenza G.L. and Isner J.M. Age-dependent defect in vascular endothelial growth factor expression is associated with reduced hypoxia-inducible factor 1 activity. *J Biol Chem* 2000; 275(38)**:** 29643-29647.

51. Rivard A., Fabre J.E., Silver M., Chen D., Murohara T., Kearney M., Magner M., Asahara T. and Isner J.M. Age-dependent impairment of angiogenesis. *Circulation* 1999; 99(1)**:** 111-120.

52. Rowart P., Erpicum P., Detry O., Weekers L., Gregoire C., Lechanteur C., Briquet A., Beguin Y., Krzesinski J.M. and Jouret F. Mesenchymal stromal cell therapy in ischemia/reperfusion injury. *J Immunol Res* 2015; 2015**:** 602597.

53. Sadoun E. and Reed M.J. Impaired angiogenesis in aging is associated with alterations in vessel density, matrix composition, inflammatory response, and growth factor expression. *J Histochem Cytochem* 2003; 51(9)**:** 1119-1130.

54. Sahin H., Tholema N., Petersen W., Raschke M.J. and Stange R. Impaired biomechanical properties correlate with neoangiogenesis as well as vegf and mmp-3 expression during rat patellar tendon healing. *J Orthop Res* 2012; 30(12)**:** 1952-1957.

55. Sieveking D.P., Lim P., Chow R.W., Dunn L.L., Bao S., McGrath K.C., Heather A.K., Handelsman D.J., Celermajer D.S. and Ng M.K. A sex-specific role for androgens in angiogenesis. *J Exp Med* 2010; 207(2)**:** 345-352.

56. Simo R., Sundstrom J.M. and Antonetti D.A. Ocular anti-vegf therapy for diabetic retinopathy: The role of vegf in the pathogenesis of diabetic retinopathy. *Diabetes Care* 2014; 37(4)**:** 893-899.

57. Takayama K., Kawakami Y., Mifune Y., Matsumoto T., Tang Y., Cummins J.H., Greco N., Kuroda R., Kurosaka M., Wang B., Fu F.H. and Huard J. The effect of blocking angiogenesis on anterior cruciate ligament healing following stem cell transplantation. *Biomaterials* 2015; 60**:** 9-19.

58. Tsutsui J.M., Xie F. and Porter R.T. The use of microbubbles to target drug delivery. *Cardiovasc Ultrasound* 2004; 2**:** 23.

59. Wang B., Cheheltani R., Rosano J., Crabbe D.L. and Kiani M.F. Targeted delivery of vegf to treat myocardial infarction. *Adv Exp Med Biol* 2013; 765**:** 307-314.

60. Wang H. and Keiser J.A. Vascular endothelial growth factor upregulates the expression of matrix metalloproteinases in vascular smooth muscle cells: Role of flt-1. *Circ Res* 1998; 83(8)**:** 832-840.

61. Wang H., Keiser J.A., Olszewski B., Rosebury W., Robertson A., Kovesdi I. and Gordon D. Delayed angiogenesis in aging rats and therapeutic effect of adenoviral gene transfer of vegf. *Int J Mol Med* 2004; 13(4)**:** 581-587.

62. Wang K., Chen X., Pan Y., Cui Y., Zhou X., Kong D. and Zhao Q. Enhanced vascularization in hybrid pcl/gelatin fibrous scaffolds with sustained release of vegf. *Biomed Res Int* 2015; 2015**:** 865076.

63. Yang X., Coleman D.P., Pugh N.D. and Nokes L.D. A novel 3-d power doppler ultrasound approach to the quantification of achilles tendon neovascularity. *Ultrasound Med Biol* 2011; 37(7)**:** 1046-1055.

64. Yoshida S., Aihara K., Ikeda Y., Sumitomo-Ueda Y., Uemoto R., Ishikawa K., Ise T., Yagi S., Iwase T., Mouri Y., Sakari M., Matsumoto T., Takeyama K., Akaike M., Matsumoto M., Sata M., Walsh K. and Kato S. Androgen receptor promotes sex-independent angiogenesis in response to ischemia and is required for activation of vascular endothelial growth factor receptor signaling. *Circulation* 2013; 128(1)**:** 60-71.

65. Younesi M., Knapik D.M., Cumsky J., Donmez B.O., He P., Islam A., Learn G., McClellan P., Bohl M., Gillespie R.J. and Akkus O. Effects of pdgf-bb delivery from heparinized collagen sutures on the healing of lacerated chicken flexor tendon in vivo. *Acta Biomater* 2017; 63**:** 200-209.

66. Zeytin K., Ciloglu N.S., Ates F., Vardar Aker F. and Ercan F. The effects of resveratrol on tendon healing of diabetic rats. *Acta Orthop Traumatol Turc* 2014; 48(3)**:** 355-362.

67. Zhang H., Jia X., Han F., Zhao J., Zhao Y., Fan Y. and Yuan X. Dual-delivery of vegf and pdgf by double-layered electrospun membranes for blood vessel regeneration. *Biomaterials* 2013; 34(9)**:** 2202-2212.

68. Zhu S. and Segura T. Cell-demanded vegf release via nanocapsules elicits different receptor activation dynamics and enhanced angiogenesis. *Ann Biomed Eng* 2016; 44(6)**:** 1983-1992.

APPENDIX 1: Achilles Tendon Incisional Injury Surgical Protocol
Updated on 02/19/2018 by Cori Riggin

Equipment and Supplies:
- Isoflurane
- Knock-out box
- Ear punch
- Sharpie
- Artificial Tears
- Betadine
- Isopropyl Alcohol
- Nair
- Clippers
- Lidocaine
- Buprenorphine Sustained-Release (1mg/kg)
- Buprenorphine (0.05mg/kg)
- Heat lamp
- Circulating Warm Water Blanket
- Hot bead sterilizer
- #61 blades (2 per animal, MYCO Medical 2002-61, ordered from VWR 10148-784, sterile)
- #61 blade holder (sterile)
- Sterile surgical pack
  - Hemostats
  - #15 blade holder
  - Small forceps
  - Rat-tooth forceps
  - Surgical scissors
  - Extra scissors for cutting suture
  - Needle drivers
  - Gauze
  - Folded drape
- Sterile drape
- #15 scalpel blades (1 per animal, sterile)
- Suture (4.0 Vicryl) (1 for every 6 animals, sterile)
- 10mL syringe
- Sterile saline
- Sterile gowns
- Sterile gloves
- Face masks
- Hair nets
- New cages with alpha-dry bedding
- Special requirement cards

- Hydrogels
- Surgical event form

Pre-Surgery Procedures:
1. Provide all rats with the pre-surgical dosage of Buprenorphine (0.05mg/kg) administered subcutaneously 30 minutes prior to surgery.
2. Prepare the surgical table for an aseptic surgery
    a. Secure a heating pad to the surgical table and place an absorbent pad over the circulating warm water blanket.
    b. Secure the isoflurane nose cone to the center of the table, leaving enough room for the length of the rat between the nose cone and the end of the table (the tail can hang off the table).
    c. Place the hot bead sterilizer at the end of the table near the wall
    d. Using sterile technique, open the surgical drape and place it over the table
        i. From this point on, the surgical table is sterile, and should not be touched except by the scrubbed in surgeon/assistant
    e. Drop surgical supplies needed on to the surgical table by opening them and letting them fall directly on the table.
        i. This includes unwrapping the outer layer of the sterile pack (inner layer is sterile and can be placed on the table), all scalpel blades, suture, #61 blade holder, 10mL syringe
        ii. Do not touch the sterile supplies when opening them, only touch the wrappers
3. Prepare the prep table
    a. Put an absorbent pad in the hood
    b. Place a knock-out box and nose cone in the hood
    c. Set out all supplies needed
        i. Artificial tears
        ii. Sharpie
        iii. Ear punch
        iv. Clippers
        v. Nair
        vi. Gauze
        vii. Cup of water (for nair removal)
        viii. Cup of 1:1 betadine and isopropyl alcohol mixture
        ix. Hemostats
        x. Lidocaine (1:3 dilution)
4. Prepare the post-surgical supplies
    a. Fill-out special requirement cards indicating use of alpha-dry for 1 week post-surgery
    b. Place cards behind each cage card
    c. Place hydrogels in the alpha-dry cages
5. Surgeon and assistant scrub-in
    a. Open gown pack so gown and towel are showing

b. Open sterile gloves onto open gown pack
c. Put your face mask and hair net on (must do this before washing!)
d. Wash hands
    i.   Wet hands and arms, up to elbows
    ii. Use scrub brush to wash from finger tips to elbows, 10 seconds on each surface
        1. Fingertip
        2. 4 sides of each finger
        3. Front, back, and sides of hands
        4. Arms
    iii. Repeat 3x
    iv. Rinse off soap, fingertips to elbows
e. Grab corner of towel and allow it to drape open
f. Dry hand and arm, then pick up opposite corner of towel and dry other hand and arm
g. Put on drape (see image below)
    i.   Pick up down by the top of the inside portion (lighter color)
    ii. Let it drape open
    iii. Slide arms in arm holes WITHOUT exposing fingers until gloving
    iv. Have an assistant Velcro the neck and tie the back of the gown

1. DRY HANDS   2. PICK UP GOWN

3. LET GOWN UNFOLD   4. OPEN TO LOCATE   5. SLIP ARMS INTO SLEEVES
                         SLEEVE / ARM HOLES

6. HOLD ARMS OUT AND SLIGHTLY UP   7. CIRCULATOR PULLS GOWN ON

h. Open sterile gloves and put them on (see image below)
    i.   Keep hands in gown until the glove is over the gown
    ii. Slip your first hand in the glove, using your other hand (still inside the gown)

iii. Make sure there are a few inches of overlap of the gown under the glove
iv. Put your second glove on
i. Have assistant help you tie the gown around the waist by handing them the cardboard pull tab and spinning around so the tie wraps around you
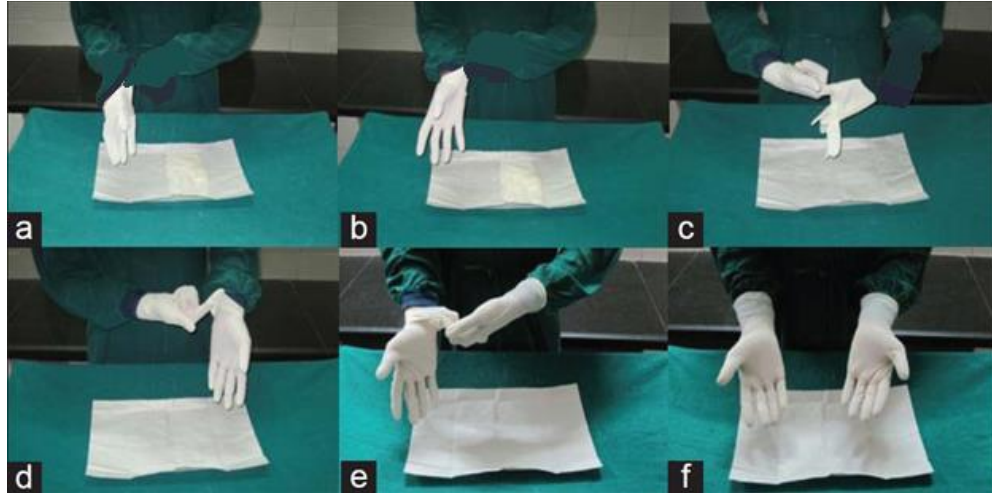
Animal Prep Procedures:
1. Anesthetize rat in the knock-out box using 5% isoflurane and oxygen set to 1 L/min
2. Once rat is under, transfer to the prep-table nose cone and lower the isoflurane to 2%
3. Apply artificial tears to both eyes
4. For odd rats only – ear punch right ear and mark the tail with sharpie
5. Use the clippers to remove hair from both hind limbs, making sure to take extra time around the Achilles tendon and calcaneus region
6. Apply nair to the skin around the Achilles tendon and let sit for a few minutes
   a. Remove nair with water and gauze and check that hair is sufficiently removed
   b. If not, re-apply nair, but do not leave on too long or you could burn the skin
7. Inject lidocaine subcutaneously in both limbs on top of the gastrocnemius muscle and on top of the Achilles
   a. Be sure to avoid large vessels
   b. Only inject a very small quantity – should be a small bubble under the skin
8. Scrub both hind limbs with isopropyl alcohol and betadine using gauze clamped in a hemostat
9. When ready, transfer the rat to the surgical table nose cone while scrubbed-in surgeon or assistant lift the sterile drape
10. Re-apply the betadine once on the surgical table

Animal Surgical Procedure:

1. Cut a hole in the top drape that just fits the hind limb of the rat, and pull the first limb through the hole
2. The surgeon will be positioned at the end of the table, and the assistant on the side of the table closest to the limb being operated on
3. The assistant will hold the limb with the ankle at 90deg flexion
   a. Hold the foot between the pointer and middle fingers of the hand closest to the surgeon, with your hand lying flat on the table
   b. The ankle should be bent around the pointer finger
   c. Use the hold on the foot to extend the leg out straight so there is tension on the leg/Achilles
4. Using a #15 scalpel blade, make an incision on the medial side of the Achilles tendon
5. Use surgical scissors to bluntly open the surgical site above the Achilles tendon
   a. The assistant can use the rat-tooth forceps to hold open the skin flap to visualize the tendon
6. Locate the plantaris tendon (medial to Achilles) using the small forceps, and separate it from the Achilles
7. Bluntly dissect between the plantaris and under the Achilles tendon so that the Achilles is isolated and above the scissors
8. Use the #61 blade to make an incisional injury immediately distal to the bifurcation of the Achilles tendon, perpendicular to the long axis of the tendon, making sure that the blade does not cut through either side of the tendon (see images below). Use the scissors as a backing to protect underlying tissues.
   a. The assistant can support the end of the scissors with a finger
   b. The tendon will flatten out wider as the blade is pressed to the tendon, allowing space in the center of the tendon for the center partial injury
   c. Press the blade down until you feel contact with the scissors below the tendon
   d. Gently rock the blade to make sure the full edge of the blade is fully through the tendon
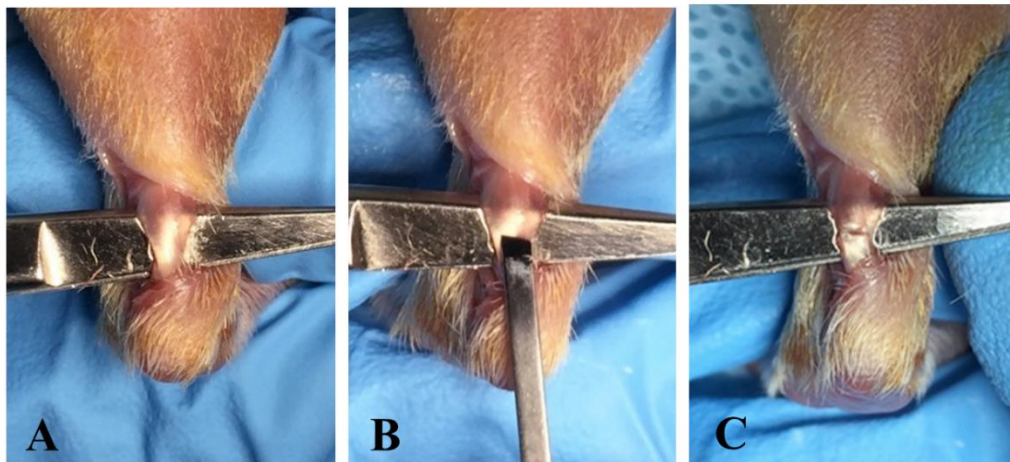
9. Flush the injury with saline
10. The assistant can relax the grip on the foot so that it can be set into plantarflexion for the skin closure
11. Close the skin using 2-3 interrupted stitches
    a. This stitch type is used to allow the skin to be as flat as possible above the Achilles for ultrasound imaging
12. Repeat procedure on the other limb
    a. The assistant will need to move to the other side of the table
    b. Re-apply the betadine solution before inserting leg through hole in top drape

Post-Surgical Procedures:
1. Once the animal has been operated on both limbs, measure and record the animal weight in the surgical form
2. Transfer to the alpha-dry cage and place under the heat lamp to recover
3. Use the weights of the animals to calculate individual Buprenorphine SR dosages.
4. Administer Bup SR 4-6 hours after surgery

APPENDIX 2: Angiogenic Factor Injection Protocol
Updated on 02/19/2018 by Cori Riggin

Injection Solutions:
- Rat recombinant VEGF-165 (PeproTech, 400-31)
  - Reconstitute and dilute to 0.25mg/mL in saline
  - Aliquot into 150μl
    - Need 120μl per animal (6 injections/animal, 2 limbs for 3 days)
    - Added 5μl/syringe to account for dead space when filling syringe
  - Store aliquots at -20°C
- Murine anti-VEGF-A antibody (Genentech, B20-4.1.1)
  - Stock solution at 17.26 mg/mL
  - Dilute to 12.5 mg/mL in saline
  - Store in sterile vial at 4°C
- Sterile pouch of saline

Equipment and Supplies:
- 0.3cc insulin syringe (Harvard Apparatus, 722419)
- Isoflurane
- Betadine
- Isopropyl alcohol
- Gauze
- Absorbent pad
- Heat lamp

Preparation Procedures:
1. No earlier than the day before the first day of injections, draw up the syringes needed for that surgical group
   a. Need a total of 6 syringes for each animal (2 limbs, 3 days of injections)
2. Label bags to store syringes
   a. 3 larger bags with the injection date for the 3 injection days
   b. 9 smaller bags, 3 each labeled with saline, B20, or VEGF
   c. Place one of each group bag into each injection day bag
3. Saline and B20
   a. Wipe the injection port with an alcohol pad before drawing up syringes
   b. Draw up 20μL of solution into the syringe
4. VEGF
   a. Thaw an aliquot for each animal that is in the VEGF group (each aliquot should supply 6 syringes)
   b. Draw up 20μL of VEGF into each syringe
5. Place the syringes needed for each injection day in the designated bags (determined by which group each animal is allocated to)
   a. Be sure to keep injection groups clearly labeled and separated so that they

don't get mixed up – they will look the same once drawn up!
6. Place all syringes in the refrigerator (4°C) until use in the next 3 days

Injection Procedures:
1. Remove syringes needed for the days injections from the refrigerator, keeping the syringes in their group labeled bags
2. Secure an absorbent pad and isoflurane nose cone on the procedure table
3. Put the animal under in the knock-out box using 5% isoflurane
4. Transfer the animal to the nose cone at the table at 2% isoflurane
5. Wipe down the skin over the Achilles tendon with the betadine and isopropyl alcohol
6. Use one hand to hold the hind limb so the ankle is at 90° flexion and in tension (like the surgical position)
7. Inject 10µl of the solution above (proximal) and 10µl below (distal) the injury site
    a. The injections are delivered percutaneously in the coronal plane from the medial side of the tendon
8. Use gauze to stop any bleeding that may occur
9. Allow the rat to recover in its cage under a heat lamp

Equipment and Supplies:
- Vevo LAZR Ultrasound with LZ550 and MS250 Transducers (VisualSonics)
- Imaging platform attachment
- Foot restraint
- Zip-ties
- Scissors
- Heating pad with re-charger and battery (Kent Scientific, DCT-20)
- Clippers (Philips Norelco, FS9185/42)
- Extra AA battery for clippers
- Nair
- Isoflurane
- Artificial tears
- Definity microbubble contrast (Lantheus Medical Imaging, DE4) on ice
- Catheters (Medline, 24 gauge ¾", NPMCI2420Z)
- Catheter injection caps (Medline, male ¾", BMG418030)
- Alcohol pads
- Tape
- Syringes (1cc) and needles (25G) for contrast injection
- Saline Solution
- Lab notebook
- Procedure form
- External hard drive
- Adjustable wrench

Preparation Procedure:
1. Turn on all imaging equipment
    a. Turn on the photoacoustics laser system (warm up for 20-30 min before imaging)
    b. Turn on the ultrasound machine (switch in the back-right first, then switch on the left side)
    c. Make sure you have the LZ550 transducer attached, and if not, switch to it:
        i. Detach the transducer from both the 3D scanner and the wall mount
        ii. Place the transducer you are not using on the rack in the back of the box
        iii. Attach the LZ550 transducer to the 3D scanner and the wall mount
        iv. Attach the ultrasound connection to the port on the ultrasound machine (far right)
        v. Place the detached plug on top of the imaging box on the Velcro

strip

      vi. Plug the laser cord into the laser box (2 connections)

     vii. For the large metal connection, loosen the screws around the plug, lift up the red rim, and remove previous plug. Place new plug in and tighten screws (lightly)

   viii. Smaller connection has a screw mechanism to secure it

   d. Once the computer is on, log into profile (password: CR01)

   e. Set-up a new study with study name as your imaging group and day, and a new series for each animal ID

   f. Set the Application to "Riggin_RatAchilles"

2. <u>Initialize the probe</u>

   a. Select Riggin_RatAchilles in the initialization drop-down

   b. Connect the 3D motor to the system if it is not already connected (back of the US machine)

   c. Make sure that the probe is free of any obstructions so the 3D scanner can move it back and forth freely.

   d. Accept the prompt to initialize the 3D motor (it will move through its range of motion)

3. <u>Calibrate the photoacoustics probe</u>

   a. Take the cap off the calibration disk and place it on the imaging platform

   b. Position the probe directly over the disk (with no gel) so that it is as close as you can get without touching

   c. Close the imaging box doors

   d. Switch to PA mode, and then hit freeze

   e. Under management, there are two buttons on the upper left of the screen: Optimize and Calibrate

   f. Click Optimize and let it run

   g. Click Calibrate and let it run

   h. By the end of the calibration, the yellow bar on the green-to-black bar on the bottom of the screen should be all the way to the right (optimized).

   i. At any time during imaging, if the yellow bar moves to the left and starts to get out of the green region, freeze and re-optimize the laser

       i. This can be done while imaging an animal – you don't need to put the probe back over the calibration disk

      ii. Do not re-calibrate unless you are on the calibration disk (just re-optimize).

4. <u>Set up the imaging platform</u>

   a. Attach the platform to the imaging linear stage so the screws are oriented closer to you

   b. Attach the foot restraint to the right side of the platform

   c. Place the heating pad on top of the set-up, tape down, and turn on to setting 4

   d. Place a diaper pad on top of that and tape down

   e. Secure the isoflurane nose cone on the left side of the set-up

5. <u>Set-up the prep table</u>
    a. Tape down a diaper pad on the prep table
    b. Tape down an isoflurane nose cone with an attached tube to the top of the pad
    c. Place on the table:
        i. Nair
        ii. Q-tips for nair application and gel adjustments
        iii. Artificial tears
        iv. Clippers
        v. Small beaker of water (to wash nair off)
        vi. Gauze
        vii. Alcohol pads
        viii. PBS bag
        ix. Catheters
        x. Catheter injection cap
        xi. Syringes (1mL)
        xii. Needles
        xiii. Gel packet
        xiv. 1 vial definity contrast (to warm to room temp)
        xv. Place sharps container and trash near by
6. <u>Prep the animal for imaging</u>
    a. Make sure that the isoflurane is filled
    b. Make sure air flow is switched to oxygen
    c. Turn on the air to 1 and the isoflurane to 5%
    d. Direct the flow to the knock-out box using the valves on the air tubes
    e. Place the rat in the box until unconscious
    f. Attach the nose cone on the prep table to the supply tube in the imaging box
    g. Adjust the valves to switch the flow to the table nose cone
    h. Place the rat on the table
    i. Turn the isoflurane down to 1.5-2%
    j. Apply artificial tears
    k. Shave over the left Achilles tendon and up the gastrocnemius, making sure to get the hair on the heel
    l. Apply Nair to the limb to further remove hair
7. <u>Insert catheter into tail vein</u>
    a. Place the animal on its side
    b. Place a piece of gauze under the left limb so that nair does not get on other parts of the rat
        i. We will remove the nair after the catheter insertion so it has time to work
        ii. If you are struggling with the catheter insertion and taking a while, remove the nair after a few minutes so that it doesn't burn the skin and resume the catheter insertion

c. Fill a syringe with 0.5mL saline
d. Unwrap a catheter injection cap and insert the saline syringe needle into the rubber port and pre-fill it with saline (~0.1mL)
e. Set to the side in a clean place
f. Use an alcohol pad to wipe the tail down over the vein – this will allow you to visualize the vein better
g. Find the vein by following the blue straight line down the tail
h. Start close to the tip of the tail so you can move up the tail if you do not get it right away
i. Hold the tail taught
j. Follow the line of the vein and insert the needle underneath a scale of the tail and just along/under the surface of the skin. Note that the skin is thicker as you move towards the base of the tail
k. Pull the needle out of the catheter slightly to see if you are in the vein – blood would fill the catheter tip if you are
l. If you do not see blood, re-insert the needle, adjust the location, and try again
m. Once you are in the vein, advance the catheter forward while simultaneously removing the needle
    i. Continually take note that the catheter is still filling with blood as you retract the needle
    ii. If it is not, you are no longer in the vein and need to re-adjust
    iii. Sometimes it is best to get a new catheter if you do not get it because you can puncture or bend the catheter and cause it to not work well anymore (only making your life harder!)
n. Make sure the catheter is all the way in, up to the hub
o. If you are still in the vein, the catheter will start filling with blood
p. Let the hub fill, and then place the injection cap on the end
q. Tape the catheter to the tail by first wrapping the tail under the catheter with tape, and then bringing that piece of tape up and over the catheter
r. Place your saline syringe needle in the hub of the injection cap and flush with saline so that the saline syringe is left with 0.2mL (flush with about 0.3mL)
    i. You should see the catheter/vein get lighter in color
    ii. It should be easy to flush with saline – if there is resistance then you are probably no longer in the vein
s. Remove the nair from the limb with gauze and water
t. If you cannot confirm placement of the catheter, remove it and try again in a different location
8. Position the animal
a. Transfer the iso to the nose cone on the imaging platform
b. Place the rat on the platform on its stomach and secure the hind foot into the foot restraint using the zip tie
    i. I insert the foot in the holder towards the back of the box, and then

slide the foot towards the front of the box where the zip tie is tighter to hold it in place

c. Pull the animal forward to make sure the ankle is tensioned

d. Adjust the animal/foot positioning so that the Achilles is as straight as possible

e. Apply ultrasound gel above the Achilles tendon and in the well of the ultrasound probe (LZ550)

f. Position the ultrasound above the Achilles tendon as well aligned as you can
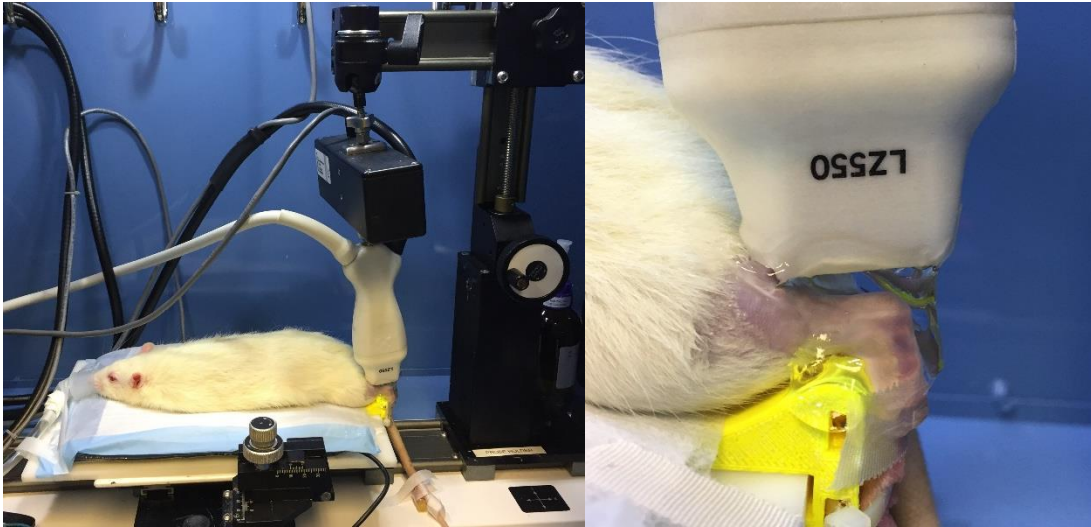
Imaging Procedure:

1. <u>Position the Transducer</u>

    a. Align the probe first so that the Achilles tendon appears parallel to the top of the screen when it is positioned at the 7mm focal zone

    b. Move the linear stage of the imaging platform back and forth to see if the length of the Achilles tendon is parallel to the imaging plane

    c. Adjust the probe angle as needed so that the tendon is parallel in both directions

        i.   If your tendon is injured, try to align the "best" plane for the injury region with the "best" plane for the calcaneus to tell if it is aligned

        ii. If your tendon is uninjured, look for the collagen fibers "traveling" along the length of the tendon – that means you are out of plane. If the whole tendon comes into focus at the same time, then you are in plane. Keep in mind that the Achilles bifurcates and gets wider proximally towards the muscle, so you are looking for the distal portion to be more aligned.

    d. Once you are happy with your probe positioning, make sure that there are no bubbles interfering with the ultrasound image – remove the bubbles or re-apply gel if necessary

    i. You should be able to raise the probe up and carefully re-apply gel without moving the tendon or probe out of place

  e. Move the probe vertically so that the tendon centered on the 7mm depth focal zone and lock the probe holder in place

  f. Make sure the entire image depth is 10mm, and the tendon is centered in the image with both the calcaneus and the myotendinous junction visible

2. <u>B-mode Imaging</u>

  a. Make sure the pre-set is set to "Riggin_Bmode"

    i. Gain: 20 dB

    ii. Focal zone: 1 located at 7mm

  b. Move the manual TGC control sliders on the keyboard all the way to the left so that you notice the image is dark if you forget to set your TGC pre-set

  c. Select the "Riggin_TGC" preset

  d. Take several still frames by navigating the probe using the linear stage attached to the animal platform

  e. Move the probe to the center plane of the tendon and take a 3D image scan over a distance of 3.5mm, with a step width of 0.1mm

    i. You can change the distance to whatever you want for your application as long as you can see the whole tendon in your 3D scan. Injured tendons might need a 5mm scan distance to capture everything

    ii. However, keep the step width consistent at 0.1mm

  f. Load your scan into 3D mode, and check the re-constructed transverse view to make sure your tendon is aligned and that the whole tendon is captured in your 3D distance

  g. Save the 3D image by pressing Cine Store

3. <u>Doppler Imaging</u>

  a. Make sure you are still in the ideal positioning in b-mode and your focal zone is still at 7mm centered on the tendon

  b. Turn on Color Doppler imaging

  c. Adjust ROI to be as small as possible while including the entire tendon and skin surface

  d. Move your focal zone back up to 7mm (it automatically moves to 8mm)

  e. Set pre-set to "Riggin_ColorDoppler"

    i. Priority = 100%

    ii. PRF = 2kHz

    iii. Wall filter = low

    iv. Doppler gain = 35dB

    v. Sensitivity = 5

    vi. Frame Rate = 18

    vii. Line Density = Full

    viii. Persistence = Med

    ix. Beam Angle = 0°

      f.   Take several still frames by navigating the probe using the platform linear stage

      g. Take a 3D image scan over a distance of 3.5mm with a step width of 0.1mm with persistence turned on

4. <u>Photoacoustics Imaging</u>

      a. Go back to your b-mode imaging to make sure your settings and positioning are all still the same

      b. Switch the air flow to medical air instead of oxygen

      c. Close the doors to the animal enclosure box

      d. Set pre-set to "Riggin_PA"

           i.   Mode: Oxy-Hemo

          ii.   Persistence: 6

         iii. PA gain: 52dB

      e. Re-adjust the ROI so it is around the tendon and skin surface

      f.   Make sure the laser energy is optimized (yellow indicator to the right on the green bar at the bottom of the screen). If energy is not full, optimize the laser before acquiring images.

      g. Take several 2D image clips in at least 3 different cross-sections by using the 3D scanner motor to navigate the probe across the ROI

      h. Navigate back to the 0 location of the 3D motor

      i.   To take a 3D image scan, press the 3D button

      j.   Set the scanner to image over a distance of 3.5mm with a step width of 0.1mm and persistence turned on

      k. Press cine store after completion of image acquisition

      l.   Open the animal enclosure box and check on animal

           i.   Note: if imaging is taking longer than expected, interrupt PA imaging and open animal enclosure box to check on animal breathing since we do not have respiratory monitoring while the box is closed

5. <u>Contrast-Enhanced Imaging</u>

      a. Switch the air flow back to oxygen

      b. The contrast should be warmed to room temperature by now

      c. Switch to the MS250 transducer

           i.   Detach the LZ550 transducer from the 3D scanner and the ultrasound port

          ii.   Attach the MS250 transducer to the 3D scanner and the ultrasound port

         iii. Initialize the transducer when prompted

         iv. Check that your tendon positioning is still the same as when scanning with the other probe

          v. If positioning is good, lock the probe holder

      d. Set pre-set to "Riggin_NonLinearContrast"

           i.   Under Preferences in the "General" tab, click the box for extended buffer

        ii. Under the "Mode Settings" tab, in the Contrast Mode section, select Nonlinear

      iii. Frame rate: 5 fps

      iv. Gain: 35 dB

       v. Image depth: 12mm

      vi. Focal zone: 7mm

e. Switch the system to non-linear contrast mode

f. Adjust the size of the ROI box so it includes the whole tendon (the buffer size should be around 4000 frames)

g. Prepare Definity contrast agent

       i. Use a VIALMIX to Shake the vial for 45 seconds – it should appear as a milky white suspension

      ii. Either use the contrast immediately after activation, or if not used within 5 minutes of activation, the microspheres should be re-suspended by 10 seconds of hand agitation by inverting the vial

      iii. Invert the vial and withdraw 100ul agent

      iv. Use the product immediately after being withdrawn – do not let it stand in the syringe

       v. *Note: Activation duration*

          1. *Activated Definity can be used up to 12 hours from time of activation, but only by hand agitation re-activation*

          2. *If not used, refrigerate and reactivate agent for 12-36 hours from initial activation*

h. Tape the rat tail down so it doesn't move during contrast injection

i. Place the 200ul saline syringe into the injection cap

j. Place the contrast syringe in the injection port as well

k. Press "Pre-Trigger"

l. Inject the 100ul contrast immediately followed by the injection of the 200ul flush of saline

       i. Make sure your injection rate is steady and consistent

      ii. Do not touch the animal or ultrasound controls while acquiring contrast data

m. Freeze acquisition after you get 1000 frames

n. Save the clip by clicking Cine Store (NOT Frame Store)

o. Double check that it saved as a clip of ~1000 frames by looking in study management

       i. If the animal/probe moves during acquisition, or the clip is pre-maturely stopped before completion, wait another 10 minutes before re-doing the injections and acquisition so that the contrast can clear.

6. <u>Recovery</u>

a. Once you have completed imaging on the animal, close the series

b. Remove the rat's foot from the restraint

c. Remove the catheter from the tail vein, and apply pressure with gauze to

stop the bleeding
d. Allow the animal to recover from anesthesia under a heat lamp

Data Transfer:
7. Use the "Copy to" function to copy the entire study to the external hard drive
   a. You use this to transfer the data in the VisualSonics format to the analysis computer, and also to back-up your acquisition data
   b. Immediately transfer this study copy to Maxine as a back-up
8. Export 3D scan clips (B-mode and Doppler) as dicom files to convert to a stack of tiff files
9. Can also export images directly as tiffs if desired.

Analysis:
10. See individual analysis protocols
    a. 2D Doppler images/Dicom files will be analyzed with the IDS Vascular Analysis code (Chandra Sehgal's lab)
    b. PA imaging will be analyzed using the VisualSonics software (imaging machine or desktop software)
    c. Contrast imaging will be analyzed using the VevoCQ software (imaging machine or desktop software)
    d. B-mode alignment images will be analyzed using the Soslowsky lab alignment MATLAB software
    e. Any 3D analyses can be analyzed using the VisualSonics software (imaging machine or desktop software)

APPENDIX 4: Ratwalk Protocol
Updated on 02/19/2018 by Cori Riggin

Set-up Protocol:
1. Plug light into power strip.
2. Remove lens cap from camera.
3. Log into computer and set-up screen:
    a. On desktop, double click "shortcut to pawstrike," a LabView program.
    b. Click the outlined arrow in the toolbar to run. After clicking, it should appear as a black filled in arrow.
    c. Simultaneously, a new dialog box should open.
4. Take calibration pictures
    a. Set up box for calibration by typing the following into the text boxes:
        i. Animal ID: block
        ii. Group ID: near, middle, or far
            1. This refers to the location of the calibration block on the walkway
        iii. Walk #: right or left
            1. This refers to the direction that the calibration block grid is facing
            2. Remember: right and left are with respect to the rats.
            3. For example, "right near" would have the grid facing the right side and be closest (nearest) to the right wall.
    b. Once you've entered the data for one calibration trial, for example, block_right_near, you need to save to the right path.
        i. In the dialog box, click the mini picture of a folder.
        ii. Navigate to the folder where you want to save your data
        iii. Create a new folder for the date
        iv. Hit "CURRENT folder", NOT "save".
    c. Place the calibration block on the walkway in the designated position for the information you just inputed
    d. Hit "PUSH to Record," which should then say "Recording…"
    e. Hit "Recording…" again to stop recording. You can click it and unclick it very quickly for this step.
    f. Hit "Save recording"
    g. Move block to next position.
    h. Hit "New trial." Change parameters to fit block position.
    i. Hit "push to record." Hit it again to stop recording. Save recording.
    j. Repeat for other sides and positions.
5. Once you are done taking calibration pictures, zero the loads (making sure nothing is touching the load cells).

Data Collection Protocol:

6. Now that you're all calibrated, hit "New Trial"
7. Fill in box appropriately:
    a. Animal ID: 43-119 (for example)
    b. Group ID: W1
        i. The number indicates which walk is recorded for the particular rat
    c. Walk #: M03
        i. This number indicates the measurement number, which I associate with the day post-surgery: M0 (pre), M03, M07, M10, or M14
        ii. Yes – Walk # and Group ID labels seem to be flipped… this is correct for my thesis work, but should be updated in future versions of the software
    d. Save under the date folder you have created.
8. Place a barrier (I use the calibration block) over the entrance to the walkway
9. Add fruity gems to the end box (should be the opaque box) as an incentive to walk across, and cover the box with the lid
10. Place the rat in the tupperware entrance
11. Let your computer mouse hover over "Push to Record" button and lift the barrier so that the rat can freely walk across the walkway
12. Once the rat looks like he is starting to walk across, click "push to record" – it should now say "Recording…"
    a. Pray he walks.
13. Click "Recording…" to stop recording once he has walked across both force plates.
14. If the walk was worth saving, hit "Save recording." If not worth saving at all, click erase recording.
    a. This is where you note:
        i. Give him a grade for the walk (this is independent of if he isolated a foot on the force plate).
        ii. If isolated, what plate was a hind limb isolated on?
            1. For my thesis right or left can be recorded since my injury is bilateral
        iii. If not isolated, give the reason why
            1. Were there two paws on the same plate?
            2. Did he strike between the plates?
        iv. Make any extra notes, such as if he paused, walked fast or slow, seemed jumpy or acting strange, etc.
15. If you have saved that recording, click new trial, and enter new text into box like "W1" or enter in data for a new rat.
16. If you did not save it and you are recording the same rat, you do not have to press "new trial" again, you just click "push to record" once the walks again.
17. Once you are done with the rat, weigh him and record the weight
18. Give some fruity gems in the cage as a reward

Clean-up:
19. Wipe down the ratwalk thoroughly, being careful of the force plates
20. Transfer your data to an external drive or to the network drive
21. Unplug the light and re-cover the camera lense

Other Notes:
- Clean the walkway frequently, especially if the rats seem scared because the smells they give off can influence the next rats in the walkway
- Walk before any anesthesia procedures
- Try to make a habit of being patient and letting them walk themselves back and forth instead of picking them up immediately at the end of a walk
    - If you pick them up right when they get to the end, they will stop wanting to go there
    - This way they get more comfortable, and are more willing to walk back and forth (makes your life easier in the long run, I promise!)
- If you are having trouble with a rat here are some tips:
    - Let him hang out without touching him for a while until he gets comfortable (as a rule, I try to pick them up as little as possible when they are in the ratwalk so that they feel relaxed)
    - Place their tube at the end of the walkway
    - Put him back in his cage and come back to him later
    - When you do take him out back out to try again, cuddle him for a few minutes before putting him in the ratwalk
    - Put his cagemate into the ratwalk with him and let them run around together to get comfortable
    - More fruity gems!
    - NEVER try to scare the rat into going down the walkway
        - This will lead to a non-representative walk
        - It will also train them to be scared in the ratwalk which will make it impossible to get them to walk the next measurement day.
- When deciding if the rat has isolated, you can click through the images using the arrows on the GUI interface BEFORE you click "save recording"
- Always double-check that your data is recording as you expect as you go. Sometimes you can accidentally record over walks, or only record the text file and not the images if things are set-up incorrectly. The last thing you want is to lose good walks!

Equipment and Materials:
- Ratwalk computer and set-up
- Zip ties
- Scissors
- Isoflurane
- Isoflurane knock-out box
- Isoflurane nose cone
- External hard drive

Set-Up and Calibration:
1. Turn on computer
2. Meanwhile, put animal in knock-out box with isoflurane at 5% and air at 1 L/min
3. Sign in using password under keyboard
4. Open "ratomoware" in labview
5. Click run
6. Unclick "remove bias"
7. Label as calib
8. Change to right limb
9. Click "erase"
10. Click "Push to record"
11. Start at 0, go internal (towards rat platform), then external about 3 times
12. Save to computer data folder

Animal Measurement:
13. Click "load calibration" and select the file you just created
14. Click "no correction" so it says "remove bias"
15. Write in animal number 43-XXX_c1
    a. c1 refers to Cori recording the first run (will continue c2, c3, etc)
16. Change to right limb
17. Write M0, M03, M07, etc for measurement number
    a. This refers to the day post-injury that the measurement is taken on (M0 is pre-surgery)
18. Move animal to the platform with iso at 2% and strap in securely
19. Put the next animal in the knock-out box with iso at 5%
20. Move the platform up and down so that the leg is resting on the raised portion of the platform
    a. The line between the knee and ankle joints should look horizontal (the tibia is curved so it is hard to tell based on the bone shape)
21. Loosely loop the zip ties around the foot
22. Re-position the foot so that the ankle joint is along the axis of rotation (the bottom of the foot should be close to the bottom of the plastic foot support)

23. Tighten the zip tie slowly and carefully with the foot in the right place until there is no wiggle room
24. Cut the zip tie ends so they won't hit the platform during testing
25. Double check your platform position
26. Remove the holders so that it can rotate freely, and hold the foot upright
27. Click "push to record"
28. Apply pressure on the knee so that the leg does not move
29. Start moving in dorsiflexion, then plantarflexion, and do a total of 4 passes going slowly
30. Torque no higher than 50 Nmm, and stop before hitting the tibia
31. Click "stop recording"
32. Click "save"
33. Change the specimen name to 43-XXX_c2
34. Repeat steps 26 – 32 another time to get a second reading
35. Remove zip ties, return animal to cage, and allow animal to recover under the warming lamp
36. Start procedure at step 15 to begin the next animal measurement

APPENDIX 6: Rat Sacrifice and Achilles Tendon Dissection Protocol
Updated on 02/19/2018 by Cori Riggin

Materials:
- PBS
- Animal storage biohazard bags
- Small specimen bags
- Sharpie
- Dissection mat
- Cup of formalin
- Histology cassettes
- Pencil
- Forceps
- Blade holder
- Hemostats
- Bone crunchers
- Microscissors
- #11 blades
- Gauze
- Kim wipes
- Liquid Nitrogen
- RNase-free 1.5mL Eppendorf tubes
- RNaseZap spray
- Ethanol
- Sacrifice form and lab notebook

Procedure:
1. Pre-label all of the bags, cassettes, and eppendorf tubes prior to the sacrifice
   a. Make sure the Eppendorf tubes are handled cleanly
   b. Label with animal number, and injured or uninjured
2. Set up your dissection table with supplies and tools
3. Sacrifice first animal or cage of 2 animals
   a. Place in CO_2 chamber and press the start button
   b. CO_2 will flow for 10 min
   c. After the 10 minutes is up, double-check that the rat is dead by feeling for a heartbeat
4. Record animal weight in your notebook and on the pre-labeled mechanics specimen bag
5. General dissection instructions:
   a. Clamp foot with a hemostat to stabilize the ankle and keep it at a 90° flexion position
   b. Make a skin incision (2cm) lateral to the tendon from the calcaneus parallel to the tibia

  c. Tension the skin and use the scalpel blade to peel back the skin and expose the Achilles tendon and gastrocnemius muscle

  d. Holding on to the muscle with your forceps, place the scalpel blade deep to the Achilles tendon and cut proximally along the tibia, leaving about 2 cm of muscle intact before rotating your blade posterior and cutting the muscle off

  e. Grab the free muscle end with foreceps and run your blade distally under the Achilles to remove additional connective tissue up to the talus.

6. For Protein/RNA harvest:

  a. Prior to dissection, spray down all surfaces and your gloves with RNaseZap

  b. Clean tools with ethanol, and spray them down with RNaseZap

  c. Start dissection immediately after animal is sacrificed

  d. Re-spray your gloves before beginning

  e. Spray down the limb until it is soaking

  f. Clamp foot with a hemostat to stabilize the ankle and keep it at a 90° position

  g. Make a single incision (2cm) lateral to the tendon from the calcaneus parallel to the tibia and peel skin back to expose the Achilles tendon/muscle

  h. Replace the blade and spray down tools

  i. Place the scalpel blade deep to the Achilles tendon and cut proximally along the tibia

  j. At the myotendinous junction, rotate your blade posterior and cut the tendon

  k. Grab the free end with foreceps and run your blade distally under the Achilles to remove additional connective tissue up to the talus.

  l. Use your blade or microscissors to quickly remove any connective tissue surrounding the tendon

  m. Use your blade to remove the proximal tendon region above the injury and discard

  n. Use your blade to remove the injury region and carefully place it in the labeled "injured" Eppendorf tube

  o. Use your blade to remove the distal part of the tendon at the insertion site and carefully place it in the labeled "uninjured" Eppendorf tube

  p. Place both tubes directly in liquid nitrogen

7. For Histology

  a. First, follow the general dissection instructions above

  b. Use the bone crunchers to break the calcaneus

  c. Spray the tendon down with PBS if it has hair attached

  d. Place it in a folded kim wipe

  e. Place it in the pre-labeled cassette and put the cassette in formalin

8. For Mechanics

  a. Disarticulate the hindlimb at the hip

      b. Wrap the end with PBS soaked gauze
      c. Place in the labeled specimen bag
9. Wrap the incisions in PBS soaked gauze and place animal in biohazard bag
10. Record any notes about the tendon or dissection
11. Store hind limbs for mechanics at -20°C until testing
12. Store tendon samples in Eppendorf tubes in a -80°C freezer
13. Process fixed histology samples for paraffin embedding

APPENDIX 7: Achilles Mechanical Preparation Protocol
Updated on 02/19/2018 by Cori Riggin

Equipment and Materials:
- Weighboats for specimens
- PBS
- Gauze
- Kim wipes
- Rat-tooth forceps
- Fine forceps
- Hemostats
- Bone crunchers
- #11 scalpel blade holder
- #11 scalpel blades
- Medium/small microscissors
- Dissection mat
- Ruler
- Dental wax
- Verhoeff stain
    - 5% hematoxylin solution (0.4g Hematoxylin + 20 ml 95% EtOH)
    - 10% aqueous ferric chloride (2g Ferric chloride + 20 ml dH2O)
    - Weigert's iodine solution (2g potassium iodide + 1g iodine + 100 ml dH2O)
- Suture for stain lines
- Stain dot application tool
- Raiser for gismo measurements
- Sandpaper
- Superglue
- PMMA
- Polycarbonate tubing, 5/8" ID, ¾" OD, 1/16" thickness (McMaster, 9176T38)
- 10-24 stainless steel socket head screw, 5/8" long (McMaster, 92196A244)

Gross Dissection:
1. Make a single incision lateral to the tendon from the calcaneus parallel to the tibia
2. Use the scalpel blade to peel back the skin and expose the Achilles tendon and muscle
3. Dissect off muscle overlaid on the gastrocnemius so that the gascroc can be clearly seen
4. Place the scalpel blade deep to the Achilles tendon and cut proximally along the tibia, rotating your blade posterior and cutting the muscle off at its most proximal position
5. Grab the free muscle end with forceps and run your blade distally under the Achilles to remove additional connective tissue up to the talus.

251

6. Use bone crunchers where the tibia meets the ankle joint and detach the tibia
7. Remove a piece of skin from the leg for storing the tendon during freezing later.

Fine Dissection:
1. Perform all fine dissection under a stereomicroscope
2. Grip the foot with hemostats to reduce movement of the tissue
3. Use microscissors, foreceps, and scalpel blade to remove surrounding musculature and soft tissue
4. Use the blunt side of the scalpel blade to gently scrape off muscle
5. Remove plantaris
   a. This tendon lies over the Achilles near the insertion, and wraps medially to insert into the anterior side of the muscle unit
   b. Using your microscissors, find the plantaris tendon distal to the Achilles insertion, detach it, and carefully pull up and proximally on the tendon, detaching connections as you go to peel it away from the Achilles
6. Once all of the muscle and the plantaris tendon are removed, thoroughly inspect the tendon and remove any non-tendinous tissue
   a. There will be "gooey" tissue overlaying the entire tendon. Pull this up starting as distal as possible and cut if off moving proximally, being very careful not to cut tendon fibers
   b. Near the scar region, gently tug on surrounding scar tissue to determine if it should be removed
      i. If it is soft, mobile, and does not appear to be load bearing – remove it
      ii. If it is firm and appears to be structural or load bearing – leave it
7. Make sure you are continually hydrating the tendon with PBS as you go
8. Prepare the foot for potting
   a. Use bone crunchers to cut the toes off of the foot
   b. Use your forceps and scalpel blade to remove the skin from the foot

Stain Lines:
1. Make Verhoeff stain
   a. Add in order B to A (mix thoroughly), then add C (and mix thoroughly) in the following ratio of A:B:C = 2:1:1
      i. Solution A: 5% hematoxylin solution (0.4g Hematoxylin + 20 ml 95% EtOH)
      ii. Solution B: 10% aqueous ferric chloride (2g Ferric chloride + 20 ml dH2O)
      iii. Solution C: Weigert's iodine solution (2g potassium iodide + 1g iodine + 100 ml dH2O)
   b. Place small amount (~0.5 to 1 ml) of stain in angled weigh boat
2. Remove tendon from PBS and dry with a kim wipe
3. Place tendon on a wax riser with posterior side facing up and tendon fanned out.
4. Place a stain line on the posterior side of the tendon at the insertion site. The goal

is to place the stain line directly on the insertion site so that it does not move under tension.

5. Position a ruler so that it is lying next to the tendon with 0mm aligned at the insertion stain line
6. Apply a stain line at 12 mm (gage length)
7. Place additional stain lines at the top and bottom of the injury region
8. Make stain dots at even increments along the rest of the tendon (~3-5 across the width of the tendon)
9. Dab the stain with a dry kim wipe before placing tissue back in PBS

Cross-Sectional Area Measurement (GISMO):
1. Turn on laser and allow it to warm up for 20 min before starting
2. Lightly dry tendon with a piece of gauze
3. Place specimen on riser with posterior end facing up.
4. Position the laser so it is to the side of the first stain line and on the riser
5. Press the "run" button and make sure that the "Capture" button is activated
6. Zero the x, y, and z positions
7. Make passes across the tendon every ~2 mm on the tendon from the first to last stain lines.
8. Place tendon back into PBS
   a. Be consistent with the amount of time the specimen is out of PBS
9. Save each specimen in a folder for a specific date set
10. Turn off laser and cover

Sandpaper:
1. Cut small pieces of sandpaper (~2 cm x 1.5 cm)
2. Apply a (very!) tiny bit of superglue on your dissection mat and place the non-coarse side on it to hold sandpaper in place on the mat
3. Remove the tendon from PBS and dry with gauze/kim wipe
4. Place tendon in proper anatomical position with posterior side facing up next to the sandpaper
5. Place thin layer of super glue on sandpaper glued to mat.
6. Pick up the tendon by holding the foot with one hand and sliding the tendon between your fine forceps until you are holding the foot and the very proximal end of the tendon and the tendon is tensioned
7. Hover it over glued-sandpaper, lining up the tendon so that it sits on the sandpaper at the 12 mm stain line
8. Smooth the tendon out over the superglued sandpaper
9. Apply glue on 2nd piece of sandpaper and compress parts together. Be careful not to squish glue onto tendon
10. Apply pressure to the sandpapered tendon for a few more seconds

253

11. Remove newly sandpapered tendon from black mat and place in PBS

Potting:
1. Machine cylindrical pots
    a. McMaster, 9176T38: durable clear polycarbonate tubing, 5/8" ID, ¾" OD, 1/16" thickness
    b. Cut with the bandsaw about 1.5"
    c. Drill a #25 drill bit hole through one side 0.5" from one end
    d. Tap the hole with a 10-24 tap
    e. Sand the outer sides to fit easily into the fixture
    f. Tape one side of pot shut (side furthest from tapped hole) and label specimen ID on pot
    g. Insert a 10-24, 5/8" long screw into the tapped hole part way
2. Mix PMMA/powder together with low viscosity
3. Fill up cylinder about 2/3rd of the way
4. Remove foot-tendon-sandpaper complex from PBS and dry foot
5. Dunk foot in bone cement making sure all portions have been covered
6. Position foot so the posterior side is facing the screw and the anterior side is up against the pot wall
7. Ensure that the Achilles tendon can bend to 90° flexion so it is perpendicular to the pot and the pot is not touching the tendon
8. Tighten screw such that the screw touches the bottom of the foot to lock foot in place
9. Fill the rest of the space in the pot if needed, making sure the PMMA is as close to the tendon insertion as possible
10. Let PMMA cure for 10 minutes before placing tendon back in PBS.

Storage for testing:
1. Once the PMMA is fully cured, wrap the tendon with the piece of skin harvested during gross dissection.
2. Wrap the whole tendon-pot unit with PBS soaked gauze
3. Place tendon in labeled specimen bag.
4. Place all specimen bags in a biohazard bag, and put in the -20°C freezer for testing on another day.

APPENDIX 8: Achilles Tendon Mechanical Testing Protocol
Updated on 02/19/2018 by Cori Riggin

Testing Set-up:
1. Turn on Instron machine – switch in the back
2. Adjust cross-head to the right height: handles facing each other means it is tight, loosen to move the crosshead and tighten once in place.
3. Place biopuls bath on the instron and lightly secure it with L-brackets
4. Hook up pneumatic hoses to pneumatic hose inputs in electropuls
5. Plug in power supply cord to bath heater
6. Place thermometer into thermometer port and tighten seal
7. Install bottom fixture to rod and line it up parallel to the imaging window in the tank
8. Add PBS to the tank (~1800mL)
9. Turn on the heating unit to 37°C
10. Set instron power setting to 1 (low)
11. Turn on the air from the orange valve on the wall
12. Confirm that the tank goes up and down
    a. Start with both buttons to the right
    b. Switch the top button to the left to move the tank up or the bottom button to the left to move the tank down
    c. Once it is in location, switch it back so both buttons are to the right
13. Attach the top fixture to the instron load cell
14. Move the cross bar down so that the top fixture is right above the bottom fixture (not touching)
15. Make sure your linear stage below the tank is centered, and then line up the fixtures
16. Tighten the L-brackets securing the tank into place
17. Remove the top fixture so that we can now test and calibrate the load cell
18. Turn on the Instron computer (left) and log in (McKay)
    a. Open Instron Console
    b. Open WaveMatrix
    c. In the console, click "calibrate" (nothing should be attached to the load cell)
    d. Save the calibration file
2. Test your loads
    a. Use 2 different weights: 4.903N and 22.24N
    b. Zero the load cell
    c. Hang each weight and record the load to check that it is within reason
19. Camera set-up
    d. Set-up the tripod for the camera in front of the bath, making sure it is not touching the benchtop
    e. Attach the camera lens to the tripod and attach the camera to the lens
        i. Both camera and lens are located on the shelf above the two

computers

  f. Plug the cord with the yellow tape into the camera and make sure the green LED is on

    i. Tape the cord to the tripod so that the plug is supported and wont fall out of the camera

  g. Position the light source so that it is directed towards the tank and turn on the lights

    i. Alternate covering up one light at a time to make sure both lights are centered just above the bottom fixture (where the tendon will be)

20. DAQ Set-up

  h. Plug in BNC cable to B-BNC port in the front of the instron under the lid

  i. Plug alligator clips to corresponding red/black wires

  j. Plug in USB cable into the far left port

21. Attach the top grip

  a. Place the pin through the fixture-load cell junction

  b. Tighten the knob to secure the fixture in place

22. Plug in the LVDT

  a. The LVDT is plugged in on the right side of the instron behind the key pad

Image Capture Computer Set-up:

1. Turn on the image capture computer and log in (McKay)

  k. Open Labview, and then select "Data\software\DigiVlepo-2013-03-22\cooker\v2.0.1\digi-Vlepo_Trigger.vi"

  l. Click Run in digi_vlepo_trigger program in Labview

  m. Select file destinations: navigate to the Data folder in the C-drive and create a folder for the test day, and then a folder each specimen within that day.

  n. Change frame rate to 1 fps

3. Check the file save location on the image capture computer

4. Type the file name for your first image (SpecimenID_part1~)

5. Check that your camera image is appearing live in the GUI

  a. Adjust the camera so that you can just see the top of the bottom fixture and focus the camera

Instron Computer Set-up:

2. Check the limits on the instron console

  a. Position

    i. Upper: 13mm

    ii. Lower: -3mm

    iii. Limit Action: System stop

  b. Load

    i. Upper: 200N

    ii. Lower: -100N
    iii. Limit Action: Unload
  c. Digital Position
    i. Upper: 13mm
    ii. Lower: -3mm
    iii. Limit Action: System stop
  d. Strain (LVDT)
    i. Upper: 0.51mm
    ii. Lower: -0.51mm
    iii. Limit Action: System stop
3. In wavemaker, adjust you directory path for the folder you want to save in
  e. Go in Admin
  f. Change default method and project folders for your testing day
4. Click "test" in wavemaker
5. Enter your specimen ID that you are testing under "Project Name"
6. Select the correct testing method: "**RatAT_FreqSweep_RampFail_CNR**." This protocol performs:
  g. Pre-conditioning (0.5% to 1.5% strain at 0.25Hz for 30 cycles)
  h. Stress-relaxation (6% strain for 10 minutes)
  i. Frequency sweep (0.125% strain amplitude at 0.1, 1, 5, and 10 Hz, 10 cycles each)
  j. Ramp to failure (0.1% strain/sec)

Specimen Set-up:
1. Remove the tape from the pot on your first specimen
2. File down the end so that it is smooth
3. Place the sandpaper in the center of the top grip, lining up the edge of the sandpaper (12mm gauge length line) with the edge of the grip
4. Use an allen wrench to tighten the grip by loosely tightening all 4 screws first, and then tightening them all up in rotating order
5. Being careful not to load the tendon, pick up the specimen and slide the pot into the bottom grip on the instron
6. Slide the top grip into the top fixture from the back side of the fixture, making sure the tendon is slack the whole time
7. Raise the tank so the tendon is submerged
8. Use the linear stages to roughly line up the tendon so that it is straight
9. Making sure the tendon is slack in the grips, click the "load" button, and then calibration, and then "balance" to zero the load
10. Use the fine adjust knobs to carefully load the tendon to 0.1N
11. Align the axis of the tendon by moving it back and forth in both planes and watching the load to find the minimum load position
12. Return the tendon to a slack position to let it relax and balance the load again
13. Preload the tendon to 0.15N
14. Insert LVDT

a. Before inserting the LVDT on the instron, click "restore calibration"
b. Set the LVDT to "controllable"
c. Make sure unloaded state of the LVDT now reads "-0.6mm"
   i. If it does not say this, balance the LVDT to 0 in the unloaded state, then push the tip 0.6mm and then re-zero.
d. Insert the LVDT into the mount so that it read "-0.30 ± 0.01mm" on the screen.
   i. The black plastic piece should mount firmly to the actuator and the side part should be snug, but allow the LVDT to slide into it.
e. Arm limits (-0.51 and 0.51 mm) for LVDT.

15. Adjust the camera location and focus and the lighting on the tendon
16. Zero the load and digital position
17. Arm all limits for position, load, digital position, and strain
18. Set the instron to high power (II)

Begin Test:
1. Stop and re-start your image capture program, and confirm that it is taking live images
2. Press the start button in WaveMatrix
3. A dialogue button will pop up – press ok at the same time that you zero the time on the image capture program
4. This will start the first part of the test (preconditioning, stress-relaxation, frequency sweep)
5. After the 10Hz frequency sweep, the instron will ramp to 0mm digital position and pause.
   a. During this time, **disable LVDT limits** <u>then</u> **remove the LVDT**
      i. Place the tip in its protective metal covering.
   b. Change your image capture name to "SpecimenID_part2~"
   c. Click continue, and when the dialogue box pops up press ok and zero your time on the image capture computer simultaneously
6. After test completes, lower the trigger voltage below the threshold to stop the image capture program
7. Click pause on wavematrix and record your max load
8. A dialogue box will pop-up – say ok and then click finish to end your test
9. Disable all limits
   a. If your limits are already tripped, go to general > system stop > clear system stop
10. Move the frame up slightly (careful not to hit the LVDT bracket on the top of the frame)
11. Change your image capture name to "SpecimenID_fail~" and take an image of the tendon failure
12. Change your image capture name to "SpecimenID_calib~" and take a calibration image with a ruler in plane with the tendon
13. Remove you specimen from the fixtures

14. Remove the screw from the pot to re-use
15. Store or discard your sample
16. Begin your next specimen at "Specimen Set-up"

Clean up:
1. Turn off the console
2. Turn off the instron
3. Turn off the heating unit
4. Remove the LVDT and put it away in the padded box
5. Remove grips and the upper fixture
6. Tank
    a. Use suction tube to remove most of the PBS from the tank – use paper towels to remove the rest
    b. Lift the tank off of the stand (carefully untangling the cord)
    c. Spray down with rocal and rinse it out
    d. Wipe it down with paper towels to dry it off
    e. Put it back on the stand
    f. Unclamp the tank set-up from the instron base
    g. Wipe down the instron base
7. Put the camera and tripod away
8. Turn the lights off and bend them in out of the way
9. Wash the grips with rocal, rinse and dry them off
10. Wipe down all surfaces
11. Copy all data files onto an external hard drive and then over to Maxine

APPENDIX 9: Histology Specimen Preparation Protocol
Updated on 02/19/2018 by Cori Riggin

Equipment and Materials:
- Formalin
- Immunocal
- 70% Ethanol
- Histology Processing Machine
- Paraffin Wax
- Histology molds
- Sectioning blades
- Rubber mat
- Microtome
- Water bath
- Forceps
- Glass slides
- Slide boxes
- Ice bath container

Processing and Embedding:
1. Let histology samples (harvested as described in the sacrifice protocol) sit in formalin for 1 week
2. Transfer samples to Immunocal for 1 week, changing out the immunocal every 2-3 days
3. Remove the kim wipes from inside the cassettes and place the samples in 70% ethanol
4. Submit samples for processing (either the McKay histo core or VA processor) using the 5mm tissue protocol

Reagent	Duration (Hours)	Temperature (°C)
Ethanol 70%	1.0	37
Ethanol 95%	1.0	37
Ethanol 100%	1.3	37
Ethanol 100%	1.3	37
Ethanol 100%	1.3	37
Xylene	1.3	37
Xylene	1.3	37
Xylene	1.3	37
Paraffin Wax	1.5	62
Paraffin Wax	1.5	62
Paraffin Wax	1.5	62

5. Once the samples have been processed, place them in the embedding paraffin bath to warm up
6. Remove from cassettes and use a sectioning blade to cut the specimen sagittally down the center of the tendon
7. Place the larger/better piece in the cassette to be the "A" block, and the other piece in another cassette with the specimen ID and labeled "B" block.
8. Place both cassettes back in the paraffin bath to warm back up
9. Once warm, put a layer of paraffin wax on the bottom of a plastic mold
10. Place the specimen, cut-side down, into the wax in the mold and press it down until it feels stuck there
11. Put the labeled cassette lid on top of the mold and fill the rest of the mold with wax
12. Put the sample on the cooling platform until solidified

Sectioning Protocol:
1. Place the specimen on ice while you are setting up so it is cooled through
2. Clean and/or re-fill the water bath with dH$_2$O (it should be very full)
3. Turn the water bath on so it can warm up to about 45°C
4. Load the sample onto the microtome so the bone will be sectioned first, and the tendon will be cut along its length (as shown)
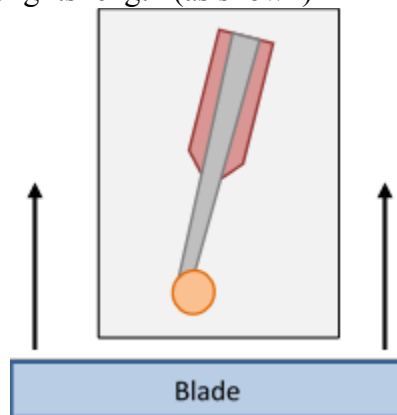
5. Carefully line it up so it is parallel to the blade (both horizontally and vertically)
6. Face-off the section with 7-10 µm slices until you just start seeing the sample
7. Switch to sectioning at 5 µm thickness
8. If needed, re-adjust your positioning so that the tendon sample is being sectioned parallel
   a. Ex. if you are only sectioning through muscle to start, re-align to move the calcaneus forward slightly, move your block back (so you don't remove a thick block) and re-face-off until you are sectioning through the full block again
   b. You want to see close to the whole sample in one section
9. Once you are happy with your positioning, place the block back in ice for a few minutes (leaving the positioning exactly where it is)
10. Once you start sectioning again, use forceps to try to get clean continuous ribbons

of sections
- a. I rehydrate and cool the sample after each cut using a kim wipe soaking in the ice bath
11. Once you have a ribbon or two (depending on what you can handle), place the ribbon carefully in the water bath
12. I use curved forceps to gently separate the ribbon into 2-3 section strips
13. Once the section has spread out on the surface and is not wrinkly, insert your slide at an angle in the bath, and touch the side of a strip to the top of the slide, and gently lift the section out of the water
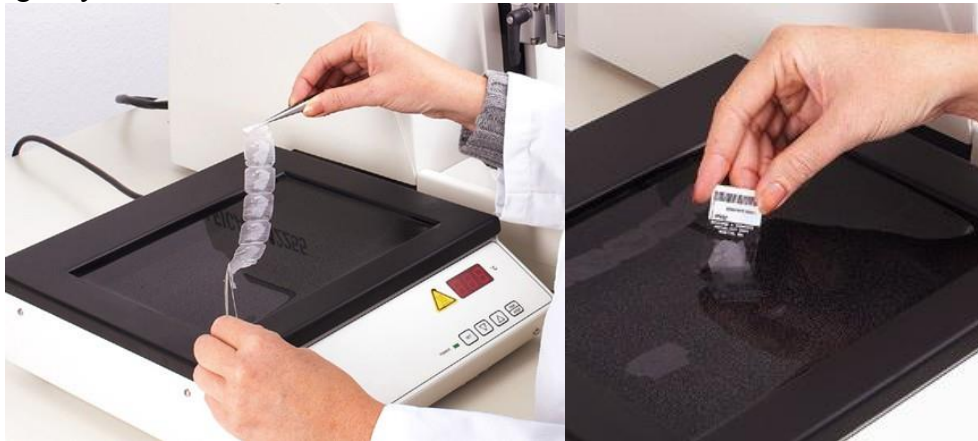
14. Allow slides to dry on a paper towel before collecting them in a slide box
15. Make thorough notes about each sample in your histology sectioning log
16. Make sure slides are completely dry (free of water bubbles under the wax) before baking slides
17. Once dry, bake the slides in the slide box for 1 hour at 60-62°C, or until the wax has melted and the section is adhered to the glass slide

APPENDIX 10: H&E Histology Staining Protocol
Updated on 02/19/2018 by Cori Riggin

Reagents:
1. Xylene
2. Ethanol (70, 95, and 100% EtOH)
3. Deionized water (dH$_2$O)
4. Hematoxylin (American MasterTech, HXHHE)
5. Clarifier
6. Bluing
7. Eosin (Sigma-Aldrich, HT110132-1L)
8. Glass slides
9. Coverslips (22-50mm, No 1.5, Azer Scientific, 1152250)
10. CytoSeal 60 (Electron Microscopy Sciences, 18007)

Staining Protocol:
1. Deparaffinize and Rehydrate Sections:

Xylene	5 min x 3
100% EtOH	2 min x 3
95% EtOH	2 min x 2
70% EtOH	2 min x1
dH$_2$O	2 min x1

2. Staining

Hematoxylin	10 min (clean off iodized surface)
dH$_2$O	Until Clear (~3 min, replacing water 2x at beginning)
Clarifier	3 Dips
dH$_2$O	2 min
Bluing	3 Dips
dH$_2$O	2 min
95% EtOH	2 min
Eosin	10 sec

3. Dehydration and Cleaning

95% EtOH	2 min x2
100% EtOH	2 min x3
Xylene	5 min x3

4. Coverslipping
    a. Leave samples in Xylene and coverslip one at a time
    b. Place 3-4 drops of CytoSeal on the section
    c. Use fine forceps to lower the coverslip onto the slide at an angle to push out bubbles
    d. Allow to dry flat for 48 hrs under the hood before putting in a slide box

Reagents:
1. Primary: Rabbit Anti-CD34 antibody [EP373Y] (Abcam, ab81289, purified 0.53mg/mL)
   a. Thaw and centrifuge before opening vial
   b. Aliquot 5 ul into small Eppendorf tubes
   c. Store at -20°C
2. Universal Vectastain ABC Kit (Vector Laboratories, PK-6200)
   a. Contains horse serum (yellow), biotinylated secondary antibody (blue), and ABC (grey)
   b. Store at 4°C
3. Ethylenediaminetetraacetic acid disodium salt dehydrate (EDTA) (Sigma, E5134)
4. Hydrogen Peroxide (H_2O_2) (Electron Microscopy Sciences, 16790)
   a. Store at 4°C wrapped in aluminum foil
5. SIGMAFAST™ 3,3′-Diaminobenzidine tablets (DAB) (Sigma, D4293-50SET)
   a. Store at -20°C
6. 10x Tris Buffered Saline (TBS) (Bio-Rad Laboratories, 1706435)
   a. Store at room temperature

Solutions:
1. TBS
   a. 1:10 dilution: 50 mL TBS in 450 mL dH_2O
2. EDTA Buffer
   a. 1 mM EDTA: 0.37g EDTA in 1L dH_2O
   b. Adjust pH 8.0 (add 1N NaOH)
3. Protein Blocker Solution
   a. Add 1 drop horse blocking serum stock (yellow label) for every 5 mL TBS
4. Primary Antibody
   a. 1:1000 dilution in TBS
5. H_2O_2
   a. 1:10 dilution of 30% hydrogen peroxide in TBS (3% solution)
6. Secondary Antibody
   a. Add 2 drops horse blocking serum stock (yellow label) for every 5 mL TBS buffer
   b. Add 2 drops biotinylated antibody stock (blue label)
7. ABC Reagent
   a. Add 2 drops of reagent A (gray label) for every 5 mL buffer, mix well
   b. Add 2 drops of reagent B (gray label) to the solution
   c. Mix immediately and allow to sit for 30 min before use
8. DAB Reagent
   a. Remove DAB tablets from freezer 30 min prior to use (warm to RT)
   b. Add 1 gold + 1 silver for every 5 ml dH_2O and vortex to dissolve tablets

Other supplies needed:
1. Xylene and Alcohol
2. IHC slide chamber
3. Pap pen
4. Shortened slide holder
5. 500 mL beaker
6. Aluminum foil
7. High temperature water bath for IHC
8. CytoSeal
9. Coverslip

Staining Day 1
1. **Set-up**
   a. Bake slides at 60°C for at least 2 hours before starting
   b. Check all alcohol and xylene solutions and replace with fresh if needed
   c. Turn on the water bath to 75°C to pre-heat
2. **Deparaffinize sections:**

Xylene	5 min. x 3
100% EtOH	2 min. x 3
95% EtOH	2 min. x 2
70% EtOH	2 min. x 1
dH$_2$O	5 min. x 1

3. **Heat induced antigen retrieval**
   a. Place a blank slide below sample slides in broken slide holder (that fits in 500 ml beaker)
   b. Add enough EDTA buffer to the beaker to cover slides
   c. Place slides in the beaker while holding the beaker on a diagonal to prevent bubbles from getting trapped between slides
   d. Cover the beaker with aluminum foil
   e. Place the beaker in the pre-heated water bath (75°C)
   f. Temperature will drop a little- wait until the temperature is back up to 75°C ± 1°C (~10 min)
   g. Once the temperature is reached, let slides incubate for <u>20 min</u>
   h. Remove the beaker from the bath and remove the aluminum foil
   i. Allow the slides to cool in the beaker of EDTA for <u>20 min</u>
4. **Prepare Slides:**
   a. Line IHC chambers with wet paper towels to create a humid environment when lid is closed
   b. One by one, remove the slides from the EDTA solution
      a. Circle sections with pap pen
      b. Put slides face up in slide box and apply TBS to circled samples
   c. Rinse samples with TBS for 3 min x2
5. **Block non-specific binding**
   a. Incubate in blocking serum solution for <u>20 min</u> at room temp

      b.   Vacuum off solution (without rinsing)
6. **Primary antibody**
      a.   Incubate with primary antibody <u>overnight</u> at 4˚C
      b.   Optional: leave 1 slide with only TBS for a negative control for background

<u>Staining Day 2</u>
1. Rinse with TBS for 3 min x 3
2. **Block for endongenous peroxidase**
      a.   Incubate in 3% H_2O_2 for <u>30 min</u> at room temp.
      b.   Rinse with TBS for 3 min x3.
3. **Biotinylated secondary antibody**
      a.   Incubate with secondary antibody for <u>30 min</u> at room temp
      b.   Meanwhile, make ABC reagent to let stand for 30 min before use
      c.   Rinse with TBS for 3 min x3
4. **ABC Reagent**
      a.   Incubate with ABC reagent for <u>30 min</u> at room temperature
      b.   Meanwhile, remove DAB tablets from freezer 30 min prior to use to warm to room temp
      c.   Rinse with TBS for 3 min x3
5. **DAB enzymatic reaction**
      a.   Add 1 gold + 1 silver to 5 ml diH_2O and vortex to dissolve tablets
      b.   Incubate in DAB solution (under hood) at room temp for <u>10 minutes</u>
            a.   Begin the 10 minute timer and apply the DAB to each slide at 10 second intervals
      c.   Immediately vacuum off solution and place in dH_2O bath to end reaction
            a.   Once the 10 minutes is up, go in the same order as you applied the DAB and vacuum/wash slides at 10 second intervals
6. **Hematoxylin, Dehydration, and Coverslip**

dH_2O	5 min x1
Hematoxylin	1 dip
dH_2O	gentle running water in the tupperware in the sink until water is clear (~3 min)
Clarifier	3 dips
diH_2O	2 min
Bluing	3 dips
diH_2O	2 min
70% EtOH	2 min
95% EtOH	2 min x2
100% EtOH	2 min x3
Xylene	5 min x3

7. Leave slides in Xylene while coverslipping one at a time
8. Apply a few drops permount and lower coverslip at an angle to push out bubbles
9. Allow to dry flat at room temp for 48 hours

APPENDIX 12: Angiopoietin-1 Immunohistochemistry Protocol
Updated on 02/19/2018 by Cori Riggin

Reagents:
1. Primary: Rabbit Anti-Angiopoietin 1 antibody (Abcam, ab102015, 500ug/ml)
    a. Shipped lyophilized: dilute in 0.2ml distilled water to yield a
       concentration of 500ug/ml
    b. Once in solution, centrifuge to get all liquid at the bottom of the tube
    c. Aliquot 6 ul into small Eppendorf tubes
    d. Store at -20°C
2. Universal Vectastain ABC Kit (Vector Laboratories, PK-6200)
    a. Contains horse serum (yellow), biotinylated secondary antibody (blue),
       and ABC (grey)
    b. Store at 4°C
3. Tri-sodium citrate dihydrate (Sigma, S1804)
4. Hydrogen Peroxide (H_2O_2) (Electron Microscopy Sciences, 16790)
    a. Store at 4°C wrapped in aluminum foil
5. SIGMAFAST™ 3,3′-Diaminobenzidine tablets (DAB) (Sigma, D4293-50SET)
    a. Store at -20°C
6. 10x Tris Buffered Saline (TBS) (Bio-Rad Laboratories, 1706435)
    a. Store at room temperature

Solutions:
1. TBS
    a. 1:10 dilution: 50 mL TBS in 450 mL dH_2O
2. 10 mM Sodium Citrate Buffer
    a. 2.94g tri-sodium citrate dihydrate in 1L dH_2O
    b. Adjust pH 6.0 (~5mL 1N HCl)
3. Protein Blocker Solution
    a. Add 1 drop horse blocking serum stock (yellow label) for every 5 mL TBS
       buffer
4. Primary Antibody
    a. 1:100 dilution in TBS
5. H_2O_2
    a. 1:10 dilution of 30% hydrogen peroxide in TBS (3% solution)
6. Secondary Antibody
    a. Add 2 drops horse blocking serum stock (yellow label) for every 5 mL
       TBS buffer
    b. Add 2 drops biotinylated antibody stock (blue label)
7. ABC Reagent
    a. Add 2 drops of reagent A (gray label) for every 5 mL buffer, mix well
    b. Add 2 drops of reagent B (gray label) to the solution
    c. Mix immediately and allow to sit for 30 min before use
8. DAB Reagent

a. Remove DAB tablets from freezer 30 min prior to use (warm to room temp)
b. Add 1 gold + 1 silver for every 5 ml diH$_2$O and vortex to dissolve tablets

Other supplies needed:
1. Xylene and Alcohol
2. IHC slide chamber
3. Pap pen
4. Broken slide holder
5. 500 mL beaker
6. Aluminum foil
7. High temperature water bath
8. 2 and 1000 µL pipettes and tips
9. CytoSeal
10. Coverslip

Staining Day 1

1. **Set-up**
   a. Bake slides at 60°C for at least 1 hour before starting
   b. Check all alcohol and xylene solutions and replace with fresh if needed
   c. Turn on the water bath to 95°C to pre-heat

2. **Deparaffinize sections:**
Xylene	5 min. x 3
100% EtOH	2 min. x 3
95% EtOH	2 min. x 2
70% EtOH	2 min. x 1
dH$_2$O	5 min. x 1

3. **Heat induced antigen retrieval**
   j. Place a blank slide below sample slides in broken slide holder (that fits in 500 ml beaker)
   k. Add enough sodium citrate buffer to the beaker to cover slides
   l. Place slides in the beaker while holding the beaker on a diagonal to prevent bubbles from getting trapped between slides
   m. Cover the beaker with aluminum foil
   n. Place the beaker in the pre-heated water bath (95°C)
   o. Temperature will drop a little- wait until the temperature is back up to 95°C ± 1°C (~10 min)
   p. Once the temperature is reached, let slides incubate for <u>10 min</u>
   q. Remove the beaker from the bath and remove the aluminum foil
   r. Allow the slides to cool in the beaker of sodium citrate buffer for <u>20 min</u>

4. **Prepare Slides:**
   d. Line IHC chambers with wet paper towels to create a humid environment when lid is closed
   e. One by one, remove the slides from the sodium citrate solution

          a. Circle sections with pap pen
          b. Put slides face up in slide box and apply TBS to circled samples
    f. Rinse samples with TBS for <u>3 min x2</u>.

5. Block non-specific binding
    c. Incubate in blocking serum solution for <u>20 min</u> at room temp
    d. Vacuum off solution (without rinsing)

6. Primary antibody
    c. Incubate with primary antibody <u>overnight</u> at 4˚C
    d. Optional: leave 1 slide with only TBS for a negative control for background

Staining Day 2

1. Rinse with TBS for 3 min x 3

2. Block for endongenous peroxidase
    c. Incubate in 3% H_2O_2 for <u>30 min</u> at room temp.
    d. Rinse with TBS for 3 min x3.

3. Biotinylated secondary antibody
    d. Incubate with secondary antibody for <u>30 min</u> at room temp
    e. Meanwhile, make ABC reagent to let stand for 30 min before use
    f. Rinse with TBS for 3 min x3

4. ABC Reagent
    d. Incubate with ABC reagent for <u>30 min</u> at room temperature
    e. Meanwhile, remove DAB tablets from freezer 30 min prior to use to warm to room temp
    f. Rinse with TBS for 3 min x3

5. DAB enzymatic reaction
    d. Add 1 gold + 1 silver to 5 ml diH_2O and vortex to dissolve tablets
    e. Incubate in DAB solution (under hood) at room temp for <u>10 min</u>
          a. Begin the 5 minute timer and apply the DAB to each slide at 10 second intervals
    f. Immediately vacuum off solution and place in dH_2O bath to end reaction
          a. Once the 10 minutes is up, go in the same order as you applied the DAB and vacuum/wash slides at 10 second intervals

6. Hematoxylin, Dehydration, and Coverslip

dH_2O	5 min x1
Hematoxylin	1 dip
dH_2O	gentle running water in the tupperware in the sink until water is clear (~3 min)
Clarifier	3 dips
diH_2O	2 min
Bluing	3 dips
diH_2O	2 min
70% EtOH	2 min
95% EtOH	2 min x2

100% EtOH   2 min x3
          Xylene   5 min x3
7. Leave slides in Xylene while coverslipping one at a time
8. Apply a few drops cytoseal to the slides and lower coverslip on at an angle to push out bubbles
9. Allow to dry flat at room temp for 48 hours

APPENDIX 13: VEGF Immunohistochemistry Protocol
Updated on 02/19/2018 by Cori Riggin

Reagents:
1. Primary: Rabbit Anti-VEGF antibody (Abcam, ab46154)
    a. Thaw and centrifuge before opening vial
    b. Aliquot to 10µl and store at -20°C
2. EnVision+ System HRP Labelled Polymer Anti-Rabbit (Dako, K4002-15mL)
    a. Store at 4°C
3. Hyaluronidase (Sigma-Aldrich, H4272)
    a. Dilute to 0.5 mg/mL in PBS
    b. Aliquot to 1 mL and store at -20°C
4. Hydrogen Peroxide (H_2O_2) (Electron Microscopy Sciences, 16790)
    a. Store at 4°C wrapped in aluminum foil
5. SIGMAFAST™ 3,3′-Diaminobenzidine tablets (DAB) (Sigma, D4293-50SET)
    a. Store at -20°C

Solutions:
9. <u>Hyaluronidase</u>
    a. Thaw aliquots needed and use un-diluted
10. <u>H_2O_2</u>
    a. 1:10 dilution of 30% hydrogen peroxide in methanol (3% solution)
11. <u>Protein Blocker Solution</u>
    a. Dilute horse serum in PBS (10%)
12. <u>Primary Antibody</u>
    a. 1:400 dilution in horse serum-PBS
13. <u>Secondary Antibody</u>
    a. Dako EnVision+ System HRP Labelled Polymer Anti-Rabbit
    b. Use undiluted – 1 drop per section
14. <u>DAB Reagent</u>
    a. Remove DAB tablets from freezer 30 min prior to use (warm to room temp)
    b. Add 1 gold + 1 silver for every 5 ml diH_2O and vortex to dissolve tablets

Other supplies needed:
1. Xylene and Alcohol
2. IHC slide chamber
3. Pap pen
4. 2 and 1000 µL pipettes and tips
5. CytoSeal
6. Coverslip

Staining Day 1
1. **Set-up**
   a. Bake slides at 60°C for at least 1 hour before starting
   b. Check all alcohol and xylene solutions and replace with fresh if needed
2. **Deparaffinize sections:**
   Xylene   5 min. x 3
   100% EtOH   2 min. x 3
   95% EtOH   2 min. x 2
   70% EtOH   2 min. x 1
   dH$_2$O   5 min. x 1
3. **Prepare slides:**
   a. Line IHC chambers with wet paper towels to create a humid environment when lid is closed
   b. Circle sections with pap pen
   c. Put slides face up in slide box and apply PBS to circled samples
2. **Digestion**
   a. Incubate samples in Hyaluronidase solution for <u>60 min</u> at 37°C
      i. Be careful not to let slides dry out (check at 30 min and put more solution on if needed)
   b. Rinse with PBS for 3 min x3
3. **Block for endogenous peroxidase**
   a. Incubate in 3% H$_2$O$_2$-MeOH for <u>10 min</u> at room temperature
   b. Rinse with PBS for 3 min x 3
4. **Block non-specific binding**
   a. Incubate samples in 10% horse serum for <u>30 min</u> at room temperature
   b. Vacuum solution off <u>without</u> rinsing
5. **Primary antibody**
   a. Incubate with primary antibody <u>overnight</u> at 4˚C
   b. Optional: leave 1 slide with only PBS for a negative control for background

Staining Day 2
1. Rinse with PBS for 3 min x3
2. **Secondary antibody**
   a. Incubate with Dako EnVision+ HRP Labelled Polymer solution for <u>30 min</u> at room temperature
      i. Apply 1 drop/ section
   b. Meanwhile, remove DAB tablets from freezer 30 min prior to use to warm to room temp
   c. Rinse with PBS for 3 min x3
3. **DAB enzymatic reaction**
   a. Add 1 gold + 1 silver to 5 ml diH$_2$O and vortex to dissolve tablets
   b. Incubate in DAB solution (under hood) at room temp for <u>50 sec</u>
      i. Begin the minute timer and apply the DAB to each slide at 10

second intervals
    ii. Only do 5 slides at a time (to fit within the 50 sec incubation time)
  c. Immediately vacuum off solution and place in dH$_2$O bath to end reaction
    i. Once the time is up, go in the same order as you applied the DAB and vacuum/wash slides at 10 second intervals

4. **Hematoxylin, Dehydration, and Coverslip**

dH$_2$O	5 min x1
Hematoxylin	1 dip
dH$_2$O	gentle running water in the tupperware in the sink until water is clear (~3 min)
Clarifier	3 dips
diH$_2$O	2 min
Bluing	3 dips
diH$_2$O	2 min
70% EtOH	2 min
95% EtOH	2 min x2
100% EtOH	2 min x3
Xylene	5 min x3

5. Leave slides in Xylene while coverslipping one at a time
6. Apply a few drops cytoseal to the slides and lower coverslip on at an angle to push out bubbles
7. Allow to dry flat at room temp for 48 hours

APPENDIX 14: TNFα Immunohistochemistry Protocol
Updated on 02/19/2018 by Cori Riggin

Prepare and aliquot antibodies:
1. Primary: Rabbit Anti-TNF-α antibody (Novus Biologics, NBP1-19532)
    a. No Rreconstitution necessary (already liquid form 1mg/ml)
    b. Thaw and centrifuge before opening vial
    c. Aliquot 10 ul into small eppendorf tubes, store at -20°C
2. Secondary: Peroxidase Goat anti-Rabbit IgG (Jackson Co. 111-035-003)
    a. Reconstitute powder in 2 ml with sterile water
    b. Once in solution, centrifuge to get all liquid at the bottom of the tube
    c. Aliquot 50 ul into small eppendorf tubes, store at -20°C
3. Hydrogen Peroxide (H_2O_2) (Electron Microscopy Sciences, 16790)
    a. Store at 4°C wrapped in aluminum foil
4. Pepsin (Sigma-Aldrich, P7012)
    a. Aliquot dilution = 1000mg in 100mL DiH2O to make 10 mg/mL stock
    b. Aliquot into 500 µl units store at -20°C
5. Normal Goat Serum (EMD Millipore, 566380)
    a. Reconstitute in 10 mL dH_2O
    b. Aliquot to 0.5 mL and store at -20°C
6. Blotting-Grade Blocker, Nonfat Dry Milk (Bio-Rad, 1706404)
    a. Store at room temperature
7. SIGMAFAST™ 3,3′-Diaminobenzidine tablets (DAB) (Sigma, D4293-50SET)
    a. Store at -20°C

Solutions: Make up enough for 200 ul for each section (adjust calculations as necessary)
1. H_2O_2
    a. 3% solution
    b. Dilute 30% hydrogen peroxide in methanol
    c. 1 ml H_2O_2 in 9 ml methanol
2. Pepsin
    a. Make 0.01N HCl (dilute in DiH20)
    b. Dilute 500 µl pepsin (prepared aliquot) with 9,500 µl 0.01N HCl (1:20 dilution)
3. Milk solution
    a. 4% solution
    b. 0.4 g dry milk in 10 ml 1x PBS
4. Combined serum and milk solutions
    a. 1:328 goat serum in milk
    b. 30 uL goat serum in 9,810 uL milk solution
5. Primary Antibody
    a. 1:750 dilution
    b. Dilute 14 µl Ab in 10,472 µl PBS
6. Secondary Antibody

    a. 1:100 dilution

    b. Dilute 100 µl Ab to 9,900 µl PBS

Other supplies needed:
1. PAP pen
2. IHC slide chamber
3. 1 ml pipette
4. 20 ul pipette

Staining Day 1
1. **Set-up**
   a. Bake slides at 60°C for at least 1 hour before starting
   b. Check all alcohol and xylene solutions and replace with fresh if needed
2. **Deparaffinize sections:**

Xylene	5 min. x 3
100% EtOH	2 min. x 3
95% EtOH	2 min. x 2
70% EtOH	2 min. x 1
PBS	5 min. x 1

3. Circle sections with pap pen
4. Line plastic chambers with wet paper towels (close lid during incubations)
5. **Block for endongenous peroxidase**
   a. Incubate in 3% H_2O_2 (solution 1) for <u>30 min</u> at room temp.
6. Rinse with PBS for 5 min.
7. **Pepsin digest (antigen retrieval; unmasking)**
   b. Incubate in pepsin (solution 2) for <u>20 min</u> at room temp.
8. Rinse with PBS 5 min x 3
9. **Block non-specific binding**
   c. Incubate in serum/milk mixture (solution 5) for <u>20 min</u> at room temp
   d. Vacuum off solution (without rinsing)
10. **Primary antibody**
    e. Incubate with primary antibody (solution 6) <u>overnight</u> at room temperature
    f. Optional: leave 1 slide with only PBS for a negative control for background

Staining Day 2
1. Rinse with PBS 5 min x 3
2. **Secondary antibody**
   a. Incubate with secondary antibody (solution 7) for 2 hours at room temp
3. Rinse with PBS for 5 min x3
4. **DAB enzymatic reaction**
   a. Remove DAB tablets from freezer 30 min prior to use (warm to room temp)
   b. Add 1 gold + 1 silver to 5 ml dH_2O and vortex to dissolve tablets

     c. Incubate in DAB solution (under hood) for <u>2 min</u> at room temp

     d. Immediately rinse with dH$_2$O to end reaction

5. Dehydration and coverslip

dH$_2$O	5 min x1
70% EtOH	2 min x1
95% EtOH	2 min x2
100% EtOH	2 min x3
Xylene	5 min x3

8. Leave slides in Xylene while coverslipping one at a time

9. Apply a few drops cytoseal to the slides and lower coverslip on at an angle to push out bubbles

10. Allow to dry flat at room temp for 48 hours

APPENDIX 15: Collagen III Immunohistochemistry Protocol
Updated on 02/19/2018 by Cori Riggin

Reagents:
1. Primary: Mouse Anti-Collagen Type III Antibody (Sigma-Aldrich, C7805)
   a. Thaw and centrifuge before opening vial
   b. Aliquot 10 µL and store at -20°C
2. Secondary: Biotin Rat Anti-Mouse IgG1 (BD Biosciences, 550331)
   a. Store at 4°C
3. Protease K (Sigma-Aldrich, P2308)
   a. Make 30mM Tris HCl (dilute HCl in dH$_2$O)
   b. Dilute Protease K in 30mM Tris HCl at a concentration of 0.4 mg/mL
   c. Aliquot 1 mL and store at -20°C
4. Hyaluronidase (Sigma-Aldrich, H4272)
   a. Dilute to 0.5 mg/mL in PBS
   b. Aliquot 1 mL and store at -20°C
5. Acetic Acid (___)
6. Normal Horse Serum (Abcam, ab139501)
   a. Aliquot and store at -20°C
7. Universal Vectastain ABC Kit (Vector Laboratories, PK-6200)
   a. Only using the ABC portion (grey vials)
   b. Store at 4°C
8. Hydrogen Peroxide (H$_2$O$_2$) (Electron Microscopy Sciences, 16790)
   a. Store at 4°C wrapped in aluminum foil
9. SIGMAFAST™ 3,3′-Diaminobenzidine tablets (DAB) (Sigma, D4293-50SET)
   a. Store at -20°C

Solutions:
1. <u>Protease K</u>
   a. Thaw aliquots needed and use un-diluted
2. <u>Hyaluronidase</u>
   a. Thaw aliquots needed and use un-diluted
3. <u>Acetic Acid</u>
   a. Glacial concentration 17.4N
   b. Dilute in dH$_2$O to obtain 0.5N acetic acid
4. <u>H$_2$O$_2$</u>
   a. 1:10 dilution of 30% hydrogen peroxide in methanol (3% solution)
5. <u>Protein Blocker Solution</u>
   a. Dilute horse serum in PBS (10%)
6. <u>Primary Antibody</u>
   a. 1:500 dilution in 10% horse serum-PBS solution
7. <u>Secondary Antibody</u>
   a. 1:100 dilution in 10% horse serum-PBS solution
8. <u>ABC Reagent</u>

a. Add 2 drops of reagent A (gray label) for every 5 mL buffer, mix well
b. Add 2 drops of reagent B (gray label) to the solution
c. Mix immediately and allow to sit for 30 min before use

9. <u>DAB Reagent</u>
   a. Remove DAB tablets from freezer 30 min prior to use (warm to room temp)
   b. Add 1 gold + 1 silver for every 5 ml diH$_2$O and vortex to dissolve tablets

Other supplies needed:
1. PAP pen
2. IHC slide chamber
3. 1 ml pipette
4. 20 ul pipette

<u>Staining Day 1</u>
1. **Set-up**
   a. Bake slides at 60°C for at least 1 hour before starting
   b. Check all alcohol and xylene solutions and replace with fresh if needed
2. **Deparaffinize sections:**

Xylene	5 min. x 3
100% EtOH	2 min. x 3
95% EtOH	2 min. x 2
70% EtOH	2 min. x 1
PBS	5 min. x 1

3. Circle sections with pap pen
4. Line plastic chambers with wet paper towels (close lid during incubations)
5. **Antigen retrieval**
   a. Incubate in Protease K for <u>4 min</u> at room temperature
   b. Rinse with PBS for 3 min x2
   c. Incubate in Hyaluronidase for <u>60 min</u> at 37°C
      i. Be careful not to let slides dry out (check at 30 min and put more solution on if needed)
   d. Rinse with PBS for 3 min x2
   e. Incubate in Acetic Acid for <u>4 hr</u> at 4°C
   f. Rinse with PBS for 3 min x2
6. **Block endogenous peroxidase**
   a. Incubate in 3% H2O2-MeOH for <u>10 min</u> at room temperature
   b. Rinse with PBS for 3 min x2
7. **Block non-specific binding**
   a. Incubate in 10% horse serum-PBS for <u>20 min</u> at room temperature
   b. Vacuum off solution without rinsing
8. **Primary antibody**
   a. Incubate in Col III primary for 2 nights and 3 days (approximately <u>34-38 hours</u>) at 4°C

     b. Optional: leave 1 slide with only 10% horse serum-PBS for a negative control for background

Staining Day 2
1. Do nothing – Incubation in primary taking place

Staining Day 3
1. Rinse with PBS for 3 min x3
2. **Secondary antibody**
    a. Incubate in biotin rat anti-mouse IgG for <u>30 min</u> at room temperature
    b. Meanwhile, make up ABC so it can sit for 30 min prior to use
    c. Rinse with PBS for 3 min x2
3. **ABC Reagent**
    a. Incubate in Vectastain ABC for <u>30 min</u> at room temperature
    b. Meanwhile, remove DAB tablets from freezer 30 min prior to use to warm to room temp
    c. Rinse with PBS for 3 min x2
4. **DAB enzymatic reaction**
    a. Add 1 gold + 1 silver to 5 ml diH$_2$O and vortex to dissolve tablets
    b. Incubate in DAB solution (under hood) at room temp for <u>4 min</u>
      i. Begin the minute timer and apply the DAB to each slide at 10 second intervals
    c. Immediately vacuum off solution and place in dH$_2$O bath to end reaction
      i. Once the time is up, go in the same order as you applied the DAB and vacuum/wash slides at 10 second intervals
5. **Dehydration and coverslip**
    dH$_2$O   5 min x1
    70% EtOH   2 min x1
    95% EtOH   2 min x2
    100% EtOH   2 min x3
    Xylene   5 min x3
6. Leave slides in Xylene while coverslipping one at a time
7. Apply a few drops cytoseal to the slides and lower coverslip on at an angle to push out bubbles
8. Allow to dry flat at room temp for 48 hours

APPENDIX 16: MMP13 Immunohistochemistry Protocol
Updated on 02/20/2018 by Cori Riggin

Reagents:
1. Primary: Rabbit Anti-MMP13 Antibody (abcam, ab39012)
   a. Thaw and centrifuge before opening vial
   b. Aliquot 10 µL and store at -20°C
2. Secondary: Biotin Goat Anti-Rabbit IgG (BD Sciences, 550338)
   a. Store at 4°C
3. Hyaluronidase (Sigma-Aldrich, H4272)
   a. Dilute to 0.5 mg/mL in PBS
   b. Aliquot 1 mL and store at -20°C
4. Hydrogen Peroxide (H_2O_2) (Electron Microscopy Sciences, 16790)
   a. Store at 4°C wrapped in aluminum foil
5. Bovine Serum Albumin (BSA) (Sigma-Aldrich, A-8022)
   a. Store at 4°C
6. Universal Vectastain ABC Kit (Vector Laboratories, PK-6200)
   a. Only using the ABC portion (grey vials)
   b. Store at 4°C
7. SIGMAFAST™ 3,3′-Diaminobenzidine tablets (DAB) (Sigma, D4293-50SET)
   a. Store at -20°C

Solutions:
1. <u>Hyaluronidase</u>
   a. Thaw aliquots needed and use un-diluted
2. <u>H_2O_2</u>
   b. 1:10 dilution of 30% hydrogen peroxide in methanol (3% solution)
3. <u>Protein Blocker Solution</u>
   a. Dissolve BSA in PBS to make a 3% solution (1.5g BSA in 50mL PBS)
4. <u>Primary Antibody</u>
   c. 1:250 dilution in 3% BSA-PBS
5. <u>Secondary Antibody</u>
   d. 1:200 dilution in 3% BSA-PBS
6. <u>ABC Reagent</u>
   e. Add 2 drops of reagent A (gray label) for every 5 mL buffer, mix well
   f. Add 2 drops of reagent B (gray label) to the solution
   g. Mix immediately and allow to sit for 30 min before use
7. <u>DAB Reagent</u>
   h. Remove DAB tablets from freezer 30 min prior to use (warm to room temp)
   i. Add 1 gold + 1 silver for every 5 ml diH_2O and vortex to dissolve tablets

Other supplies needed:
5. PAP pen
6. IHC slide chamber
7. 1 ml pipette
8. 20 ul pipette

Staining Day 1
9. **Set-up**
   a. Bake slides at 60°C for at least 1 hour before starting
   b. Check all alcohol and xylene solutions and replace with fresh if needed
10. **Deparaffinize sections:**

Xylene	5 min. x 3
100% EtOH	2 min. x 3
95% EtOH	2 min. x 2
70% EtOH	2 min. x 1
PBS	5 min. x 1

11. Line plastic chambers with wet paper towels (close lid during incubations)
12. Circle sections with pap pen
13. Rinse with PBS for 3 min
14. **Antigen retrieval**
    a. Incubate in Hyaluronidase for <u>60 min</u> at 37°C
       i. Be careful not to let slides dry out (check at 30 min and put more solution on if needed)
    b. Rinse with PBS for 3 min x3
15. **Block endogenous peroxidase**
    a. Incubate in 3% H2O2-MeOH for <u>30 min</u> at room temperature
    b. Rinse with PBS for 3 min x3
16. **Block non-specific binding**
    a. Incubate in 3% BSA-PBS for 3<u>0 min</u> at room temperature
    b. Vacuum off solution without rinsing
17. **Primary antibody**
    a. Incubate in primary <u>overnight</u> at 4°C
    b. Optional: leave 1 slide with only 3% BSA-PBS for a negative control for background

Staining Day 2
9. Rinse with PBS for 3 min x3
10. **Secondary antibody**
    a. Incubate in biotin goat anti-rabbit IgG for <u>60 min</u> at room temperature
    b. Meanwhile, make up ABC so it can sit for 30 min prior to use
    c. Rinse with PBS for 3 min x3
11. **ABC Reagent**
    a. Incubate in Vectastain ABC for <u>30 min</u> at room temperature
    b. Meanwhile, remove DAB tablets from freezer 30 min prior to use to warm

to room temp
c. Rinse with PBS for 3 min x3

12. DAB enzymatic reaction
a. Add 1 gold + 1 silver to 5 ml diH$_2$O and vortex to dissolve tablets
b. Incubate in DAB solution (under hood) at room temp for <u>4 min</u>
   i. Begin the minute timer and apply the DAB to each slide at 10 second intervals
c. Immediately vacuum off solution and place in dH$_2$O bath to end reaction
   i. Once the time is up, go in the same order as you applied the DAB and vacuum/wash slides at 10 second intervals

13. **Dehydration and coverslip**

dH$_2$O	5 min x1	
70% EtOH	2 min x1	
95% EtOH	2 min x2	
100% EtOH	2 min x3	
Xylene	5 min x3	

14. Leave slides in Xylene while coverslipping one at a time
15. Apply a few drops cytoseal to the slides and lower coverslip on at an angle to push out bubbles
16. Allow to dry flat at room temp for 48 hours

APPENDIX 17: Color Doppler Analysis Protocol
Updated on 04/08/2014 by Cori Riggin

Convert Dicom files to a folder of tiff images
1. Run dicom2tif.m function
    a. \\maxine\soslowskylab\software cooker-freezer\dicom2tif
2. Select the dicom file of interest (can run in batch if multiple dicoms in a folder)
3. Will output a new folder with the dicom name containing a stack of tiff files
4. Look through tiffs and remove images on either side of the tendon
5. Transfer these tiff files to the ultrasound lab analysis computer for the rest of the analysis

Convert image files to .mov
1. Open quicktime (must have correct plug-ins. I used computers in the imaging lab)
2. Click on >> File >> Open Image Sequence
3. Select an image from in the specimen folder of tiffs from the 3D scan you want to analyze
    a. I analyzed each set of images for a particular specimen on a particular day
4. Click on >> File >> Export >> Options >> Settings
    a. Select: Millions of Colors, Quality – Best, Dimensions – current, Number of frames - current
5. Save as .mov
    a. The .mov file should have a sequence of your tiff files for that specimen
6. Repeat for all specimens

IDL Program – Select ROI
1. Open IDL program
2. Type into command line: IDL>upenn
3. Go to Programs >> ROI tool (vascular analysis)
4. Click File >> load quicktime, and find your .mov file
5. Click first image – the window comes up with tools to select a region
6. Select the region of interest using the tool that works best for the application
    a. I use the free-form button (second from the left)
    b. Press the center button on mouse to un-do the last click
    c. Double click to finish outlining ROI
    d. Select 1 in box that pops up >> save
7. Either continue to do this for each image in the sequence, or replicate the ROI and apply to other images
8. To replicate:
    a. Command >> Replicate an ROI
    b. Indicate which image to replicate, and which to apply the ROI to
    c. Once ROI is applied, right click on the ROI to move it around, and right click again to set into place.

9. To import ROI:
    a. Command >> Import an ROI
    b. Select a previously analyzed .roivrt file
    c. Indicate which slice and which ROI you want to replicate
    d. Click on the image where you want to use the ROI
    e. Right click the location you want to place the ROI
    f. You can continue to other image slices with this same imported ROI
    g. Once you are finished with the imported ROI, change the ROI type to trace
10. Finish tracing all of your ROIs in all your image slices. You can skip slices if needed.

IDL Program – Color/Vascular Analysis
1. Command >> Color/Vascular Analysis
2. Click: skip slices (images that you did not include a ROI on)
3. Select: ROI 1 (or whatever ROI(s) you want to use for analysis)
4. Select: Done – ready for analysis
5. Click: Options >> Area, sum, mean, stdev
6. Define new sets >> Slice #1 >> Color set #2 >> Name: Red >> Linear Gradient
7. Use the square tool to select the red region of the color scale on the image – right click to finish
8. Redefine the zoomed selected region – right click to finish
9. Click minimum gradient region first, then click max on gradient – right click to finish
10. Set min and max to the values in the image scale [0 min, 24.1mm/s max]
11. Name and select the blue scale the same way
12. Choose highlight – Medium. See if it selected the color Doppler properly for both red and blue scales
13. Select: Okay – use colors
14. Put the created .inf file into a folder to keep the color sets for other analyses
15. For following image sets, you can say "use existing color set" to select this file.

Excel File
1. An excel file of data was created with the following headings:
    a. Slice: Image number
    b. Area: Total area of the image
    c. For Red and Blue
        i. # of Pixels: Total number of pixels with color
        ii. Sum (Grad): Velocity value x Pixels
        iii. Avg (Grad): Mean Velocity [Sum (Grad)/# Pixels]
        iv. STD(Grad): Standard deviation of Mean Velocity
    d. Combined Values
        i. MCL (Grad): Mean Color Level – Average velocity of colored pixels not taking into account number of colored pixels

284

  ii. % Area: Also known as fractional area – Fraction of colored pixels to total pixels in image

  iii. CWFA: Color weighted fractional area – Velocity or flow per unit area. Takes into account both velocity measurement, as well as area with flow.

2. The headings are a bit shifted, so you need to shift one line down and re-label red and blue in the right place. It should look like:

		Red				Blue				Combined		
Slice:	Area:	# of Pixel	Sum(Grad	Avg(Grad	STD(Grad	# of Pixel	Sum(Grad	Avg(Grad)	STD(Grad	MCL(Grad	% Area(G	CWFA(Gra
0	8324	147	25	0.2	0.2	85	16	0.2	0.2	0.18	2.79	0.01

3. Average together the slices for each animal for each parameter to get a representative reading

APPENDIX 18: Photoacoustic Imaging Analysis Protocol
Updated on 11/20/2017 by Cori Riggin

Data Analysis
1. After image acquisition, use the "copy to" command to copy the data and transfer it to the ultrasound analysis computer
   a. John Morgan Rm 170-180
   b. Computer in the first bay on left side
   c. Password: coffee
2. Open the VisualSonics software and select your Oxy-Hemo PA image
3. Select the "Measure" tab, and click the photoacoustics region measurement button
   ⚬
4. Click on the point of the insertion site, click your second point at the myotendinous junction (~10mm from the insertion), and then click a point at the anterior and posterior borders
5. Continue to place points along the border of the tendon until you have defined your ROI
6. Right-click to finish your ROI selection
   a. You can move the points on the ROI around once it is defined, or add more
7. Your oxy-hemo measurements will appear next to your ROI
8. You can re-name your ROI if needed

Export PA Region Measurements
1. After selecting the PA images that you have defined ROIs in, select "Export"
2. Export the PA analysis as a report
3. Navigate to the folder you want to export your data
4. Your report will show the series information, but not which particular image each ROI is from within each series (Specimen ID). This doesn't matter to me because I average all measurements within a single specimen, but if you need to differentiate you can re-label the ROIs and that info will appear in the report.

Output Parameters
1. sO2 Avg (%): Average blood oxygenation %
2. sO2 Tot (%): Average tissue oxygenation % (takes into account % area of signal detected in ROI)
3. HbT Tot (a.u.): Total quantity of hemoglobin detected
4. HbT Avg (a.u.): Average quantity of hemoglobin detected/unit area of ROI
5. Area: area of ROI

APPENDIX 19: Non-Linear Contrast-Enhanced Ultrasound Analysis
Updated on 11/20/2017 by Cori Riggin

Data Analysis
1. After image acquisition, use the "copy to" command to copy the data and transfer it to the ultrasound analysis computer
   a. John Morgan Rm 170-180
   b. Computer in the first bay on left side
   c. Password: coffee
2. Open the contrast clip up in the VisualSonics analysis software
3. Select the clip, and click "VevoCQ" at the top of the screen
4. If your image clip is more than 1000 frames, a prompt will alert you that you can only load the first 1000 frames – click OK
5. Your clip will be loaded into the clip editor
   a. Select Bolus injection type
   b. Frame Selection
      i. Here you can include/exclude images for quantification. Use the (-) and (+) controls to indicate frames to remove or include. You can drag the indicator on the bar at the bottom to include or exclude groups of frames
   c. Draw your ROIs
      i. Select your type of ROI tracer (rectangle, ellipse, polygon, closed curve)
      ii. The ROIs can be traced on either the b-mode or contrast image and they will be replicated to the other image simultaneously
      iii. A default label is placed next to the ROI, but can be edited if desired
      iv. You can save or copy/paste ROIs to other images or within an image as well
   d. Motion Correction
      i. If you have some motion in your image clip, select motion correction while you are on a frame that you want to adjust your other frames to match
      ii. It applies a spatial realignment correction to all the frames in the cine loop
   e. Once you have set up your clip in the editor, you can select "Quantify"
6. Quantification Window
   a. The program will try to pre-define the start of your injection curve.
   b. You can use that or re-define it yourself by dragging the bar along the graph
   c. Your output will be in 4 quadrants on the screen
      i. Q1: Original clip with ROIs – you can still adjust or move these in the quantification mode
      ii. Q2: Processed clip or parametric image
      iii. Q3: Chart displaying time intensity curved (both linearlized and fitted signals for each ROI

iv.   Q4: Table listing the computed values from each ROI
7.   To export data, select "Export"
   a.   You can define what data you want to export
      i.   TSV: Your quantification data and time intensity curve numbers
      ii.   Images: Can choose which quadrants you want images of (BMP or Tiff)
      iii.   Cine Loop: of original or parametric data
   b.   In settings, make sure you have export of extrapolated data checked so that you can get AUC, mTT, and PI parameters.

Perfusion Curve-Fitting Algorithm:
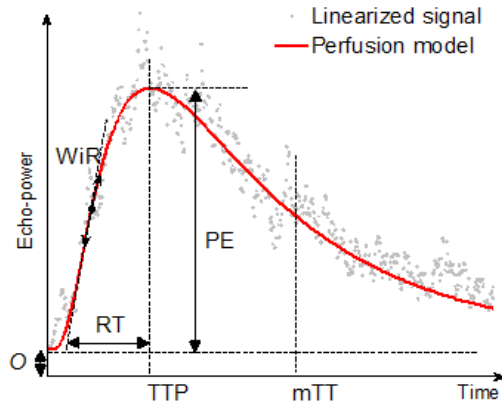
$$f(t) = O + AUC \frac{1}{st\sqrt{2\pi}} e^{-\frac{(\ln(t)-m)^2}{2s^2}}$$

$$Where \quad m = \ln(mTT) - \frac{s^2}{2}$$

Abbreviation	Definition	Unit
f(t)	Best-fit function of echo-power	[a.u.]
t	Time variable	[s]
AUC	Area under the curve to infinite time	[a.u.]
mTT	Mean transit time	[s]
O	Offset amplitude	[a.u.]

Perfusion Parameters:

Abbreviation	Definition	Unit
PE	Peak Enhancement	[a.u.]
WiAUC	Wash-in Area Under the Curve	[a.u.]
RT	Rise Time	[s]
TTP	Time to Peak	[s]
WiR	Wash-in Rate	[a.u.]
WiPI	Wash-in Perfusion Index (WiAUC/RT)	[a.u.]
PI	Perfusion Index (AUC/mTT)	[a.u.]
QOF	Quality of Fit	[%]

APPENDIX 20: B-mode Ultrasound Alignment Analysis
Updated on 02/20/2018 by Cori Riggin

us_align2

1. Open up MATLAB (compatible with MATLAB 2012 -2015)
2. Set current folder to Z:\software cooker-freezer\rat_US\cooker\cooker-CNR_thesis
    a. Z: is \maxine
3. Type "close all; clear all; clc; us_align2; " into the Command Window
4. *Modal Dialogue Box*: Navigate to where your ultrasound images are located. Choose any image.
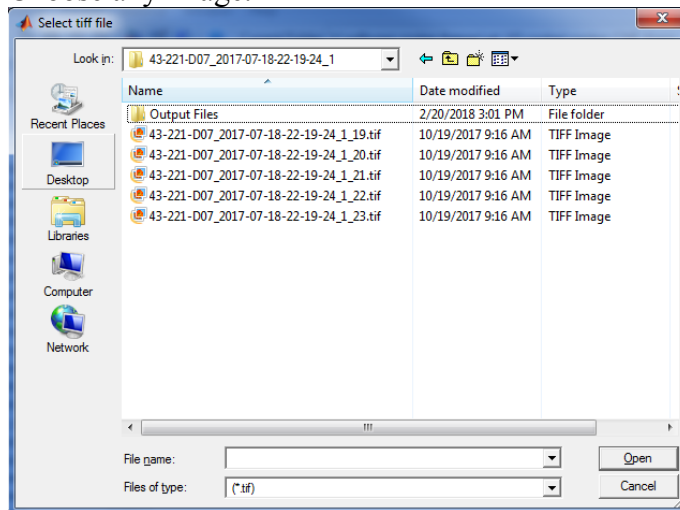
5. *List Dialogue*: Select the image files you wish to analyze
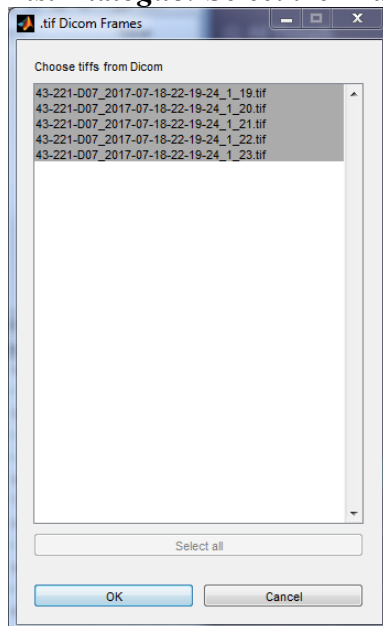
6. ***Polymasking tool***: Each image that you chose in the previous step should pop up. Crop the region of interest (ROI) for each image. Double-click inside the ROI after connecting the vertices.
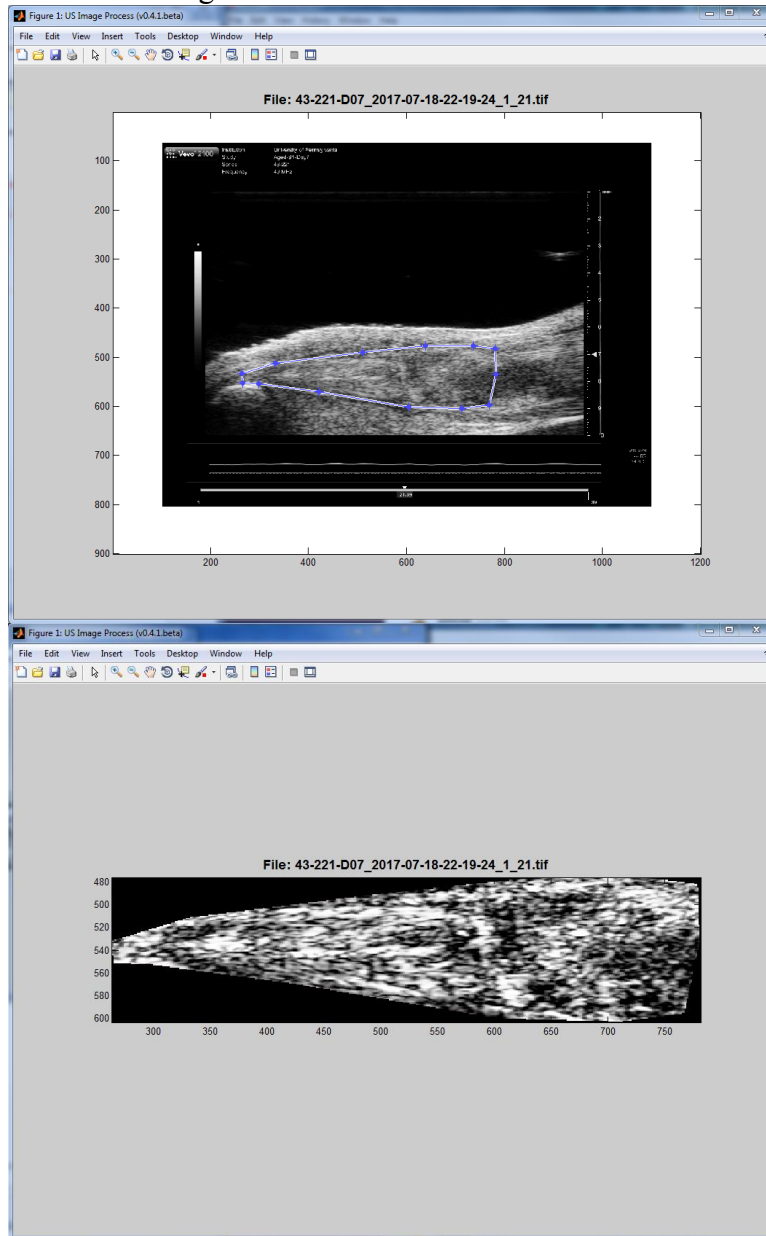
7. ***Enter Bundle Width and Spacing***: Enter 3 for the Bundle Width and 3 for the Bundle Spacing
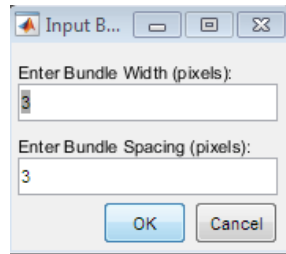
8. **Choose Output Location**: Navigate to the location where you would like to save your output file

9. The code will run and will save the *_usi.txt files to the location specified earlier.

batch_usi_fit_alt

1. Type "close all; clear all; clc; batch_usi_fit_alt; " into the Command Window

2. **Modal Dialogue Box**: Navigate to where your _usi.txt files are located. Choose any file.

   a. These are the output files from the us_align2 code.
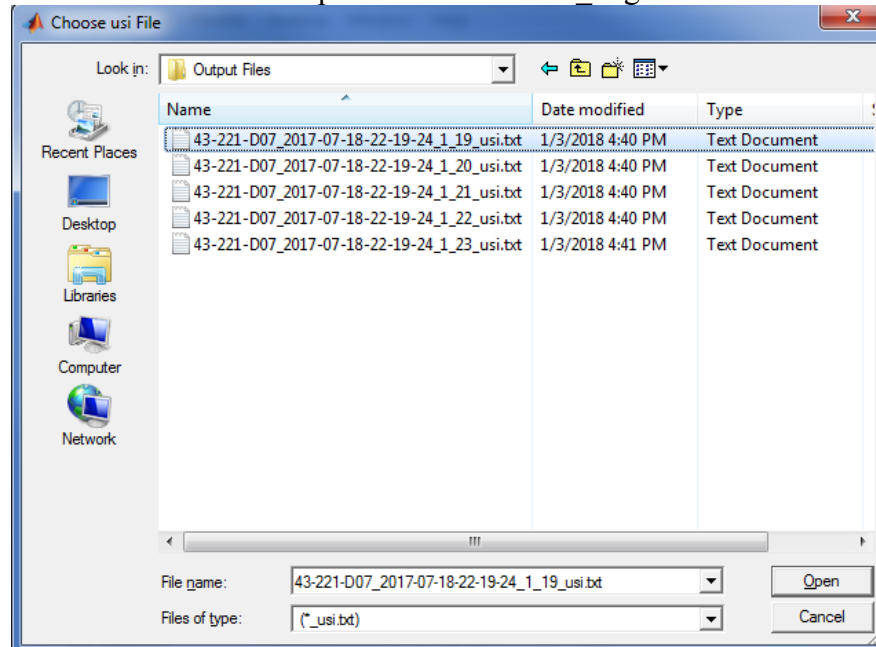
3. MATLAB will open up its parallel processing capabilities. Once the parallel processor has initialized, the code will run every *_usi.txt file in the directory.

   a. The code takes a long time to run.

usf_threshbj

4. Type "close all; clear all; clc; usf_threshbj; " into the Command Window

5. **Modal Dialogue Box**: Navigate to where your *_usf.txt files are located. Choose any file.

6. These are the output files from batch_usi_fit_alt

7. *List Dialogue:* Select the *_usf.txt files you wish to analyze.
8. ***Threshold Parameters****:* Enter 0 for the p2p Thresh, 0 for the Range Thresh, and 10 for the Phase 95CI Thresh
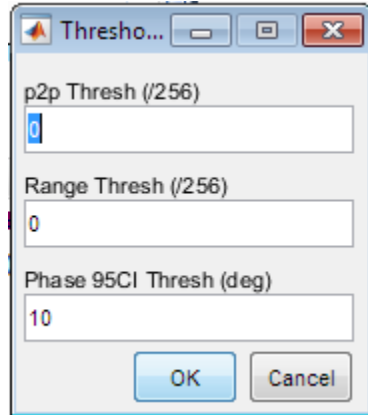
9. ***Choose Output File:*** Navigate to where you would like to save your output files.
10. The code will run on each *_usf.txt file you chose previously and save all output files to the location specified.

batch_usf_thresh_avg

1. Copy all the usf.txt files from usf_threshbj to a separate folder labeled "usf thresh copies"
2. Type "close all; clear all; clc; batch_usf_thresh_avg; " into the Command Window
3. ***Modal Dialogue Box****:* Navigate to where your *_usf_thresh.txt files are located. Choose any file.
4. ***List Dialogue****:* Select the *_usf.txt files you wish to analyze.
5. ***Choose Output File****:* Navigate to where you would like to save your output files
6. The code will execute and save the average output for all specimen to a single text file

echo_us

1. Type "clear all; close all; clc; echo_us;" into the Command Window
2. Modal Dialogue Box: Navigate to where your ultrasound images are located. Choose any image.
3. ***List Dialogue***: Choose the images you wish to analyze.
4. **Draw or Load Mask**? Choose whether you wish to draw the mask or load a mask if it has already been created.
   a. If a mask was created and saved while running **us_align2**, this mask should be loaded and used for echogenicity analysis.

292

File: 43-221-D07_2017-07-18-22-19-24_1_19.tif
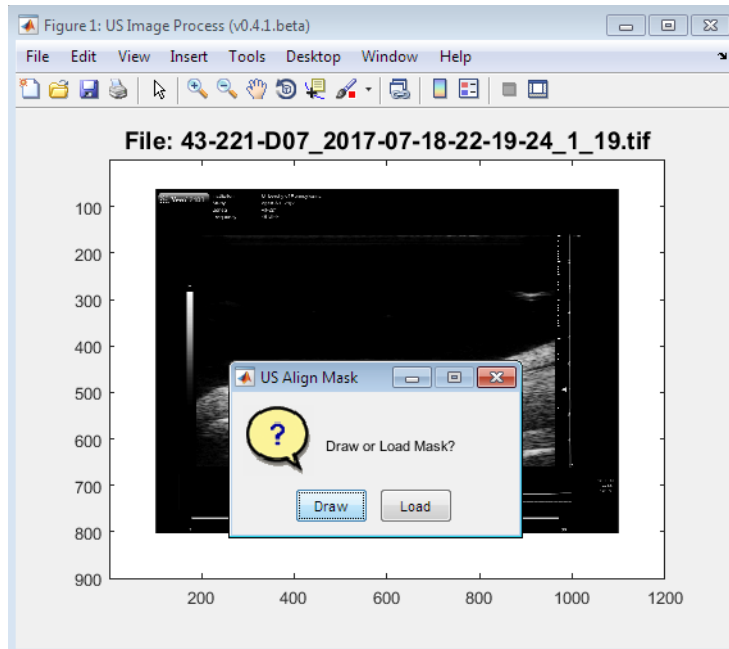
5. Draw → Polymasking tool
   a. The first image should pop up. Crop the region of interest (ROI). Double-click inside the ROI after connecting the vertices.
   b. Once you have connected the vertices, a modal dialogue box will pop up and ask you to save the _msk.txt file. Navigate to where you wish to save the file.
6. Load → Modal Dialogue Box
   a. Navigate to where the mask file for this image is saved. Choose the mask and a question box should pop up asking whether it is correct. If it is correct, the code will continue, if it is incorrect, the modal dialogue box will pop back up for you to choose the correct one.
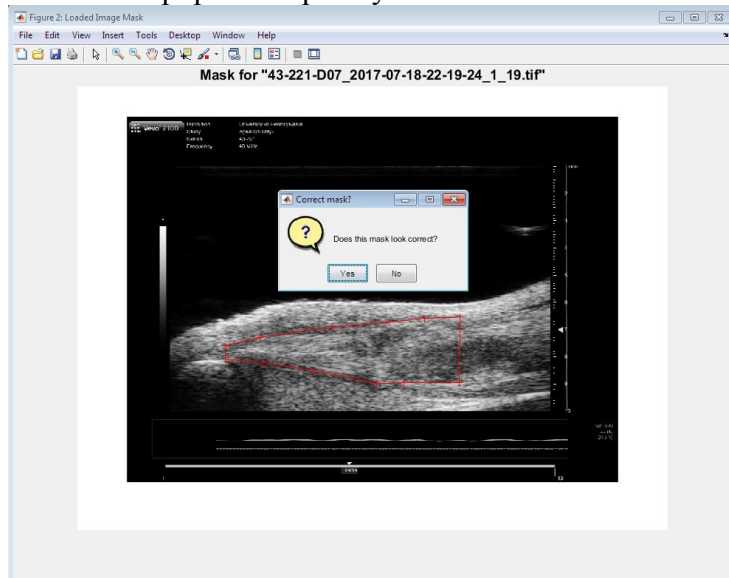
1. ***Choose Output File***: Navigate to where you wish to save the _echo.txt output file

batch_echo_avg

2. Copy all the *_echo.txt files from echo_us to a separate folder labeled "echo us copies"
3. Type "clear all; close all; clc; batch_echo_avg;" into the Command Window
4. ***Modal Dialogue Box***: Navigate to where you saved all the copies of the _echo.txt files. Choose any file.
5. ***List Dialogue***: Choose the files you wish to analyze
6. ***Choose Output Location***: Navigate to where you wish to save your output.

APPENDIX 21: Mechanical Testing Analysis Protocol
Updated on 06/01/2017 by Cori Riggin

This protocol should be used for all mechanical analysis performed on Achilles tendon specimens tested using the "RatAT_FreqSweep_RampFail_CNR" protocol with a midsubstance partial-width, full-thickness incisional injury.

Gage and Injury Length
1. Open Image J
2. Open your part1 image file for your first specimen
3. Select the line tool, and draw a vertical line from the top of the tendon at the grip to the top of the insertion stain line
4. Select Analyze > Set Scale
5. Copy the pixel length into your excel spreadsheet
6. Move the line to go from the insertion to the top of the first injury stain line
7. Select Analyze > Set Scale
8. Copy the pixel length into your excel spreadsheet
9. Move the line to go from the insertion to the top of the second injury stain line
10. Select Analyze > Set Scale
11. Copy the pixel length into your excel spreadsheet
12. Close part1 image, and open the corresponding calib image
13. Draw a line from the top-left side of the highest mm mark, to the top-left side of the lowest mm mark
14. Select Analyze > Set Scale
15. Copy the pixel length into your excel spreadsheet
16. Count the number of mm you measured from and input that value into the spreadsheet
17. The spreadsheet should calculate the pix/mm and corresponding gage and injury lengths

Gismo
1. Open MATLAB
2. Set your directory to Z:\Software- Released\gismo_area\released (in medfiles)
3. Run **>>gismo_area;**
4. On the GUI that pops up, click Load and select your gismo file
5. Mark the beginning and end of each pass across the tendon
6. Press enter when done
7. Copy and paste the output from the command window into excel (note: the 1D and 2D areas should be very similar)
8. To calculate injury area, input the "Injury bottom" distance calculated in imageJ into "Pass 1" and "Injury Top" into "Pass 2" (make sure the values are negative)
9. Click **"Local Area"** to calculate the local area in the injury region
10. Record the output from the command window into your excel spreadsheet

Specimen Dimension Files
1. Create an excel file formatted with columns: Spec ID, Gage length, Area (total)
2. Open MATLAB
3. Set your directory to V:\software cooker-freezer\Fatigue\criggin_thesis\cooker (in Maxine)
4. Run **>>make_specDimTxt;**
5. Select the excel file you created
6. Select the location you want to save the files

Stress-Relaxation, Frequency Sweep, and Structural Fit
1. Open MATLAB
2. Set your directory to V:\software cooker-freezer\Fatigue\criggin_thesis\cooker (in Maxine)
3. Run **>> csv2txt_ePuls_CNR;**
4. Select the instron file for your specimen
5. Re-name the csv.txt file to include the name of your specimen and save the file in your analysis folder under "Grip Analysis" and then in a separate folder for the specimen number.
6. Run **>> benware;**
   a. If you have previously created the csv.txt file, click **"Load Text File"** to load your csv.txt file
   b. If you just created the file, it should already be loaded into the program
7. Click **"Input Specimen Dimensions"**
   a. Do input specimen dimensions exist? Select yes
   b. Choose your SpecDim file for the specimen you are analyzing
8. Click **"Stress Relaxation"**
   a. The input parameters should be:
        i. Vector of block numbers: [7]
        ii. Vector of Frequencies: [0.01 0.01 0.01]
        iii. Seconds to subtract: 0.002
   b. Click OK
   c. The next input parameters should be:
        i. Vector of block numbers: [8]
        ii. Vector of Frequencies: [0.01 0.01 0.01]
        iii. Seconds to subtract: 0.002
   d. Click OK
   e. Save the figure (SR.fig) showing the stress relaxation plot in your analysis folder in a folder for the specimen you are analyzing (grip analysis)
   f. Copy the output SR information from the command window into your excel spreadsheet
9. Click **"Frequency Sweep"**
   a. Click "Select all" in the pop-up window, and choose the txt file
   b. The input parameters should be:
        i. Vector of block numbers: [9 10 11 12]

        ii.   Vector of Frequencies: [0.1 1.0 5 10]
       iii.   Seconds to subtract: 0.002
  c. Click OK
  d. Cycle Analysis should be:
        i.   Enter Cycle# Start: 4
        ii.   Enter Cycle# End: 8
  e. Select Output Style 2
  f. Save Output Files? Select No (will save them individually)
  g. Save all 3 figures (FS1.fig, FS2.fig, FS3.fig)
  h. Copy and paste the output from the command window into your excel spreadsheet

10. Click **"Structural Fit"**
  a. Select No, a _fail.txt file has not been created
  b. Select RT Fatigue
  c. On the ramp to failure graph that comes up, select the max point at the end of the linear region (this should be before the max load)
  d. The sfit figure and file should save automatically, along with a fail.txt file in the same folder as the csv.txt file.
  e. Copy the output from the command window into your excel spreadsheet

Optical Strain Analysis
1. Open MATLAB.
2. Set the directory to or set a path to: V:\Software_released\optikos\released (in Maxine)
3. Run **>>optikos;**
4. Click **"Load"**
  a. Select the images for your specimen. If you load one the rest will automatically load.
  b. Change the display from Not Enhanced to Contrast + Filtered
5. Click **"Instron Restrict"**
  a. Select the _fail.txt file that was created during the structural fit analysis (note: you will have to change the dropdown to look for all files - it is looking for a _raw.txt file)
  b. When prompted for the image capt correction (sec), enter **1167**
  c. A warning will come up "more images than instron data…" – press OK
  d. When prompted to choose the maximum point, click ok and use the cursor to choose the point at the end of the linear region.
  e. After you select the point a warning dialog will pop up and tell you how many images there are to analyze. The software defaults to analyze 20 and will automatically determine how many images to skip. You can keep this number, or change the number of images to skip if you want to analyze more images (for instance if it is not tracking well).
6. Click **"Choose ROIs"**
  a. You will be choosing 2 ROIs for each location you want to track.

b. For this project, we will track ROIs at the insertion (ins) and distal (dist) ends of the tendon, as well as the top (injT) and bottom (injB) of the injury region.
c. For ROI1, choose a region on a stain line or dot on the left side of the tendon, and for ROI2 choose the right side
d. You want these boxes to be unique enough to track the region wells

7. Click **"Track ROIs"**
   a. As it goes through (or once it is complete) use the scroll bar on the GUI to make sure the points tracked well.
   b. If they did not, re-do the "Choose ROIs" command and choose different regions

8. If they look good, click **"Text Output"**
   a. Insert the identifier of the region into the file name that pops up (ins, dist, injT, or injB), and save in your analysis folder within the specimen ID name folder
   b. Move on to each of the other regions and track the ROIs and save them in this folder.

9. To compare movement between ROIs, run **>>trk2element;**
   a. For the whole tendon analysis, choose the file for the insertion ROI, then choose the file for the distal ROI
   b. When the tracking is complete, save as "Specimen Name_ins-dist_ eopt2D.txt".
   c. Repeat the same steps for injB to injT

10. To calculate the stiffness, run **>> el2d_stiffness;**
    a. Choose the _eld2D.txt file for the full tendon (ins-disp).
    b. Open the mechanical test data file (fail.txt).
    c. Set the Image capture correction to **1167**
    d. Select Y as the primary loading direction
    e. A graph will appear with Load against Optical Strain and a box with the image number will appear. Each image is represented on the graph with a diamond, and included images have a circle around them. The black line represents the best fit to these images.
    f. In order to achieve the best fit, delete the images associated with the toe region or failure region that are not part of the linear region (hold ctrl and click on image # you want to remove)
    g. Try and get the line to fit as best as possible, while keeping as many images as possible that are part of the linear region.
    h. In the figure window, click "Save as" and save the figure in the Analysis folder
    i. Click close on the image selector when your graph looks good and save the graph as the default name.
    j. Copy and paste output from Matlab command window into excel in a tab for full tendon Optikos.
    k. Repeat for the injury region (injB-injT) and copy the output into a separate

tab for injury Optikos.

Excel Calculations
1. Stress-Relaxation
   a. % Relaxation = (Fpk-Feq)/Fpk
   b. This should be calculated automatically
2. Frequency Sweep
   a. Dynamic Modulus (E*) = (F_Amp/Area)/(u_Amp/Gage Length)
   b. Tanδ = Tan(phi*π/180)
3. Structural Fit
   a. Max Displacement = DispFmax (mm)
   b. Max Force = Fmax (N)
   c. Grip Stiffness = Kel (N/mm)
   d. Modulus = (Kel*Gage length)/Area
4. Optical Strain
   a. Stiffness = Kopt*Calib (pix/mm)
   b. Modulus (Full Tendon) = Kstrn*100/(full tendon CSA)
   c. Modulus (Injury) = Kstrn*100/(local injury CSA)

APPENDIX 22: Ratwalk Analysis Protocol
Updated on 02/20/2018 by Cori Riggin

DRW
- *Purpose*: analyzes the forces (min, max, avg), moments, and stance time for specimens that isolated a hind limb on a force plate during ratwalk.
- *Directory*: medfiles\ort\McKay_Lab_Folders\Sosloswky_Lab\shared\Released-Software\DRW\released
- *Command:* >>drw;

Procedure:
1. Load images
2. Mark when each foot of interest (indicated as isolated) first makes contact and lifts off
    a. 1 and 2 represent the force plate number
3. After each specimen – click Export
4. After the day of analysis – click Summary to get COP, GRF, and Averages
5. Summary outputs, the min/max/avg for all force directions, moments, stance times, torque, ratio of loading, etc.
6. Usually only analyze best run for each rat – choose based on notebook chart

Ambipaws
- *Purpose*: since we can evaluate both left and right hind limbs in this study (bilateral injury), we need to convert the data to have matching conventions so specimen walks can be averaged even if taken from both left and right limbs.
- *Directory*: medfiles\ort\McKay_Lab_Folders\Sosloswky_Lab\shared\Released-Software\DRW\cooker
- *Command:* >>ambipaws;

Procedure:
1. Modal Dialogue Box: Navigate to the folder were you saved your processed DRW data. Choose the first file.
2. List Dialogue: Select all files you wish to analyze.
    a. Note: The original _grf.txt and _down.txt files aren't edited. All data is copied and edited to new text files.
3. Modal Dialogue Box: Create a new folder labeled "ambipaws" and save your data to that folder.
4. MATLAB will process and save all files the ambipaws folder
    a. Only right back paws were converted to match the orientation of the left back paw. Converted files contain the label _LC1 or _LC2 (depending on the force plate) to distinguish which files were changed.
    b. Left back paws were left unchanged and are labeled _LB1 or _LB2 after the animal ID.

Tiptoe
- *Purpose:* analyzes the paw placement data collected from the images captured during ratwalk.
- *Directory*: medfiles\ort\McKay_Lab_Folders\Sosloswky_Lab\shared\Released Software\TipToe\released
- *Command*: >>tiptoe;

Procedure:
1. Load images
2. Calibrate using length of force plate (68mm)
3. Mark toes by selecting the correct foot from the drop-down
   a. 1 and 2 represent the 1st and 2nd placement of the same foot
   b. Make sure you select the foot when it first is placed down (so your speed measurement will be accurate)
4. Save when done with a specimen
5. Summarize when done with the day (data set)

Note that all measurements are made twice (ex. Denoted as "c1" and "c2" for cori1 and cori2). Both should be analyzed, and then averaged together to obtain a representative measure for each specimen.

Procedure:
1. Set your matlab directory to:
   \\maxine\soslowskylab\software cooker-freezer\Ratonalysis\Released\v10.2.0

2. Type **ratonalysis;**

3. Choose data file
   a. My thesis data is located: \\maxine\criggin\Thesis\Experimental Data\Ratometer

4. Select "**Torque**" for determining the metric for defining cycles

5. The window will ask you to select the beginning/end of each cycle. Note that there are 4 cycles. The first cycle is a "pre-conditioning", so **ignore the 1st** and start counting at the 2nd (each cycle consists of a peak followed by a valley - the beginning of a cycle is at the start of the positive peak at torque = 0 - see image below).
   a. Enlarge the window so you can see the data better
   b. Pick cycles at **ZERO torque**. E.g.,
      i. Select beginning of cycle #1, 2, and 3
   ii. Select end of cycle #3
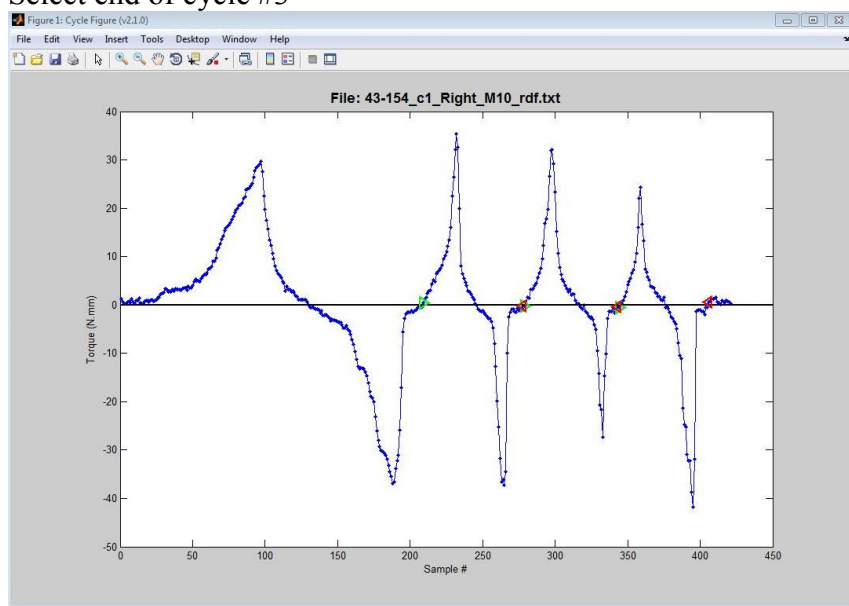
c. Set the peak and min torque values
  i. **Peak** torque (external) = **25** Nmm
  ii. **Min** torque (internal) = **35** Nmm

d. Select "**Torque**" when it asks for the metric for defining cycles.

e. **Save** the output file into an "**Analysis**" folder that you can create within the particular date you are analyzing.

f. Your Torque vs. Angle plots should look something like this:
  i. Internal = Plantarflexion
  ii. External = Dorsiflexion
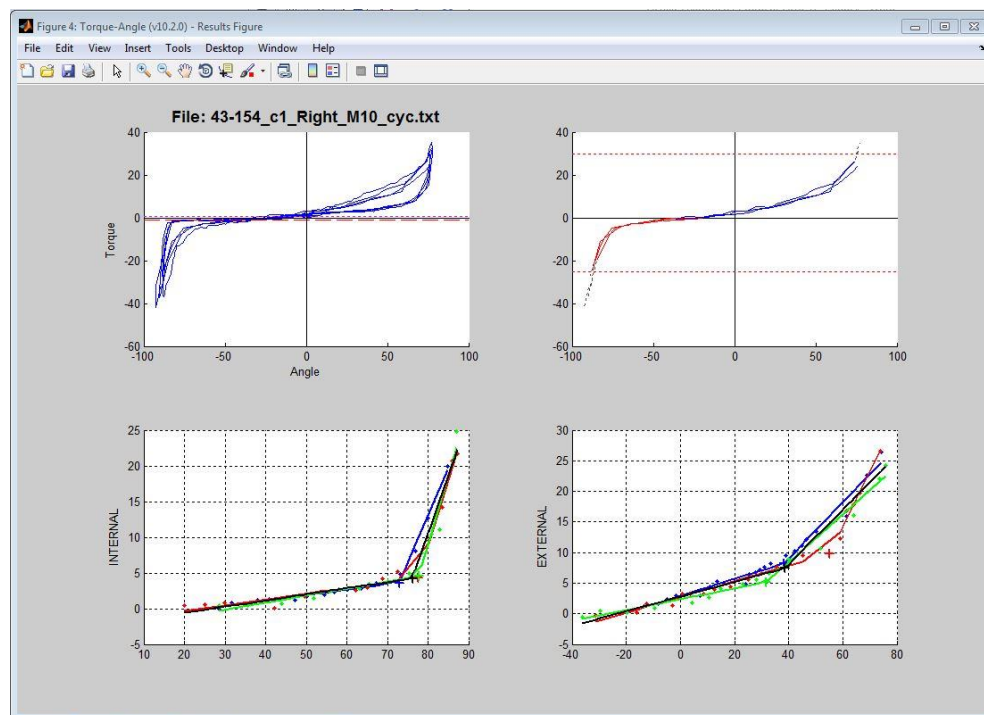
Other Commands:

>>batch_cycle_results;
    This will take the cycle file and re-analyze with a new torque cut-off
>>batch_ressum_pool;
    This will pool data from all three runs and then fit the curve
>>batch_ressum;
    This will apply the fit to each run and then average the 3 fits
>>ratonalysis_CNR;
    This will run the same ratonalysis program, but force the Boolean sign flip to

occur regardless of left or right limb label (for when data is altered does not flip sign on its own)

Outputs Parameters:

%File: File name
T_init (N.mm): Initial torque
T_off (N.mm): Torque offset; generally not important
Tmn (N.mm): Minimum torque into plantar
Amn (deg): Plantarflexion ROM
I_BP-x (deg): Plantar breakpoint for angle
I_BP-y (N.mm: Plantar breakpoint for torque
I_K1 (N.mm/deg): Plantar toe stiffness
I_K2 (N.mm/deg): Plantar linear stiffness
Tmx (N.mm): Max torque into dorsi
Amx (deg): ROM in dorsiflexion
E_BP-x (deg): Breakpoint of angle into dorsiflexion
E_BP-y (N.mm): Breakpoint of torque into dorsiflexion
E_K1 (N.mm/deg): Toe stiffness in dorsiflexion
E_K2 (N.mm/deg): Linear stiffness in dorsiflexion
Arest (deg): Resting joint angle at zero torque (ie angle at zero torque)

Now, export these into Excel and average the 2 measures together per measure.

Notes:
1. Since I am comparing between experimental groups within time points (and not across time), I do a separate grading scheme for each stain and each time point. This gives the best chance of seeing differences between groups, especially if between group changes are smaller than changes across time.
2. I am performing grading for H&E because it is the injury region, and therefore images are too cellular to accurately perform quantitative bioquant analyses.
3. I am performing grading for CD34 because we are looking specifically for vessel structure, and it is difficult for an image analysis program to accurately detect individual vessels of varying sizes.
4. All other immunohistochemistry will be quantified using a simple % area of positive signal (explained in the following protocol).

Protocol:
Randomize Images
1. Make a copy of the images you are grading and put them in a "Grading" folder (ex. H&E, Midsubstance, 20x)
2. Once in the new folder, copy the folder directory (at the top) and paste it into a web browser
3. Select all (Ctrl-A) and copy the browser window text
4. Paste the text into an excel spreadsheet in a tab labeled with the image folder information (ex. H&E Mid)
5. Remove all of the extraneous text so that you have a list of your image names in that folder
6. In the next column, put image number labels (ex. 1-15) sequentially next to each image name
7. In the next column over, type "=rand()" and drag the formula down to the last image
8. Copy the rand column, and re-paste as "values only"
9. Select column B (image number) and column C (rand)
10. Go to data -> sort -> sort by: column c (rand) -> click ok
11. Re-name the images in your grading folder (from the top) with the new randomized image numbers

Sort Images
1. Open a ppt file
2. Copy and paste your histology images so there is one image/slide
3. Put ppt into slide sorter view
4. Re-order the images to go from one end of the grading scale to the other
    a. H&E we will do this for cellularity (order images from least to most number of cells) and cell shape (order images from spindle shaped to

round shaped cells)
- b. CD34 we do this for vessel density (least to most vessels – independent of size) and vessel size (smallest to largest vessels on average in your image).
5. If you are going to have a 3 point grading scale, divide your images into 3rds
   - a. I can sometimes have a 4 point grading scale if there is enough variation between images. This depends on your image set.
6. Take roughly a center image of each group, and use this as a representative image for each grading scale (1, 2, or 3)
7. Make a new ppt presentation, with all 3 representative images and their corresponding number.

Set-up Grading
1. Create an excel file with tabs for each grading group (ex. H&E Density, H&E Shape, etc)
2. In each tab, make 3 columns: Image Number, Image Grade, Comments
3. Put in your image numbers corresponding to each group (ex. 1-15 in order)
4. Leave the other columns blank
5. Save the excel file in the "Grading" folder with the blinded, randomized images
6. Save your Image Key in the same folder
7. The graders should have: (1) the blinded, randomized images folder, (2) the Image key(s), (3) the excel spreadsheet(s) to input their grades.
8. Instruct the graders on what they are grading for, and to save a copy of the grading excel sheet with their initials.

Compiling Grades
1. Once all of the grades are in from the 3 graders, take the mode of the 3 grades as the final grade for each image
2. Compare the grades and check for any necessary re-grading that needs to happen.
   - a. There must be consistency between all 3 graders within 1 point (ex. Grades of 3, 3, and 2 would be acceptable and give a mode of 3)
   - b. If there is not consistency (ex. 3, 3, 1 or 4, 3, 2), then you need to send this image back to the graders to be re-graded.
       - i. Look at the image first to see if there is a clear reason for the discrepancy (such as some sectioning artifact that should be disregarded when grading) and indicate this to the graders.
       - ii. This should all be done in a blinded manner and only give help if there is confusion about what or how to grade the image. Do not provide suggestions for if it should be graded higher or lower, etc.
3. Most of the time re-grades will solve the discrepancies. If an image cannot get a grading consensus, then it cannot be used.
4. Once all of the grades are in, the median is taken between multiple images of the same specimen, and that value is the final grade for the specimen
5. Present the data as median and IQR, and run non-parametric statistics to compare groups.

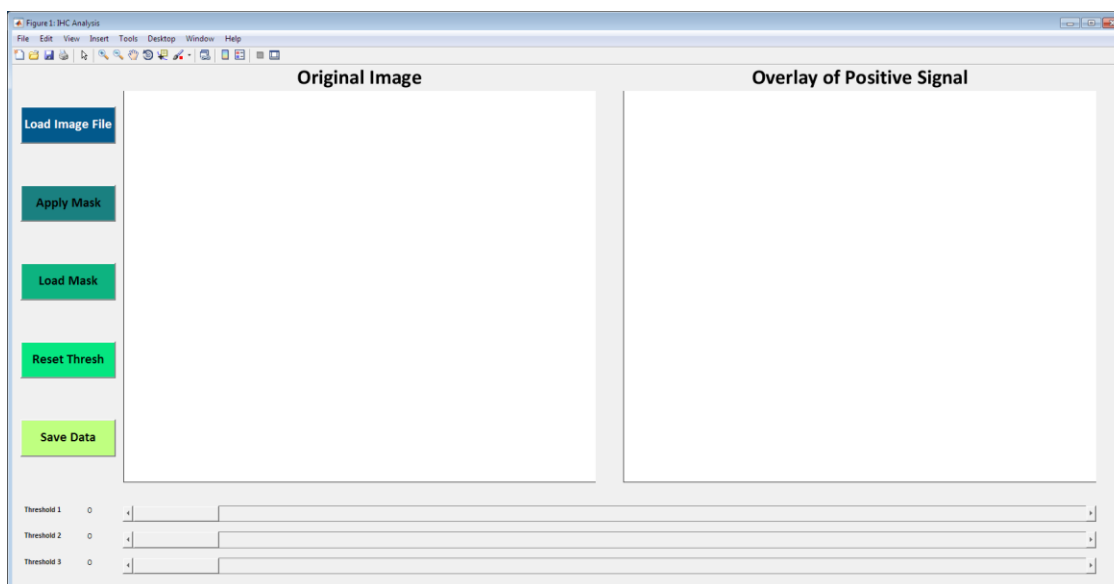## APPENDIX 25: Immunohistochemistry Quantification Protocol
Updated on 02/20/2018 by Cori Riggin

Analysis of IHC Images:

MATLAB Directory: \\maxine\soslowskylab\software cooker-freezer\Immuno\cooker\cooker_CNR thesis

Command: **IHC_analyzer;**

1. The **G**uided **U**ser **I**nterface (GUI should come up).

2. Begin by clicking the ***Load Image File*** pushbutton. A modal dialogue box will pop up. Navigate to where your image is located. Select whether there 1 or 2 stains
   a. DAB only is 1 stain, where DAB + counterstain such as hematoxylin would be 2 stains.
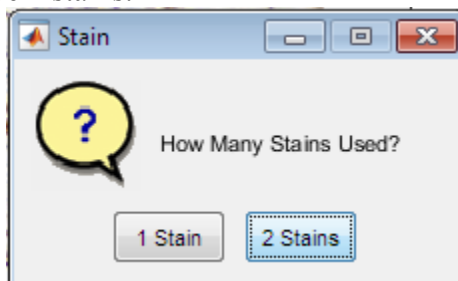
   b. The original image will come up, but the overlay image will take some time. Once the overlay image comes up, you make begin processing

the image.

c. Green is the overlay.
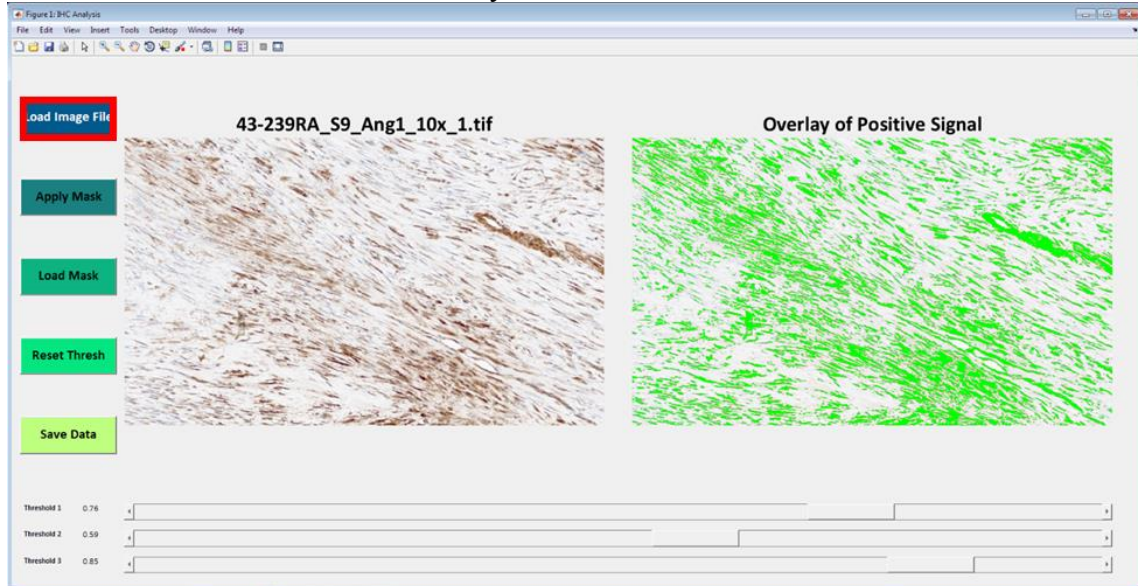
This particular example has 2 stains

3. If you wish to apply a mask, click the ***Apply Mask*** pushbutton. Use the interactive polygon tool to choose a ROI.
   a. This is used to remove any space in the image that you don't want to perform the analysis on (such as image artifact, blank slide space, etc)
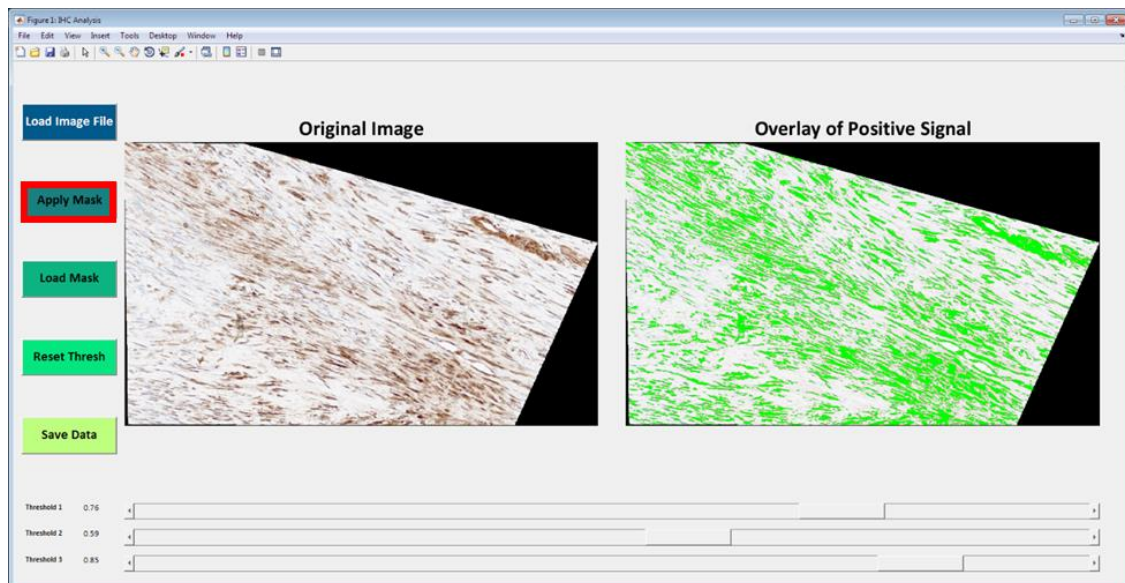
4. If a mask already exists for a particular sample, click the ***Load Mask*** pushbutton. This will bring up a modal dialogue box. Navigate to where your mask is located.
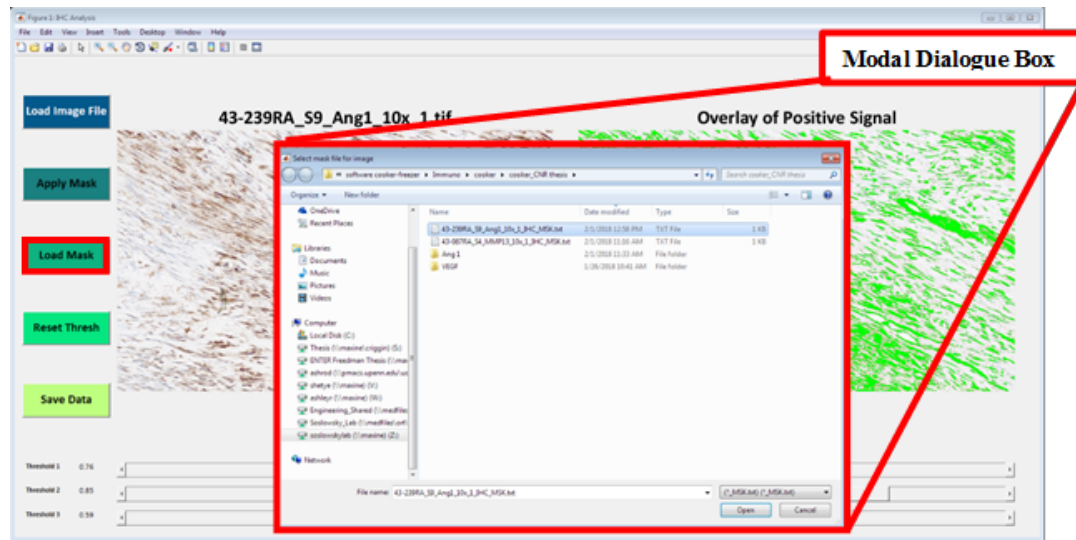
5. Move the each scroll bar left or right to adjust the threshold for brown, blue, and the background.
   a. Left – (lower threshold values) will capture less signal
   b. Right – (higher threshold values) will capture more signal

Examples:
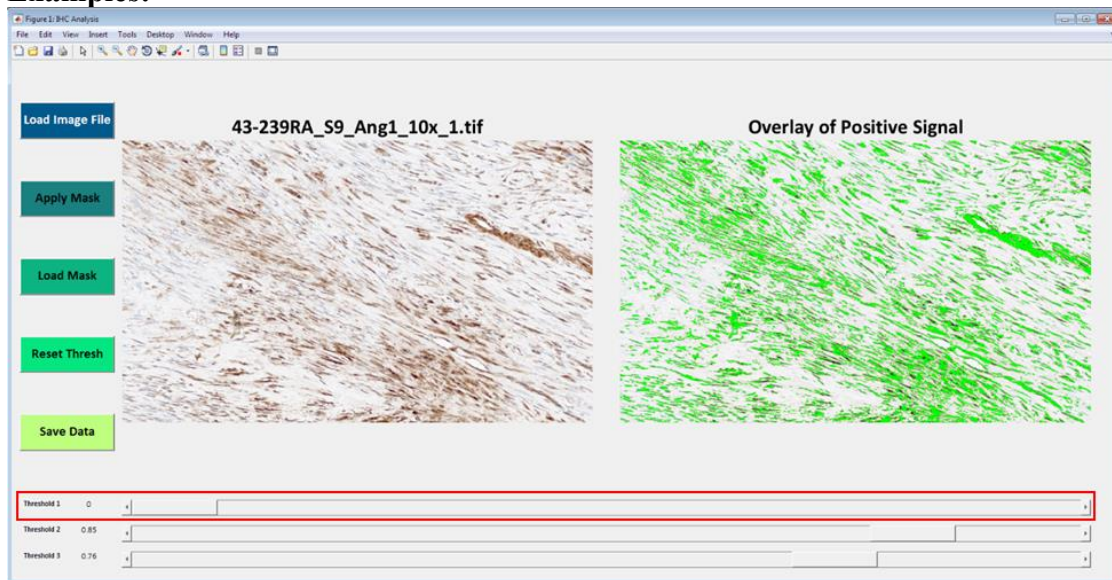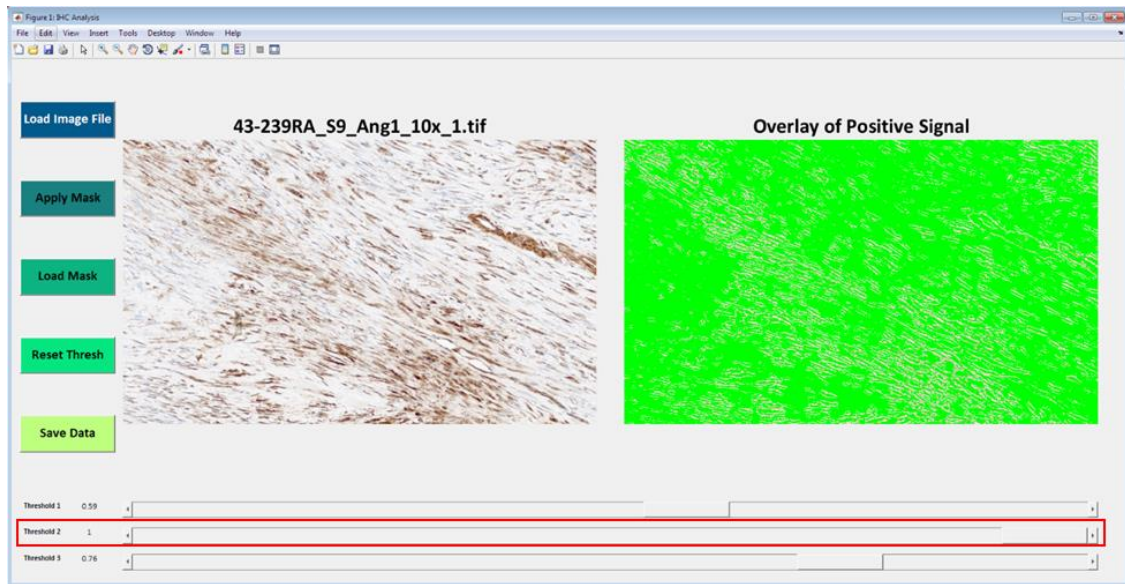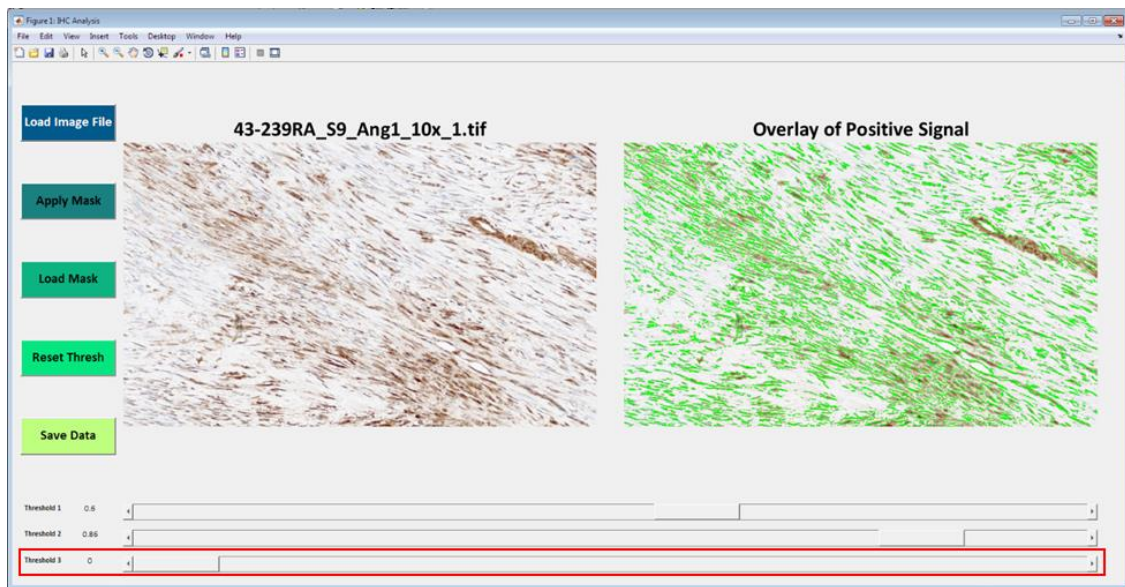

Threshold 1 set to 0
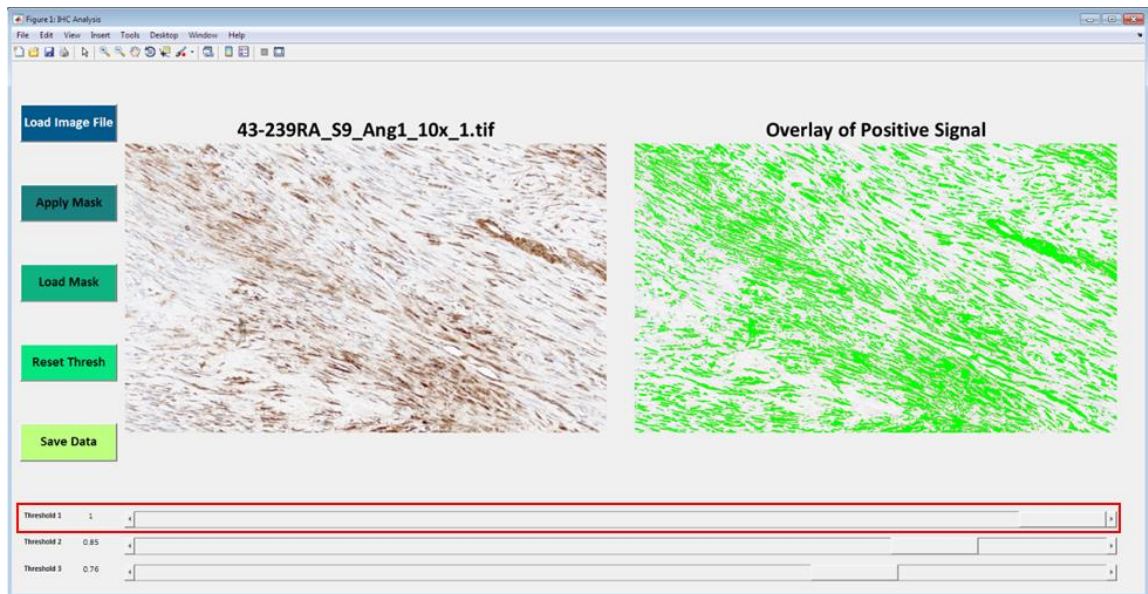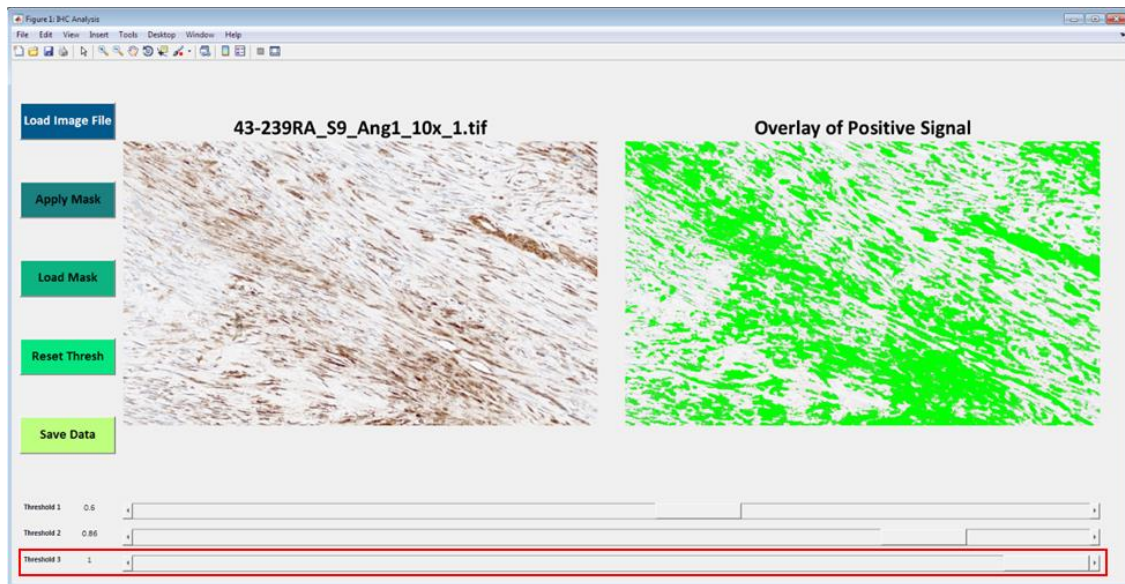
Threshold 1 set to 1
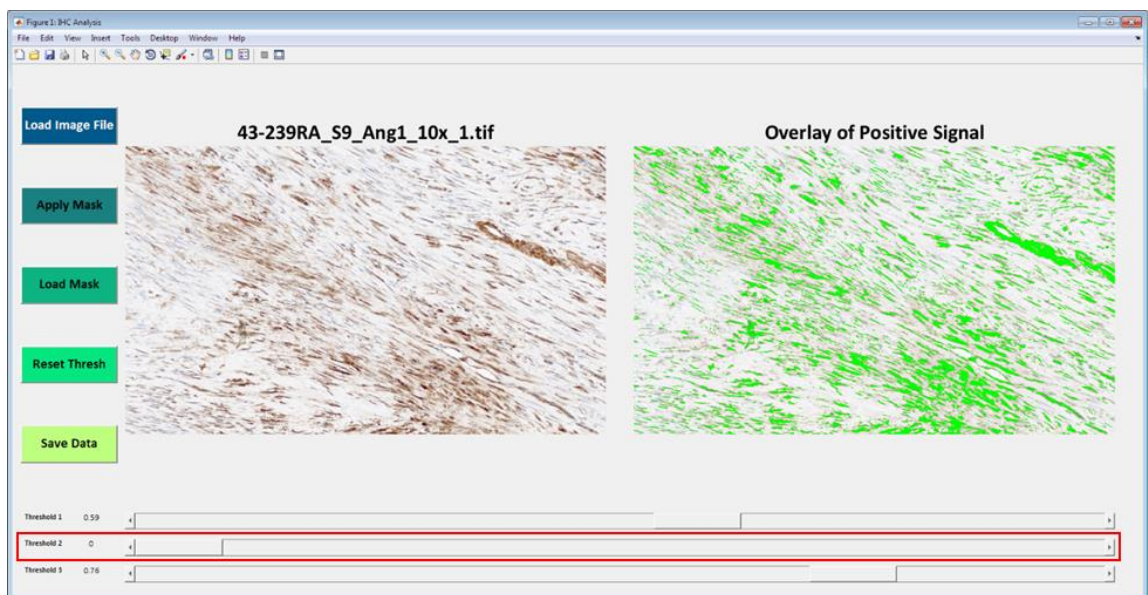
Threshold 2 set to 0

*Threshold 2 set to 1*

Threshold 3 set to 0

Threshold 3 set to 1

6. If you wish to go back to the default threshold hold, you may click the ***Reset Thresh*** button

7. Generally, a good system to use is to work with one threshold at a time
   a. Move all of the thresholds up to 1 (should be all green)
   b. Slowly lower the white threshold down until right before you start seeing color that is dark and would be part of the DAB coloring
   c. Then, move the blue threshold down until you only see white and blue color, and no brown
   d. Finally, move the brown threshold BELOW what you want, and slowly move it up to cover all positive DAB stain.
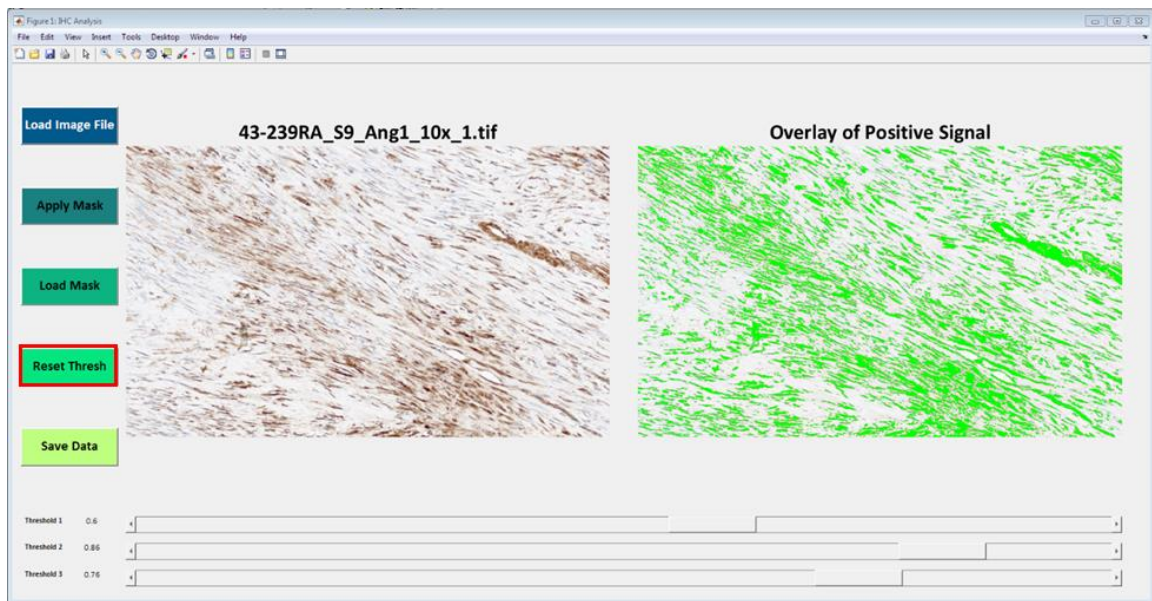
8. Once you are happy with the thresholding, click ***Save Data***. A modal dialogue box will pop up. Navigate to where you would like to save your data
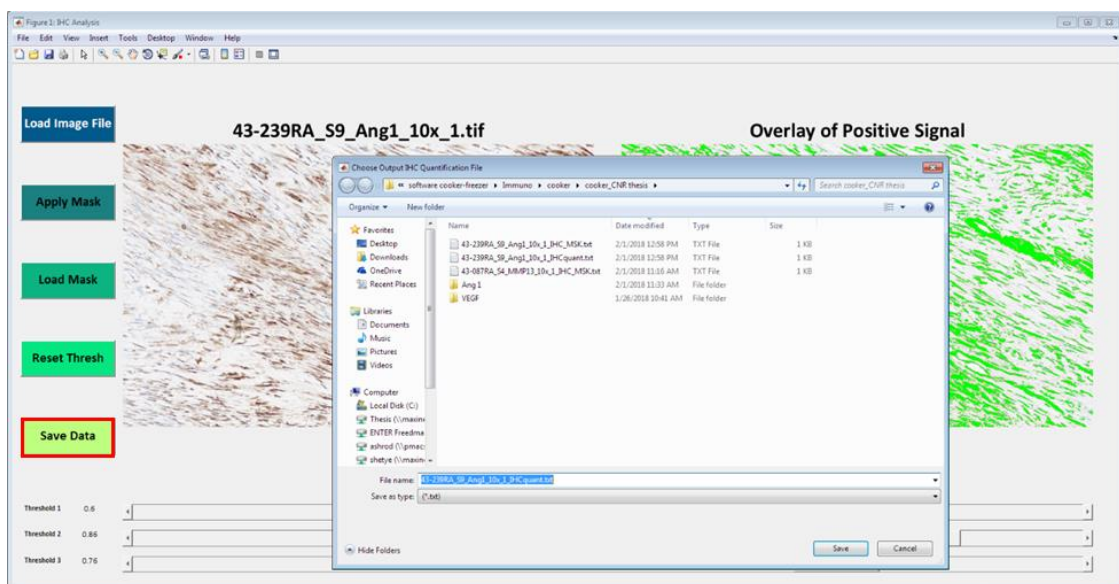
Compiling Data:

MATLAB Directory: \\maxine\soslowskylab\software cooker-freezer\Immuno\cooker\cooker_CNR thesis

Command: **batch_IHC_results;**

1. Navigate to the folder of IHC images that you are analyzing together
   a. For my project, I analyzed within each time point for each stain
2. Select all of the IHC analysis files you want to compile
3. This code will put them all into one text file so that you can easily copy and paste into excel for processing.

Pushbuttons:

Load Image File – Opens a modal dialogue box for you to navigate to the image you wish to analyze.

Apply Mask – Opens an interactive polygon tool for you to choose a ROI.

Load Mask – If you have already chosen a ROI and wish to re-analyze the image, you can load a previous ROI using this tool.

Reset Thresh - Resets to the default threshold values for brown, blue, and background.

Save Data - Opens a modal dialogue box for you to specify a name and location for your output. The output is saved to a text file.

Scrolls:

Brown Threshold – Edits the threshold for brown colors – higher values will capture darker colors

Blue Threshold – Edits the threshold for blue colors – higher values will capture darker colors

Background Threshold – Edits the threshold for background colors – higher values will capture darker colors